NASA-CR-174697-Vol-1

Configuration Study for a 30 GHz Monolithic Receive Array

Volume I: Final Report

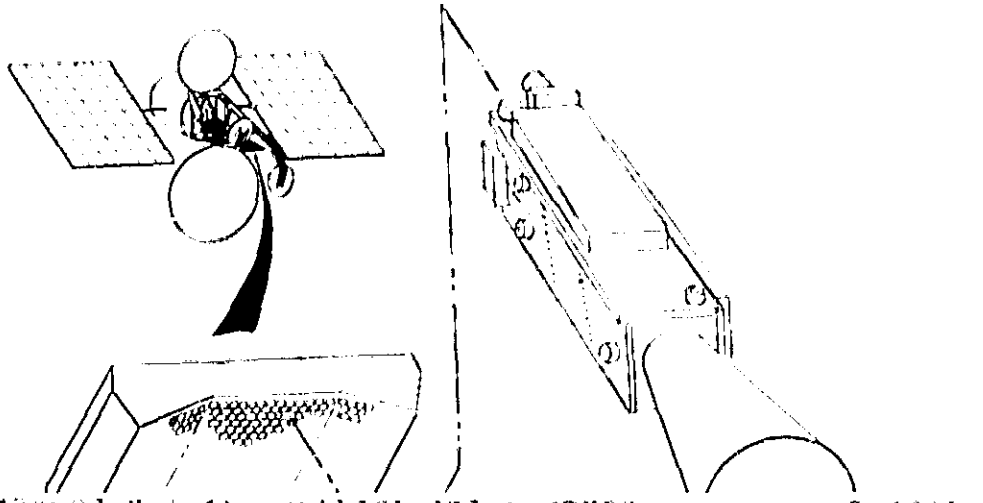

Prepared for
NASA LEWIS RESEARCH CENTER
Cleveland, Ohio

Contract NAS3-23780

ELECTRONICS LABORATORY
Syracuse, New York 13221

GENERAL ELECTRIC

1. Report No.	2. Government Accession No.	3. Recipient's Catalog No
NASA CR-174-697		

4. Title and Subtitle	5. Report Date
Configuration Study for a 30 GHz Monolithic Receive Array	1 November 1984
	6. Performing Organization Code

7. Author(s)	8. Performing Organization Report No
W.H. Nester, Bryan Cleaveland, Brian Edward, Steve Gotkis, Gary Hesserbacker, Jack Loh, Bruce Mitchell	
	10. Work Unit No.

9. Performing Organization Name and Address	11. Contract or Grant No.
General Electric Company Electronics Laboratory Electronics Park Syracuse, New York 13221	NAS3-23780
	13. Type of Report and Period Covered

12. Sponsoring Agency Name and Address	14. Sponsoring Agency Code
National Aeronautics & Space Administration Lewis Research Center 21000 Brookpark Road Cleveland, OH 44135	

15. Supplementary Notes

Technical Monitor, Richard Lee, Space Communication Division
NASA Lewis Research Center

16 Abstract

This report summarizes the results of configuration and design studies for 30 GHz receive antennas on a communications satellite. The antennas use reflector focusing systems with phased array feeds for beampointing, aberration correction, and interference suppression. The phased array feed designs are based on MMIC module technology. The antennas form simultaneous multiple beams in both scanning beam and fixed beam designs. Polarization diversity is used for beam isolation.

The initial configuration study and parametric design analyses encompassed Gregorian, Cassegrain, and single reflector systems. Parametric design and performance curves were generated. A preliminary design of each reflector/feed system was derived including radiating elements, beam-former network, beamsteering system, and MMIC module architecture. Performance estimates and component requirements were developed for each design. A recommended design was selected for both the scanning beam and the fixed beam case.

Detailed design and performance analysis results are presented for the selected Cassegrain configurations. The final design point is characterized in detail and performance measures evaluated in terms of gain, sidelobe level, noise figure, carrier-to-interference ratio, prime power, and beamsteering. The effects of mutual coupling and excitation errors (including phase and amplitude quantization errors) are evaluated. Mechanical assembly drawings are given for the final design point. Thermal design requirments are addressed in the mechanical design.

17. Key Words (Suggested by Author(s))	18. Distribution Statement
Cassegrain, Gregorian, Reflector, Phased Array Feed, MMIC Multiple Beam Antenna	For General Release

19. Security Classif. (of this report)	20. Security Classif. (of this page)	21. No. of Pages	22. Price*
Unclassified	Unclassified	549	

* For sale by the National Technical Information Service, Springfield Virginia 22161

TABLE OF CONTENTS

VOLUME I

TABLE OF CONTENTS (Continued)

VOLUME I (Continued)

TABLE OF CONTENTS (Continued)

LIST OF TABLES

LIST OF TABLES
(Continued)

1 INTRODUCTION

1.1 FUTURE COMMUNICATIONS SYSTEM SATELLITE REQUIREMENTS

Increasing satellite communications traffic has led to an increased use of the millimetric portion of the electromagnetic spectrum. Advanced communication satellites will require high performance millimeter-wave antenna systems capable of multiple beams, polarization diversity, adaptive beamforming, agile hopped beams, and reconfigurable shaped geographic coverage. Phased array fed reflector systems will satisfy these needs, but historically the cost of the phased array development has been prohibited, because of the large number of hybrid circuits and components required. However, recent advances in monolithic circuits make such a communications system technologically and economically feasible. Monolithic microwave integrated circuits (MMICs) operating at millimeter wave frequenices are in the early stages of development, and they must be upgraded to fully realize the advantages that phased array systems offer. When the technology is mature, it will provide lightweight, low-cost, highly reproducible, and high performance replacements for the currently available discrete circuits.

Forecasting studies have projected a growth in long-haul communications traffic by a factor of five between the years 1980 and 2000. This increase in traffic will result from both an expansion of services provided and from an expanded user population. Expanded sevices will include telephone, video teleconferencing, electronic mail, point-of-sale and electronic fund transfer, and other data services. The increase in users will occur principally in the government, large business, hospital, and educational sectors, and to a lesser extent will take place in small businesses and private homes. (Video services and certain data services can require very high data rates: e.g. several million bits per second.)

In the near term, the increasing traffic will be handled by the C- and Ku-band satellite systems. However, 12 of the 15 allocations for telecommunications at C-band are already committed or planned. Similarly, 10 of the 15 allocations at Ku-band are committed or planned. Allocations in both bands are for a 500 MHz bandwidth.

The millimeter-wave allocations include 24 prime slots available at 30/20 GHz with a bandwidth of 2500 MHz for telecommunications and 24 prime slots at 40/30 GHz with a bandwidth of 1000 MHz for TV broadcast. Based on the increase in traffic and the saturation of the C- and Ku-band satellite systems, it is projected that communications satellites operating in the millimeter-wave band will supply 20 to 40 percent of the total long haul communications traffic by the year 2000.

Specialized antenna designs must be used if the satellite communications system is to use the available frequency spectrum efficiently. Dual-reflector or single-reflector antennas with array feed systems are generally required. These antenna designs conserve spectrum through the use of electronic scan, multiple beams, and/or shaped beams.

Multiple-beam antennas conserve spectrum by allowing frequency re-use; they use beam directivity to provide channel isolation between geographically separated terminals on the same frequency. Rapid electronic scanning can be used to conserve spectrum by using the electronic scan to accomplish time division multiple access (TDMA). In addition to being required to implement such antenna designs, array feeds can be used to null out interference or jamming in a communications system. The basic building block of array feeds is the array module. In general, the array module must provide both phase and amplitude control of the communications signal.

Decisive technical factors drive the implementation of these array modules to MMIC form. For example, the high reliability afforded by the MMIC process uniformity and repeatability is a major asset in satellite applications. Also, the low power drain afforded by MMIC circuits is another major advantage in satellite systems. The extremely small size of millimeter-wave circuits particularly suits them to MMIC implementation, since the module size becomes too small for operator-oriented fabrication and assembly processes. In addition, MMIC technology can also provide weight and cost advantages in systems in which large numbers of modules are involved.

Furthermore, MMIC implementation at millimeter wave frequencies provides module performance advantages. The extremely small circuit sizes allow undesireable parasitics to be minimized, which results in broader band and less dispersion. Such performance considerations are important in wideband data communications systems, in which phase linearity and uniform group delay is important. Phase linearity is required for TDMA carrier recovery. Group delay variations must be minimal since such variations increase inter-symbol interference and result in an effective signal loss and/or an increase in the bit-error probability. The small size attainable with MMIC modules can also provide lower insertion loss, improved noise-figure, and the suppression of module package RF resonances.

The development of new technologies are necessary for a wideband 20/30 GHz system. Such a system must have the following performance characteristics:

- High degree of matching between predicted traffic density distribution and system communication capability.
- Efficiency in its use of the available bandwidth allocation.
- High link fidelity
- Flexibility of operation in the presence of changing traffic, propagation, and pointing error conditions.
- High reliability

These goals translate into two antenna system requirements:

1. Capability of providing high peak gain, high C/I, and large channel capacity to major communications centers (fixed beams)

2. Capability of providing high contour gain, high C/I, and variable channel capacity to the rest of the 48 states (scanning beams)

The thrust of this contract has been to investigate and develop the application of MMIC receive modules to phase array feed technology. The study included such considerations as:

- MMIC's
  - Mounting of the modules to the beam combining network
  - RF and IF transitions to the module
  - DC and logic interfaces with the module
  - Distribution of LO power to the module
  - Feed element design that takes fullest advantage of module capabilities
  - Dissipation of thermal energy
- Beam Combining Network
  - Loss
  - Weight
  - Maintaining effective noise figure
  - Inherent graceful degradation
  - Low sidelobes
  - Wide angle scan
  - Exploitation of distributed receiver with MMICs
  - Electrical limitations imposed by available prime power from the satellite
- Feed Element
  - Mutual coupling effects
  - Efficient illumination of the subreflector
  - Low cross-polarized component
  - Bandwidth
- Optics Design
  - Shapes of reflectors
  - Size of reflectors
  - Impact of module phase granularity
  - Impact of module amplitude granularity
  - Wide angle scan
  - Impact of module to module variation
  - Grating lobe suppression
  - Sidelobe level
  - Cross polarization suppression

- Satellite

  - Packaging of antenna system on the satellite
  - Shuttle compatibility of the system
  - Thermal environment of in-place satellite

Each of these will be discussed in greater detail in the following sections.

1.2 CONFIGURATION STUDY SPECIFICATIONS/REQUIREMENTS

The purpose of this section is to review the overall antenna system requirements for both the multi-beam and scanning beam systems. During this study, the multi-beam and scanning beam systems have been considered separately, although, the two functions may eventually be combined into one antenna system.

The objective requirements for the system configurations are shown in Table 1. While the optical configuration was an important part of this contract, the greatest emphasis was placed on the application of the monolithic receive modules to the receiving array design.

TABLE 1. OBJECTIVE REQUIREMENTS FOR MULTI-BEAM AND SCANNING BEAM ANTENNA

Beam Configuration		Multi-Beam	Scanning Beam
Antenna Size		Shuttle	Compatible
Operation Frequency Range (GHz)	-Uplink	27.5 - 30.0	27.5 - 30.0
Number of Beams	-Operational	10 - 18	6
Minimum Gain (dB)	-30 GHz	56	53
Bandwidth (MHz)	-30 GHz	2500	2500
Polarization		Linear	Linear
C/I Performance (dB) [1]		30	30
Pointing Accuracy (degrees)	- E & H Plane Polarization	0.02 0.4	0.02 0.4

[1] Carrier to interference ratio for each beam relative to all other beams

The general requirements consider the antenna system to be an integral part of a spacecraft launched using the shuttle space transport system, and to be operated at synchronuous altitude at a position of 100° ± 5° west longitude and 0° latitude. The spacecraft bus on which the antenna system is mounted is assumed to be three axis stabilized.

The objective requirements for the multiple fixed beam antenna include a ten (10) beam and an eighteen (18) beam concept with fixed beams positioned on the cities specified in Table 2.

TABLE 2. MULTIPLE FIXED BEAM ANTENNA COVERAGE

Ten-City Coverage	Eighteen-City Coverage
1 New York City	1 New York City
2 Washington, DC	2 Washington, DC
3 San Francisco, CA	3 San Francisco, CA
4 Chicago, IL	4 Chicago, IL
5 Los Angeles, CA	5 Los Angeles, CA
6 Denver, CO	6 Denver, CO
7 Minneapolis, MN	7 Minneapolis, MN
8 Atlanta, GA	8 Atlanta, GA
9 Dallas, TX	9 Dallas, TX
10 Houston, TX	10 Houston, TX
	11 Boston, MA
	12 Seattle, WA
	13 Detroit, MI/Cleveland, OH
	14 Buffalo, NY/Pittsburgh, PA
	15 St. Louis, MO
	16 Phoenix, AZ
	17 New Orleans, LA
	18 Miami, FL

The multiple scanning beam antenna has six (6) receive beams which are independently controlled. Each receive beam originates from different locations in each of the six CONUS sectors. For each sector, a sufficient number of beam positions exist such that any point in the sector falls within the 1 dB contour for at least one of the beam positions of the antenna.

The component requirements outlined below were assumed as typical specifications of the components used in developing the antenna systems.

Electrical and RF Performance Objective Requirements. The receive module shall be of fully monolithic construction with no discrete components, no wire bonds and no off-the-chip matching required.

RF Band: The RF band shall be from 27.5 to 30.0 GHz.

IF Center Frequency: The IF center frequency shall be between 4 and 8 GHz.

Noise Figure: The noise figure at any given frequency in the bandwidth shall be less than or equal to 5 dB.

Output Gain: The RF to IF output gain shall be greater than or equal to 30 dB at the highest level of the gain control.

Gain Control: The gain control shall provide for at least 6 levels of RF-IF gain including the following: 30 dB; 27 dB; 20 dB; 17 dB; and an off state.

Module Power Consumption in Each State: The power consumption of the entire receive module in each state of the gain control shall be in accordance to the following:

RF-IF Gain Level	Module Power Consumption
30 dB	250 mW
27 dB	250 mW
24 dB	250 mW
20 dB	250 mW
17 dB	250 mW
off	25

Gain Control Response Time: The gain control response time shall be less than or equal to 10 nanoseconds.

Gain Variation: The maximum variation in the output RF-IF gain for any state of the gain control shall be no greater than ± 0.5 dB over the entire 2.5 GHz bandwidth and no greater than ± 0.2 dB over any 500 MHz band.

Module to Module Gain Variation: For any module, the RF-IF gain at any given frequency in the bandwidth shall vary by no greater than ± 0.5 dB from the RMS average for all the modules at the given frequency.

Phase Shifter: The phase control shall contain the following 5 bits:

0° or -180° ± 3° at band center
0° or -90° ± 3° at band center
0° or -45° ± 3° at band center
0° or -22.5° ± 3° at band center
0° or -11.25° ± 3° at band center

The phase shifter is to use a true time delay phase shifter scheme. That is, in any state of the phase shifter, the total module phase shift shall be proportional to frequency, within the 27.5 to 30.0 GHz pass band, with a phase error not exceeding ± 6° i.e.

$$\Delta\Theta_i = 2\pi f\tau_i + \varepsilon_i(f)$$

where: Δ_i = total phase shift, as a function of frequency, in the i'th state of the 5 bit phase shifter; f = frequency; τ_i is a characteristic time delay associated with the i'th state of the 5 bit phase shifter, and $\varepsilon_i(f)$ is a phase error associated with the i'th state of the phase shifter. $\varepsilon_i(f)$ may vary with frequency but its maximum magnitude should not exceed 6° at any i and at any frequency.

Phase Shifter Response Time: The phase shifter response time shall be less than or equal to 10 nanoseconds.

Group Delay Variation: The group delay variation shall not exceed 0.2 nanoseconds peak to peak in any 0.5 MHz portion of the operating band and under any state of the phase shifter.

RF/IF Impedances: The nominal RF input and IF output impedance shall be 50 ohms. The input and output VSWR shall be less than or equal to 1.3:1.

Phase Control/Gain Isolation: The RF/IF gain shall not vary by more than 0.25 dB in response to any change in the phase control state.

Gain Control/Phase Isolation: The phase shift shall not vary by more than ± 5 degrees in response to a change in the gain control level.

Phase and Gain Control: The phase and gain control shall operate on digital input.

Number of Control Lines: The number of control lines shall not exceed twelve (12). Impedance and voltage level shall be TTL compatible. Input signal shall be continuously available during period of dwell.

LO Reference: A phase reference shall be provided to the receive module local oscillator from off chip. The reference signal power shall be 15 microwatts minimum.

Dynamic Range: > 30 dB.

2 EXECUTIVE SUMMARY

2.1 RECOMMENDED ANTENNA CONFIGURATION

The dual-reflector Cassegrain reflector optics with a phased array feed system using dual-polarized circular horn radiating elements has been found to be a superior design for both the multiple scanning beam and the multiple fixed beam antennas. The major design features of the recommended configuration are:

- A Dual-Reflector Antenna
- Offset Cassegrain Optics
- Offset Plane in a North-South Orientation
- A Singly-Curved Feed Array
- Dual-Polarization Circular Horn Feed Elements
- An All-RF Module (with Both Phase and Amplitude Control*)
- An RF Beam Combining Network (with Row-Column Implementation*)
- A Simple Sequential-Beamsteering Control Distribution Network

* Pertains to Scanning, Multiple Beam Design

The principal advantages of the recommended antenna configuration are summarized below:

- Dual-Reflector Antenna Provides
  - Reduced axial dimension
  - Reduced cross-polarization

- Offset Reflector Design
  - Eliminates aperture blockage by sub-reflector and feed over scan region for better gain and lower sidelobes.
  - Using north/south offset provides best gain/sidelobe performance over the scan region.

- Cassegrain Optics Provides
  - Minimum feed array size
  - Minimum sub-reflector size
  - Full exploitation of MMIC module technology (amplitude and phase control in low-noise application).

- Singly Curved Feed Array Surface Results In
  - Improved scan performance (high gain, low sidelobes)
  - Simple array combiner structure

- Dual-Polarized Circular Horn Feed Array Elements
  - Are proven design
  - Have low mutual coupling
  - Provide high polarization purity

- RF Beam Combiner Network
  - Allows simple, small, lightweight structure
  - Avoids complex LO power distribution network
  - Minimizes LO noise degradation

- Maximum Likelihood Beamforming/Beamsteering Algorithm
  - Suppresses sidelobes over full coverage region with minimum loss in gain
  - Allows sidelobe nulls to be formed by spot beam along interfering directions
  - Compensates for known reflector/feed misalignments
  - Compensates for known reflector deformations
  - Allows beam-position interpolation for full beamsteering capability with simplified beamsteering computation
  - Provides maximum residual performance capability under component failure conditions

An isometric depiction of the chosen configuration is sketched in Figure 1. A dimensioned cross-sectional line drawing of the basic antenna geometry is given in Figure 2 for the scanning beam design and in Figure 3 for the fixed spot beam design. The values of the principal design parameters for these two designs are reported in Table 3.

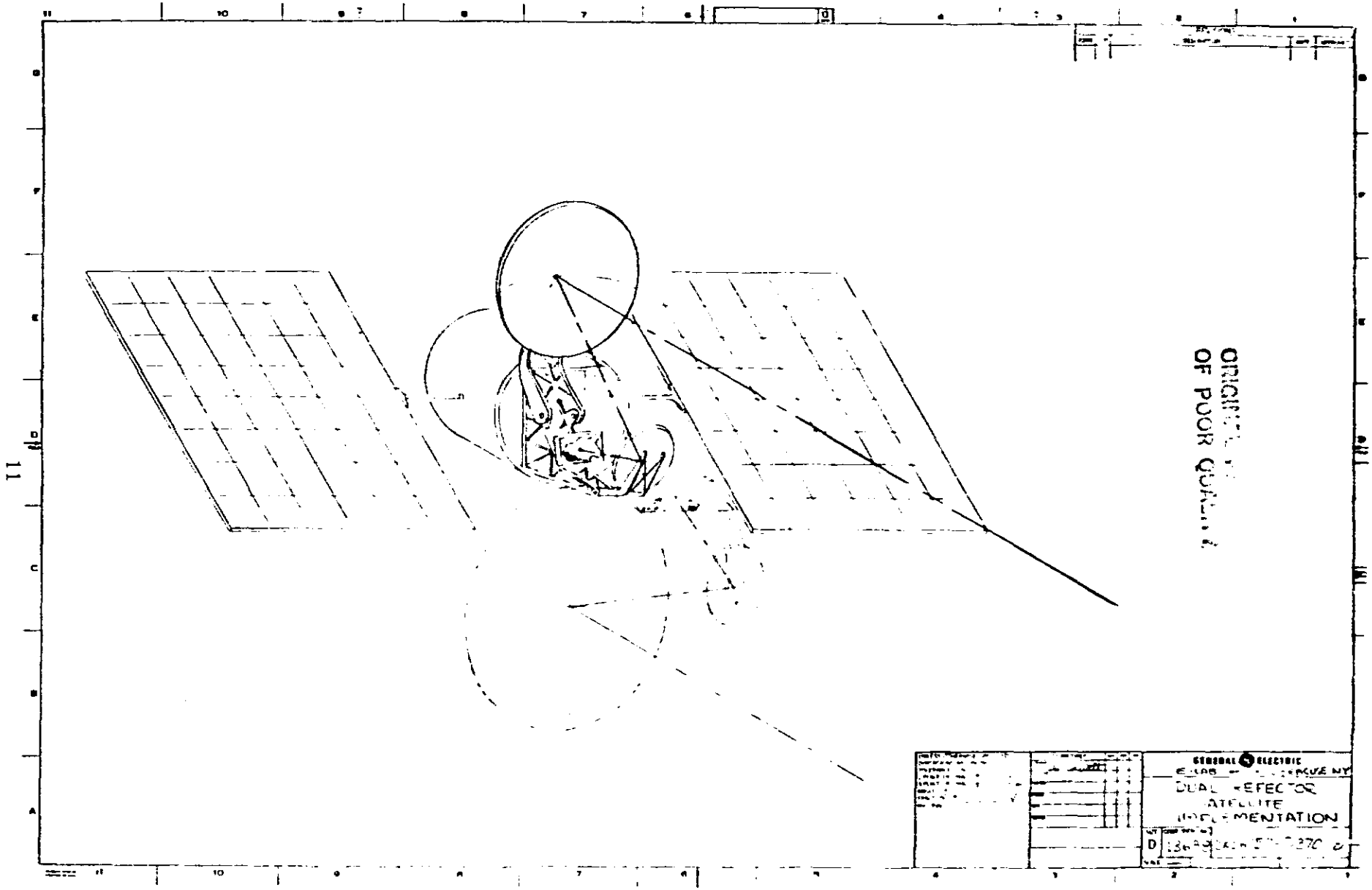

Figure 1. Isometric View of the Recommended Antenna Configuration

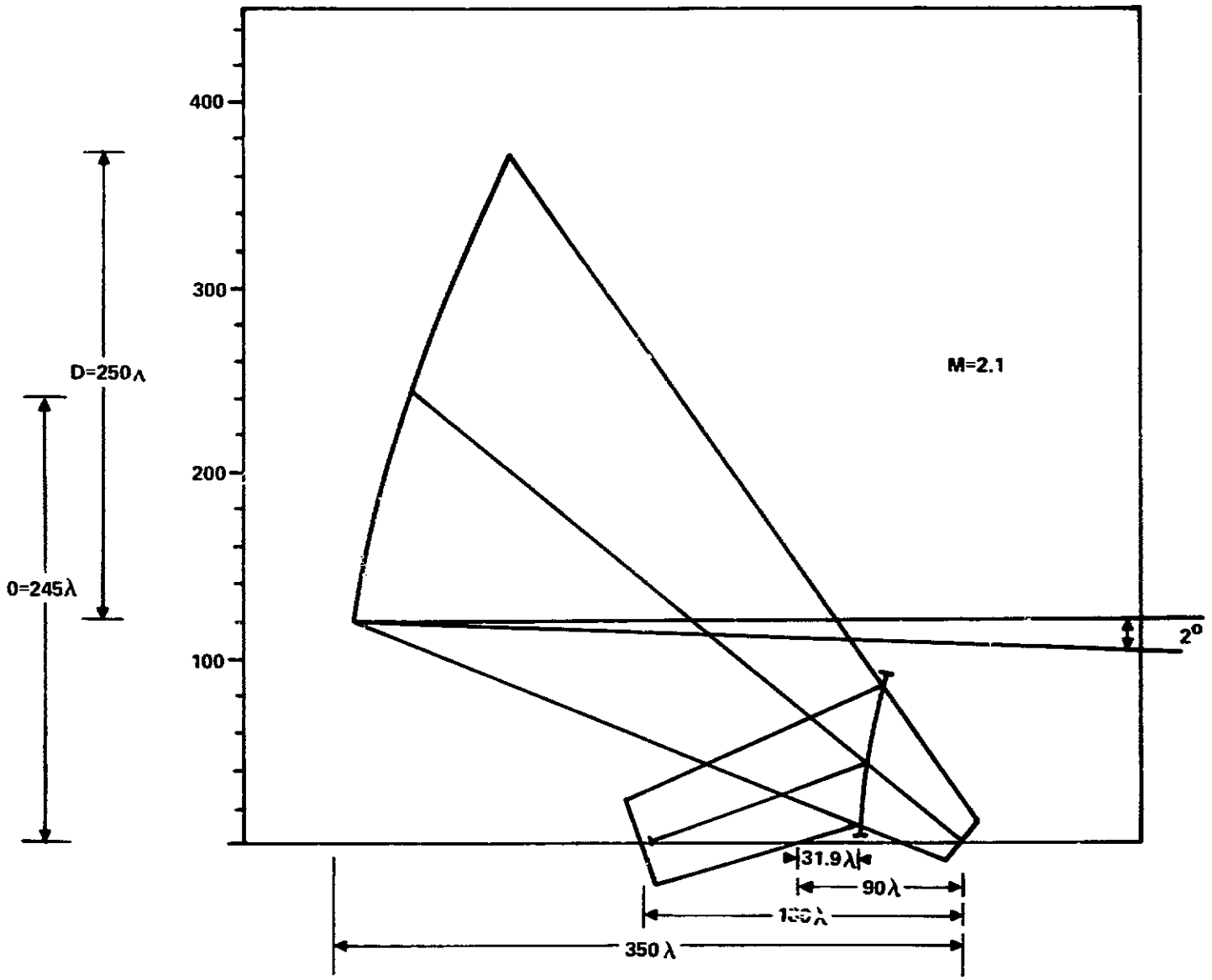

Figure 2. Line Drawing of Scanning Beam Antenna Geometry (Offset Plane)

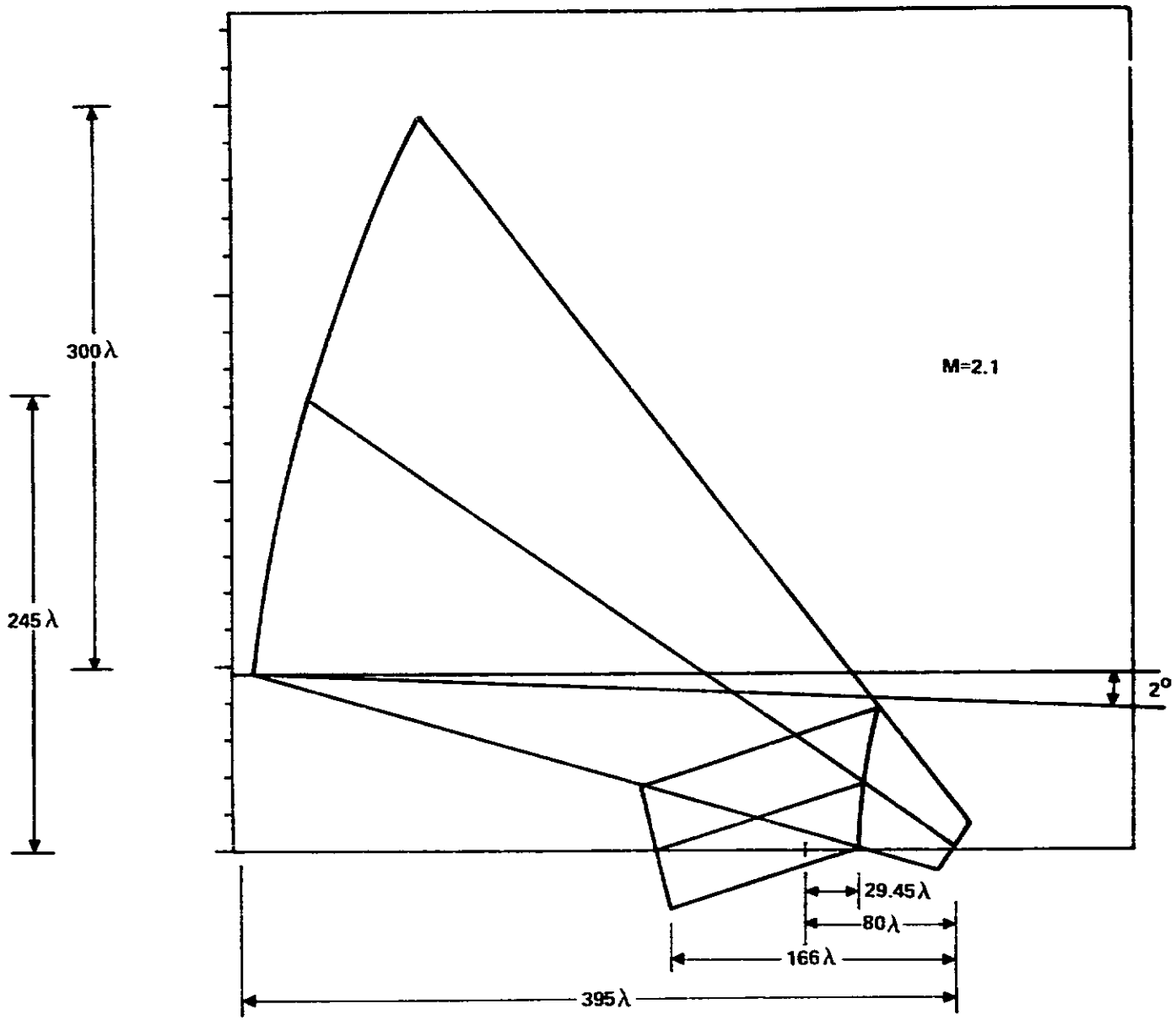

Figure 3. Line Drawing of Fixed Beam Antenna Geometry (Offset Plane)

TABLE 3. FINAL DESIGN PARAMETERS OF THE RECOMMENDED CONFIGURATIONS (DETAILED DESIGN STUDIES)

Design Parameter		Scanned Beam	Fixed Beam
• Dimension of Primary Reflector			
- Major axis (offset-plane)	:	8.94'	10.62'
- Minor axis	:	8.56'	10.28'
- Diam of projected aperture	:	8.56'	10.28'
• F/D of the Primary Reflector			
- (Focal length of parent paraboloid/projected diameter)	:	1.4	1.32
• Offset of Primary Reflector (System Axis to Reflector Center)	:	8.39'	8.39'
• Diameter of Sub-Reflector	:	3.0'	3.0'
• Offset of Sub-Reflector	:	1.71'	1.37
• Magnification Factor	:	2.1	2.1
• Effective F/D	:	2.94	2.77
• Array Feed Dimensions			
- Height (dimension in offset plane)	:	1.72'	2.33' *
- Width	:	3.45'	4.67' *
- Depth	:	0.70'	.70' *
• Array Tilt Angle (offset plane)	:	20°	20°
• Array Curvature (Azimuth Plane)	:	5.48°/FT	N/A
• Number of Beams	:	6	18
• Number of Dual-Polarized Feed Array Elements			
- Total number	:	391	243
- Number of vertically polarized ports	:	320	100
- Number of horizontally polarized ports	:	344	57
- Active number/beam	:	19	19
• Diameter of Circular Feed Horn	:	0.105'	0.105'
• Feed Horn Spacing (Equilateral Triangular Grid)	:	0.106'	0.106'

* Envelop

TABLE 3. FINAL DESIGN PARAMETERS OF THE RECOMMENDED CONFIGURATIONS (DETAILED DESIGN STUDIES) (Continued)

Design Parameter		Scanned Beam	Fixed Beam
• Overall Antenna Dimensions			
- Height	:	13.5'	14.6'
- Width	:	8.6'	10.3'
- Length	:	10.2'	12.0

The principal performance parameters for these two designs are summarized in Table 4.

TABLE 4. FINAL PERFORMANCE PARAMETERS OF THE RECOMMENDED CONFIGURATIONS (DETAILED DESIGN STUDIES)

Performance Parameter		Scanned Beam	Fixed Beam
• Antenna Gain			
- Broadside	:	54.7 dB	56.2 dB
- Worst Case Scan	:	54.2 dB	55.9 dB
• Average Design Sidelobe Level (0.5° to 2.0° Radius Annular Region About Main Beam)			
- Broadside	:	-45.3 dB	-46.4 dB
- Worst Case Scan	:	-42.9 dB	-45.3 dB
• Peak Design Sidelobe			
- Broadside	:	-36.2 dB	-35.4 dB
- Worst Case Scan	:	-33.5 dB	-34.4 dB
- Expected	:	-38 dB	-40 dB
• Degradation of Sidelobes due to Excitation Errors	:	< 1 dB	< 1 dB
• Beamwidth			
- Broadside	:	0.29°	0.24°
- Worst Case Scan	:	0.29°	0.24°
• Scan Region (or Max. Fixed Beam Displacement)			
- Azimuth , Total	:	± 3.5°	3.5°
- , Per Beam	:	± 0.6°	N/A
- Elevation, Total	:	± 1.5°	1.5°
, Per Beam	:	± 1.5°	N/A
• Noise-Figure	:	5.28 dB	4.41 dB
• C/I	:	-30 dB	-30 dB*
• DC Power Consumption/Beam	:	7.90 Watts	5.18 Watts

* Worst Case

The pattern performance of the final designs are presented in Figures 89 through 98. These patterns were computed for the ten cases summarized in the table below:

DIRECTORY OF PATTERN PLOTS FOR RECOMMENDED CONFIGURATIONS
(DETAILED DESIGN STUDIES)

Antenna Design	Case	Nominal Scan Angle	Excitation Condition Over Feed Array	Figure Number
6 Scanning Beams	203	3° Azimuth	1 Principal Element	89
	203B	3° Azimuth	3 Principal Elements	96
	207	0° Boresight	1 Principal Element	91
	207B	~0° Boresight	3 Principal Elements	92
	209	-1.5° Elevation		93
	210	+1.5° Elevation		94
18 Fixed Beams	307	3° Azimuth		95
	308	0° Boresight		96
	309	+1.5° Elevation		97
	310	-1.5° Elevation		98

The feed array layout is depicted in Figure 4 for the multiple scanning beam design and in Figure 5 for the multiple fixed beam design. In all cases, a low sidelobe beam is formed by using a 19 element feed cluster comprised of a central element surrounded by two hexagonal rings of elements as evident in Figure 5.

An isometric view of the scanning beam feed assembly is depicted in Figure 6 for the scanning beam design. The beam combining network for the scanning beam design uses a total of 48 identical column 8-way power combiners to form the six simultaneous scanning beams. There are additionally a total of 6 row power combiners of two different designs; viz.; a 16-way combiner and a 17-way combiner. Details of the scanning beam feed array assembly are shown in Figure 7. Also, details of the horn radiating element and MMIC module assembly (which along with the combiner networks comprise the feed array) are presented in Figure 8.

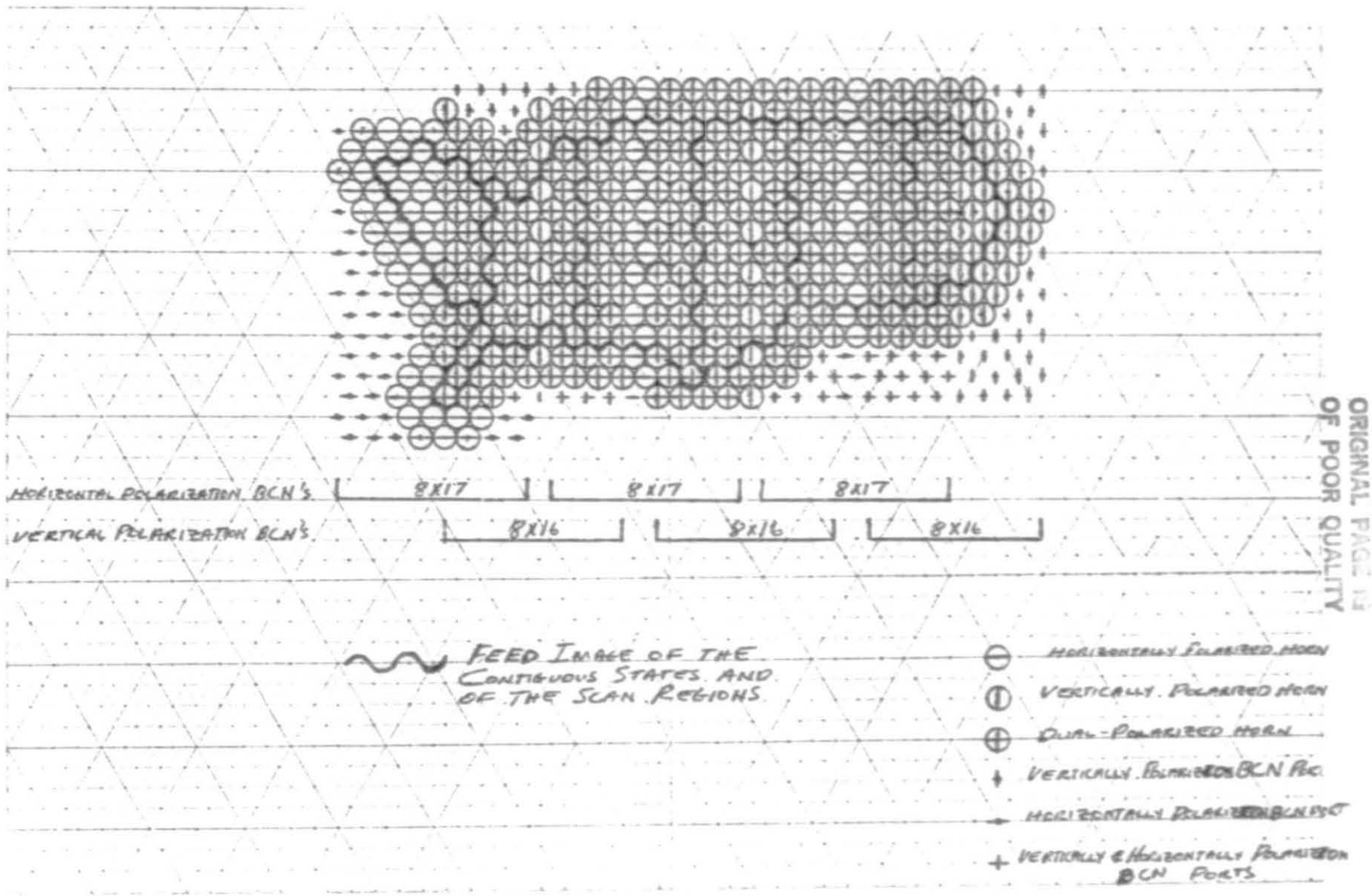

Figure 4. Feed Array Layout Geometry for the Multiple Scanning-Beam Antenna

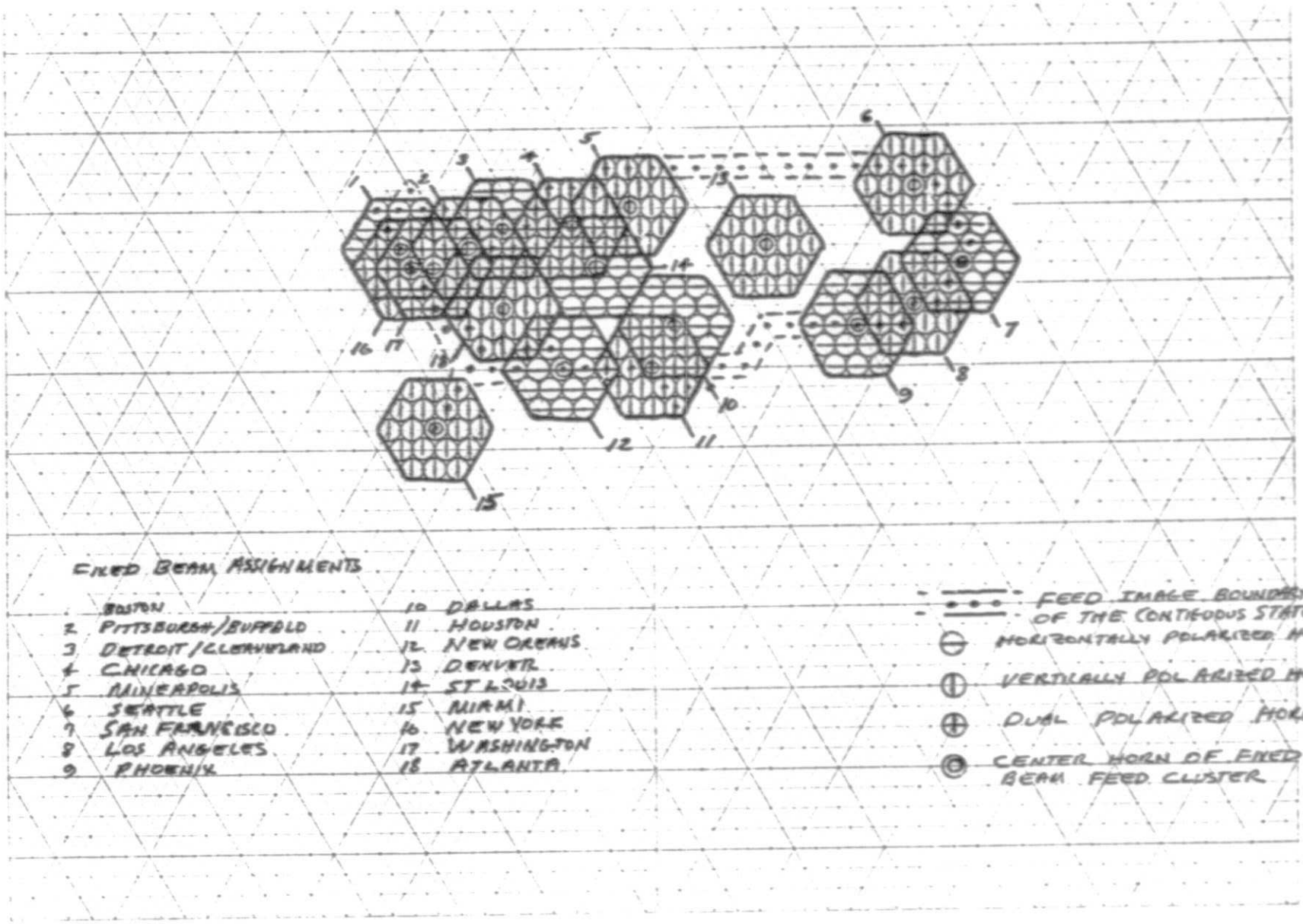

Figure 5. Feed Array Layout Geometry for the Multiple Fixed-Beam Antenna

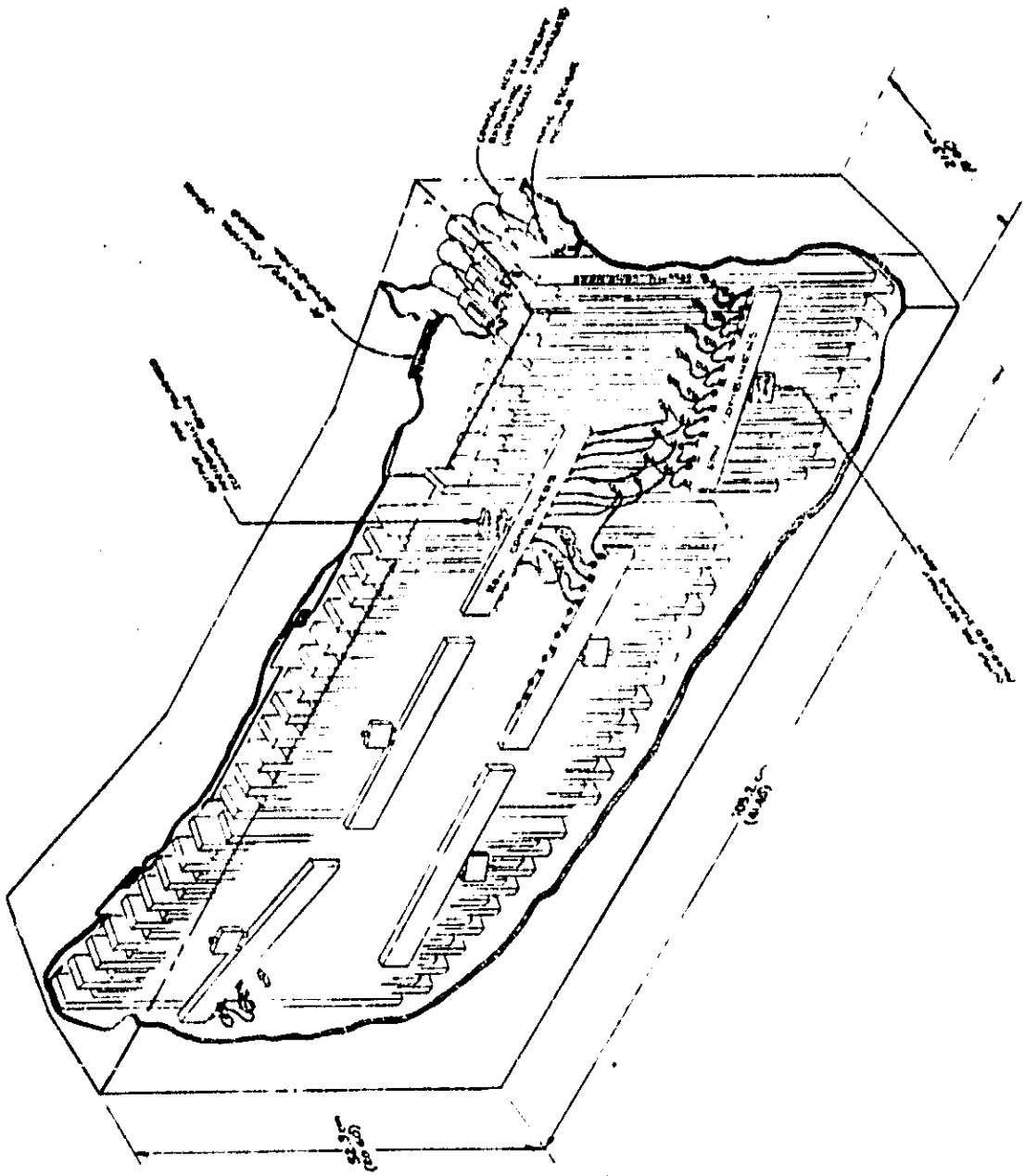

Figure 6. Isometric View of the Multiple Scanning Beam Feed Assembly

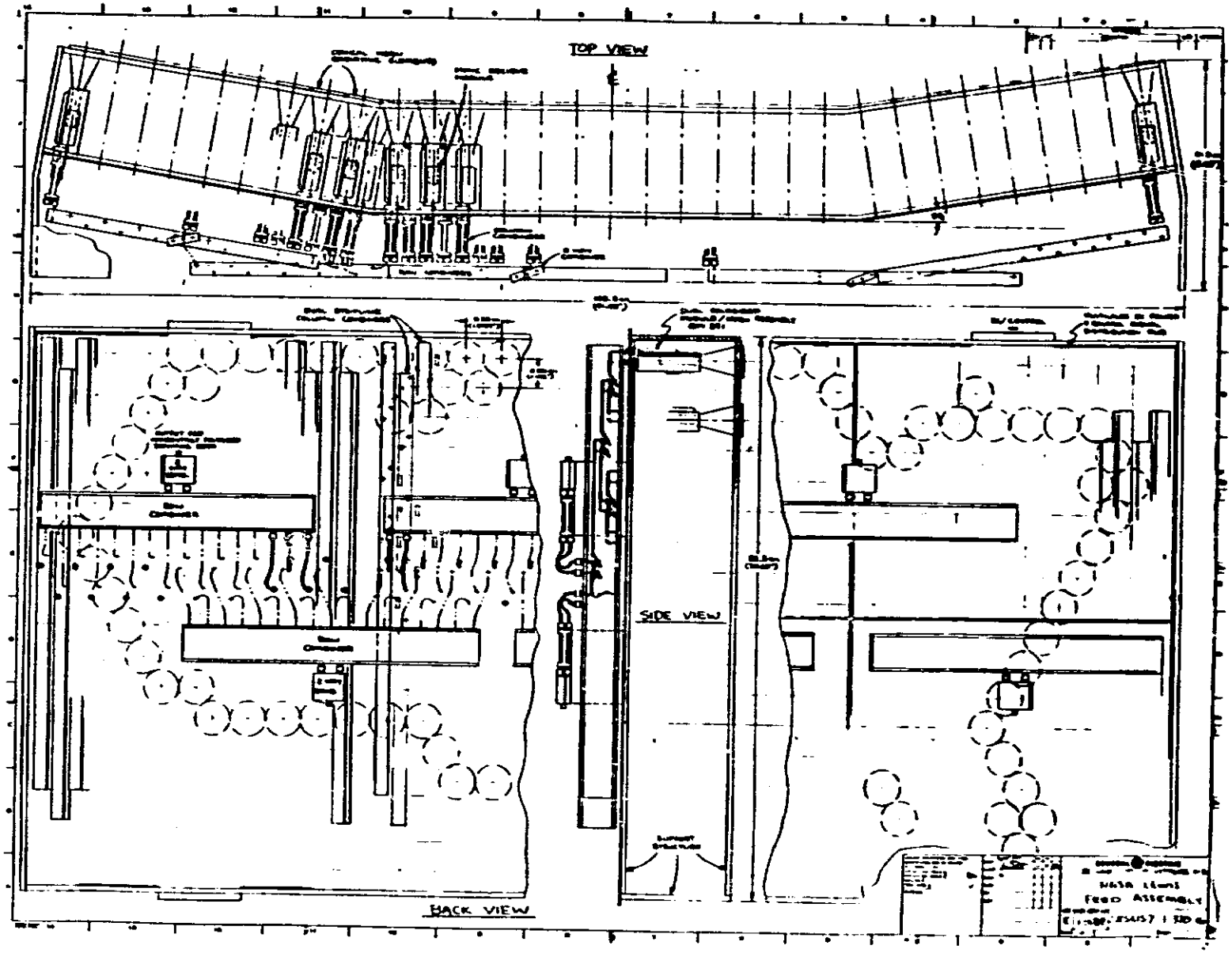

Figure 7. Feed Array Assembly Details for the Simultaneous Scanning Beam

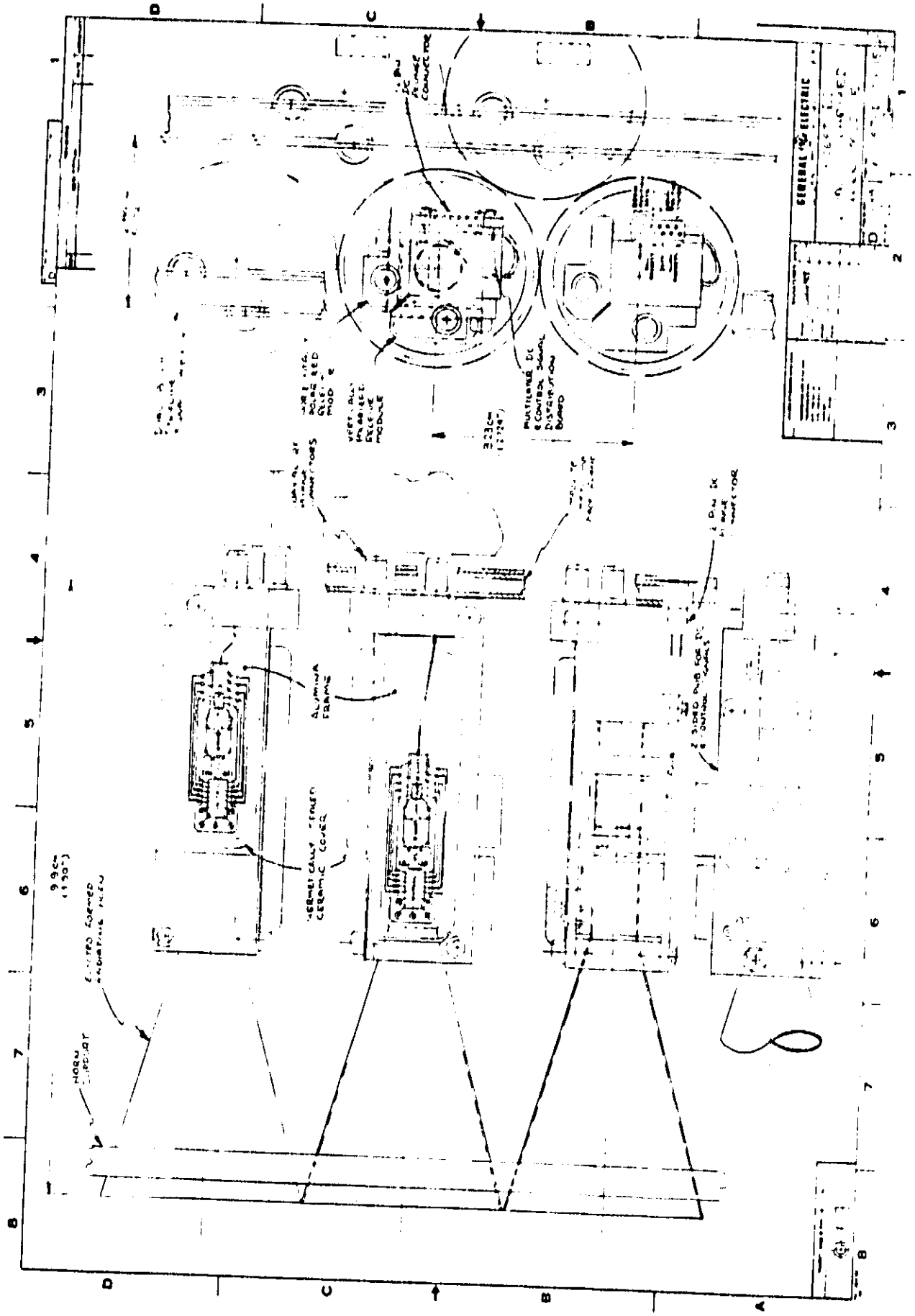

Figure 8. Horn/Module Detail

The feed array assembly for the simultaneous fixed beams design is similar to the simultaneous scanning beam design except that fewer elements are needed for the fixed beam design and the beam combining networks for each of the 18 fixed beams is of a different design to optimize the C/I performance of each beam in its assigned beam pointing direction.

The simultaneous fixed beam reflector system is larger than the simultaneous scanning beam system to meet the greater gain and C/I performance goals for the fixed beam as set forth in the statement of work. The sidelobe suppression for the fixed beam design using the larger reflector system is sufficient to meet the C/I goal without frequency diversity even for the worst case beam assignment (which exists in the Boston-New York-Washington corridor). However, the advantages of the larger reflector for the fixed beam needs to be weighed against the advantages of an integrated scanning beam/fixed beam system. The lower noise figure of the fixed beam receiver, the greater antenna gain of earth stations for fixed beam users, and the possibility of frequency diversity in the Washington-Boston corridor suggest that the fixed reflector can be reduced to the same size as the scanning beam reflector to achieve an integrated fixed beam-scanning beam system while meeting system performance requirements.

These recommended configurations resulted from detailed design studies following a preliminary design study during which a tentative design point was established. The detailed design studies resulted in the following design changes.

- An increase in the F/D of the primary reflector from 1.2 to 1.32 for the fixed beam design and 1.4 for the scanning beam design
- A decrease in secondary reflector diameter from 3.75 ft to 3.0 ft
- An increase in magnification from 2.0 to 2.1
- A reduction in feed element spacing from 0.123 ft to 0.106 ft
- The use of a circular horn radiating element rather than a printed circuit yagi
- A reduction in the number of radiating elements (578 yagis compared to 391 horns)
- A cylindrical rather than a planar feed array (19° total curvature across the array)

The changes were generally made to improve the gain and C/I performance of the receiver. However, the selection of the circular horn radiating element over the yagi was made predominantly on the superior polarization purity of the horn vis a vis the yagi in the mutual coupling environment.

2.2 PRELIMINARY DESIGN STUDIES OVERVIEW

This section narrowly reports on the Preliminary Design Study results. It does not reflect subsequent modifications from the detailed design studies. These modifications were generally minor and were already noted in the preceding section. However, one of the more significant changes was in the feed array, from 578 printed circuit yagis to 391 circular waveguide horns.

2.2.1 Initial Design Points

The configurations and design parameters for the initial design points of the four antenna systems are summarized in Tables 5 through 7. Table 5 reports the initial design point of a focal plane Cassegrain antenna considered for both the multiple scanning beam and the multiple fixed beam systems. Table 6 reports the initial design point for a focal plane single reflector and Table 7 reports the initial design point for an aperture-image plane Gregorian antenna, both of these latter two designs for the multiple scanning beam system. These initial designs were selected to provide a wide range of design options to the design trade-off studies encompassing the major design options; i.e., dual-reflector versus single reflector and focal plane array versus aperture-image plane array.

TABLE 5. FOCAL PLANE CASSEGRAIN CONFIGURATION BASELINE

- M = 2
- Diameter of Main Reflector = 250 λ .
- F/D = 1.2.
- Diameter of Subreflector = 110 λ .
- Subreflector focal length = 80 λ .
- Diameter of Array = 81.4 λ .
- 578 Elements (19 active/beam): 6 Simultaneous Scanning Beams.
  342 Elements (19/beam): 18 Simultaneous Fixed Beams.
- Element Spacing = 3.6 λ .
- Beamsteering: Amplitude and Phase (No Blockage). (Scanning Beam)
- Center Offset = 250 λ .
- Overall Length = 270 λ .

TABLE 6. FOCAL PLANE SINGLE REFLECTOR CONFIGURATION BASELINE

- Diameter of Main Reflector = 250 λ .
- F/D = 2.4.
- Diameter of Array = 40.6 λ .
- 578 Elements (19 active).
- Element Spacing = 1.7 λ .
- Beamsteering: Amplitude and Phase (No Blockage).
- Center Offset = 166 λ .
- Overall Length = 600 λ .

TABLE 7. APERTURE PLANE IMAGE GREGORIAN CONFIGURATION BASELINE

- M = 6.
- Diameter of Main Reflector = 271 λ .
- F/D = 1.
- Diameter of Subreflector = 93 λ .
- Diameter of Array = 45 λ (20 ring circular hex).
- 1039 Elements.
- Element Spacing = 1.33 λ .
- Amplitude Taper = Quasi-static.
- Beamsteering - Phase Control.
- Overall Length = 296 λ .

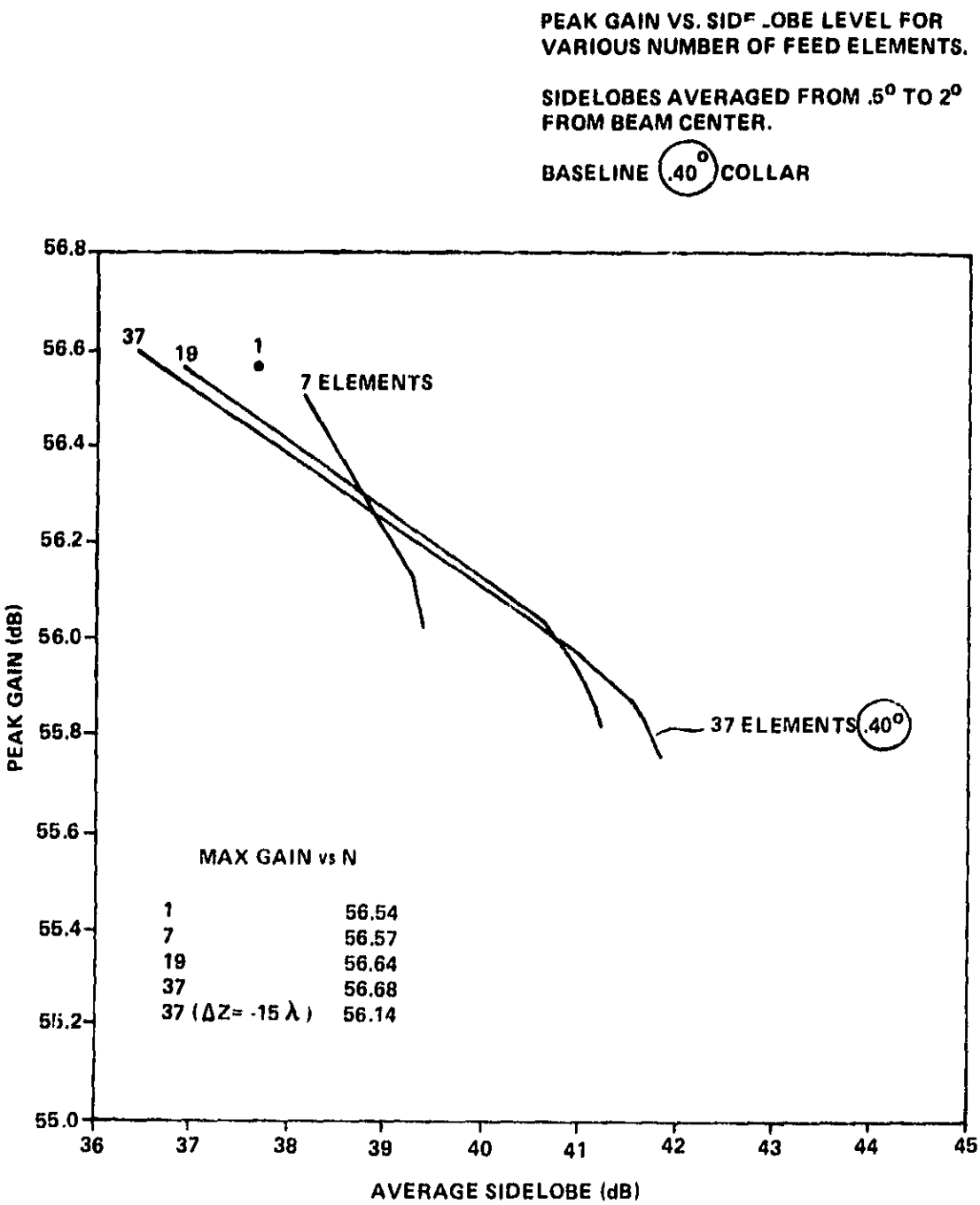

Figure 9. 0° Scan

2.2.2 Parametric Design Studies

The design parameters of the three different antenna configurations were varied about their initial design points, and the results of these design changes on performance evaluated. A summary of the scope of the design trade-off studies for the Cassegrain configuration is reported in Table 8. However, it is not to be implied that the design trade-off matrix associated with Table 8 was completely filled. Not all parameters listed are free; i.e., a change in main reflector diameter results in an implied change in F/D ratio, in magnification factor, and in unblocked scan capability. In all cases, unblocked scan of CONUS was a design constraint. Performance evaluations were principally peak antenna gain, pattern beamwidth, sidelobe level (peak and average over the sidelobe control region), and cross-polarization gain.

TABLE 8. PARAMETER TRADE OVERVIEW - FOCAL PLANE ARRAY

INDEPENDENT VARIABLES		AS REQUIRED
Aperture Diameter	150 λ - 400 λ	Offset
F/D	.6 - 2.4	Subreflector Diameter
Effective F/D	1.2 - 2.4	Subreflector Focal Length
Magnification	1.2 - 3.	Subreflector Axis Tilt
Feed Element Spacing	1.0 λ - 3.6 λ	
Number of Elements	1 - 61	
Choice of Element Set		
Element Gain	3 dB - 30 dB	
Feed Array Defocus	0 - .04F	
Scan Angle	0°, 3°	
DEPENDENT VARIABLES		
Gain		
Beamwidth		
Average Sidelobe Level		
Peak Sidelobe Level		
Peak Cross-Polarization		

Figure 9 reports typical design trade-off data obtained from studies of the Cassegrain configuration. The performance data is for an unscanned antenna. Each curve in Figure 9 depicts the gain-sidelobe tradeoff for a particular design through optimal control of the feed array excitation (obtained by a reiterative application of the maximum likelihood optimization. Refer to Appendix A). The performance curves are parametric in the number of feed array elements (1, 7, 19 and 37) and in the inner radius of the sidelobe control region (0.36°, 0.40°, 0.44°). Also shown is the performance curve for the case of the feed array displaced off-focus by 15

wavelengths, and the maximum available gain for each case is also reported. For example, a feed array of 19 elements allows a -40 dB average sidelobe level (over the control region) to be obtained with only a 0.5 dB reduction in gain relative to the maximum available gain from that feed array; i.e., 56.1 versus 56.6 dB. Figure 10 presents similar results for 2.8° of electronic scan. To maintain the 40 dB sidelobe level, the scan loss is only 0.4 dB, i.e. 55.7 dB at 2.8° scan, compared to 56.1 dB at 0° scan.

Figures 11 and 12 report some design trade-off study results from the single reflector configuration. Figure 11 shows the gain-sidelobe trades available from a single reflector using 19 feed array elements, parametric in element spacing. When element spacing was changed, element gain was also changed accordingly to keep the aperture utilization of the feed array constant. Figure 12 reports the effect of feed array defocus on maximum available gain and on sidelobe level attainable at 54.0 dB of gain for a single reflector antenna. The array excitation was re-optimized for each defocussed position of the feed array. The curves are parametric in the number of feed array elements (19 and 37).

These curves provide a glimpse of the extensive design-performance trade-off data that was generated during the course of the design trade studies. The results of these studies will be summarized in greater detail in a later section of this report.

2.2.3 Beam Combining Network (BCN)

Implementation of the BCN at both RF and IF has been evaluated. The basic assumptions that were made to perform the evaluations are reported in Figures 13 and 14. These assumptions are consistent with the over-all module specifications established by NASA/Lewis as they appeared in the 30 GHz/MMIC module development program work statement; and represent an optimized partitioning of module performance by General Electric. These assumptions were used in lieu of any results from the NASA 30 GHz MMIC module development program and will be revised as necessary as soon as such information becomes available.

Figures 15, 16 and 17 summarize the results of these BCN evaluations for the Gregorian, Cassegrain, and single reflector configurations respectively. The BCN architecture is illustrated and the resultant noise-figure, net gain, and DC power consumption are reported. The best noise-figure, 4.2 dB, is realized with the Cassegrain system with the BCNs at IF. The DC power requirements of the Gregorian system (and as will be reported later, the weight) is excessive (in excess of 360W for 6 scanning beams). The total DC power requirements for the Cassegrain system are only 50 watts for 6 scanning beams. The net-gain reported is not a critical performance measure and the reported differences not significant (since net gain can readily be equalized with IF amplifiers without significant penalty).

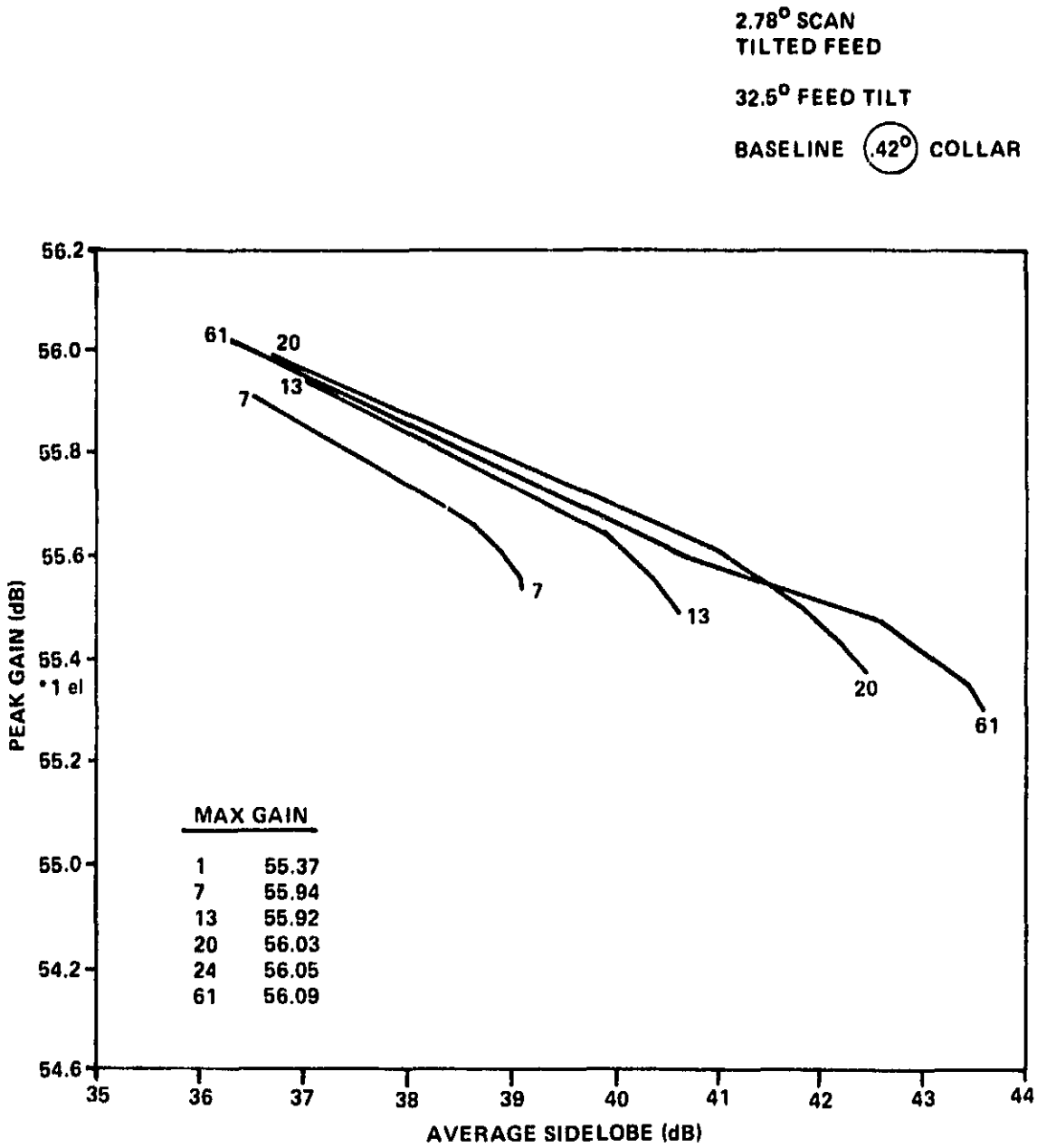

Figure 10. Gain vs Average Sidelobe Level for Various Number of Feed Elements (Focal Plane Cassegrain)

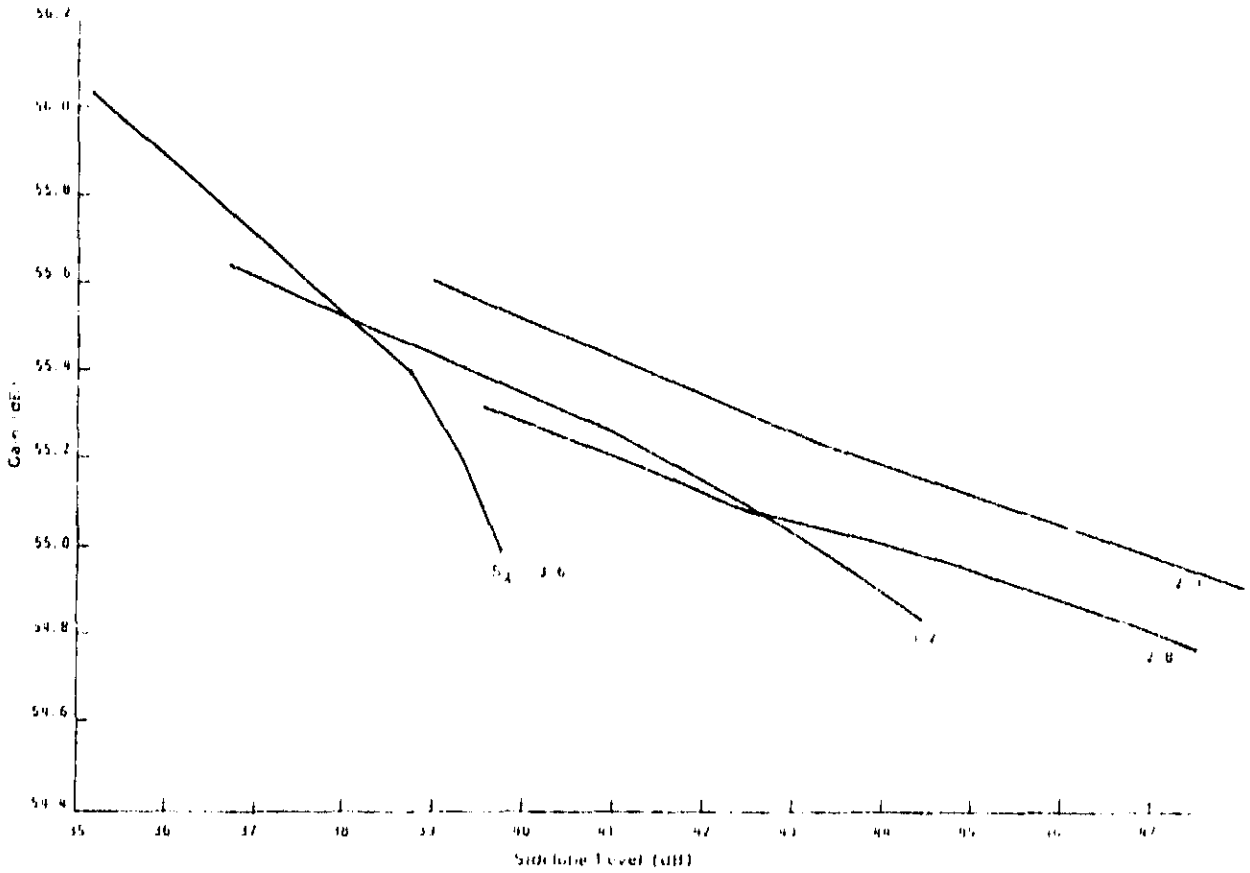

Figure 11. 0° Scan Single Ref, F/D = 2.4 Element Spacing Studies

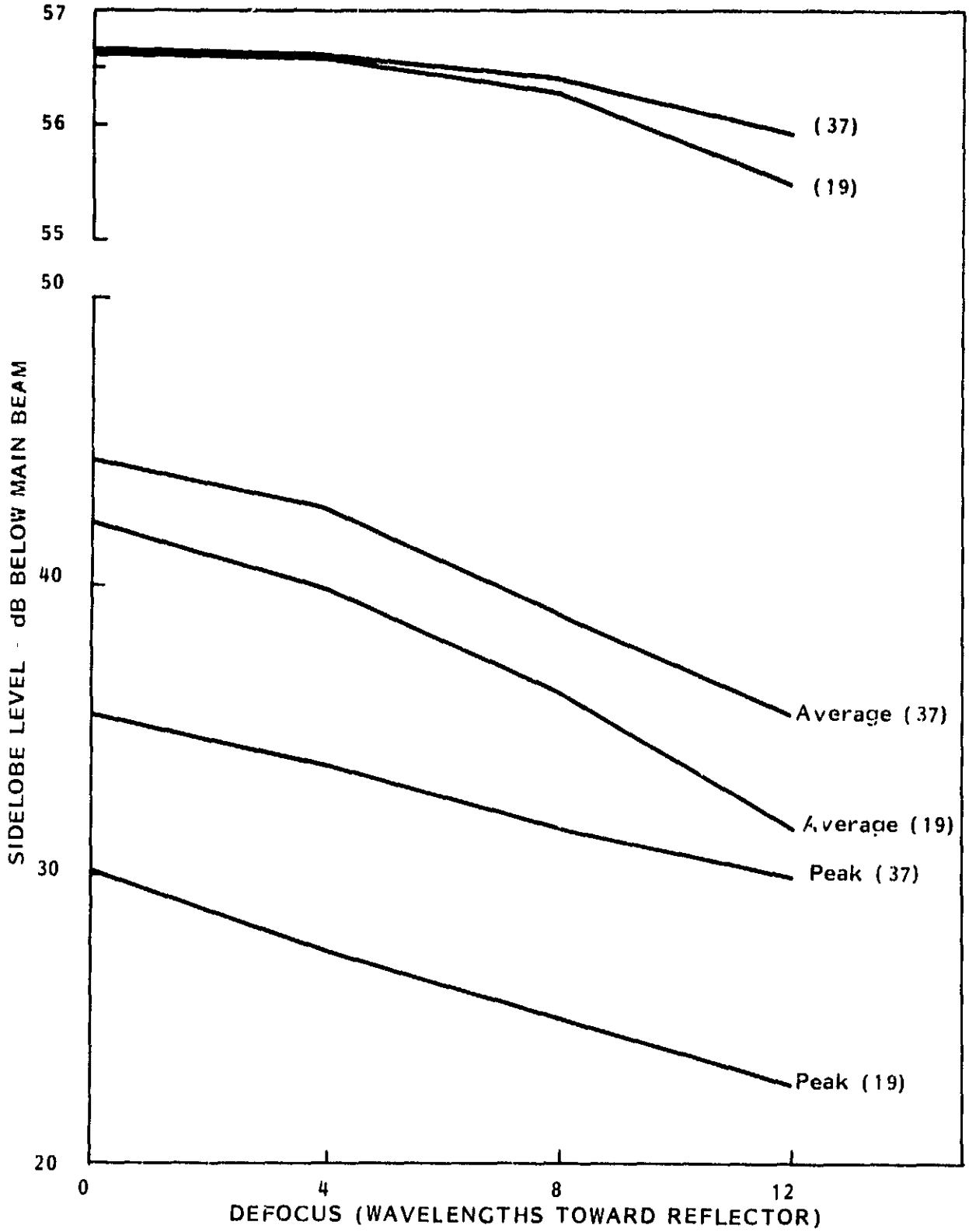

Figure 12. Element Spacing 1.7λ, n = 7 Single Reflector F/D = 1.2

LOW NOISE AMPLIFIER

Gain = 7 dB/Stage
Noise Figure = 3.5 dB/Stage
DC Power Consumption = 15 mW/Stage

ACTIVE MIXER

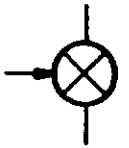

Conversion Loss = 0 dB
Noise Figure = 6.5 dB
DC Power Consumption = 80 mW

VARIABLE GAIN AMPLIFIER

Gain = -10 to +3 dB/Stage
Noise Figure = 10 to 4.36 dB/Stage
DC Power Consumption = 40 mW/Stage

LOCAL OSCILLATOR/BUFFER

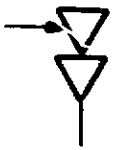

DC Power Consumption = 45 mW

5 BIT PHASE SHIFTER

Insertion Loss = 8 dB
Noise Figure = 8 dB
DC Power Consumption = 10 mW

I.F. AMPLIFIER

Gain = 7 dB/Stage
Noise Figure = 3 dB/Stage
DC Power Consumption = 15 mW/Stage

Figure 13. MMIC Performance Used for Noise Figure Calculations

SIGNAL COMBINERS (SCANNING BEAMS)

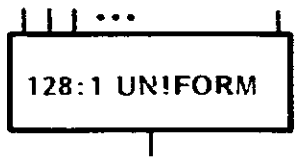

7 Levels
Insertion Loss = 4 dB

SIGNAL COMBINERS (FIXED BEAMS)

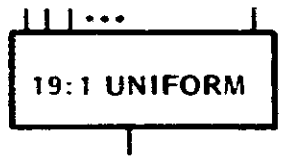

4 Levels
Insertion Loss = 2.6 dB

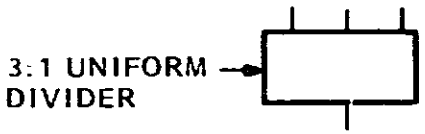

1 Level
Insertion Loss = 0.6 dB

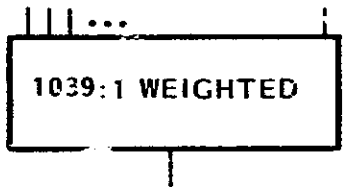

10 Levels
Insertion Loss = 6 dB

DIGITAL CONTROLLER

DC Power Consumption = 125 mW/Variable Gain Stage
12.5 mW/Phase Shifter

VOLTAGE LEVEL SET

DC Power Consumption = 50 mW

Figure 14. MMIC Performance Used for Noise Figure Calculations (Con't)

SIGNAL COMBINATION AT I.F.

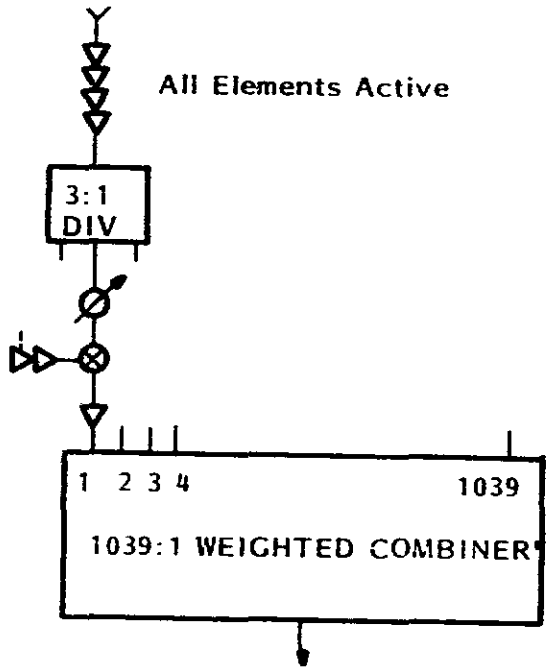

ONE SCANNING BEAM

Net Noise Figure - 4.40 dB
(No Coherent Noise)

Net Noise Figure - 20.06 dB
(All Mixer Noise Coherent)

Net Gain - 15.63 dB

Total DC Power Consumption 241.57 Watts (Per Beam)

SIGNAL COMBINATION AT R.F.

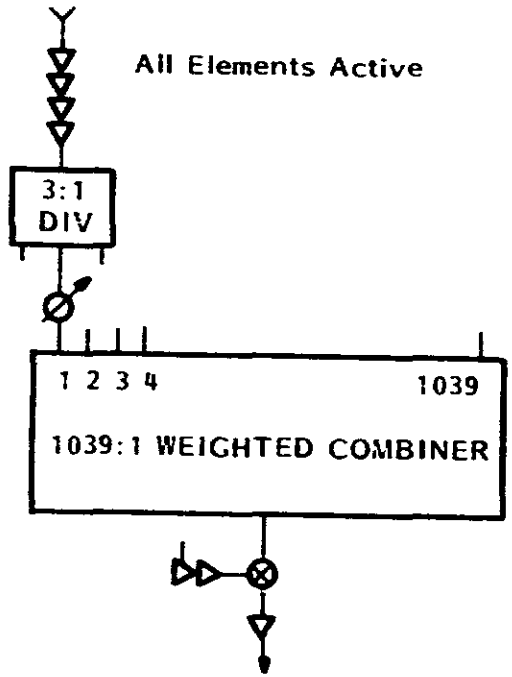

ONE SCANNING BEAM

Net Noise Figure - 5.18 dB

Net Gain 15.63 dB

Total DC Power Consumption 61.57 Watts (Per Beam)

Figure 15. Beam Combining Network Architecture - Performance Comparison Dual Reflector Gregorian Configuration

SIGNAL COMBINATION AT I.F.

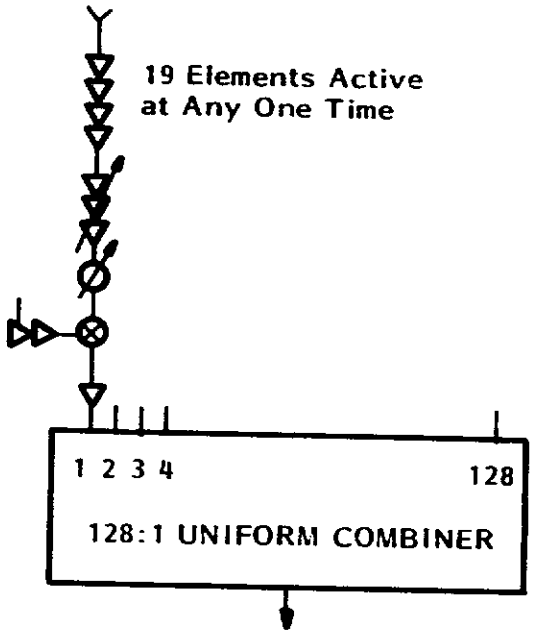

Net Noise Figure = 4.20 dB
(No Coherent Noise)

Net Noise Figure = 4.32 dB
(All Mixer Noise Coherent)

Net Gain = 15.53 dB

Total DC Power Consumption = 10.42 Watts (Per Beam)

SIGNAL COMBINATION AT R.F.

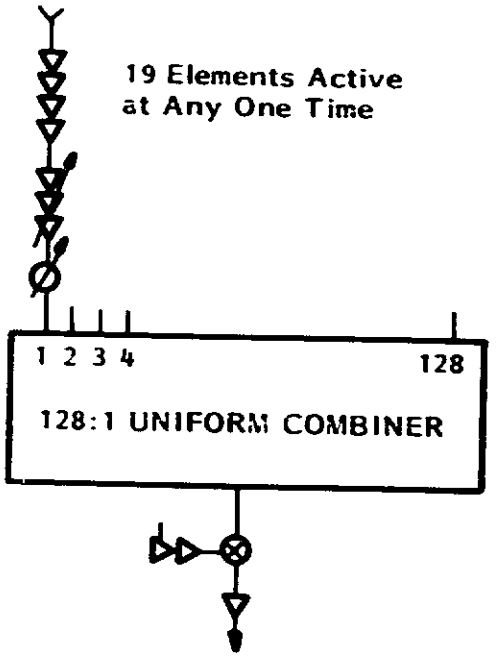

Net Noise Figure = 5.28 dB

Net Gain = 15.53 dB

Total DC Power Consumption = 7.90 Watts (Per Beam)

Figure 16. Beam Combining Network Architecture - Performance Comparison Dual Reflector Cassegrain Configuration, F/D = 0.6, Magnification Factor = 2

SIGNAL COMBINATION AT I.F.

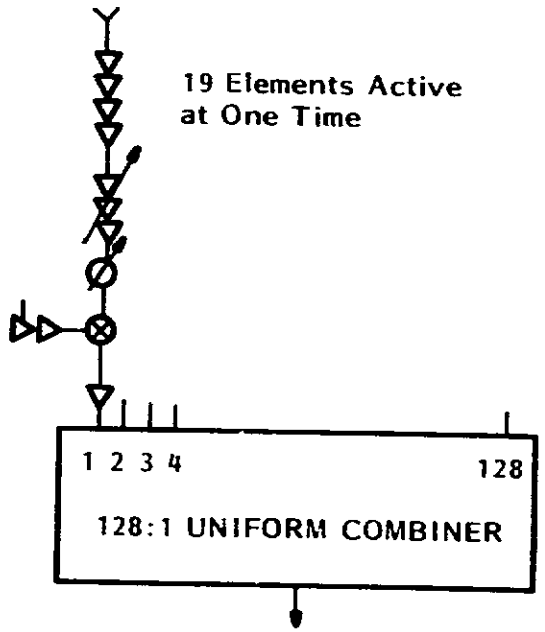

Net Noise Figure = 4.41 dB
(No Coherent Noise)

Net Nosie Figure = 4.79 dB
(All Mixer Noise Coherent)

Net Gain = 11.65 dB

Total DC Power Consumption = 10.42 Watts (Per Beam)

SIGNAL COMBINATION AT R.F.

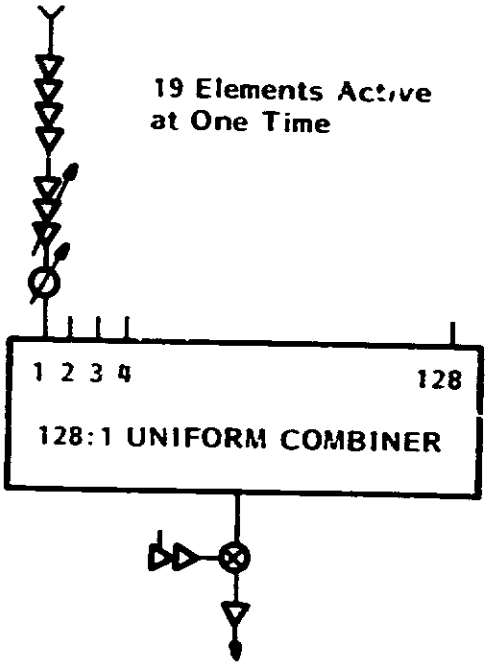

Net Noise Figure = 6.59 dB

Net Gain = 11.65 dB

Total DC Power Consumption = 7.90 Watts (Per Beam)

Figure 17. Beam Combining Network Architecture - Performance Comparison
Single Reflector Configuration, F/D = 1.2

Table 9 summarizes the principal design features of the BCN assembly. The plunge connectors for the plug-in modules have been developed for General Electric addressed to ECM phased array applications. Tables 10 and 11 summarize the performance of two types of integrated radiating elements. Performance evaluations were made for each design using the NEC (numerical electromagnetics code) computer analysis (method-of moments). Experimental verification was accomplished for the zig-zag element, and is underway for the yagi element. The zig-zag element was featured in the proposal, but the yagi design has been found to have superior performance over the operating bandwidth. A non-integrated radiating element, the multimode horn, has also been developed by General Electric for satellite communications systems. The waveguide to microstrip transitions necessary to use the multimode horn with a MMIC elemental receive module have also been developed. Figure 18 depicts an artist's conception of the feed array assembly using interleaved, orthogonally polarized integrated radiating elements.

2.2.4 Recommended Configuration

Table 12 summarizes the derived design/performance parameters of the three major antenna configurations. The principal disadvantages of the single reflector design is its greater axial length. The principal disadvantages of the Gregorian design is its larger weight (attributed primarily to the six parallel 1039:1 beamcombiner networks) and its greater DC power consumption (attributed to the large number of active modules required). The Cassegrain design emerges as a clear design choice. The principal "disadvantage" of the Cassegrain design is the requirement for variable gain amplifiers, but this requirement in fact represents an excellent match between hybrid antenna design requirements and MMIC capabilities afforded in a distributed receiver implementation.

The Cassegrain configuration is recommended both for the scanning beam and the fixed beam design. This recommendation is summarized in Table 13. The recommendation of the same configuration for both the scanning and the fixed beam systems is favorable for the eventual integration of the two systems into one antenna assembly. The rationale for the selection of the recommended configurations is summarized in Table 14.

TABLE 9. MMIC PHASED ARRAY BCN SUMMARY

- Plug-in Modules to Facilitate Assembly and Test.
- Interleaved, Linear Polarized Printed Radiating Elements, Compatible with MMIC Circuitry.
- DC and Logic Fed Through from Backside of Module.
- Each Submodule Packaged in a Separate Carrier for Easy Replacement.
- Special Molybdenum Submodule Carrier for Matched Thermal Expansion and Good Thermal Conductivity.

TABLE 10. 10-ELEMENT PRINTED YAGI RADIATING ELEMENT

- Realized on a Dielectric Substrate.
- Element Spacings and Lengths Provides Control over Directivity, Field Pattern, and Bandwidth.
- Easily Integrated with MMIC; Requires a Balun.
- Calculated Directivity = 12.0 dBi

  E-Plane HPBW = 42°

  H-Plane HPBW = 48°
- Gain Variation Over Band of Interest < 1 dB.

TABLE 11. 6-SECTION PRINTED ZIG-ZAG RADIATING ELEMENT

- Realized on a Dielectric Substrate.
- Section Length, Pitch Angle, and Ground Plane Spacing Provides Control Over Beam Directivity and Field Pattern.
- Easily Integrated with MMIC; Needs No Special Transitions.
- Calculated Directivity = 15.6 dBi.

  E-Plane HPBW = 36°

  H-Plane HPBW = 46°
- Gain Variation Over Band of Interest = 7.5 dB.

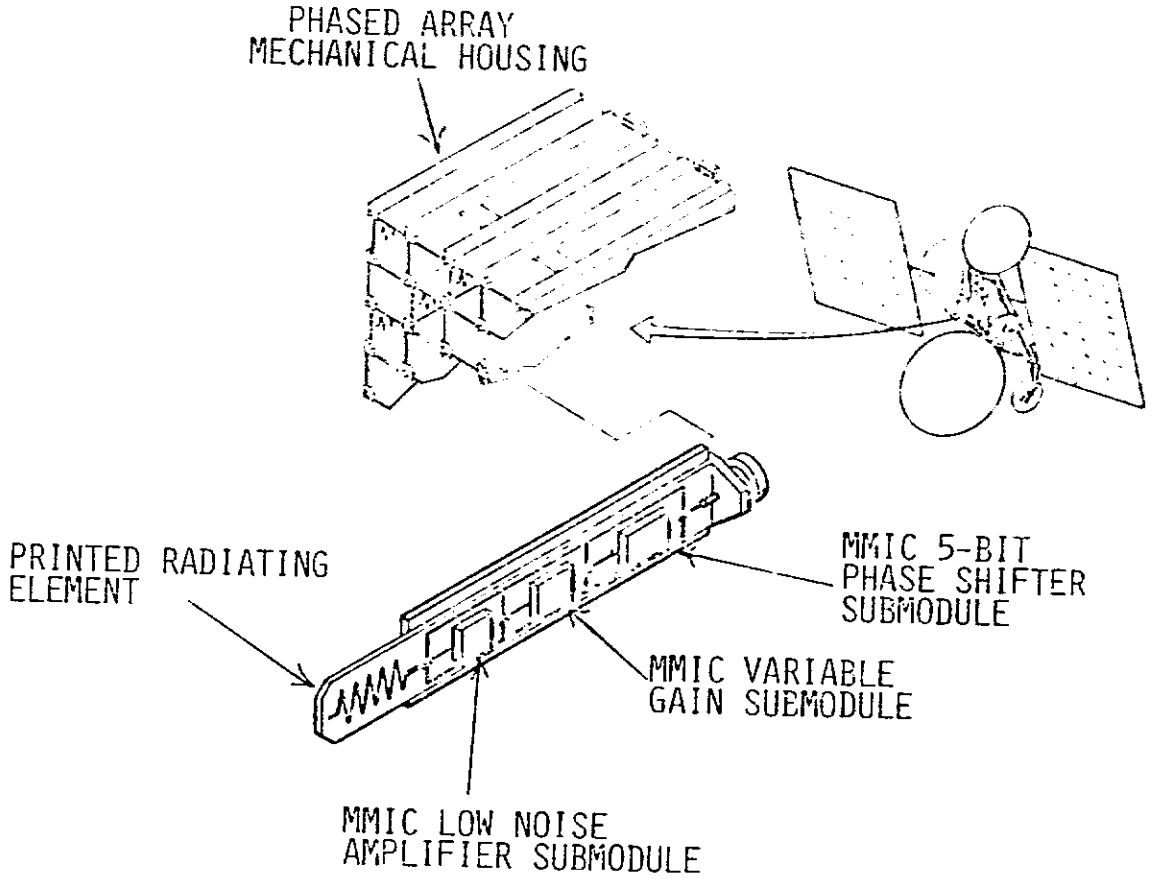

Figure 18. MMIC Phased Array Feed Concept

TABLE 12. ANTENNA CONFIGURATION SELECTION MULTIBEAM SCANNING ANTENNA COMPARISONS (PRELIMINARY DESIGN STUDIES)

	Gregorian	Cassegrain*	Single Reflector
F/D	1	1.2	2.4
Main Reflector Diameter	271 λ	250 λ	250 λ
Subreflector Diameter	93 λ	110 λ	N/AP
Feed Beam	45 λ	86 λ	76 λ
Overall Length	296 λ	270 λ	600 λ
Number of Elements	1039	578	578
Active Elements	1039	19	19
Magnification	6	2	N/AP
Gain [1]	0° : 55.7 3.5°: 54.5	0° : 56.1 3° : 55.7	0° : 55.2 3° : 54.8
Sidelobe [1,2] Average	0° : N/AV 3.5°: N/AV	0° : -40 dB 3° : -40 dB	0° : -40 dB 3° : -40 dB
Sidelobe [1] Peak	0° : -40 3.5°: TBD	0° : -32 dB 3° : -31 dB	0° : -28 3° : -27
Noise Figure	5.2 dB	5.3 dB	6.3 dB
BCN (RF Beamforming)	6× 1039:1	6× 100:1	6× 100:1
Total DC Power Consumption	6× 62 W	6× 8.0 W	6× 8.0 W
Rel. Feed Array Weight	10	1	1
Element Diameter	1.33 λ	3.6 λ	2.7 λ
Variable Gain Range	Trim Only	40 dB	40 dB

[1] Scan Angle: dB

[2] Averaged Over Annular Region of 0.5° to 2.0° Radius

* Compare with Table 3 for final design parameters of the recommended configurations as derived by the detailed design studies.

TABLE 13. RECOMMENDED ANTENNA CONFIGURATIONS DESCRIPTION

- Scanning Multiple Beam Antenna
  - Focal Plane Feed Aray with Cassegrain Optics
  - "Microstrip" Yagi Radiating Elements
  - RF Beamforming Network, Uniformly Weighted Power Combiner
  - LNA, Phase Shifter, Variable Gain Amplifier MMIC RF Modules
- Fixed Multiple Beam Antenna
  - Focal Plane Feed Array with Cassegrain Optics
  - "Microstrip" Yagi Radiating Elements*
  - RF Beamforming Network, Optimally Weighted Power Combiner
  - LNA, Phase and Gain Trim MMIC RF Modules

* Modified by the detailed design studies to be a circular waveguide horn for its superior polarization purity in an array environment.

TABLE 14. RECOMMENDED ANTENNA CONFIGURATIONS SELECTION RATIONALE

- Focal Plane Optics Requires Smaller Feed Array
  - Fewer Elements
  - Lighter Weight
  - Lower Loss
  - No RF Power Division at the Element
  - Lower N/F
  - Lower DC Power
  - Less Circuit Routing Conflicts
- Cassegrain Optics Provide Superior Performance
  - Higher Gain
  - Lower Sidelobes
  - Lower N/F
- Cassegrain Optics Results in Shorter Structure
- RF Combining Provides Less Complex LO Power Distribution Network
  - Lighter Weight
  - Less Circuit Routing Conflicts
- "Microstrip" Yagi is MMIC Compatible*
  - Minimal Transitions
  - Lightweight
  - Compact

* Modified by the detailed design studies to be a circular waveguide horn for its superior polarization purity in an array environment.

2.3 MAJOR DISADVANTAGES OF THE ALTERNATIVE ANTENNA CONFIGURATIONS

The recommended antenna configuration consists of an offset dual reflector using Cassegrain optics, a focal plane feed array, circular horn feed array elements, and RF beamforming. This design is superior for meeting the major design objectives of the 30 GHz communications satellite receive antenna; viz.,

• High Aperture Efficiency	:	56 dB Minimum Gain (Fixed Beams) 53 dB Minimum Gain (Scanning Beams)
• High C/I	:	30 dB Minimum Net
• Simultaneous Multiple Beam Operation	:	18 Fixed Beams 6 Scanning Beams
• Low Noise Figure	:	5 dB Nominal
• Short Dwell Time (Scanning Beams)	:	10-100 μ sec
• Satellite System Requirement	:	Shuttle Compatible Size Light Weight Low Power Drain High Reliability

The major disadvantages of the principal design alternatives are summarized in the following paragraphs.

2.3.1 Single Offset-Reflector

The principal disadvantage of the single, offset-reflector is its greater axial length. A large (effective) F/D is required to meet the high gain and high C/I (low sidelobes, low cross-polarization) objectives of the satellite communications antenna. A dual-reflector system achieves the required large effective F/D within a short axial dimension by (1) the F/D magnification available with the dual-reflector optics and (2) the folded optics inherent in a dual-reflector system. The large F/D requirement translates directly to axial length in a single reflector system.

2.3.2 Gregorian Reflector System

The principal alternative to a focal plane design (of which a single reflector or a Cassegrain reflector are representative) is an aperture image design (of which the Gregorian reflector system is representative). The major disadvantage of the aperture image designs is the larger number of active elements and the larger number of total elements required in the feed array. Basically, the primary aperture of the antenna system is imaged onto the feed array in an aperture imaging system. Consequently, all elements in

the feed array are active in an aperture imaging system and are used for beam shaping and beamsteering as in a conventional phased array. The larger number of active elements results in greater power dissipation. In contrast, a focal-plane array uses a relatively small number of active elements primarily for aberration correction, with the principle beamforming and beamsteering functions accomplished by the reflector system. Typically, the number of active elements in a Gregorian system is near 1000 compared to 19 per beam for a Cassegrain system (addressed to the present requirements). The small number of active elements/beam in the Cassegrain system also allows a sample serial beamsteering control within the 100 μs minimum beamdwell, whereas the large number of active elements in the Gregorian system requires a more complex parallel beamsteering control.

Not only is there a disparity in the number of active elements in the feed array, but also in the total number of elements. For typical designs addressed to the present application, the total number of feed array elements is 301 in the Cassegrain design compared to over 1000 in the Gregorian design. This larger number of elements in the feed array places the Gregorian system at a weight disadvantage considering the entire feed element module assembly and the beamforming network required.

2.3.3 IF Beamforming

The major disadvantage of an IF beamforming system is the weight and space penalties incurred through the implementation of the LO power distribution system. A second disadvantage of an IF beamformer applies to a Gregorian (or phased-array) system. Any coherent component of LO noise is increased by the number of elements in the feed (or array). Since the number of active elements is large in a Gregorian system compared to a Cassegrain system, the degradation in noise figure due to this effect is significantly greater in the Gregorian system. It is negligible in the worst case for the Cassegrain design, but totally unacceptable in the Gregorian system for the same worst case (viz., all added noise at the mixer being coherent LO noise)

2.3.4 Printed Circuit Yagi Feed Array Elements

Originally, printed circuit yagi radiating elements being microstrip compatible with the MMIC receive modules were considered for the feed array. However, the major disadvantage of these elements was the depolarizing effect by a cross-polarized neighbor on the elemental patterns. This effect is particularly serious in simultaneous multiple beam systems where the local phase and amplitude excitations are not "locally uniform". Consequently, the decision was made to use dual-polarized circular horn radiating elements of proven design.

3 DETAILED CONFIGURATION STUDY RESULTS

3.1 THE FOUR INITIAL DESIGN POINTS

The four initial design points were based on a technology assessment and consisted of three configurations for the simultaneous, multiple scanning beam system and one configuration for the simultaneous fixed beam system. Parametric design and performance trade-off studies were then performed centered on these initial design points to aid in the selection of the final design point.

The three initial design points for the scanning beam system are depicted in Figures 19, 20, and 21. These initial design points were selected because they spanned the major design options; viz., dual reflector versus single reflector and focal-plane feeds versus aperture image-plane feeds. Thus, Figure 19 and Figure 20 are focal plane systems. More specifically, Figure 19 is an offset dual-reflector Cassegrain implementation while Figure 20 is an offset single parabaloid implementation. Figure 21 is an aperture image design, specifically a Gregorian system.

Ideally, the focal plane systems focus an incident plane wave onto a spot at the feed array. The position of the focal spot changes with scan angle. Thus, ideally, beam scanning is accomplished with amplitude-only control of the feed array elements. In actual practice, both phase and amplitude control is required over a diffused focal spot to compensate for optical aberrations and to suppress side-lobes. Simultaneous multiple beam operation results in multiple focal "spots" across the composite feed array with those feed array elements within each "spot" are activate. Nineteen active elements with phase and amplitude weights are used to form each beam. A total of 578 elements were used for six simultaneous beams. The design parameters of the Cassegrain system for the initial design point in Figure 19 were

- Primary Reflector Diameter : 250 λ
- F/D of Primary Reflector : 1.2
- Offset of Primary Reflector : 250 λ
- Magnification of Cassegrain System : 2.0
- Diameter of Secondary Reflector : 110 λ
- Secondary Reflector Focal Separation : 80 λ
- Diameter of Feed Array : 81.4 λ
- Number of Feed Elements : 578 (19 Active/Beam)
- Overall Length : 270 λ

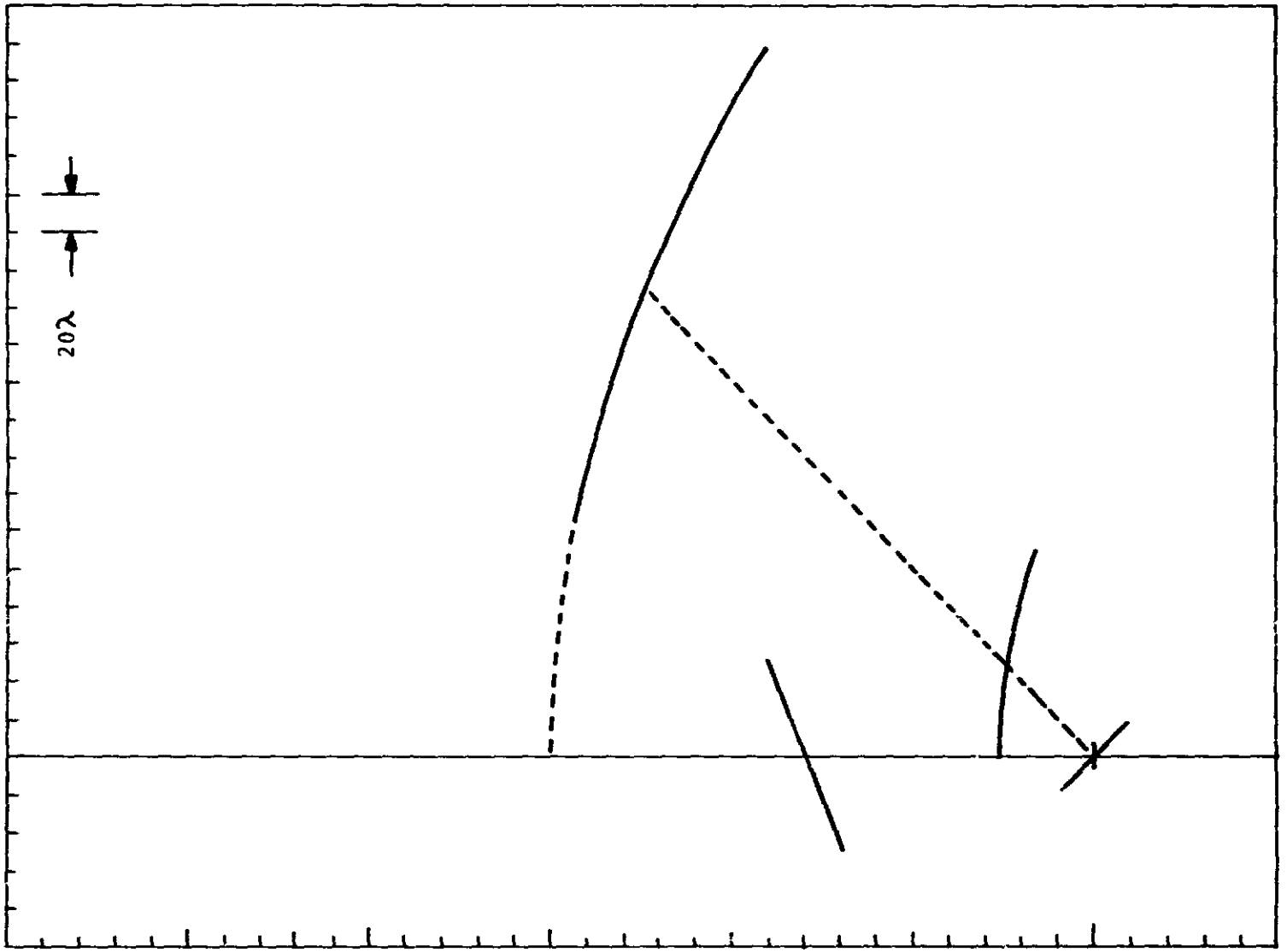

Figure 19. Initial Design-Point Geometry for Scanning Beam Antenna (Cassegrain Reflector System)

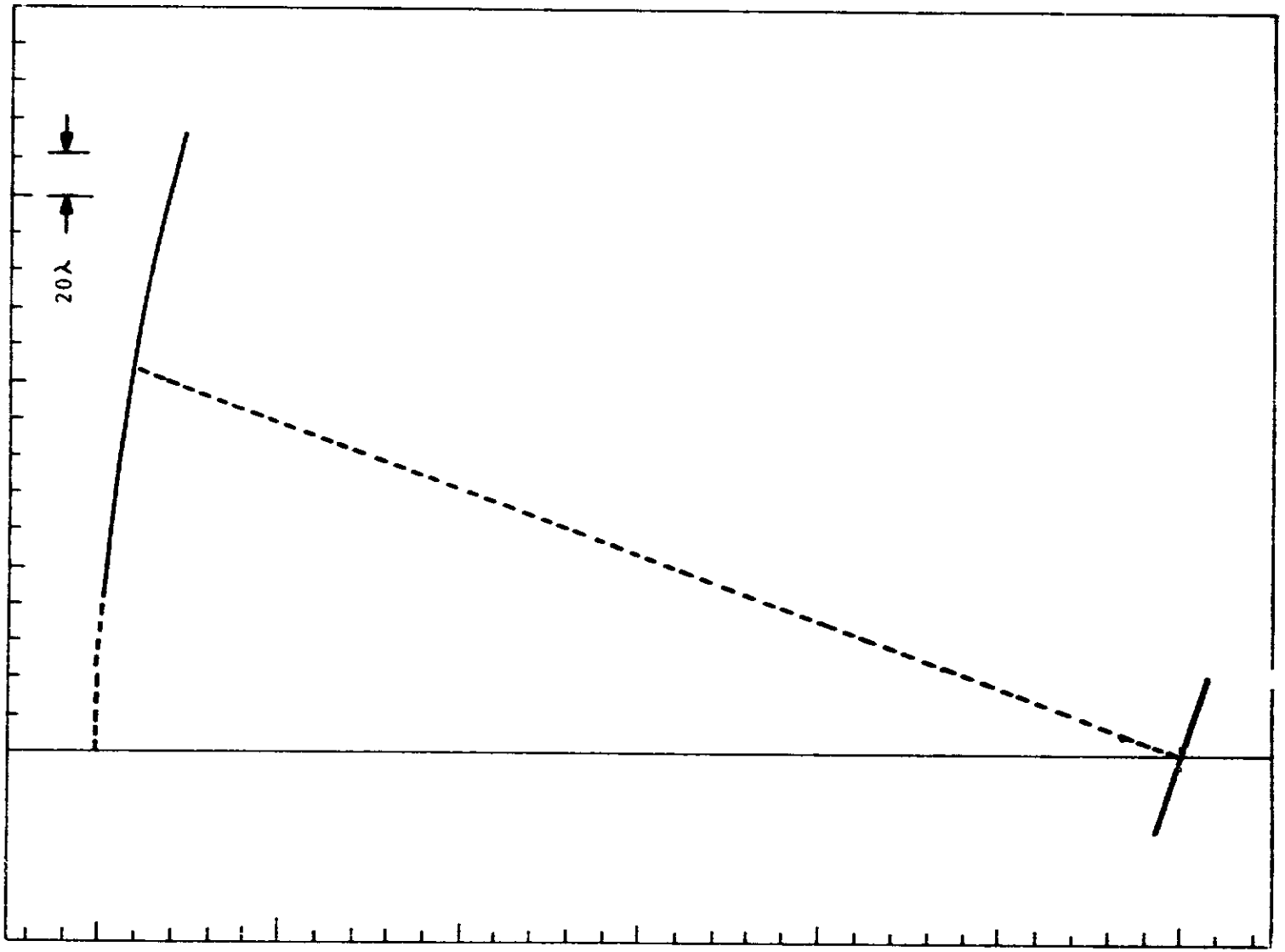

Figure 20. Initial Design-Point Geometry for Scanning Beam Antenna (Single Reflector System)

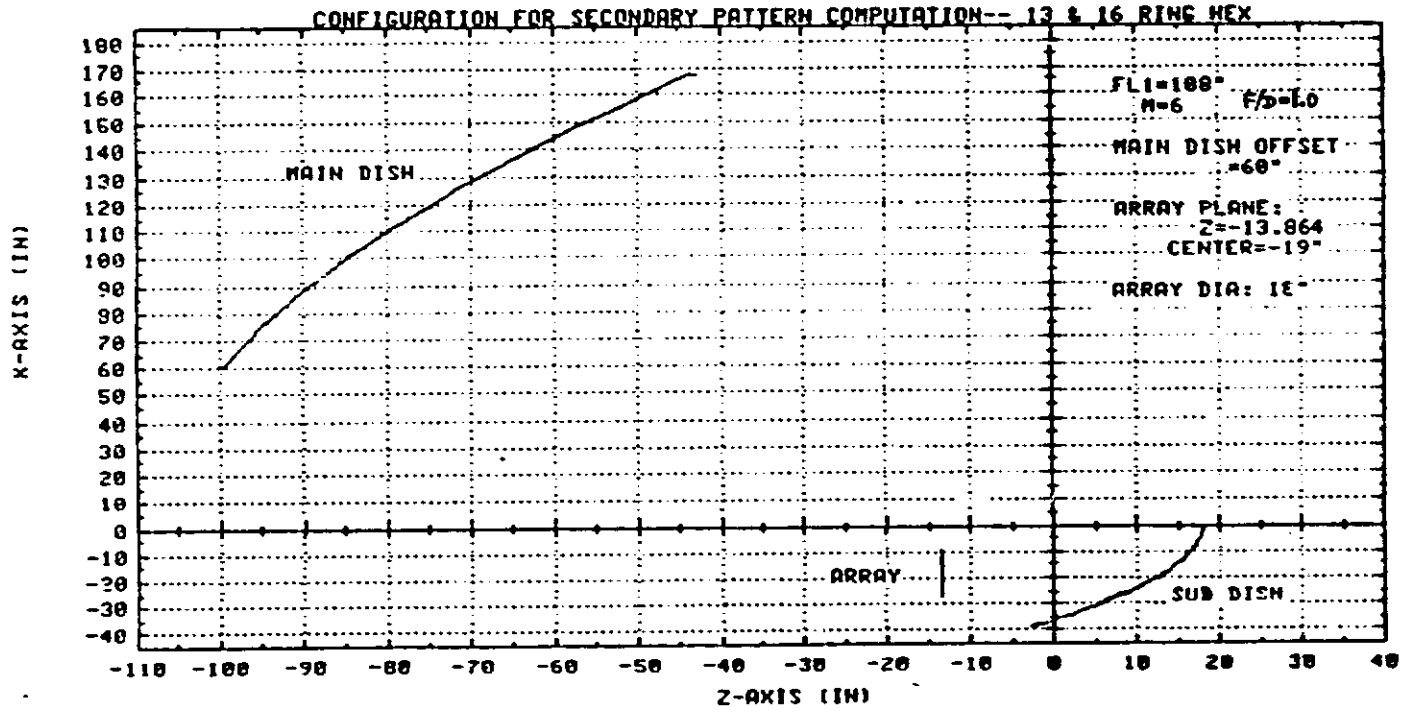

Figure 21. Initial Design-Point Geometry for Scanning Beam Antenna (Gregorian Reflector Optics)

The Design parameters of the single paraboloid reflector for the initial design points in Figure 20 were.

- Diameter : 250 λ
- F/D : 2.4
- Offset : 209 λ
- Diameter of Feed Array : 40.6 λ
- Number of Feed Elements : 578 (19 Active/Beam)
- Overall Length : 600 λ

In contrast to the focal plane systems, ideally an aperture image plane system transforms an incident plane wave to a scaled replica of the incident plane wave over the feed array. The phase slope over the plane wave changes with scan angle. Thus, ideally, beam scanning is accomplished with phase-only control of the feed array elements. In practical systems, both amplitude and phase control are required to maintain low sidelobe performance over wide scan angles. However, the more serious departure from phase-only control occurs with simultaneous, multiple beam operation. Since the same elements are involved for all beams, the complex superposition of multiple plane waves across the feed array results in an amplitude variation just as extreme for an aperture-image system as for a focal plane image system. For the Gregorian implementation depicted in Figure 21, the feed array consisted of 1039 elements of each polarization, all active. The design parameters for the Gregorian system initial design point were

- Diameter of the Primary Reflection : 271 λ
- F/D of the Primary Reflectors : 1
- Magnification of the Gregorian System : 6
- Diameter of the Secondary Reflectors : 93 λ
- Diameter of the Feed Array : 45 λ
- Number of Feed Elements (Dual Polarized) : 1039
- Overall Length : 296 λ

The initial design point for the multiple fixed beam system was selected to be an offset Cassegrain similar to Figure 19. The design parameters for the initial design point for the 18 fixed beam initial design point were the same as for the 6 scanning beam design except for the feed array which consisted of 342 elements rather than 578 elements (still 19 active per beam).

3.2 RESULTS OF PARAMETRIC DESIGN STUDIES

The range of parameters considered in the tradeoff study is summarized in Table 15.

TABLE 15. TRADEOFF STUDY OVERVIEW

INDEPENDENT VARIABLES	
Aperture Diameter	150-400 λ
F/D	.6-2.4
Effective F/D	1.2-2.4
Magnification	1.2-3.
Feed Element Spacing	1.0 λ 3.6 λ
Number of Elements/Beam	1-61
Choice of Elements/Beam	
Element Gain	3 dB-30 dB
Feed Array Defocus	0-.04F
Scan Angle	0°-3°

DEPENDENT VARIABLES

Maximum Gain
Gain
Beamwidth
Average Sidelobe Energy in a Region
Peak Sidelobe
Peak Cross-Polarization Sidelobe

AS REQUIRED:

Offset
Subreflector Diameter
Subreflector Axis Tilt
Subreflector Focal Length

COMPUTER PROGRAM DESCRIPTION

The techniques used in the computer programs for calculation of the far field antenna patterns are described below.

MAIN REFLECTOR

- Uses Jacobi-Bessel series expansion technique for offset paraboloid.*
- Efficient method of computing large number of far field points for a large reflector.
- First obtains a set of coefficients.
- Then uses coefficients to compute complex vector far field.

SUBREFLECTOR (IF USED)

- Computes scattered complex vector far field.
- Uses only geometric optical formulation,** including divergence factorresulting from surface curvature.

FEED

- $\cos^n(\theta)$ pattern assumed.
- No cross-polarization component from the feed.
- Equal E-plane and H-plane patterns.
- n chosen based on element spacing.

---

* Rahmat-Samii, Galindo-Israel, "Shaped Reflector Antenna Analysis Using the Jacobi-Bessel Series," IEEE Trans. Antennas & Propagation, Vol. AP-28, p. 425-435, July 1980.

** Lee, Cramer, Woo, Rahmat-Samii, "Diffraction by an Arbitrary Subreflector: GTD Solution," IEEE Trans. Antennas & Propagation, Vol. AP-27, p. 305-316, May 1979.

COMPUTATIONAL PROCEDURE

The following steps describe the sequence of program usage for evaluation of array fed reflector performance, exploiting the efficiency of the Jacobi-Bessel expansion technique.

1. Define geometry of optics and feed.

2. Run Jacobi-Bessel program to obtain coefficients and complex vector far field data over a $\pm$ 2° square region, Δ = 0.1°, for each element.

3. Rerun Jacobi-Bessel program, using coefficients computed in step 2, to obtain complex vector far field data at a small number of selected points, specifically to define a circular collar around the desired beam direction to control the skirts of the main beam, and principal cuts through the desired beam center direction.

4. Optimize as desired with a selected set of elements, using the sidelobe suppression technique described in Appendix A.

5. For a new beam direction for the same set of elements, repeat steps 3 and 4.

TRADEOFF STUDY GROUND RULES

The following assumptions and constraints were used for the tradeoff study.

- Sidelobe Statistical Region

  .5° - 2°
  - Average sidelobe value is average power in this region.
  - Peak sidelobe is peak in this region.

- Fixed Diameter Main Reflector
  - Approximate fixed beamwidth for similar sidelobe levels.

- Optimization Technique - Two Methods.
  - $\Delta \alpha$ Minimize average sidelobe over region for given gain, without suppressing peak sidelobes.
  - ΔP Optimum calculation is weighted incrementally to minimize the peak above average sidelobe ratio. Fixed collar has more significance, so that the null to null beamwidth is controlled. A collar of radius .42° is used for all cases, unscanned or scanned.
  - Definition of suppression region has been fixed, complete from collar out to 2°.

- Scanning 0°, and 3° as representative cases.

TRADEOFF STUDY GROUND RULES (Cont'd)

- Computed Gain Reported
  - Includes spillover loss.
  - No surface losses or errors included.
- Relationship between C/I and sidelobe level.
  - 30 dB C/I Spec.
    - Multiple beam margin requirement.
      - Assume equal contributions from all other beams.

Case	Margin	Average Sidelobe Requirement
6 beams	7.0 db	37.0 dB
10 beams	9.5 dB	39.5 dB
18 beams	12.3 dB	42.3 dB

OPTIMIZATION OF OPTICAL CONFIGURATION

- Basic Configuration - Dual Reflector F/D = 1.2, M = 2.
- Necessary to determine precise diameter for desired beamwidth, gain, and sidelobes.
  - This is dependent on element patterns.
  - To provide good sidelobes for any beam, the rule of thumb is to design for 3 dB crossover of secondary element patterns. This is primarily a function of element spacing, and secondarily dependent on element gain. The highest realizable element gain is desired to increase the overall antenna gain.
- General Approach
  - Plot beamwidth, gain, sidelobes versus n versus D, as in Figures 22, 23, and 24.
  - Enlarge plot of secondary element pattern beamwidth versus n versus D, as in Figure 25.
  - Plot the range of secondary pattern beamwidths versus element spacing by relating a range of n to element spacing.

$$n = \alpha\left(\frac{d}{\lambda}\right)^2 - 0.5$$

α_{MIN} $\alpha_{TYP} = 2.20$ $\alpha_{MAX} = 2.88$

  - On the same graph plot beam peak separation versus element spacing. This is essentially the beam deviation factor.
  - Normalized results of this exercise are plotted in Figure 26. The intersection of the appropriate curve from each family indicates the element spacing required for 3 dB secondary element pattern crossovers.
  - Optimize for low sidelobe performance with an array feed and correlate beamwidth and gain and sidelobe performance with position relative to predicted curve.
  - Plot gain versus average sidelobe convergence curve.
  - Bandwidth considerations
    - As frequency increases, element spacing increases, but F/D remains constant. This makes the element crossover levels lower and degrades sidelobe control.

3.2.1 Configuration Drawings

The configuration drawings in Figures 27 through 33 illustrate the general proportions of the range of cases considered in the parametric study. All drawings are made for a 250 λ diameter main reflector, with a range of focal lengths and magnifications. Scale is 20 wavelengths per small division. Of particular interest is the configuration for F/D = 0.6, M=2. The blockage free design algorithm correctly showed that no such design was possible, with the subreflector axis parallel to the main reflector axis. Tilting the subreflector axis as shown leads to 2 blockage free design. However, due to the subreflector's short focal length, the realized magnification falls off rapidly with the large scan angles.

3.2.2 Blockage Avoidance

A simple computer program based on geometrical optics was written to establish design curves for blockage free offset dual reflectors. The criteria is illustrated in Figure 34. The upper edge of the subreflector must fall in the shaded region in order to reflect the rays necessary for scanning down in elevation, yet not block the collimated rays from the main reflector for that same case. Furthermore, the top edge of the feed array must not block the rays between the two reflectors for scanning up in elevation.

On the basis of these criteria, a set of blockage free design curves were generated. A typical set of curves is shown in Figure 35, for a given F/D, maximum elevation scan angle, and subreflector focal length. The descending curve represents the criteria for the top edge of the subreflector. The ascending curve represents the criteria for the top edge of the feed array. The shaded area is then the allowed space from which the magnification and offset can be chosen.

3.2.3 Standard Aperture Curves

The gain and beamwidth curves in Figure 36 are included to allow the reader to readily compare antenna performance to that of several standard aperture illuminations. The relative performance level can then be used to predict performance of a similarly scaled design at a new aperture diameter. Curves are based on data given in Hansen.*

---

* Hansen, Microwave Scanning Antennas, Vol. 1, p. 66, 1964, Academic Press, New York.

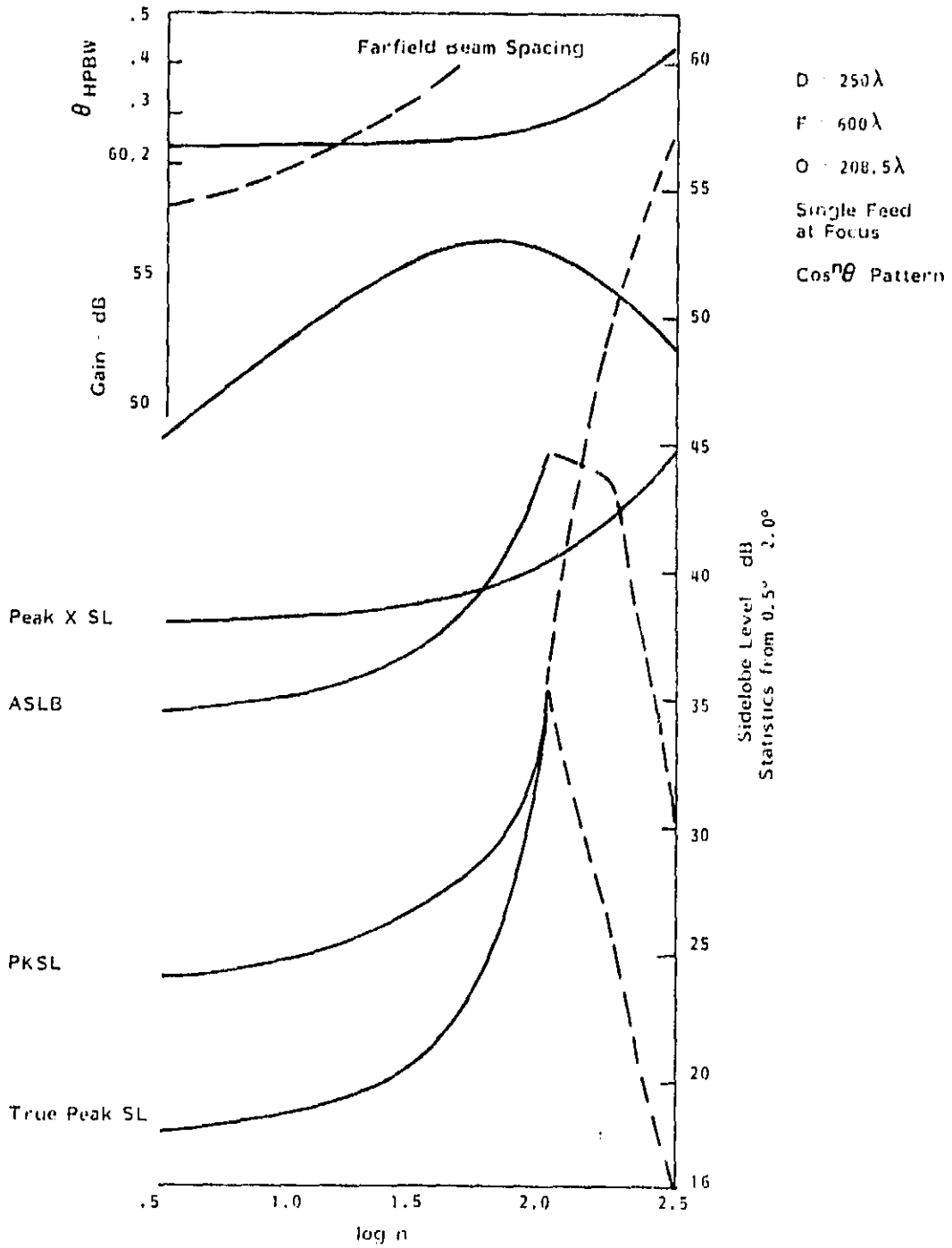

Figure 22. Performance of Single Element Beam vs Element Gain Parameter, D=250

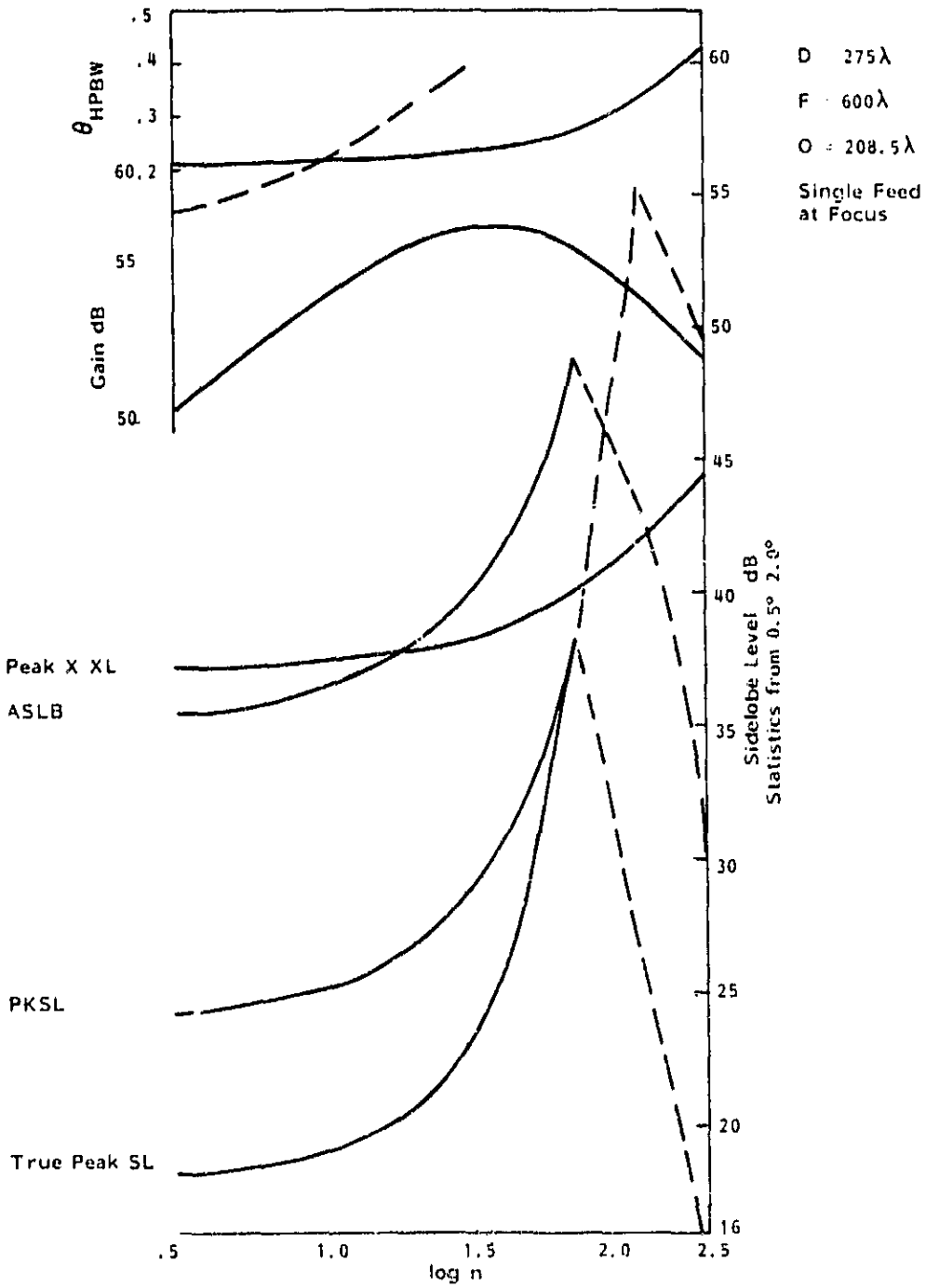

Figure 23. Performance of Single Element Beam vs Element Gain Parameter, D=275

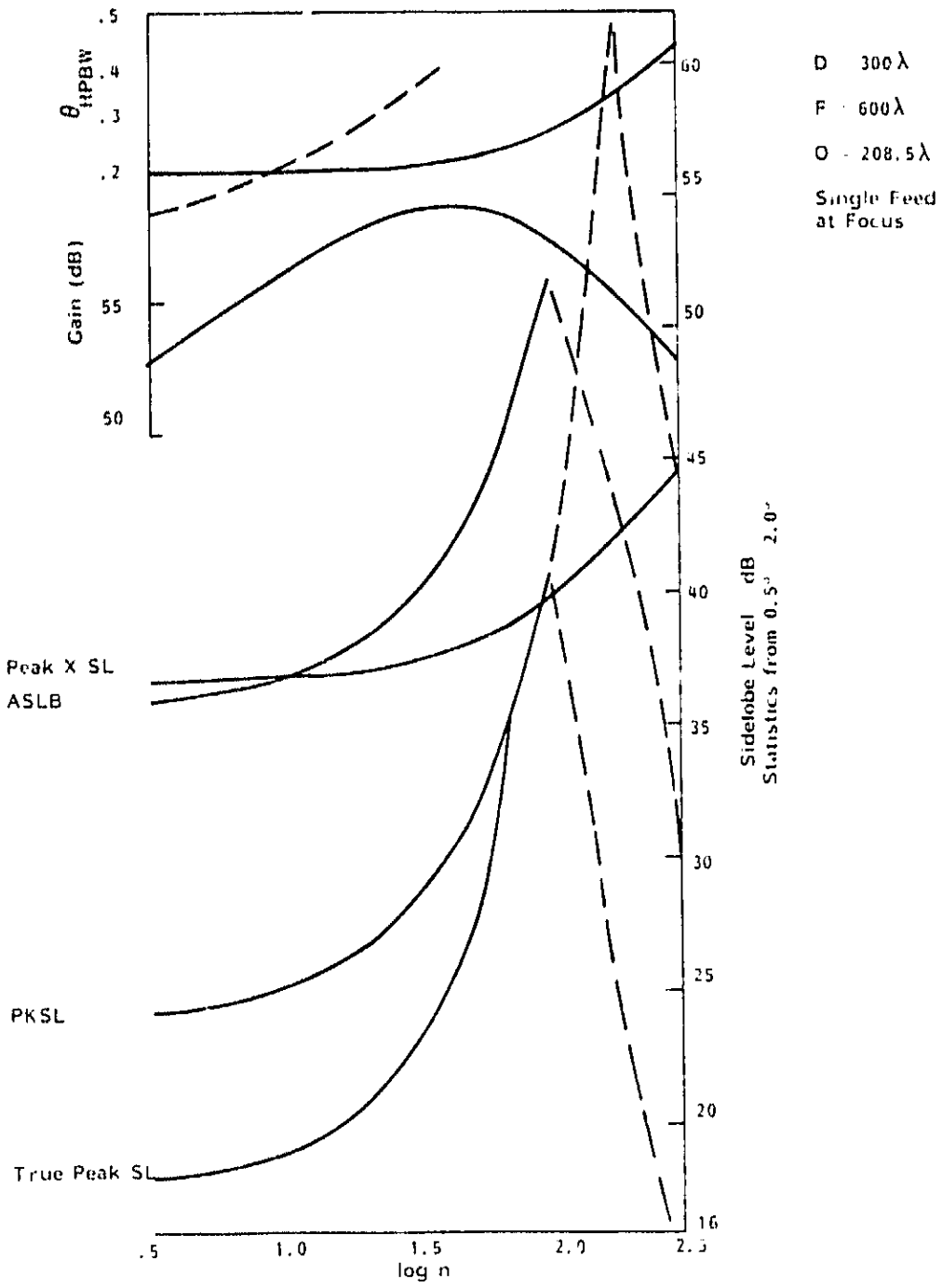

Figure 24. Performance of Single Element Beam vs Element Gain Parameter, D=300

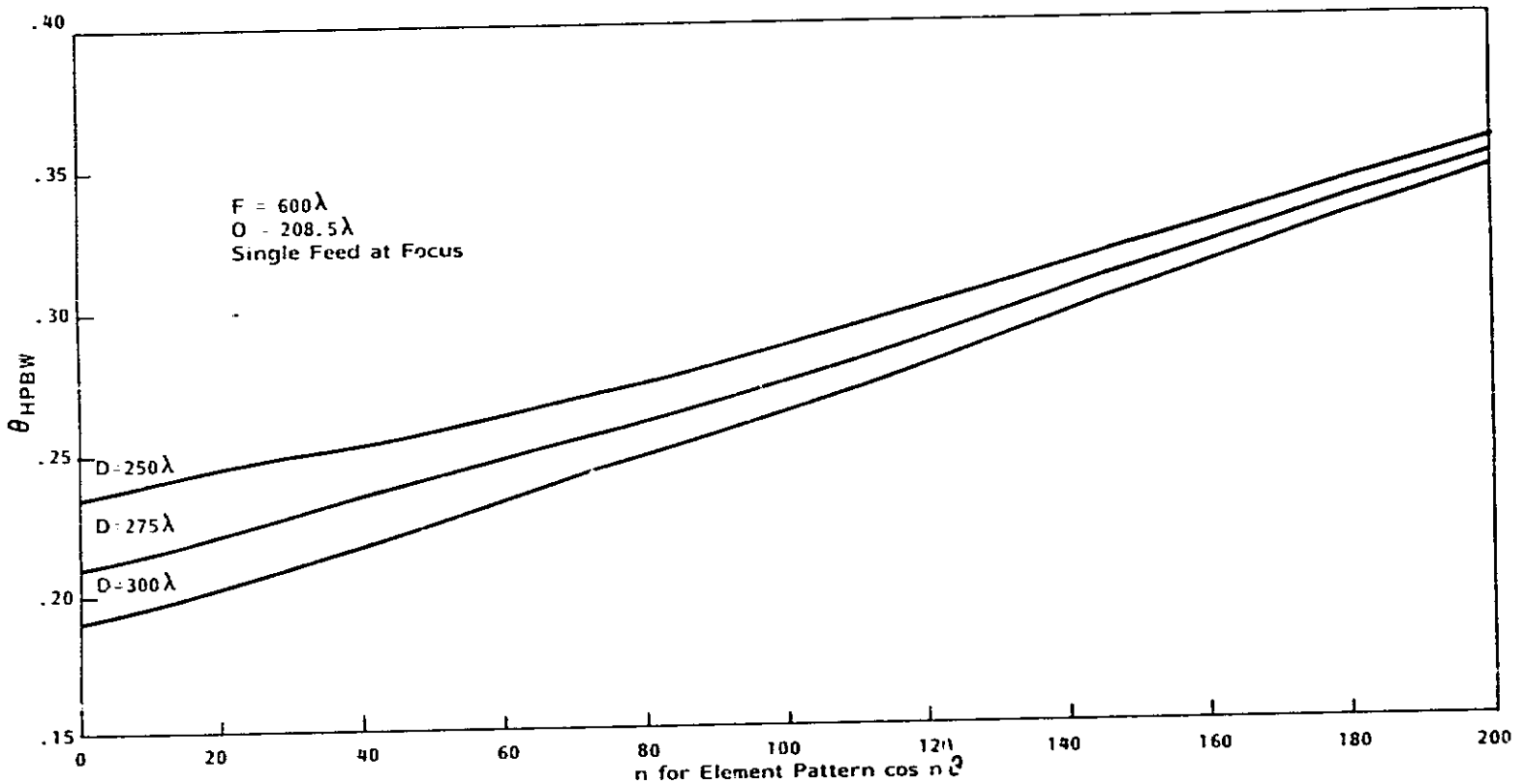

Figure 25. Secondary Pattern Beamwidth vs Element Gain Parameter

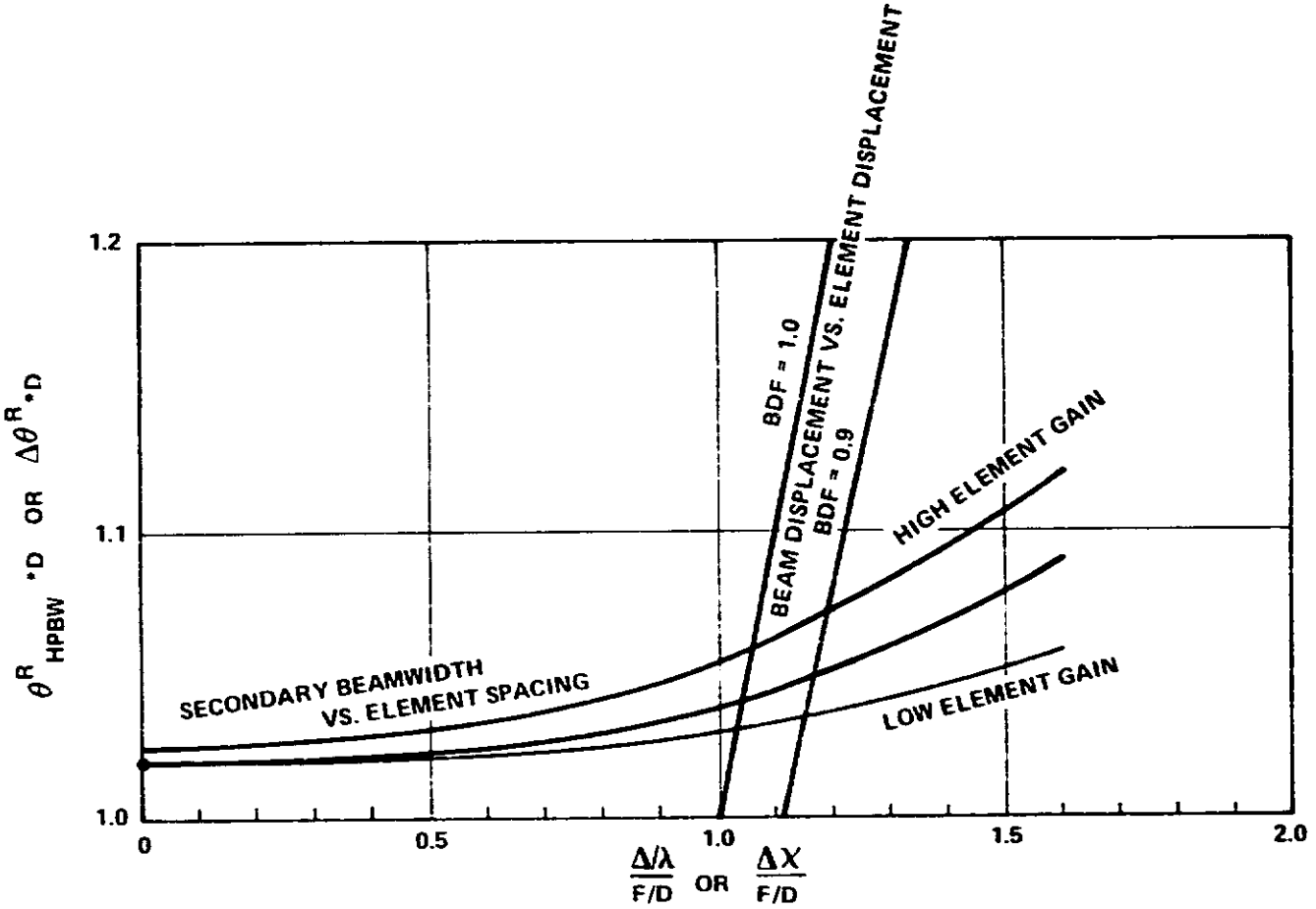

Figure 26. Normalized Beamwidth vs Element Spacing to Determine Spacing for 3dB Second Element Pattern Crossovers

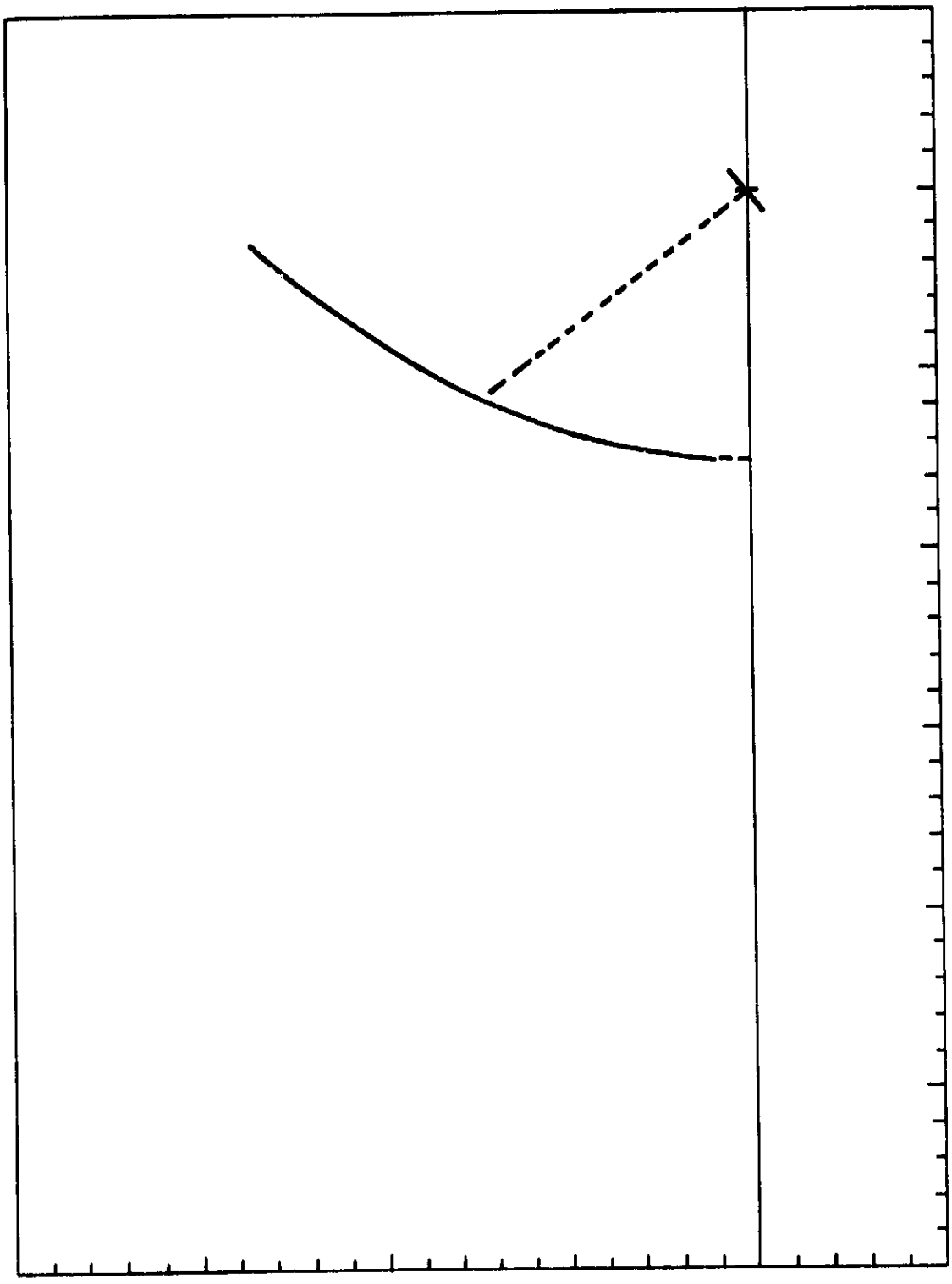

Figure 27. Single Reflector F/D = 0.6

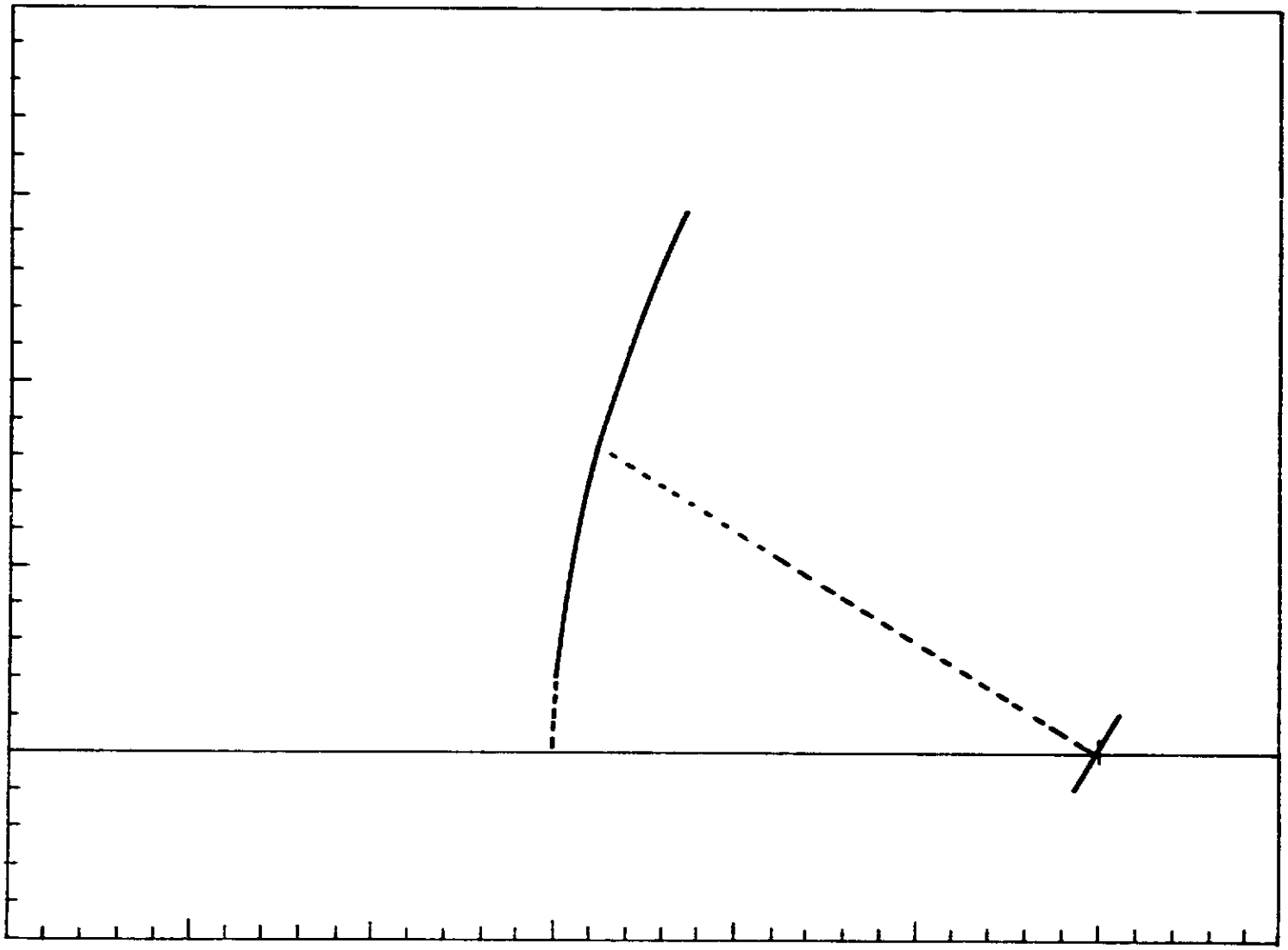

Figure 28. Single Reflector F/D = 1.2

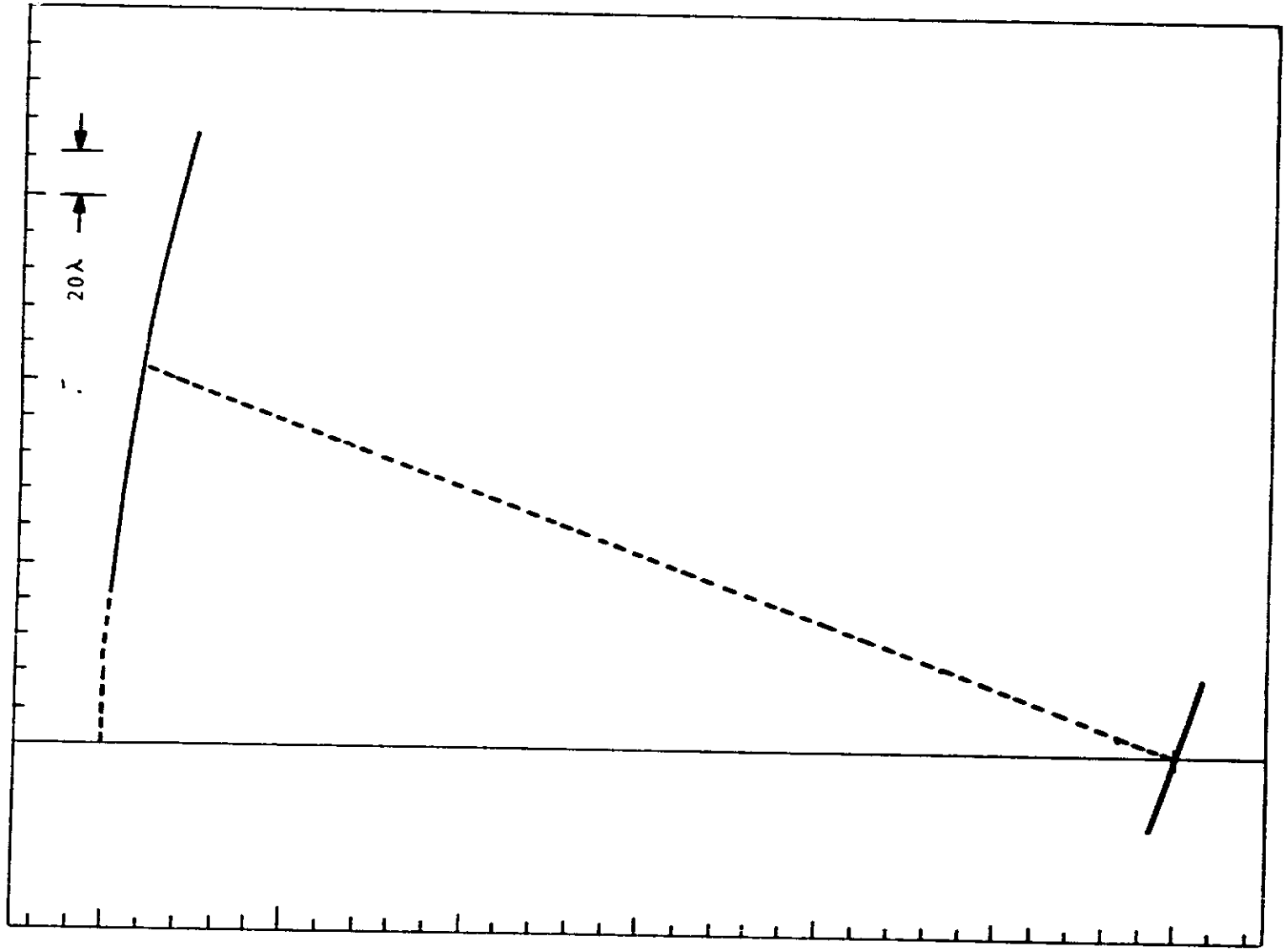

Figure 39. Single Reflector F/D = 2

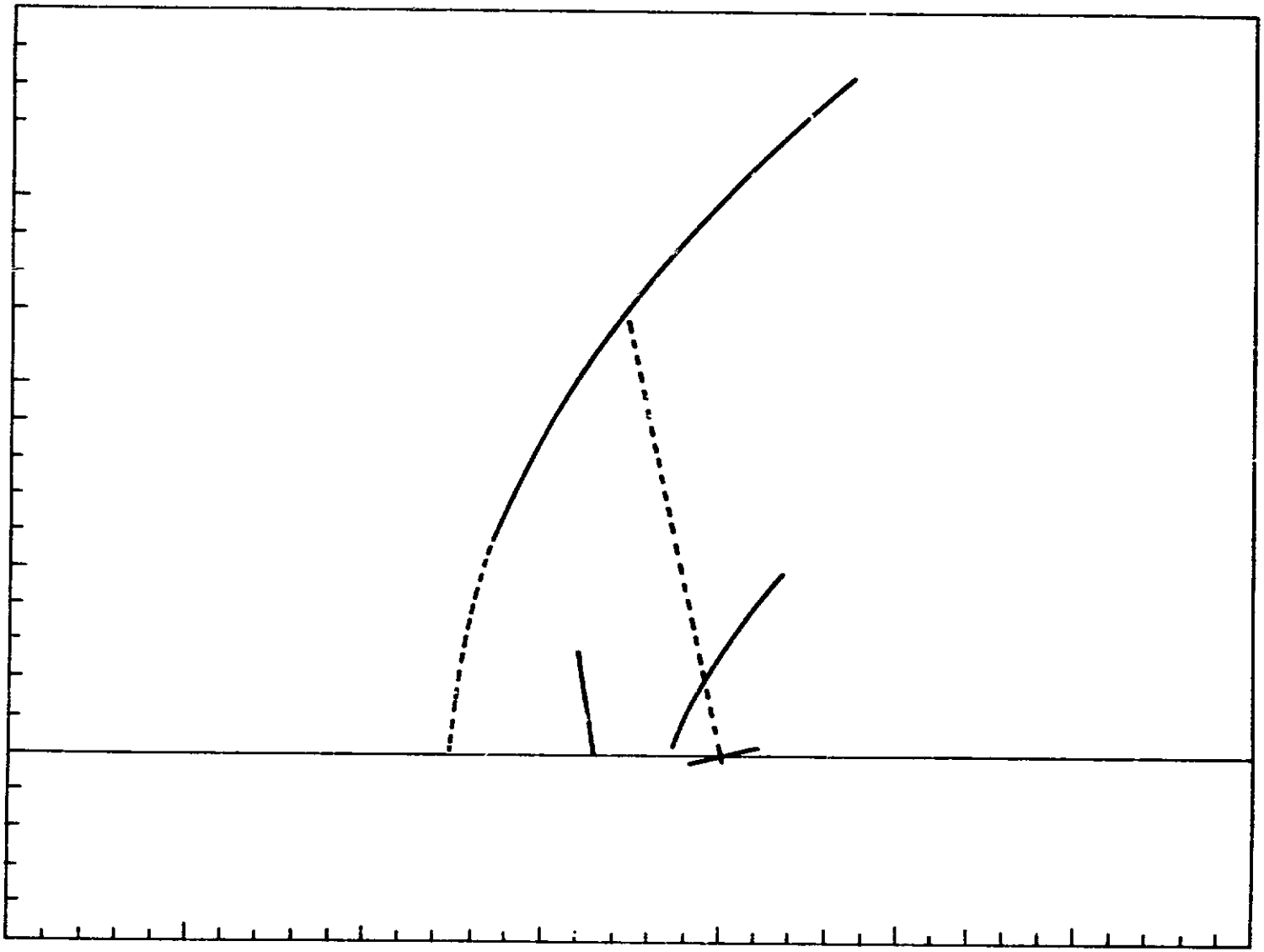

Figure 30. Cassegrain Reflector F/D = 0.6, M = 2

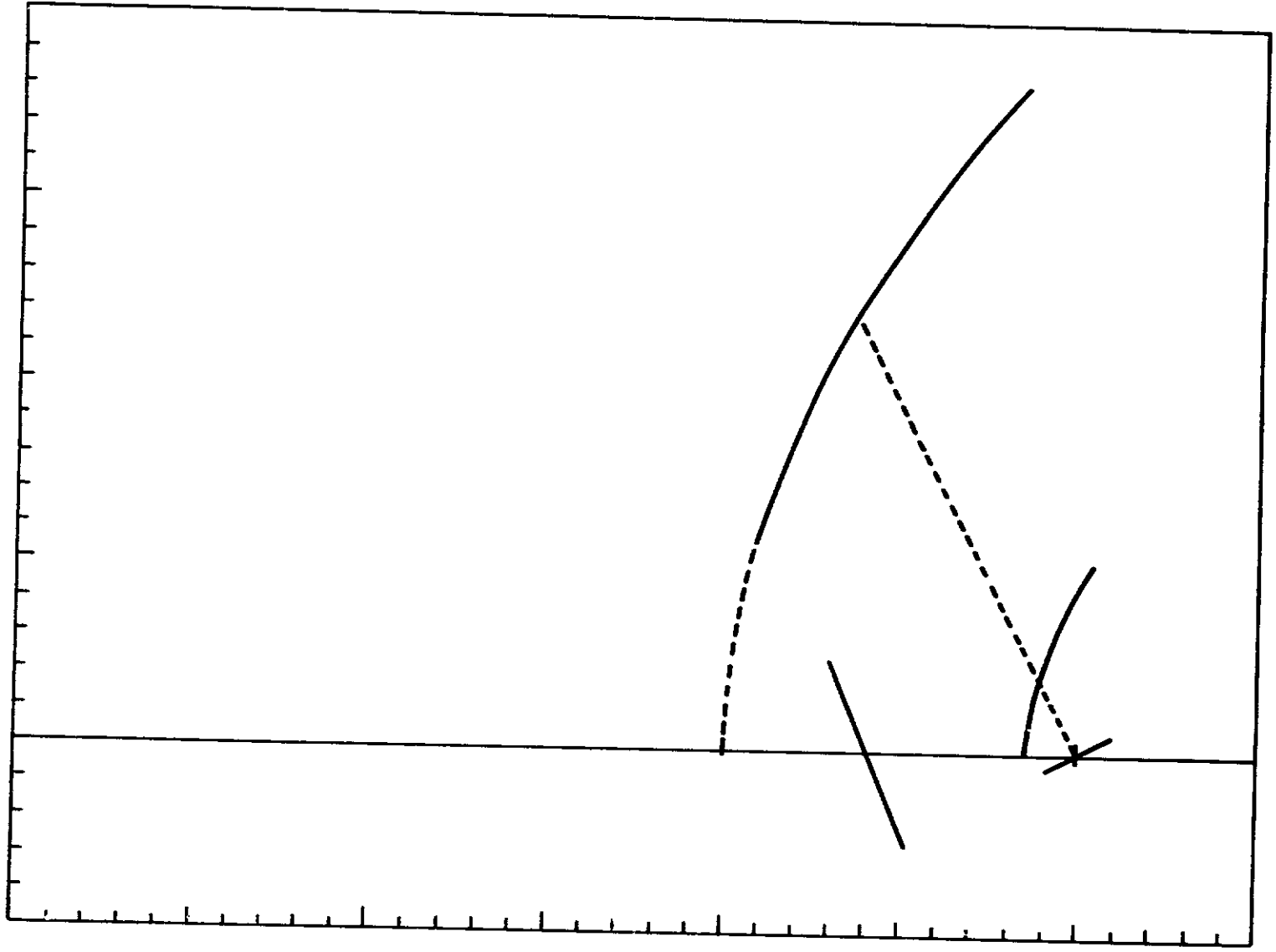

Figure 31. Cassegrain Reflector F/D = 0.8, M = 3

3.2.4 Element Pattern

A simple $\cos^n \theta$ pattern is used to model the feed elements for computer simulations. The exponent was chosen initially as a function of element spacing, based on the curves given in [1], shown in Figure 37. Values of the exponent for the final design simulations were based on the gain and beamwidth of the horn used for the final element design. The element patterns used were linearly polarized with no cross-polarization component. Potential sidelobes in the element pattern are not modeled.

3.2.5 Reflector Antenna Performance vs Element Gain

Reflector performance parameters are plotted as a function of the element pattern parameter n in Figures 22 through 24. Gain, beamwidth, and several measures of sidelobe performance are provided. The most obvious conclusion that can be drawn from these graphs is that a single element capable of providing the desired beam gain and sidelobe level is too large to permit the small element spacing required for the desired angular spacing between adjacent beams in the far field. For small n, the element pattern is broad. The reflector illumination is nearly uniform, leading to the narrowest achievable beamwidth, and lowered overall gain due to large spillover losses. The sidelobe levels are high due to the high edge illumination. For very large n, the reflector is illuminated inefficiently, so gain and beamwidth appear to behave as they would for a shrinking aperture. However, the sidelobe level continues to improve due to the decreasing edge illumination. The sidelobe curves based on the region from .5° to 2° reverse suddenly as the skirt of the main beam grows beyond .5° radius. The cross-polarized sidelobe curve is not constrained to any region. The true peak sidelobe curve reports the largest sidelobe beyond the end of the skirts of the main beam, wherever they may fall.

3.2.6 Discussion of Convergence Trade Curves

A phased array fed reflector antenna has a great deal of flexibility. The tradeoff curves describe performance as a function of design. However, for any given design, the antenna can be operated in a number of ways, as the amplitude and phase weights are varied. With an adequate design, beams of various characteristics can be generated by the beamformer. A reasonable compromise among gain, average sidelobe level, and peak sidelobe level was used for choosing the best design. Alternatively, weights can be chosen which optimize gain alone, optimize average sidelobe level over a region without regard to peak sidelobe level. Another option is to create a good lower gain beam with a wider beamwidth than would be normal for the reflector dimension. Also, specially shaped beams can be formed as an extension of this procedure.

---

[1] Y. Rahmat-Samii, "Realizable Feed-Element Patterns for Multibeam Reflector Antenna Analysis," IEEE Trans. on Antennas and Propagation, Vol. AP-29, No. 6, Nov. 1981.

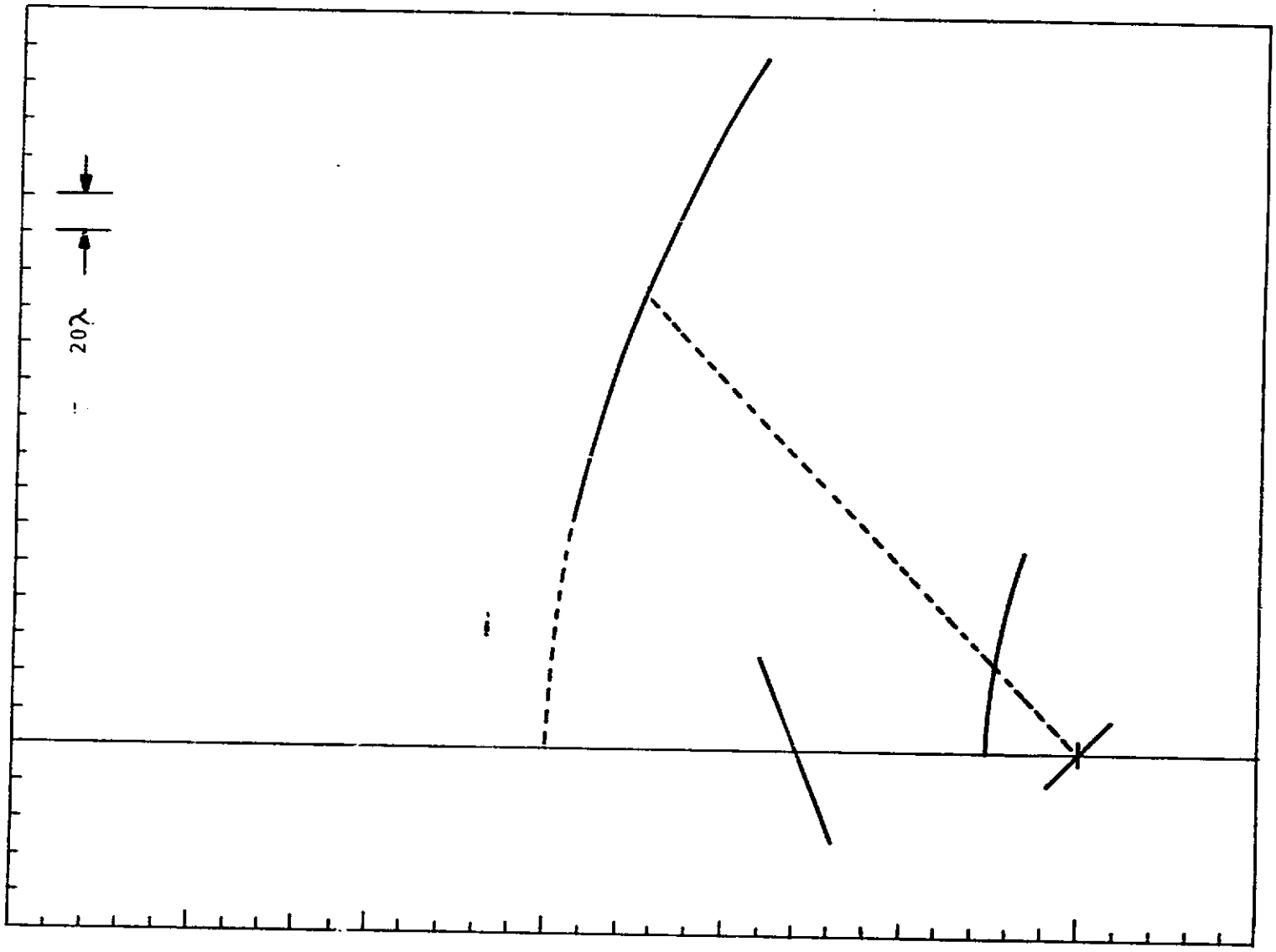

Figure 32. Cassegrain Reflector F/D = 1.2, M = 2

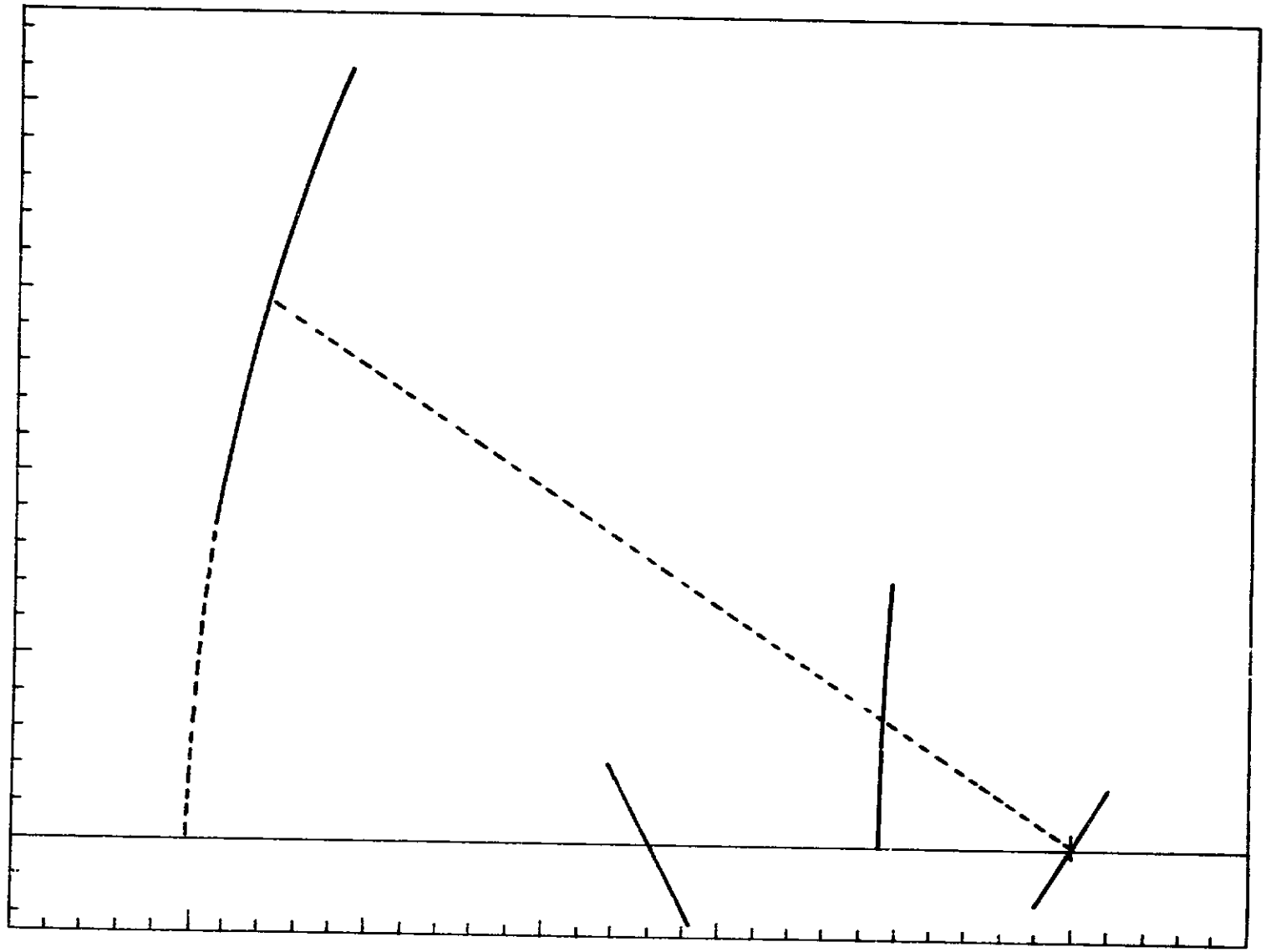

Figure 33. Cassegrain Reflector F/D = 2.0, M = 1.2

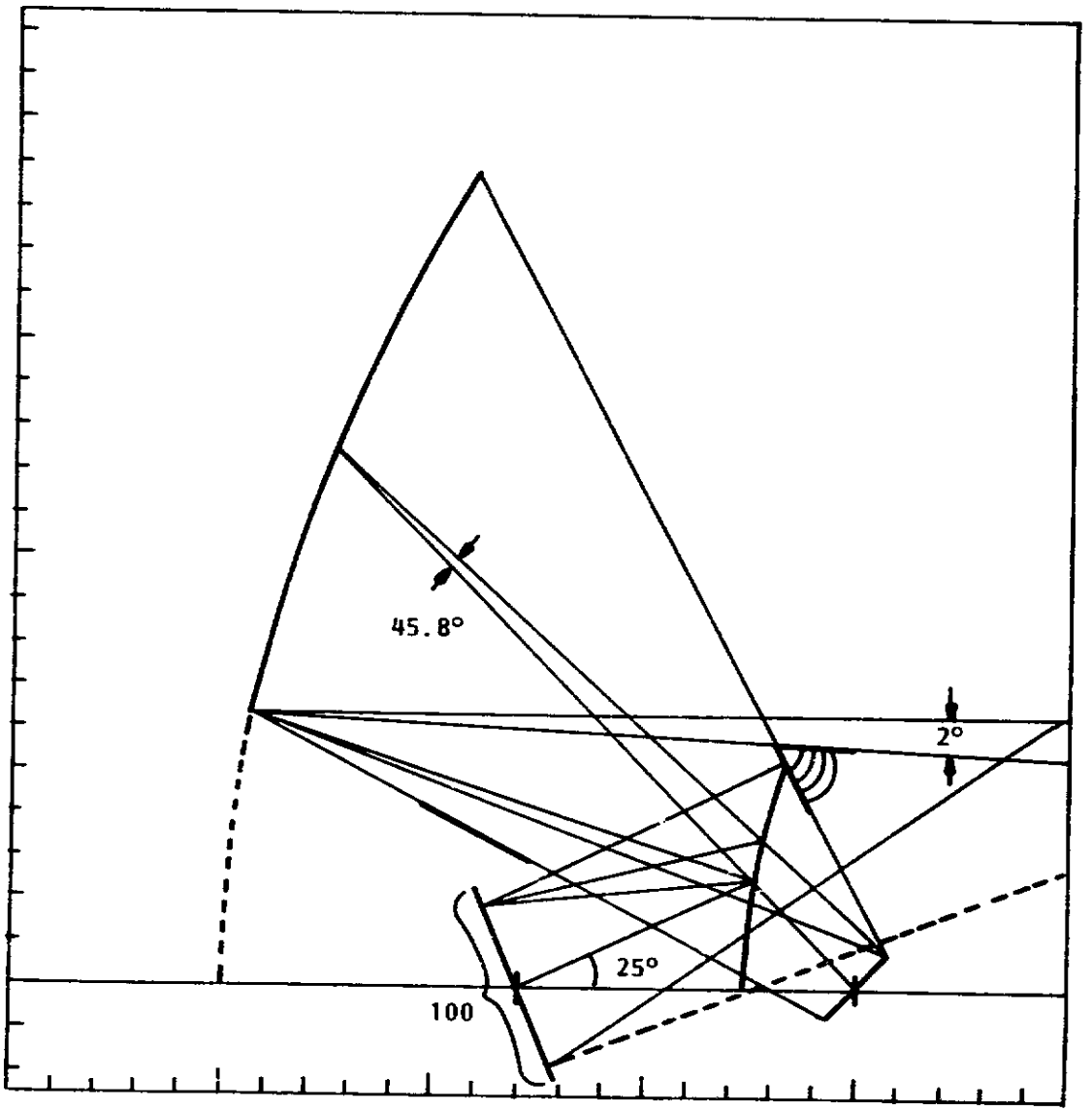

Figure 34. Cassegrain Reflector Showing Regions in which Reflector Edges Must Fall to Avoid Blockage

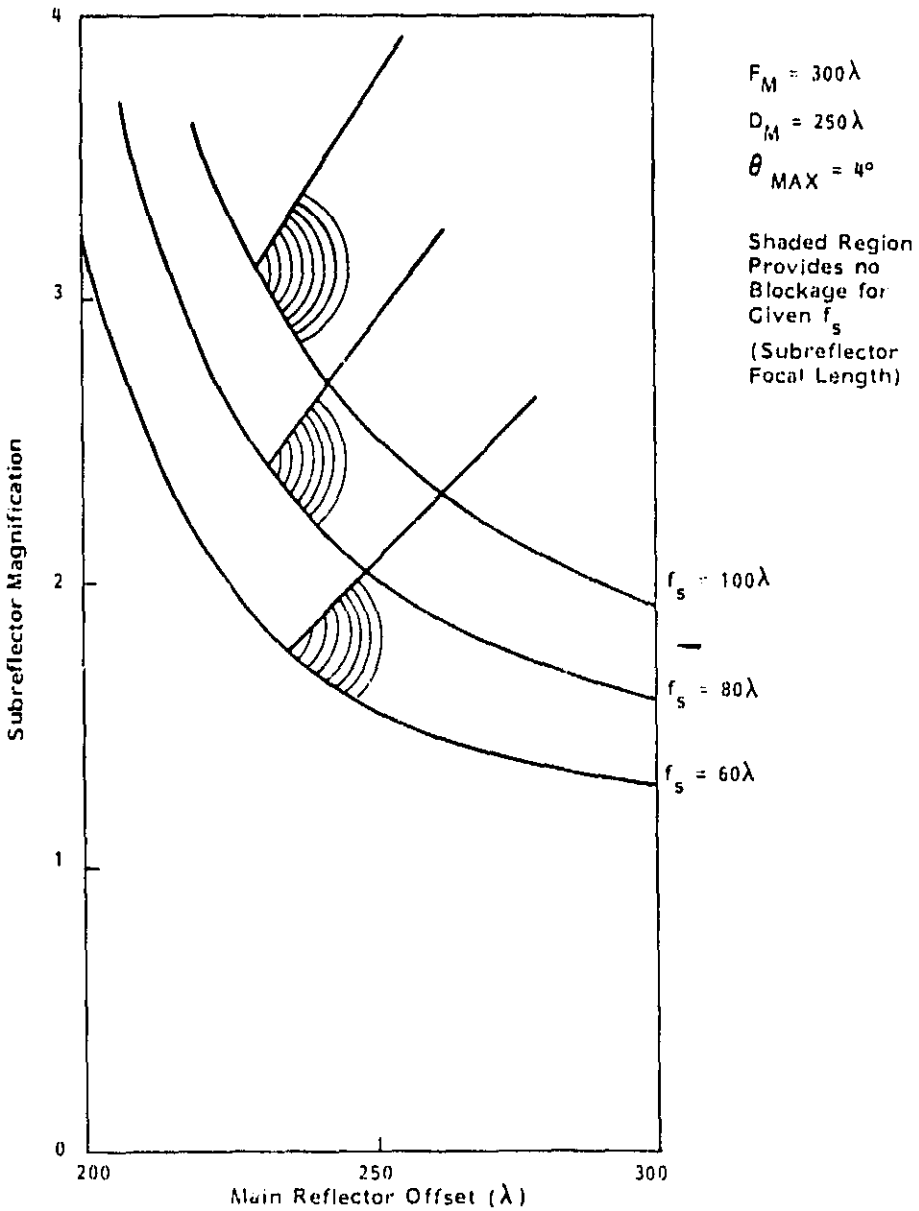

Figure 35. Sample Parametric Plot of Dimensions Required to Avoid Blockage

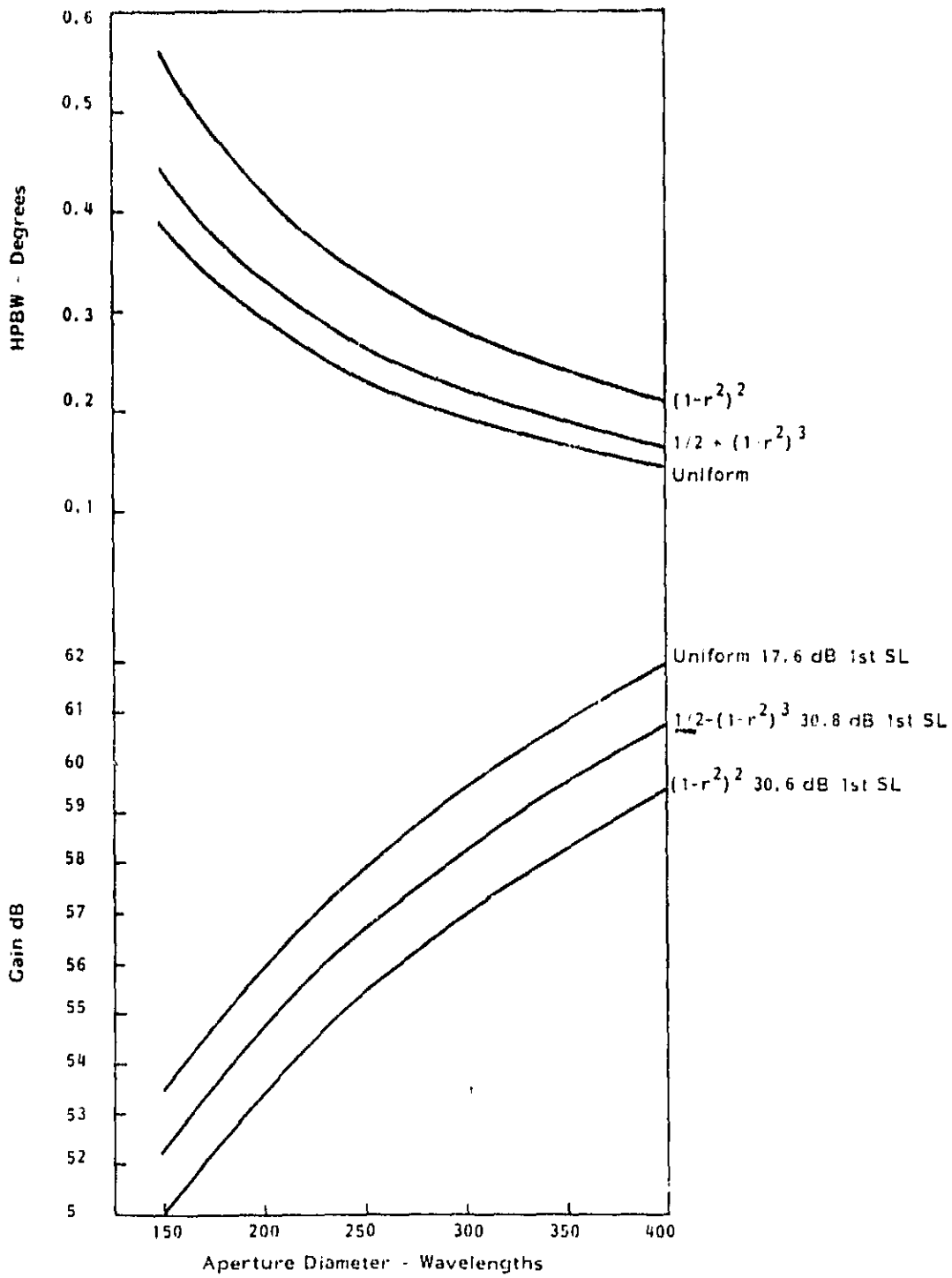

Figure 36. Standard Gain and Beamwidth for Circular Aperture

The computer program used for the design process can determine the weights and pattern for any such beam, once the secondary element patterns are known. The sample optimization curves, Figure 38, demonstrate the compromise usually taken. The starting point is near the maximum gain case. Both average and peak sidelobes are then suppressed until a satisfactory level is reached, or the gain degrades below a minimum gain requirement. Note how the peak above average ratio is compressed as the iterative procedure is continued.

The actual value given as the average sidelobe level depends on the size of the averaging region. Use of a large area makes the average artificially low, since most of the sidelobe energy is concentrated in a small region around the main beam.

Gain and sidelobe performance trades are illustrated in Figures 38, 39, 40, and 41 as functions of subreflector magnification, element gain, and scan angle.

A trade study was performed concerning the ability of an array feed to generate the narrowest possible beam for an undersized reflector. The results are plotted in Figure 42. Beamwidth is plotted vs. the peak sidelobe level in the region beyond .5" from the main beam center, in order to present a relationship between beamwidth and good performance. A 250 λ reflector was used, with F/D = 2.4. Results are plotted parametrically with number of elements used and element spacing in wavelengths.

A significant turning point is seen by comparing the graphs of 7 and 19 elements with those of 37 and 61 elements. The curves for the smaller numbers of elements show sooner or later, a steep increase in beamwidth degradation as the sidelobe level is improved. In contrast, the results for the larger number of elements show an apparent limit to beamwidth degradation as the sidelobe level is improved. However, in most applications the 19 element cluster would realize most of the improvement possible.

3.2.7 Maximum Gain Envelope

The maximum gain excitation is the simplest set of array weights to compute. Each element weight is set to simplify the complex conjugate of the secondary pattern field strength in the direction in which a beam is desired. This condition gives more gain than any other condition. A comprehensive plot of the maximum gain as a function of scan angle is known as the maximum gain envelope. This plot in itself is not an antenna pattern. The maximum gain envelope for several design conditions is shown in Figure 43.

The maximum gain envelope is useful in estimating array reflector performance. The gain vs. scan performance for low sidelobe beams has the same shape as the maximum gain envelope, but typically has from .5 to 1.5 dB less gain. When the maximum gain envelope has a significant ripple, low sidelobe performance vs. scan is found to be good near ripple peaks but

r	DIRECTIVITY 10 log (2*(2n+1))	HPBW	EDGE TAPER FOR F/D = 2.4*
0.	(3 dB)	--	0.
1.	7.8	89.9	-.2
3.	11.5	53.9	-.5
10.	16.2	29.9	-1.8
30.	20.9	17.4	-5.5
100.	26.0	9.5	-18.2
300.	30.8	5.5	-54.7

*23.4° SUBTENDED ANGLE

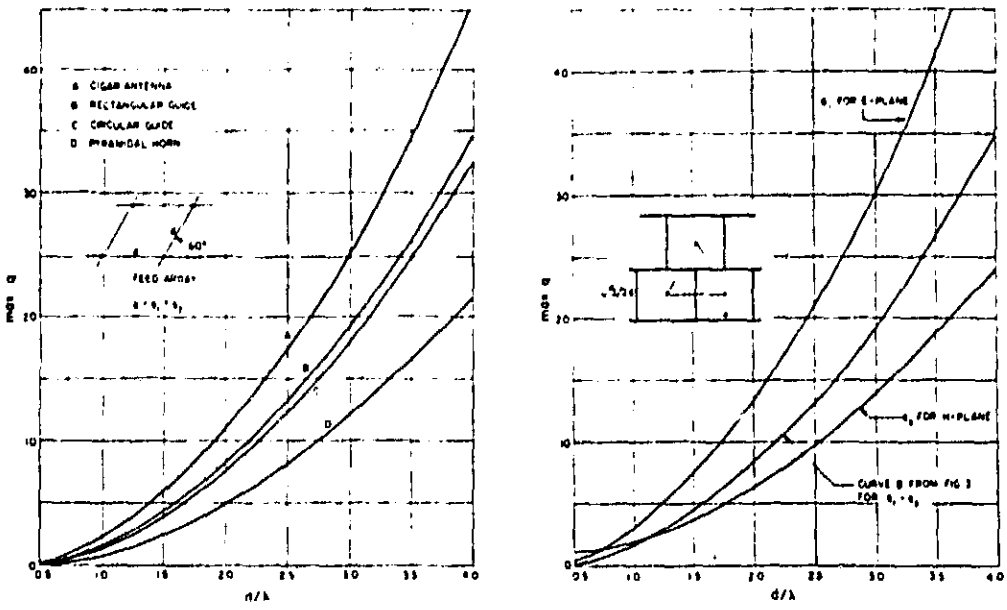

Figure 37. Element Gain Parameter n (q) vs Element Spacing

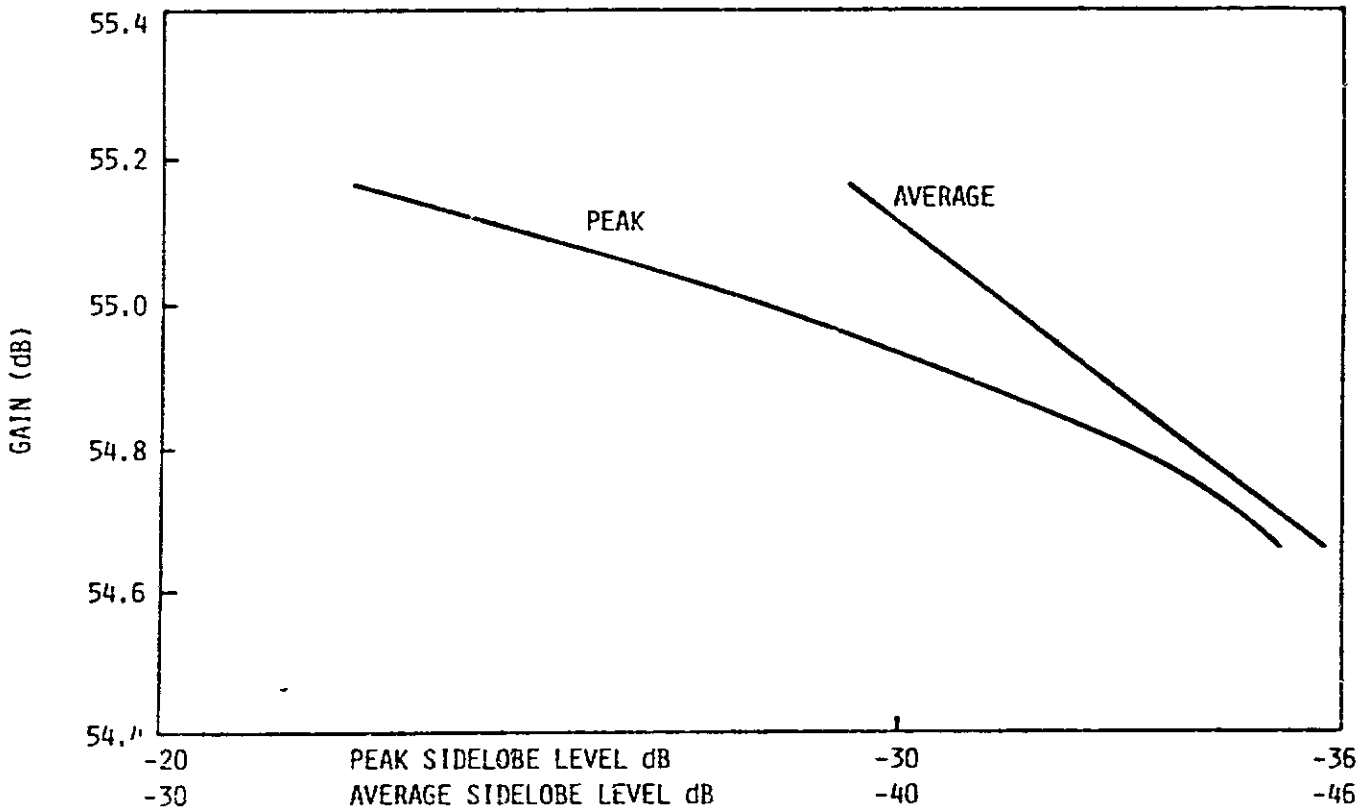

Figure 38. Optimization Convergence Curve for an Adequate Design

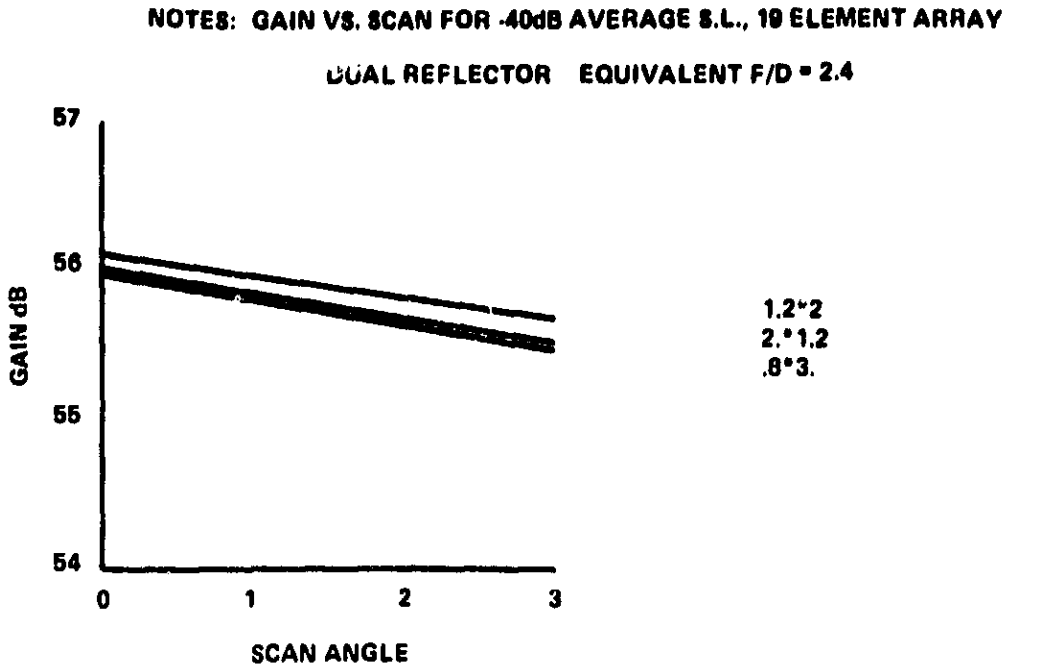

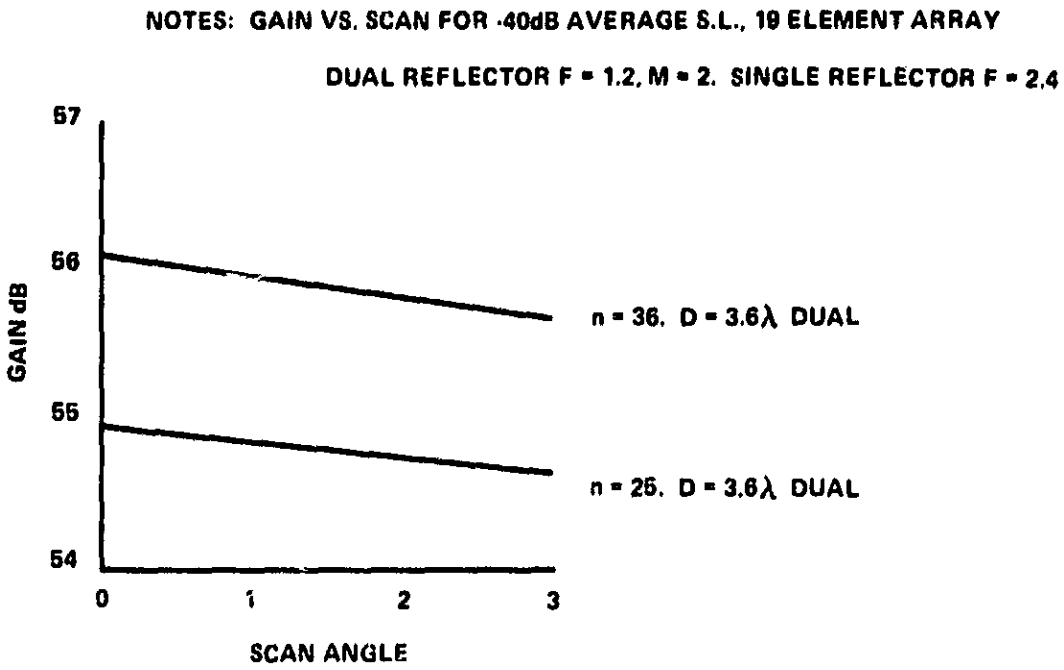

Figure 39a. Gain vs Scan Angle vs M, Constant Equivalent F/D
Figure 39b. Gain vs Scan Angle vs Element Gain Parameter n

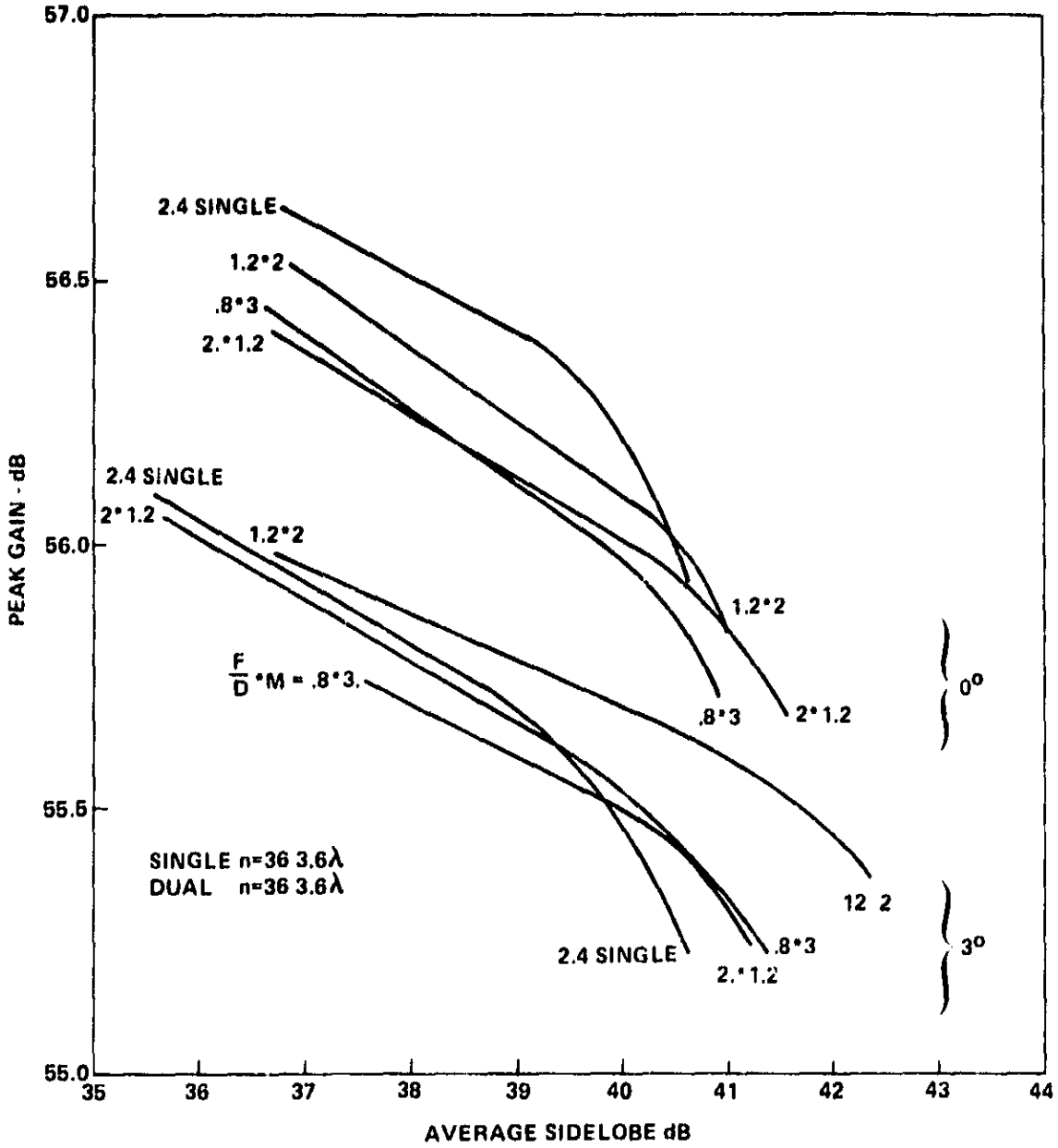

Figure 40. Optimization Curves for Constant Effective F/D

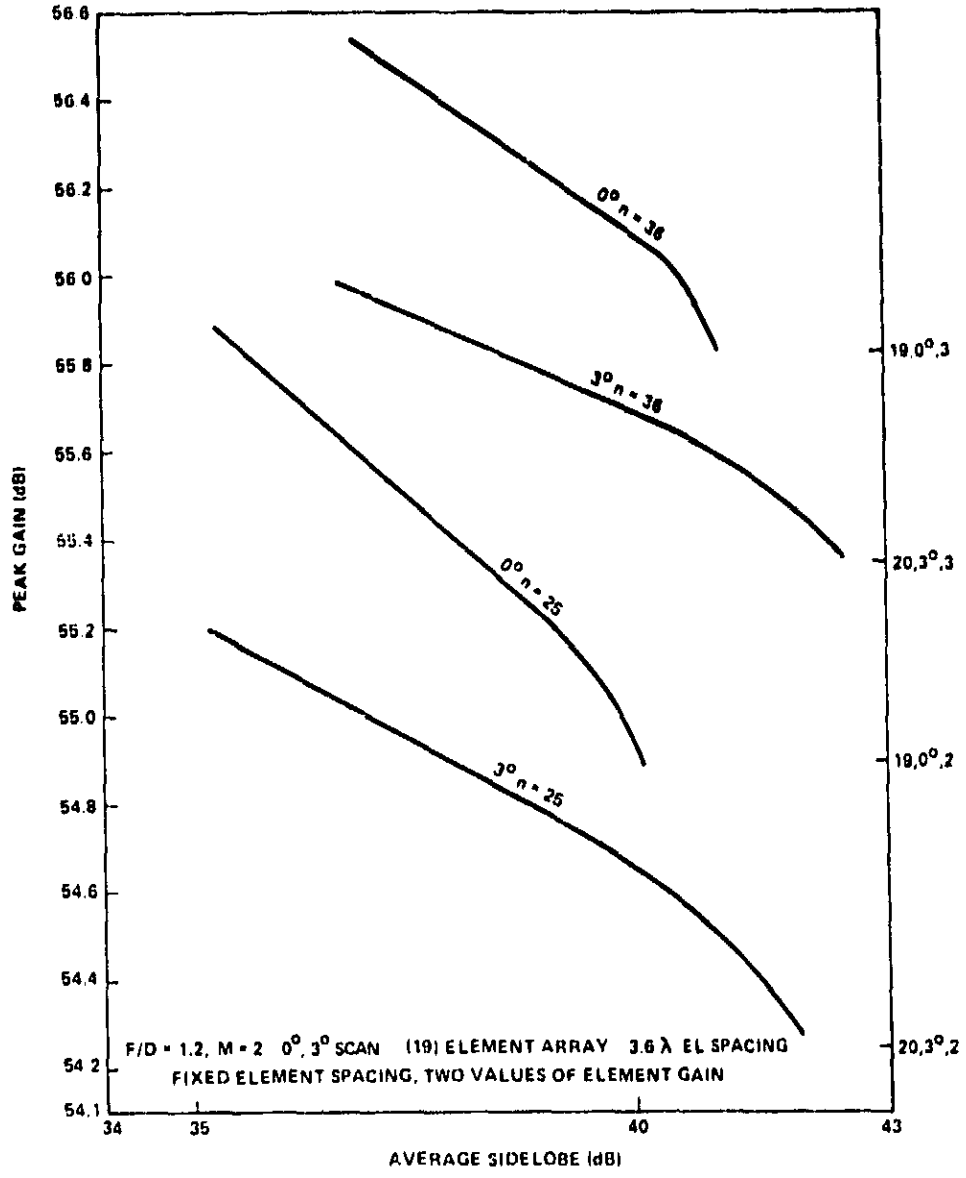

Figure 41. Optimization Curves vs Scan Angle vs Element Gain Parameter

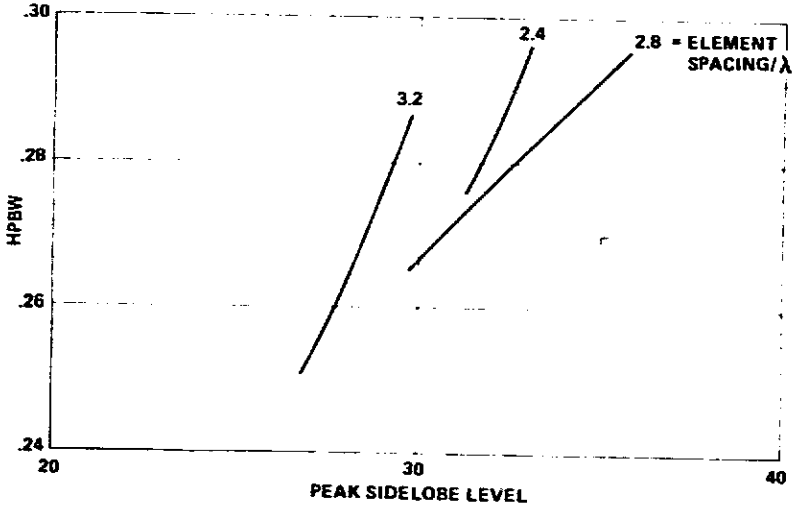

a. 7 Elements

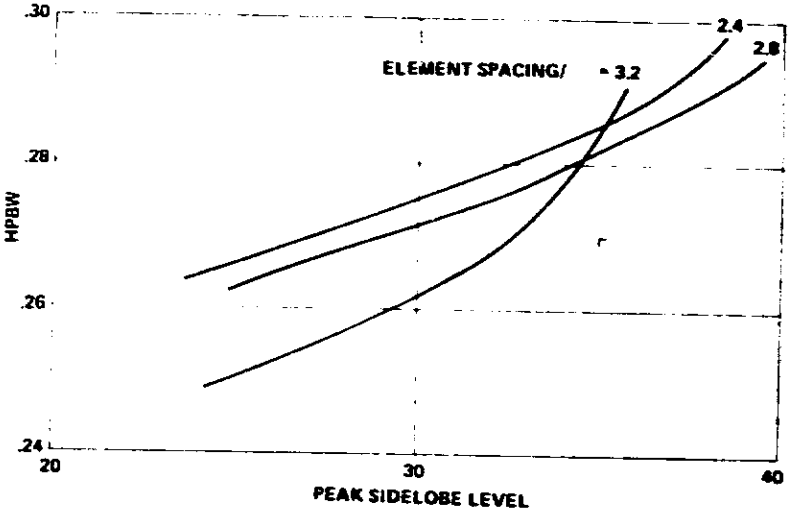

b. 19 Elements

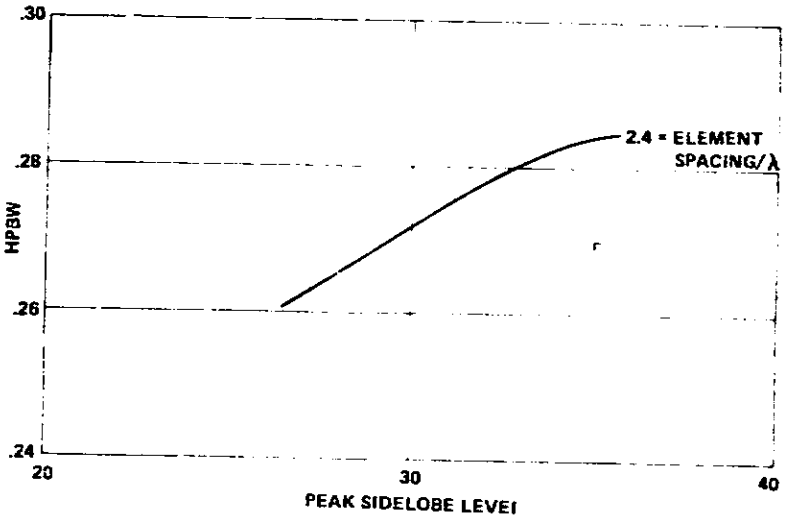

c. 37 Elements

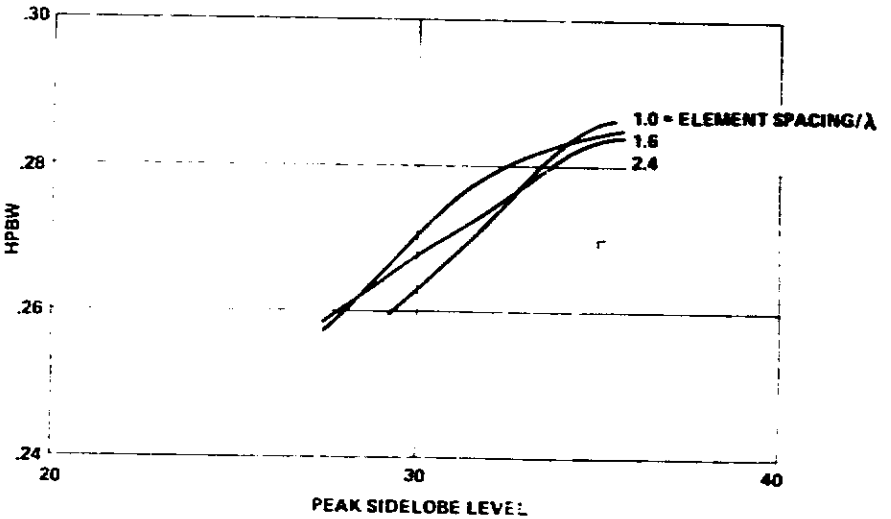

d. 61 Elements

Figure 42. Beamwidth vs Peak Sidelobe Level for Narrow Beam Optimization

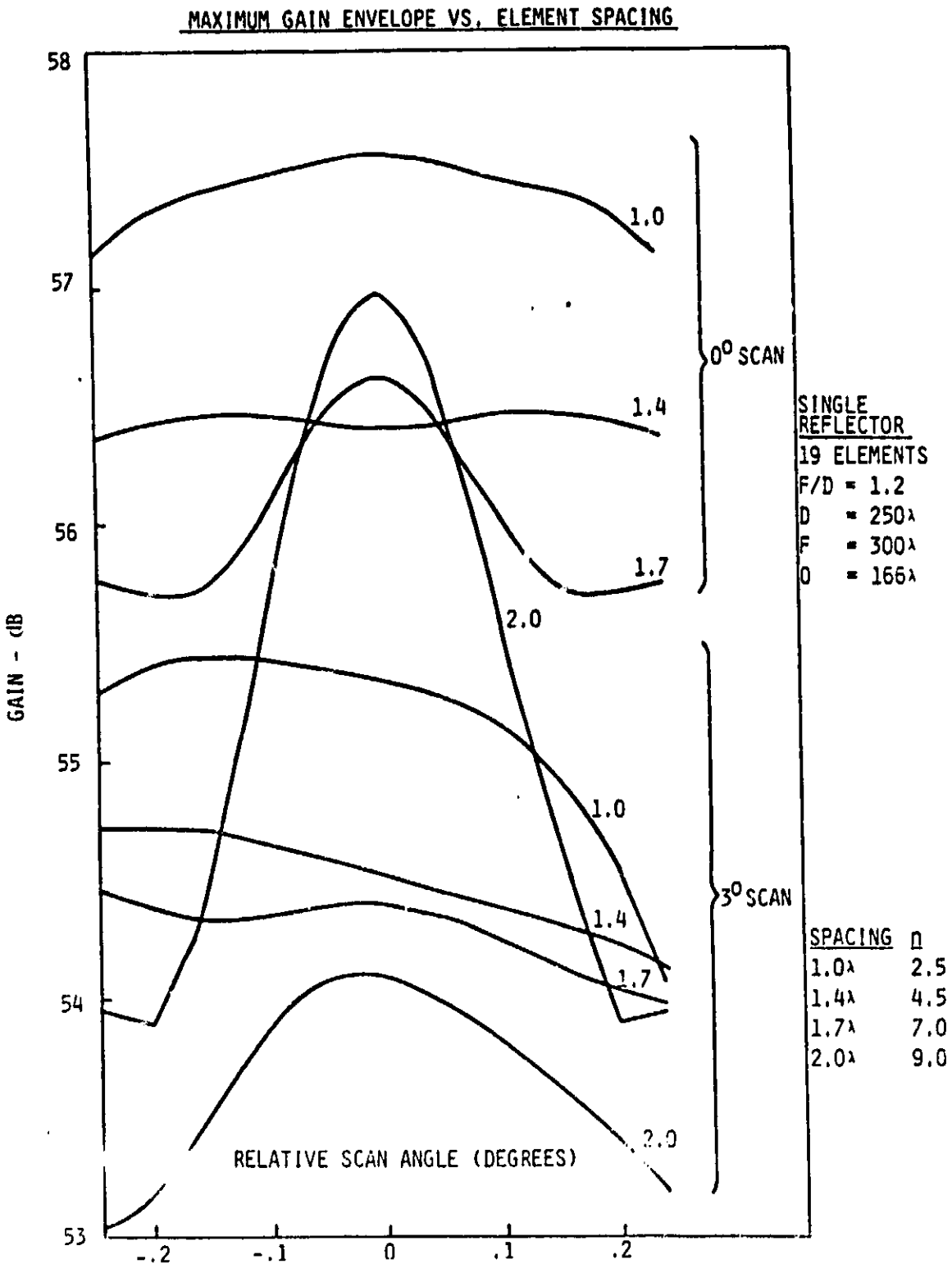

Figure 43. Maximum Gain Envelope vs Element Spacing vs Scan Angle

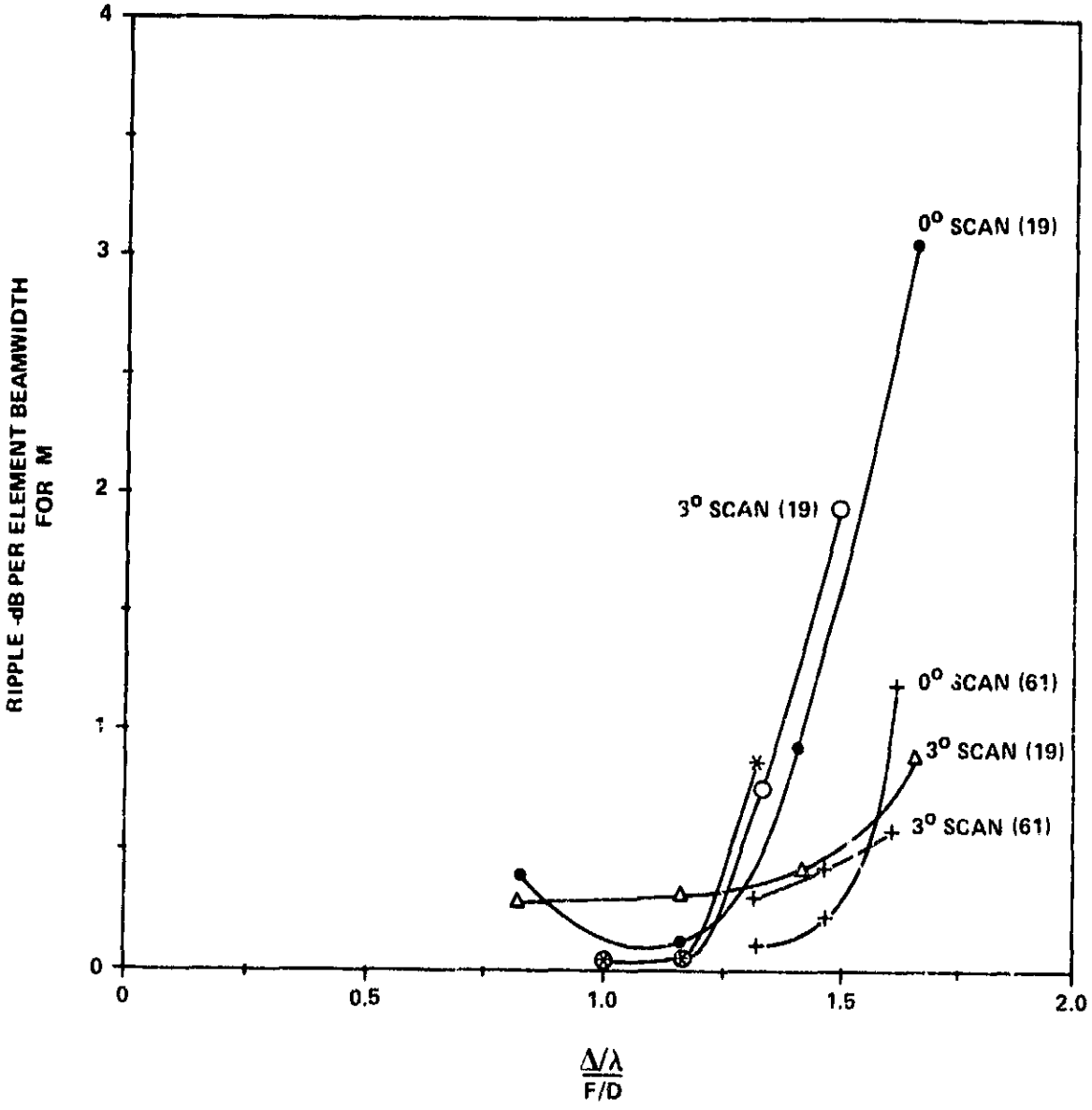

Figure 44. Maximum Gain Case Ripple vs Normalized Element Spacing

poor near ripple valleys. Therefore an antenna should be designed such that the ripple of the maximum gain envelope is less than .5 dB. Data on element spacing vs. ripple is shown in Figure 44, from a number of different design tradeoffs. Element spacing is normalized by the wavelength and the F/D ratio. Thus a design for continuous scan capability requires a normalized element spacing less than 1.25.

3.3 RECOMMENDED CONFIGURATION

Table 16 summarizes the derived design/performance parameters of the three major antenna configurations. The principal disadvantages of the single reflector design is its greater axial length, poorer noise-figure, and higher sidelobes. The principal disadvantages of the Gregorian design is its larger weight (attributed primarily to the six parallel 1039:1 beamcombiner networks) and its greater DC power consumption (attributed to the large number of active modules required). The Cassegrain design emerges as a clear design choice. The principal "disadvantage" of the Cassegrain design is the requirement for variable gain amplifiers, but this requirement in fact represents an excellent match between hybrid antenna design requirements and MMIC capabilities afforded in a distributed receiver implementation.

The Cassegrain configuration is recommended both for the scanning beam and the fixed beam design. This recommendation is summarized in Table 17. The recommendation of the same configuration for both the scanning and the fixed beam systems is favorable for the eventual integration of the two systems into one antenna assembly. The rationale for the selection of the recommended configurations is summarized in Table 18.

TABLE 16. ANTENNA CONFIGURATION SELECTION MULTIBEAM SCANNING ANTENNA COMPARISONS

	Gregorian	Cassegrain	Single Reflector
F/D	1	1.2	2.4
Main Reflector Diameter	271 λ	250 λ	250 λ
Subreflector Diameter	93 λ	110 λ	N/AP
Feed Beam	45 λ	86 λ	76 λ
Overall Length	296 λ	270 λ	600 λ
Number of Elements	1039	578	578
Active Elements	1039	19	19
Magnification	6	2	N/AP
Gain(1)	0° : 55.7 3.5°: 54.5	0° : 56.1 3° : 55.7	0° : 55.2 3° : 54.8
(SL)(1,2) Average	0° : N/AV 3.5°: N/AV	0° : -40 dB 3° : -40 dB	0° : -40 dB 3° : -40 dB
(SL)(1) Peak	0° : -40 3.5°: TBD	0° : -32 dB 3° : -31 dB	0° : -28 3° : -27
NF	5.2 dB	5.0 dB	6.3 dB
BCN (RF Beamforming)	6 × 1039:1	6 × 100:1	6 × 100:1
Total DC Power Consumption	6 × 44	6 × 6.0	6 × 6.0
Rel. Feed Array Weight	10	1	1
Element Diameter	1.33 λ	3.6 λ	2.7 λ
Variable Gain Range	Trim Only	40 dB	40 dB

(1) Scan Angle: dB

(2) Averaged Over Annular Region of 0.5° to 2.0° Radius

TABLE 17. RECOMMENDED ANTENNA CONFIGURATIONS DESCRIPTION

- Scanning Multiple Beam Antenna
  - Focal Plane Feed Array with Cassegrain Optics
  - "Microstrip" Yagi Radiating Elements
  - RF Beamforming Network, Uniformly Weighted Power Combiner
  - LNA, Phase Shifter, Variable Gain Amplifier MMIC RF Modules
- Fixed Multiple Beam Antenna
  - Focal Plane Feed Array with Cassegrain Optics
  - "Microstrip" Yagi Radiating Elements
  - RF Beamforming Network, Optimally Weighted Power Combiner
  - LNA, Phase and Gain Trim MMIC RF Modules

TABLE 18. RECOMMENDED ANTENNA CONFIGURATIONS SELECTION RATIONALE

- Focal Plane Optics Requires Smaller Feed Array
  - Fewer Elements
  - Lighter Weight
  - Lower Loss
  - No RF Power Division at the Element
  - Lower N/F
  - Lower DC Power
  - Less Circuit Routing Conflicts
- Cassegrain Optics Provide Superior Performance
  - Higher Gain
  - Lower Sidelobes
  - Lower N/F
- Cassegrain Optics Results in Shorter Structure
- RF Combining Provides Less Complex LO Power Distribution Network
  - Lighter Weight
  - Less Circuit Routing Conflicts
- "Microstrip" Yagi is MMIC Compatible
  - Minimal Transitions
  - Lightweight
  - Compact

4.0 RADIATING ELEMENT

The choice of a radiating element for use in the reflector antenna's primary feed array is based on criteria pertaining to electrical performance and mechanical interfacing. For the feed arrays under study, the element spacing in terms of wavelength is relatively wide, resulting in the formation of undesired grating lobes. The selected radiating element should therefore have relatively narrow E and H plane beamwidths (resulting in element gain) and low sidelobe levels to aid in the suppression of the grating lobes. These field pattern characteristics for the element should also remain essentially constant over the operating band.

To minimize interference between closely located fixed beams and adjacent sector scanning beams, alternate vertical and horizontal polarization is employed. Therefore, the radiating elements must provide independent dual polarization or be linearly polarized and amenable to being arranged in an interleaved orthogonal configuration. The linearly polarized elements must also have a cross polarization component that is low with respect to the co-polarized component.

To physically locate the active circuitry into the limited elemental area of the feed array, it is necessary to orientate the modules in a longitudinal fashion. To effect an efficient and reliable interface between the radiating elements and the modules, it is desirable that the elements also be orientated in a longitudinal manner. This arrangement is also dictated if the radiators are to have relatively narrow beamwidths and must fit within the elemental area.

Two classes of radiating elements were studied for application in the reflector antenna's primary feed. They are the conical horn excited for two orthogonal linear polarizations and printed end-fire radiators which include the zig-zag and the yagi. Due to its superior electrical performance for its physical size, the conical horn has been selected for application in the feed array.

4.1 CONICAL HORN RADIATOR

The conical horn antenna has been selected as the radiating element in the reflector antenna's primary feed array. For its physical size, it offers high directivity over the entire operating band (27.5 to 30.0 GHz). In addition, it may be excited to provide two orthogonal linear polarizations having coincident phase centers.

The electrical properties of the conical horn are dictated by its axial length "L", its aperture radius "a", (see Figure 45), and the propagating modes which are excited within the waveguide feed and within the horn's mouth. The initial studies considered horns which are excited in the fundamental TE_1 circular mode.

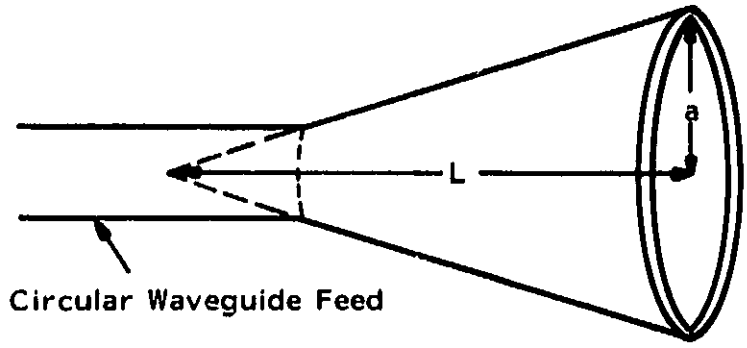

Figure 45. Conical Feed Horn

The far field radiation characteristics of various horn designs were determined using the vector diffraction formula as outlined by Narasimhan and Rao*. This technique yields the horn's radiation patterns for a calculated horn aperture field.

To achieve maximum element gain, the feed horn's aperture is selected to be as large as possible. Since the radiating elements of the primary feed array are arranged on an equilateral triangular grid with spacings of 3.232 cm. (3.1 λ at center band, 28.75 GHz), the horn outside diameter at the aperture is limited to this value. Therefore, if the horn wall thickness is 0.25 mm then the maximum conical horn aperture radius will be 1.526 λ at center band.

The calculated directivity for a 1.526 λ aperture radius horn as a function of its axial length is given in Figure 46. The longer the horn is made, the more constant the phase across its aperture becomes, resulting in higher directivity. However, it may be noted that the increase in directivity diminishes for subsequent increases of horn axial length.

A feed horn design having an axial length of 5.5 λ at center band has been selected. This design yields a far field directivity, as shown in Figure 47, of 18.5 to 19.4 dBi over the 27.5 to 30.0 GHz band. This level is compatible with the requirements for the primary feed array. The far field E- and H-plane patterns at center band are shown in Figure 48. The half-power beam widths for each of these cuts is on the order of 19°.

The fundamental TE_{11} mode conical horn will have low cross-polarization components in its principal planes. The cross-polarization in the diagonal planes may be minimized by the selection of the aperture size. Adatia, et al** have shown that cross-polarization radiation in the diagonal planes theoretically vanishes for an aperture radius of 0.575 λ. This size, however, restricts the maximum possible directivity to a level lower than that required for the elements of the primary feed array.

---

* Narasimhan and Rao, "Radiation from Conical Horns with Large Flare Angles," IEEE Transactions on Antennas and Propagation, Vol. AP-19, pp. 678-681, Sept. 1971.

** Adatia, Rudge, and Parini, "Mathematical Modeling of the Radiation Fields from Microwave Primary-Feed Antennas," Proc. 7th European Microwave Conference, Copenhagen, 1977.

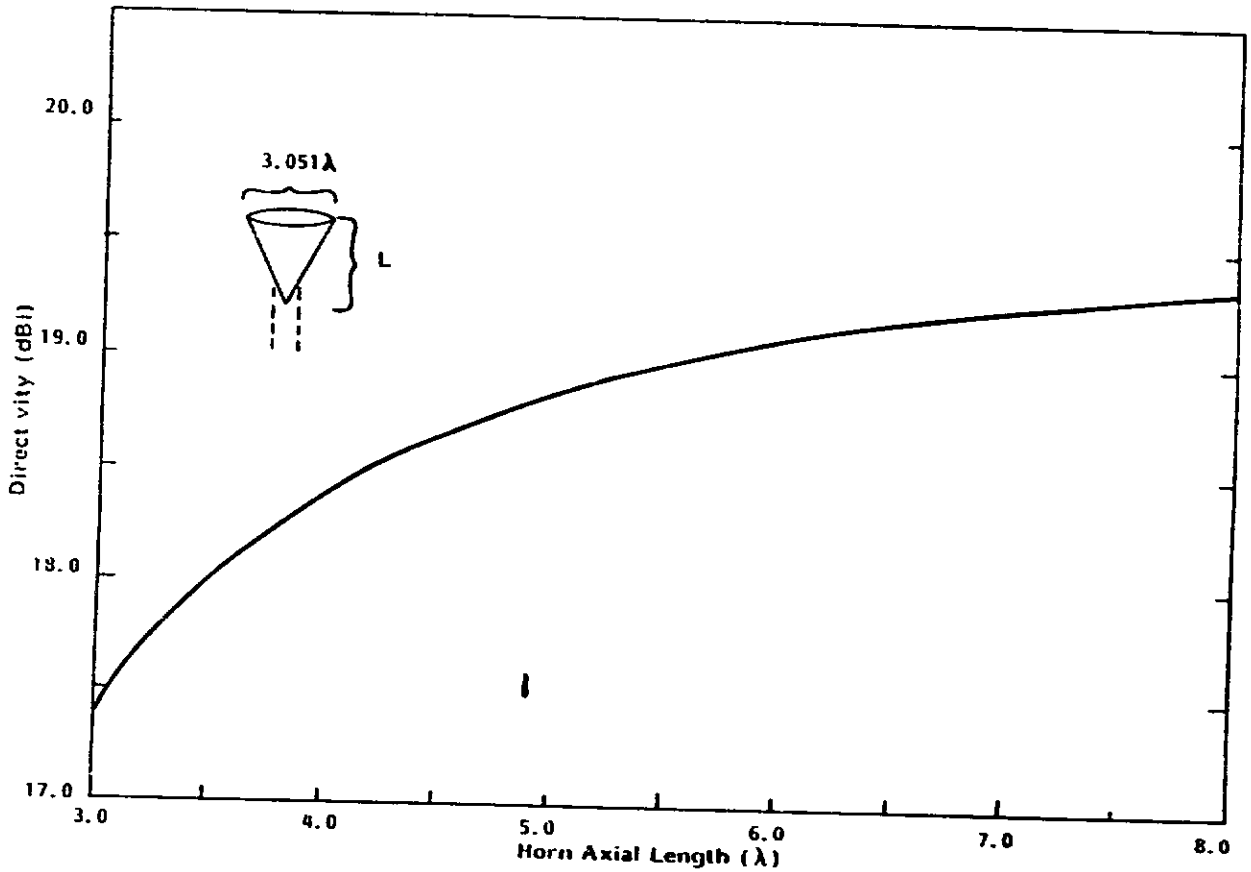

Figure 46. Directivity of a 1.526λ Aperture Radius TE_{11} Conical Horn

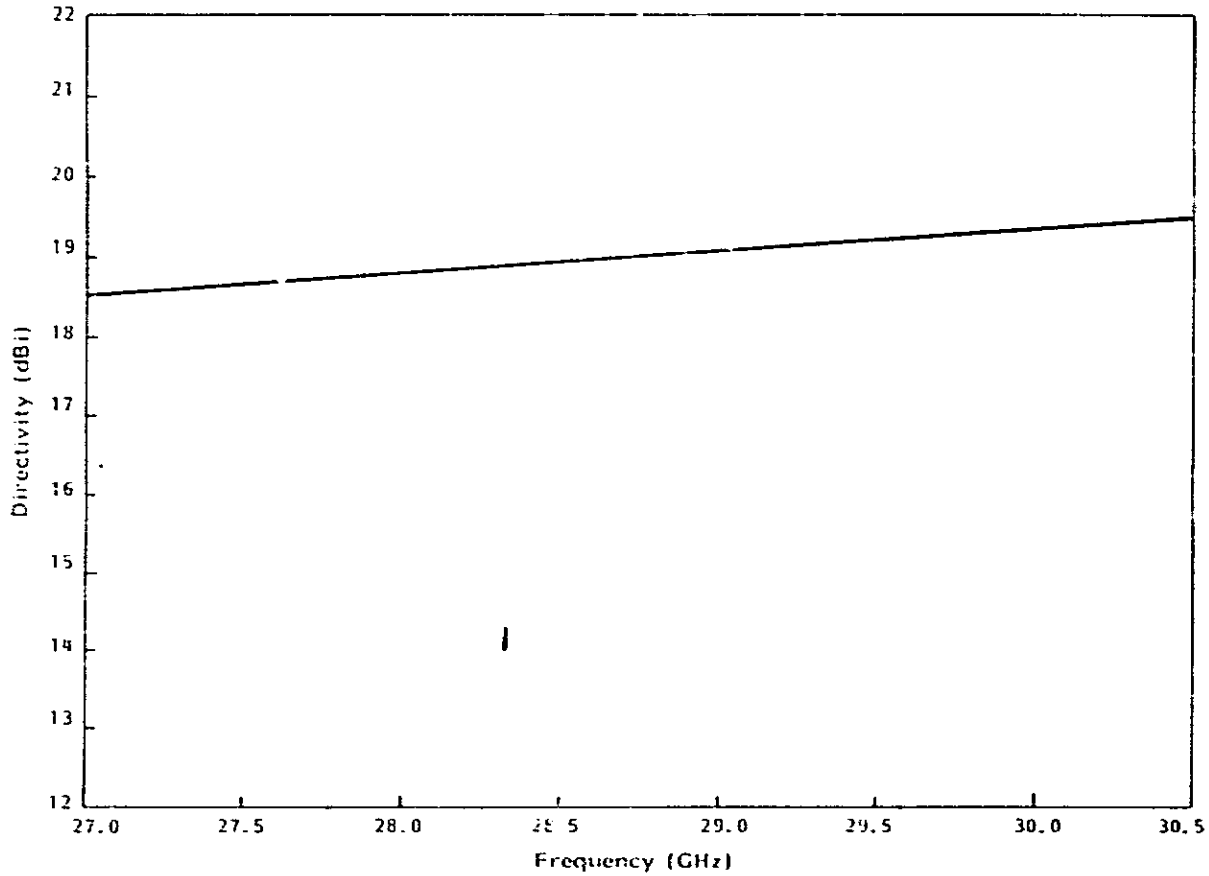

Figure 47. Directivity vs Frequency
TE_{11} Conical Horn
Aperture Radius = 1.59 cm
Axial Length = 5.73 cm

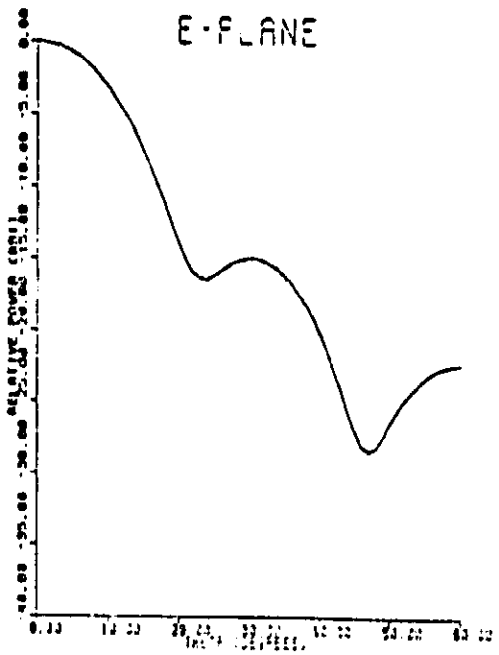

A) E-Plane

B) H-Plane

Figure 48. Far Field Patterns for TE_{11} Mode Conical Feed Horn
Aperture Radius = 1.526
Axial Length = 5.5

The cross-polarization components may alternately be reduced by the inclusion of higher order modes of the proper magnitude and phase with respect to the fundamental TE_{11} mode. As an example, the far field diagonal plane patterns for a 1.17 λ aperture radius conical horn with relative higher order mode levels at the aperture of:

$$TM_{11}/TE_{11} = 0.1453$$

$$TE_{12}/TE_{11} = -0.0052$$

are shown in Figure 49. The TM_{11} mode is in phase with the TE_{11} mode at the aperture while the TE_{12} mode is 180° out of phase (as denoted by the minus sign). The component mode main- and cross-polarization far-field patterns relative to isotropic for the TE_{11}, TM_{11}, TE_{12}, and rim current at the aperture edge are given in Figures 49A through 49E. The phase of the TE_{11} cross-polarization signal is 180° with respect to the others. Note that the TM_{11} has equal main- and cross-polarizations in this plane which approximately match the shape of the TE_{11} cross-polarization lobe. Overlaying the TE_{11} and TM_{11} patterns gives a clear indication of the difference in power levels for cross-polarization cancellation at any desired aspect angle.

4.1.1 Feed System for the Conical Horn Radiator

The conical horn radiator is fed by a section of cylindrical waveguide. The inside diameter of the guide is selected so that only the fundamental TE_{11} mode will be supported. Choosing the standard WC 28 waveguide size which has an inside diameter of 0.714 cm places the TE_{11} cutoff frequency at 24.64 GHz. The next higher TM_{01} mode cutoff frequency for this guide is at 32.19 GHz which is above the band of interest.

The fundamental mode is excited in the waveguide by a coaxial E-field probe which extends through the wall of the guide to the microstrip circuitry of the active receive module. Two orthogonal probes are employed to achieve the independent vertical and horizontal feed horn polarizations. The arrangement is shown in Figure 50. The input guide impedance at the probe is determined primarily by the probe length ℓ and the probe location with respect to the shorting back plane C*. A vertical grid within the guide provides an effective short for the vertical component of the electric field.

---

* Deshpanole and Das, "Input Impedance of a Coaxial Line to Circular Waveguide Feed," IEEE Transactions on Microwave Theory and Techniques, Vol. MTT-25, pp. 954-957, Nov. 1977.

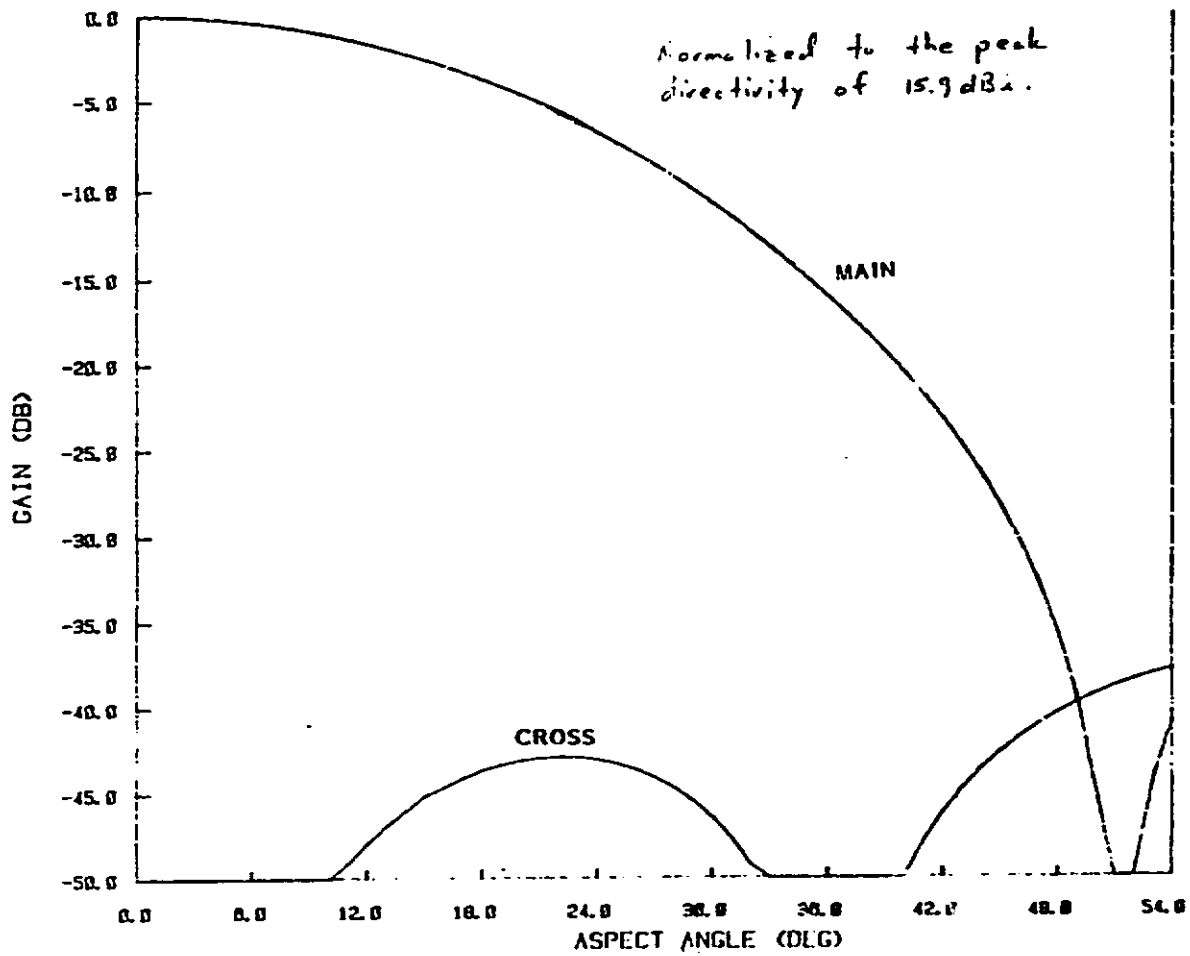

Figure 49A. Net Far-Field Pattern (Diagonal Plane)

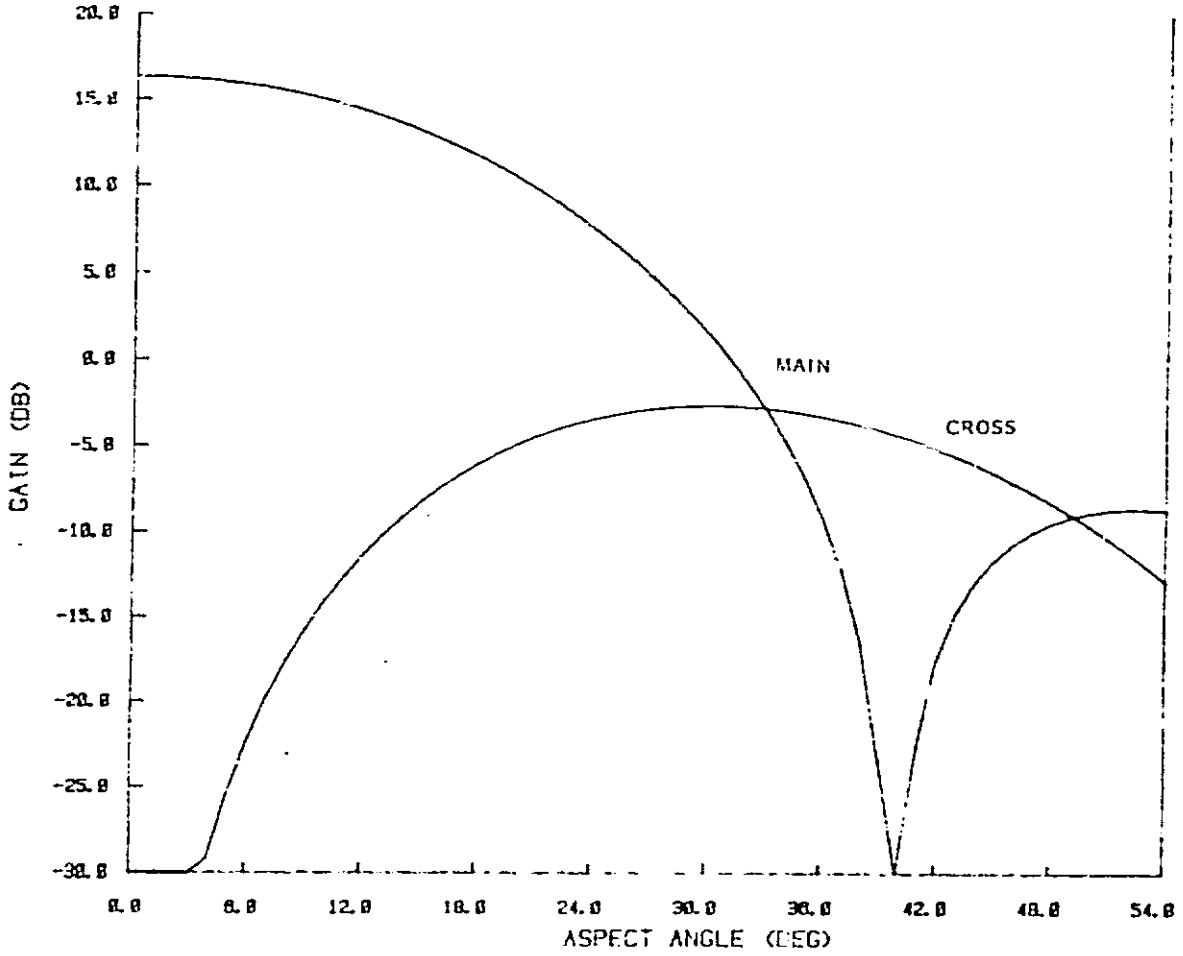

Figure 49B. TE_{11} Mode Pattern (Diagnonal Plane)

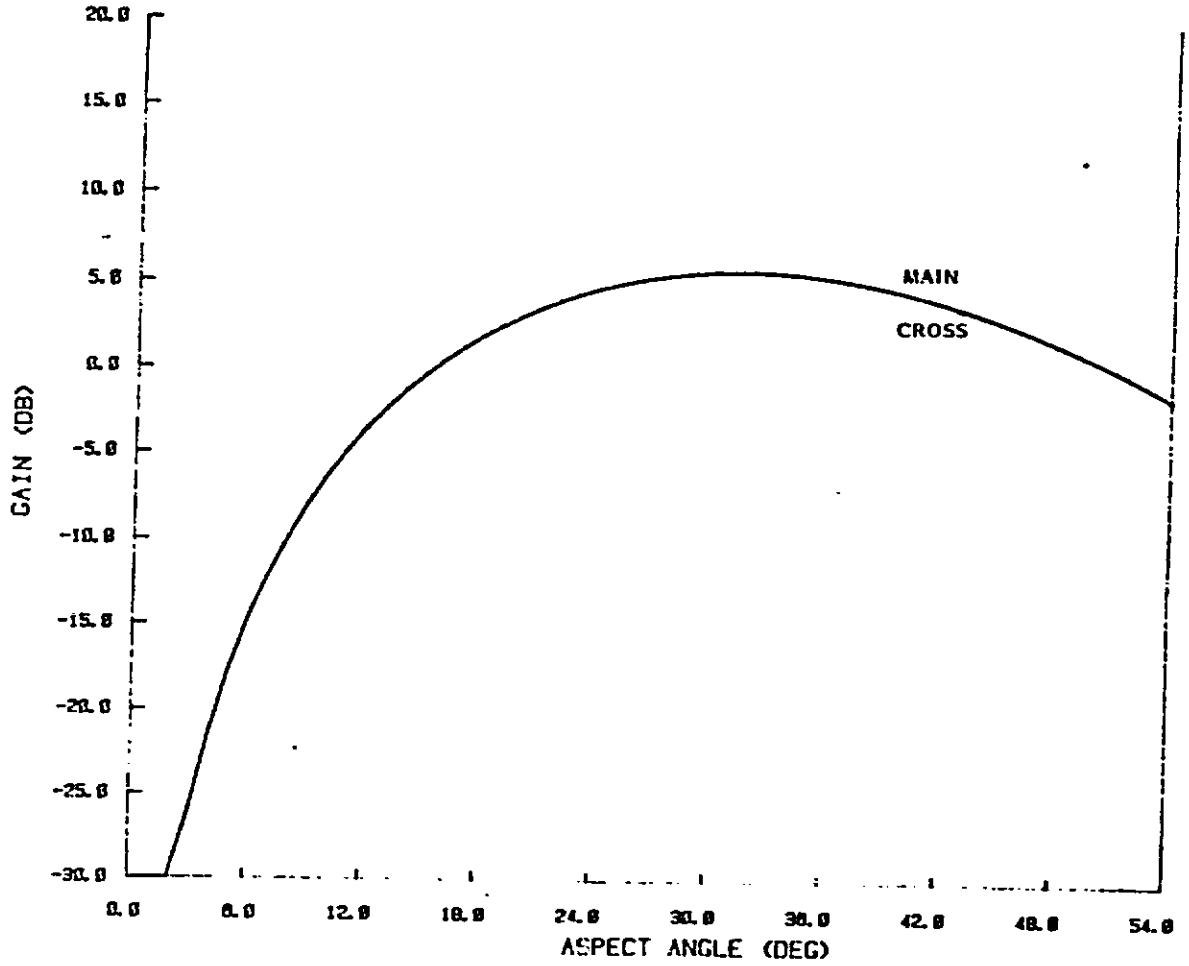

Figure 49C. TM_{11} Mode Pattern (Diagonal Plane)

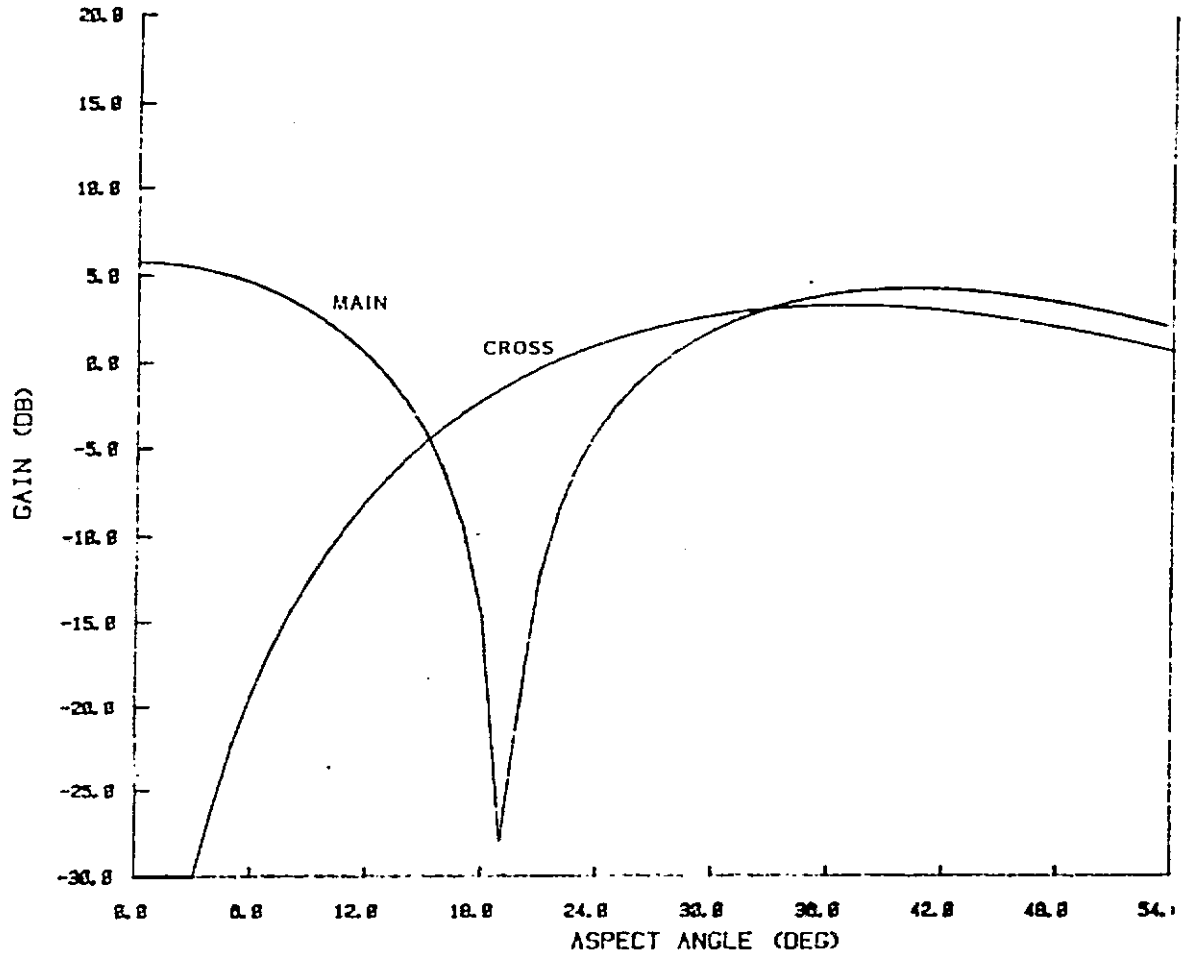

Figure 49D. TE_{12} Mode Pattern (Diagonal Plane)

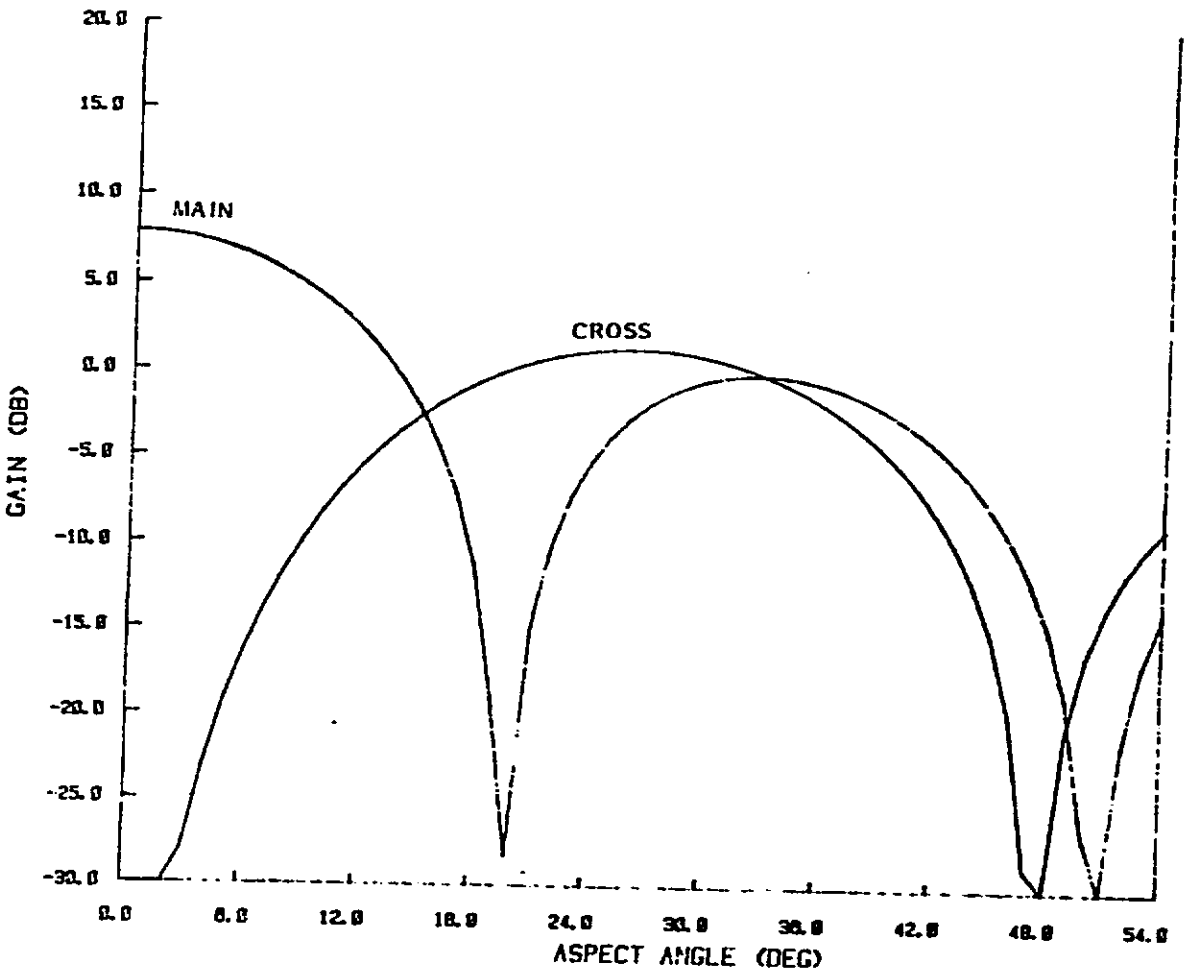

Figure 49E. Rim Current Pattern (Diagnonal Plane)

Figure 49. Computed Multi-Mode Concial Horn Diagonal Plane Far-Field Pattern

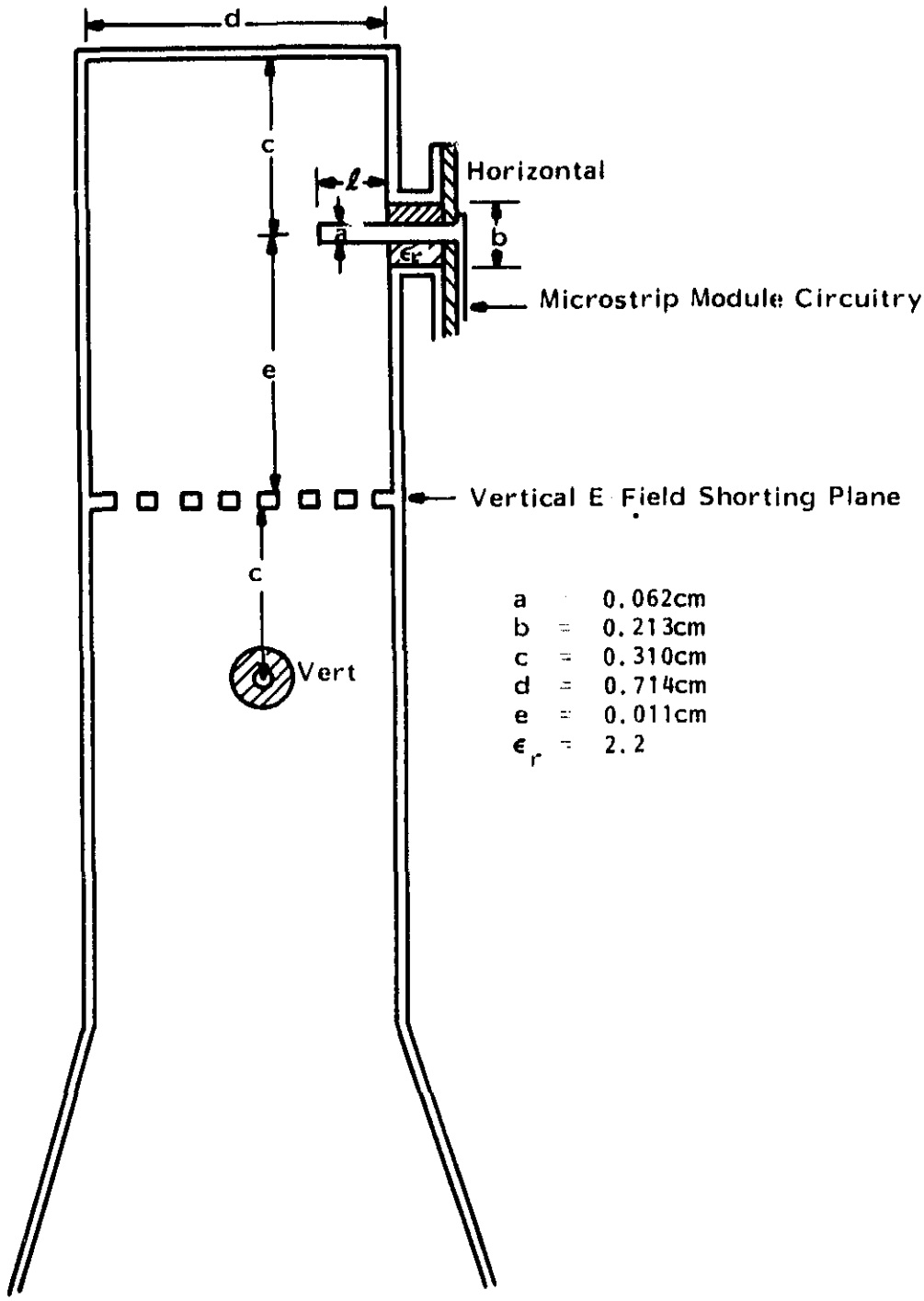

Figure 50. Coaxial Probe Transition for Interfacing the Conical Horn Radiating Elements and the MMIC Receive Modules

The inside and outside conductor diameters and the dielectric fill of the coaxial probe are selected to result in the desired probe impedance and to place the cutoff frequencies of the non-TEM coaxial modes above the 30 GHz upper band limit.

4.1.2 Mutual Coupling with Conical Horn Radiating Elements

The perturbation due to mutual coupling of the desired excitation of a cluster of conical horn feed elements has been investigated. The method used to determine element to element coupling was developed by Steyskal*.

The dual reflector scanning antenna feed array consists of a cluster of 19 active elements. The 19 elements are conical horns arranged on an equilateral triangular grid with spacings of 3.1 λ at center band. The horns have aperture radii of 1.526 λ and are excited in the TE_{11} fundamental mode. The arrangement of the feed cluster horns is shown in Figure 51.

The design excitations of the feed elements for a typical scanning beam (case 203a) are labeled in Figure 51A. Both the amplitude and phases are given normalized to the excitation of the cluster's center element. The resultant excitations, which are the design excitations modified due to mutual coupling effects, are given in Figure 51B. The perturbation defined as design minus resultant excitations are reported in Figure 51C. As is evident in this last figure, the effects of mutual coupling on the design excitations of the feed array employing high gain conical horns is insignificant.

4.2 PRINTED RADIATING ELEMENTS

End-fire radiating elements that may be printed directly onto a supporting substrate were studied as an alternative to the conical horn radiator for application in the reflector antenna's primary feed array. These type of elements offer the advantage that they can be interfaced directly with the monolithic active circuitry. However, since their practical limit of directivity appears to be in the neighborhood of 15 dBi, they were judged inadequate for application in the selected antenna configuration. These style of elements may be employed in other reflector/feed configurations which require a lower level of elemental gain.

Two types of printed end-fire radiating elements have been studied. These are the zig-zag and the yagi. The physical dimensions for both radiators were developed using a method-of-moments computer program. For the zig-zag, the peak directive gain, sidelobe level, and operating bandwidth are determined by the element's section lengths, section pitch angles, the total number of sections, and by the spacing of the radiator from the feed ground plane. A six-section 1.62 λ long design that was arrived at by

---

* Steyskal, "Analysis of Circular Waveguide Arrays on Cylinders," IEEE Transactions on Antennas and Propagation, Vol. AP-25, pp. 610-616, Sept. 1977.

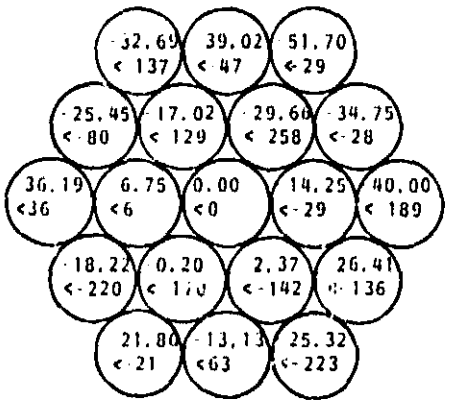

(a) Design Excitations

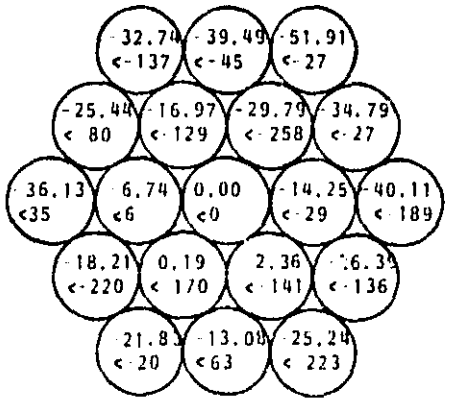

(b) Excitations Perturbed by Mutual Coupling

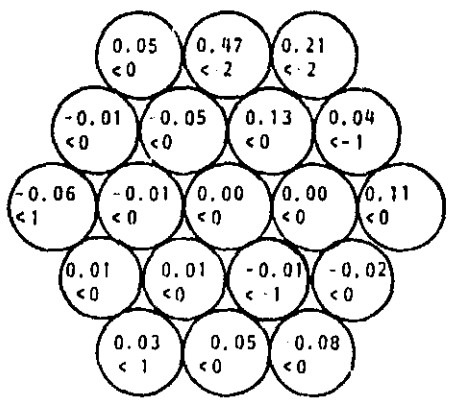

(c) Difference Between Design and Perturbed Excitations

Figure 7 Scanning Beam Feed Cluster Excitations
Element Excitation Magnitude Given in dB, Angle in Degrees

computer modeling is shown in Figure 52. The calculated E and H plane far field patterns for this design are shown in Figure 53. The directivity at center band in the end-fire direction is on the order of 15 dBi. The calculated directivity as a function of frequency is shown in Figure 54.

Two zig-zag elements were fabricated based on the dimensions from the computer model. One was self-supporting, being etched out of brass, while the other was printed onto a teflon-glass supporting substrate. Figure 55 shows the H-plane principal pattern and cross-polarization pattern for the self-supporting element operating at center band. The measured peak gain is approximately 12 dBi which is 3 dB less than the calculated maximum directivity. Some of this discrepancy may be attributed to the mismatch at the connector to feed transition in the test antenna. The cross-polarized component remains essentially 20 dB below the co-polarized component in the element's main lobe.

The six-section zig-zag radiator printed onto a supporting substrate is shown in the photograph of Figure 56. The measured H-plane principal plane pattern and cross-polarization pattern for this element is given in Figure 57. The center frequency was found to be shifted down 11% from its self-supported counterpart. It was also found that the main lobe broadened and that the cross-polarized component increased. These results indicate the segment length and pitch angle must must be altered for the dielectrically supported design.

Both calculations and measurements indicate that the zig-zag's performance is highly dependent upon frequency. This is evident in the end-fire directivity versus frequency plot of Figure 54. An alternative radiator which may be designed to have less gain variation over the required band is the Yagi - Uda array. Two of the designs investigated are shown in Figure 58A and B. One design is comprised of ten elements and has an overall length of 1.8 λ. The parasitic element spacing and taper schedule were selected so as to make the directivity relatively constant over a 12% bandwidth. The second yagi is comprised of fifteen elements and has an overall length of 4.2 λ. The parasitic element spacing and taper schedule for this antenna are based on a National Bureau of Standards maximum gain design.*

The calculated free-space end-fire directivity as a function of frequency for the two yagi designs are shown in Figure 59. It is seen that the ten-element yagi has a wide directivity bandwidth while the larger yagi provides a higher peak directivity and is more dependent on frequency. In both cases, the directivity over the required band is less frequency dependent than for the zig-zag radiator. The calculated E- and H-plane patterns at center band for these two designs are given in Figure 60A and B.

---

* Viezbicke, "Yagi Antenna Design," National Bureau of Standards Technical Note 688, Boulder, Colorado, 1976.

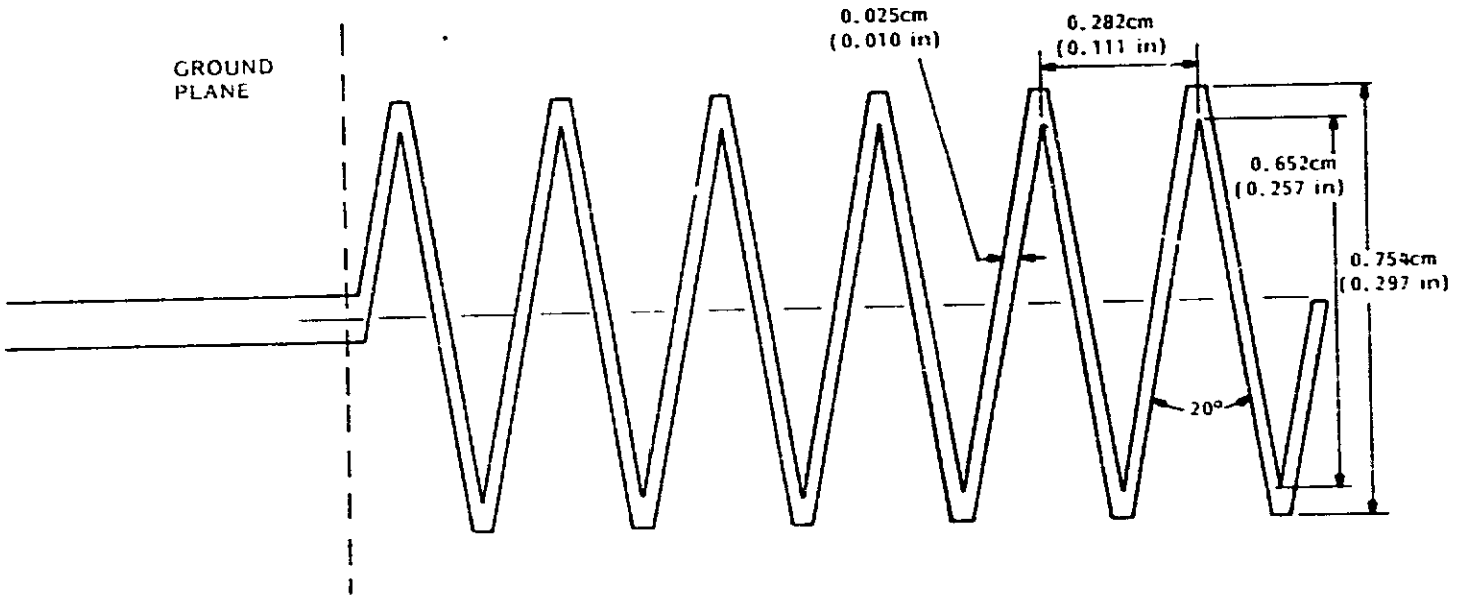

Figure 52. Six-Section Zig-Zag End-Fire Radiator

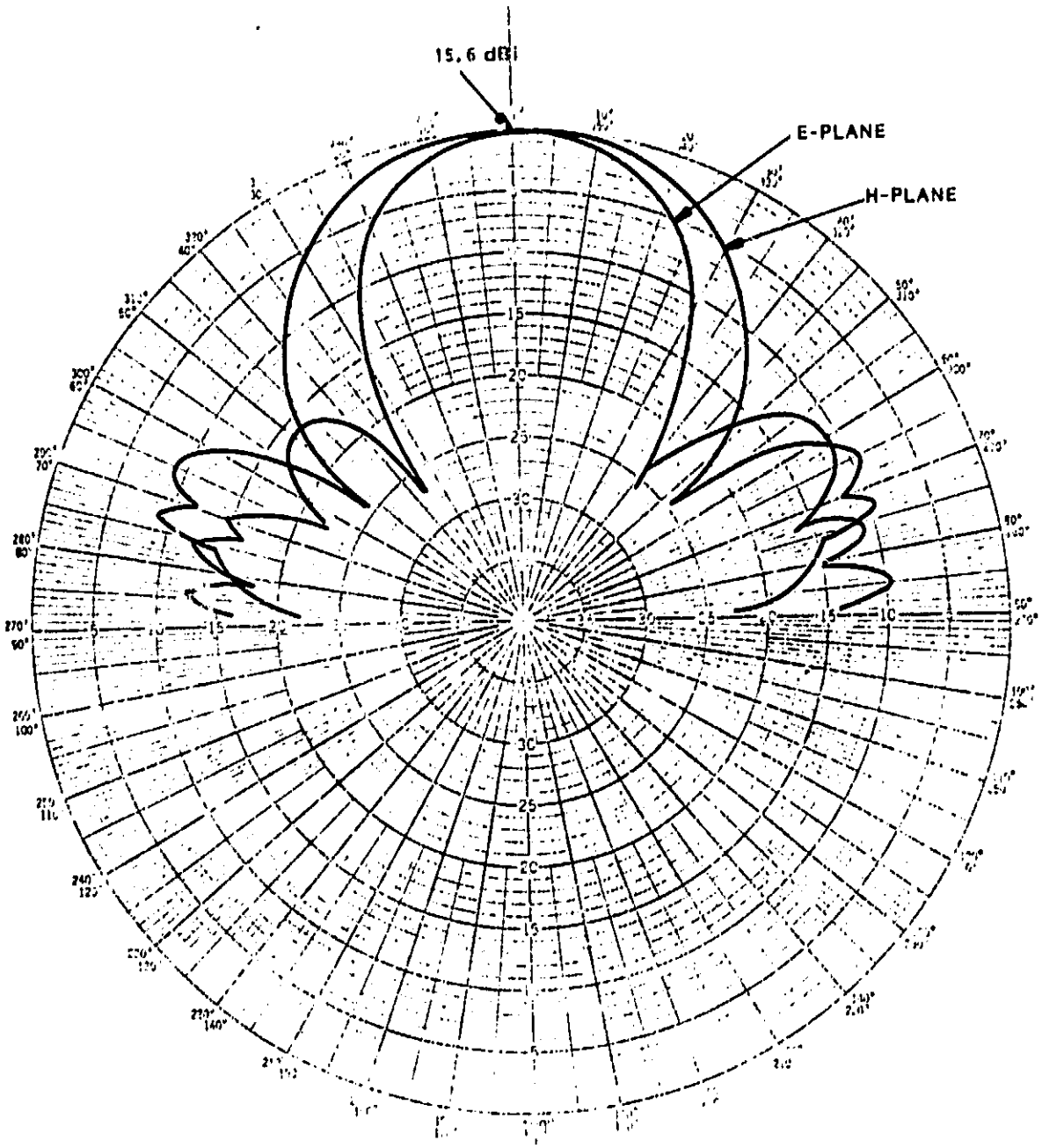

Figure 53. Six Section Zig-Zag Calculated Patterns - Center Band

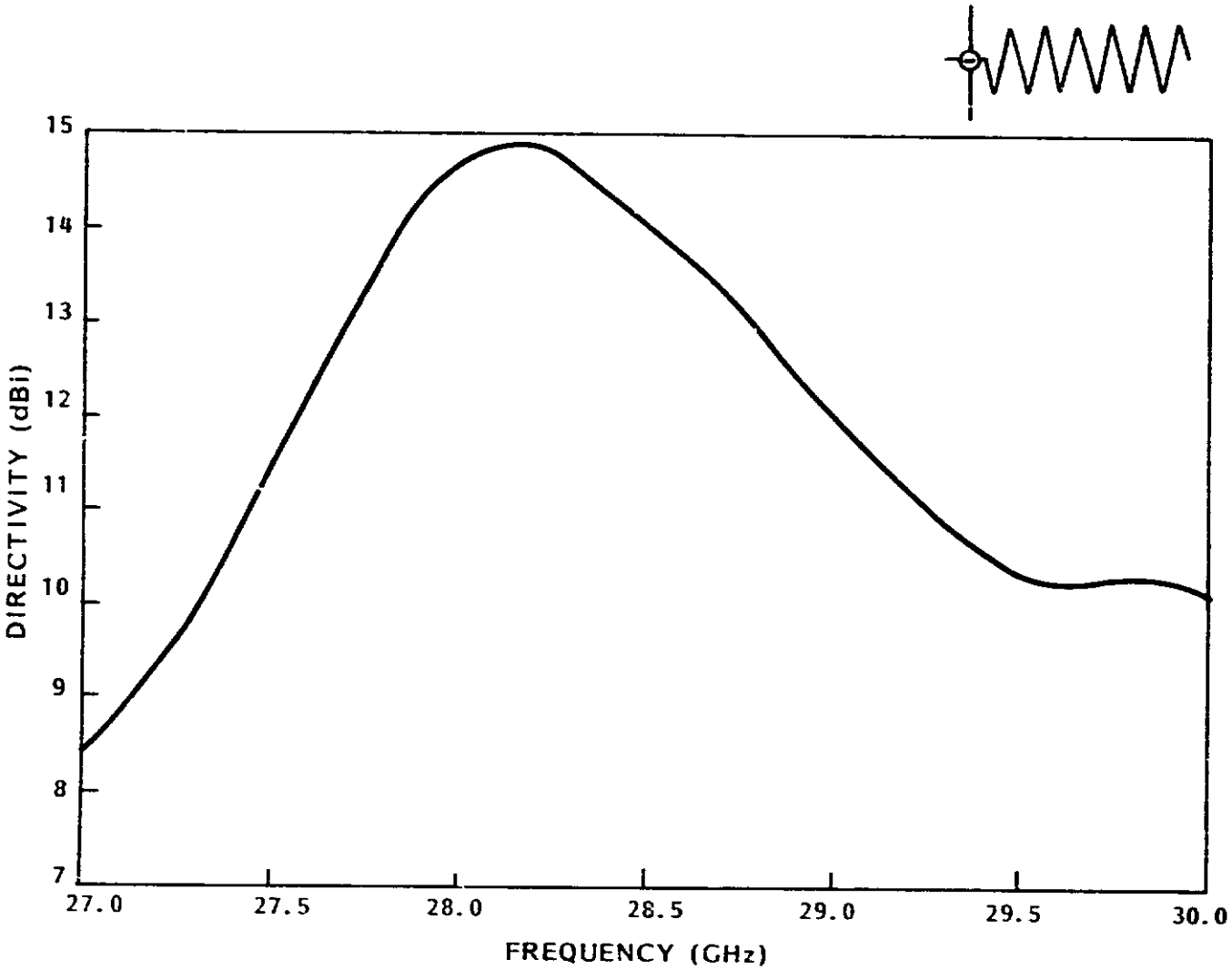

Figure 54. Calculated End-Fire Directivity vs Frequency - Six Section Zig-Zag

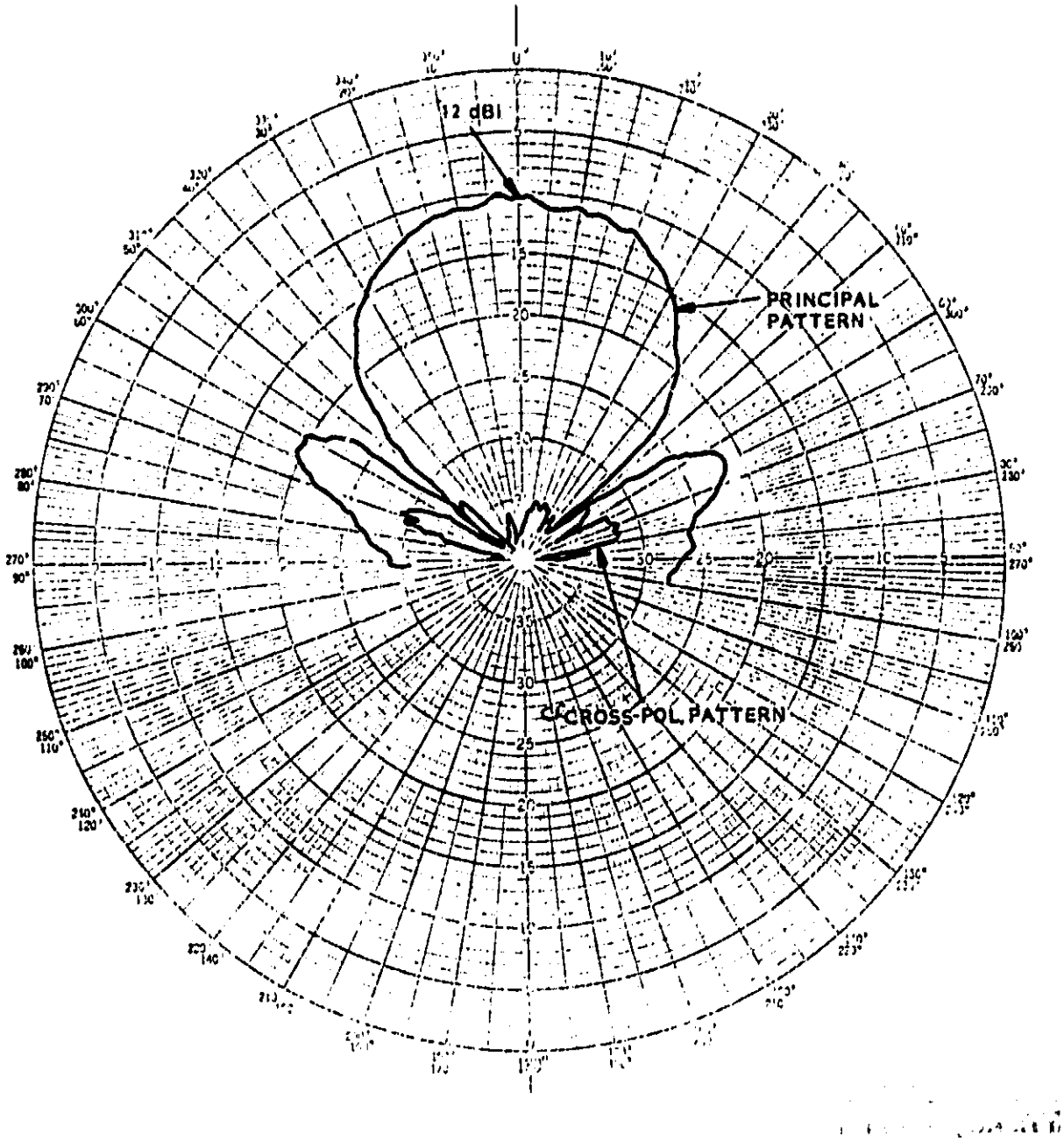

Figure 55. Six Section Self-Supported Zig-Zag H-Plane Measured Patterns

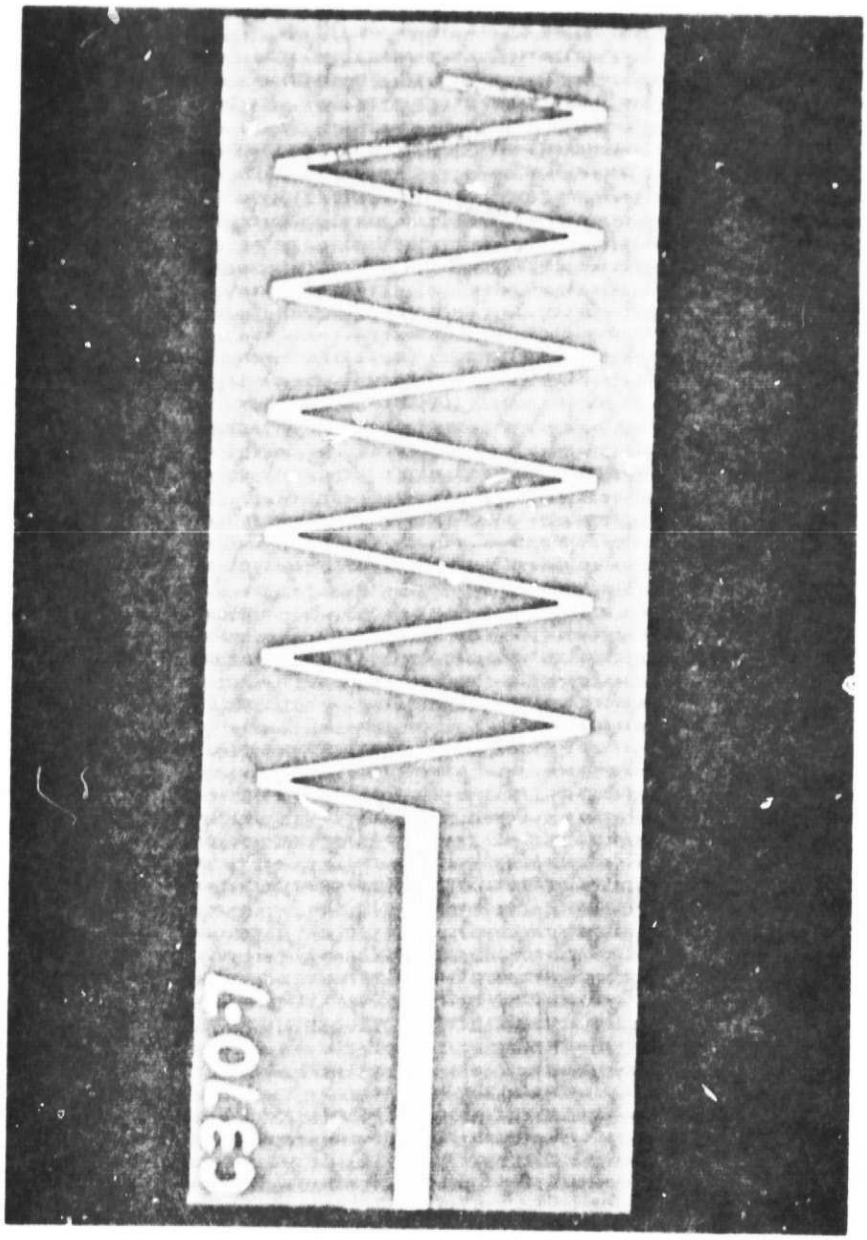

Figure 56. Six-section Zig-Zag Radiator Printed onto a Supporting Substrate

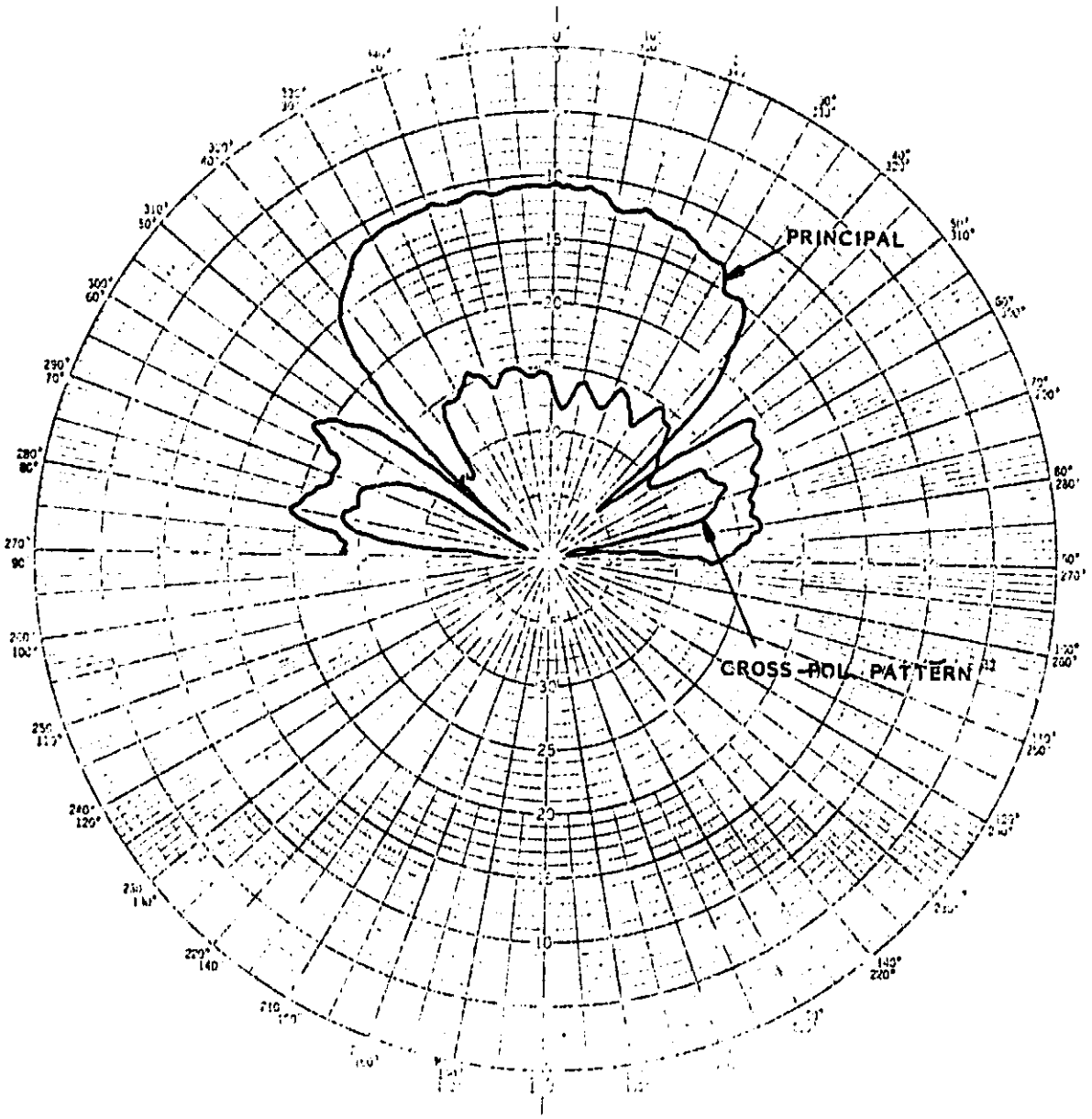

Figure 57. Six Section Dielectric Supported Zig-Zag H-Plane Measured Patterns

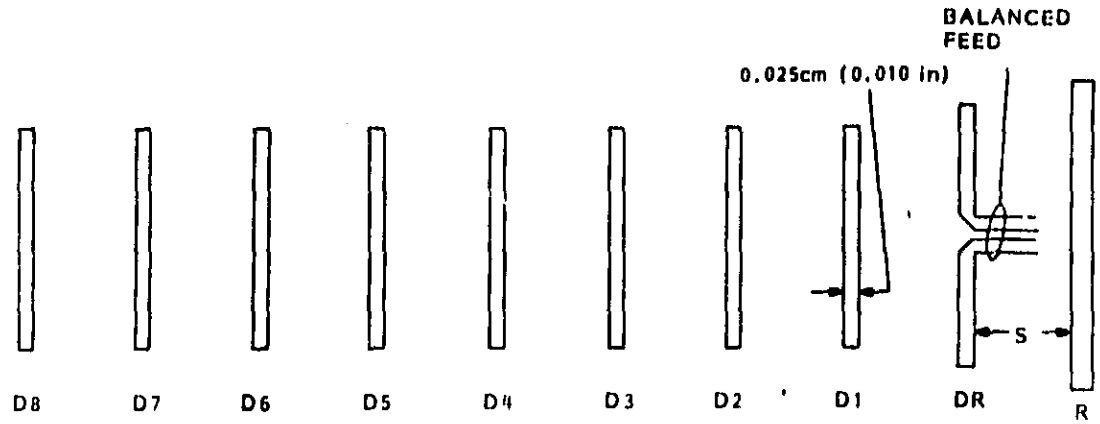

ELEMENT	LENGTH	
REFLECTOR (R)	0.547 cm	(0.215 in)
DRIVEN (DR)	0.463 cm	(0.182 in)
DIRECTORS (D1-D8)	0.394 cm	(0.155 in)

ALL ELEMENT SPACINGS ARE 0.206 cm (0.081 in)

Figure 58A. Ten Element, 1.8λ Long Design

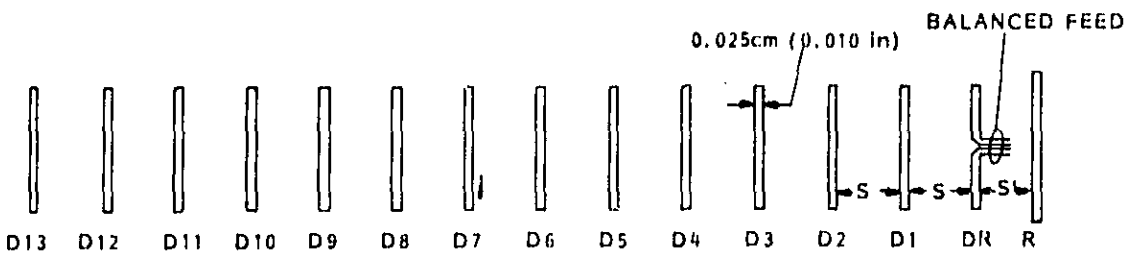

ELEMENT	LENGTH
REFLECTOR (R)	0.487 cm (0.192 in)
DRIVEN (DR)	0.456 cm (0.180 in)
DIRECTORS (D1, D2)	0.426 cm (0.168 in)
DIRECTOR (D3)	0.409 cm (0.161 in)
DIRECTOR (D4)	0.408 cm (0.160 in)
DIRECTOR (D5)	0.404 cm (0.159 in)
DIRECTOR (D6)	0.397 cm (0.156 in)
DIRECTOR (D7)	0.393 cm (0.155 in)
DIRECTORS (D8 D13)	0.388 cm (0.153 in)

REFLECTOR TO DRIVEN SPACING (S') - 0.205 cm (0.081 in)
ALL OTHER ELEMENT SPACINGS (S) - 0.316 cm (0.125 in)

Figure 58B. 15 Element, 4.2λ Long NBS Design
Figure 58. Yagi-Uda End-Fire Radiators

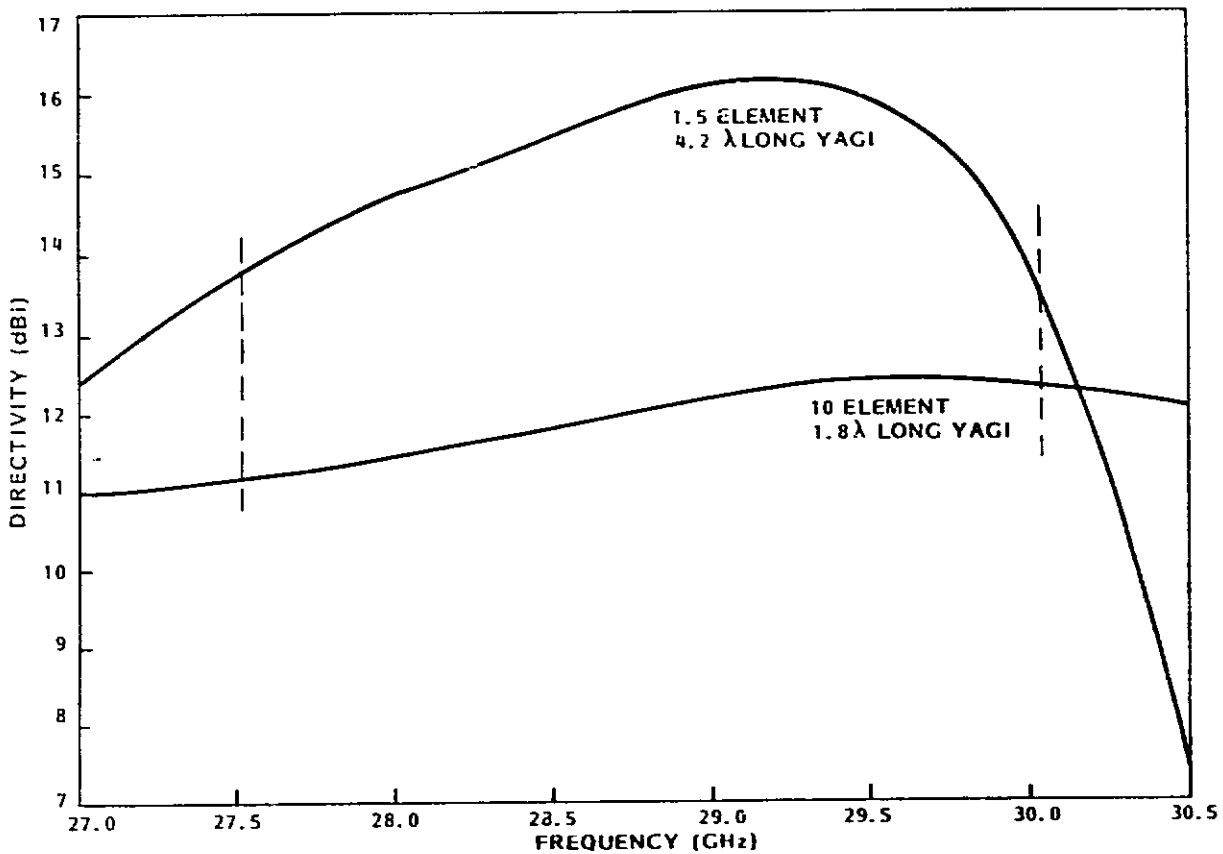

Figure 59. Directivity vs Frequency-10 and 15 Element Yagi Designs

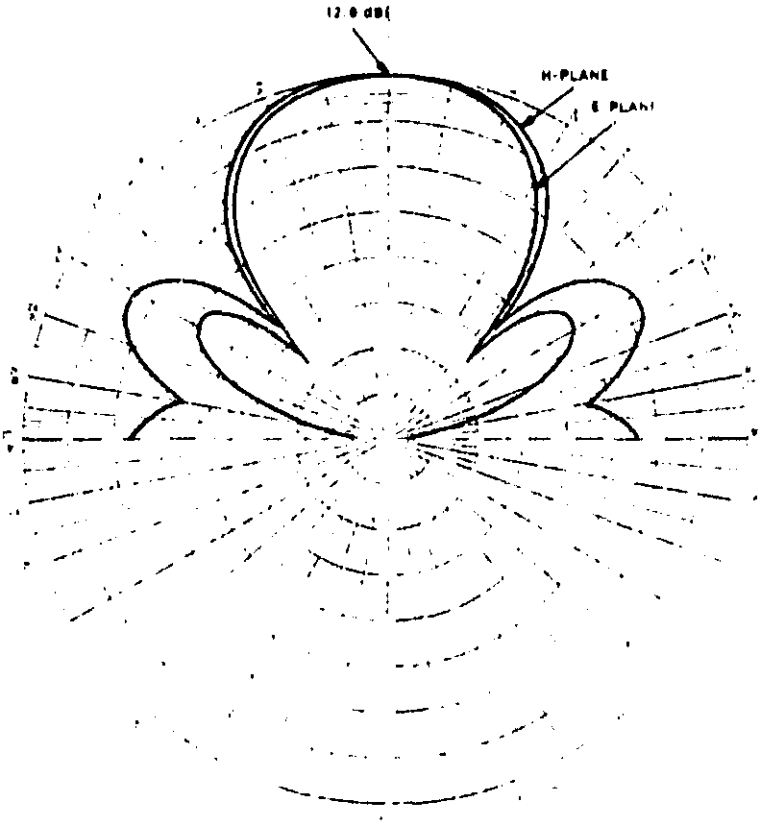

Figure 60A. Ten Element 1.8λ Long Yagi Band

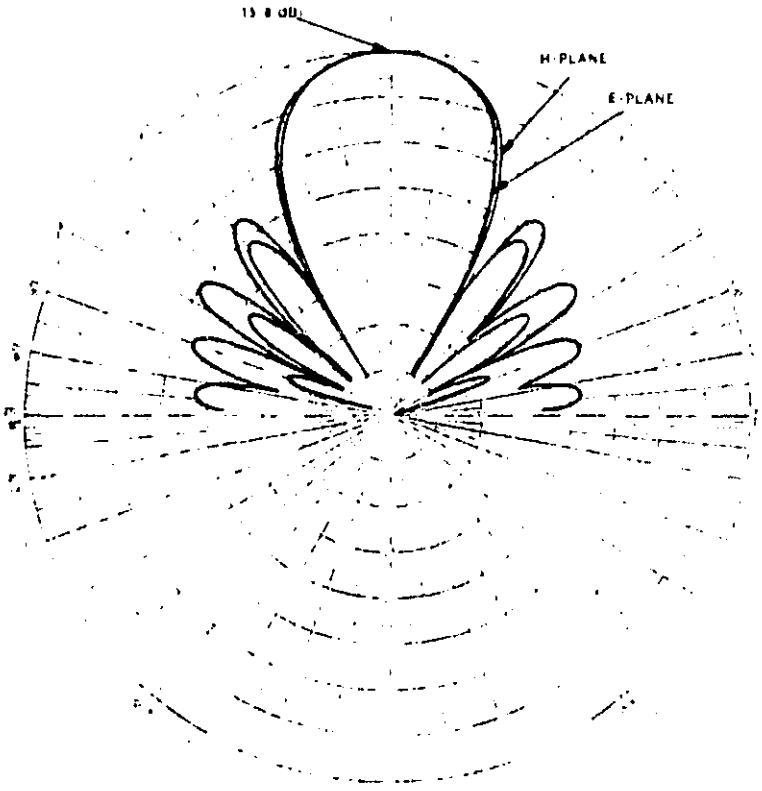

Figure 60B. 15 Element 4.2λ Long Yagi
Figure 60. Calculated Far Field Patterns - Center Band

The ten element yagi design was printed onto a teflon-glass supporting substrate which is shown in the photograph of Figure 61. The driven element is fed by a coplanar balanced transmission line. The reflector element is located on the backside of the substrate so as to avoid interference with the feed line. For testing purposes, a diode was bonded across the gap of the balanced line at the point where the two conductors diverge. Pattern measurements were then performed by detecting a modulated field signal. This allowed for evaluation of the yagi antenna exclusively as opposed to the combination of the yagi and a balanced line to unbalanced microstrip transition.

Antenna pattern measurements of the ten element yagi indicate that it has an operating bandwidth of approximately 15%. The center frequency, however, is 13% lower than the free-space design value. This lowering is due to the dielectric supporting substrate. The measured E- and H-plane patterns at 26.0 GHz are shown in Figure 62. The cross polarized components are greater than 20 dB down from the principal plane components.

4.2.1 Feed System for the Printed Yagi Radiator

The yagi radiator is fed by a balanced coplanar transmission line which is printed directly onto the same substrate that supports the yagi's elements. The characteristic impedance of the balanced line is selected to match the nominal yagi driven element feed point impedance. The balanced feed is transitioned to the microstrip format of the monolithic circuitry via a printed circuit balun.

The configuration of the dielectrically supported balanced line is shown in Figure 63. The characteristic impedance of the line may be determined by modeling it as a pair of coupled microstrip lines on a suspended substrate operating in the odd mode. The bottom ground plane is considered to be located a relatively large distance with respect to the substrate thickness so that balanced line impedance becomes equal to twice the calculated microstrip odd mode impedance;

$$Z \text{ (balanced line)} = 2\, Z_{odd}\ (\mu \text{ strip}).$$

The effective dielectric constant for the balanced line configuration is equal to that calculated for the coupled microstrip lines.

For a 0.254 mm (0.010 inch) thick alumina supporting substrate, the balanced line configuration with practical line widths and spacings has a lower impedance limit of approximately 70 ohms. This lower bound is due to the limiting value of line to line capacitance available in the coplanar configuration. An impedance of 100 Ω was selected for the yagi feed line. This corresponds to an alumina supporting substrate thickness h of 0.254 mm (0.010 inch), line widths B of 0.254 mm, and a line spacing s of 0.117 mm (0.0046 inch) (see Figure 63).

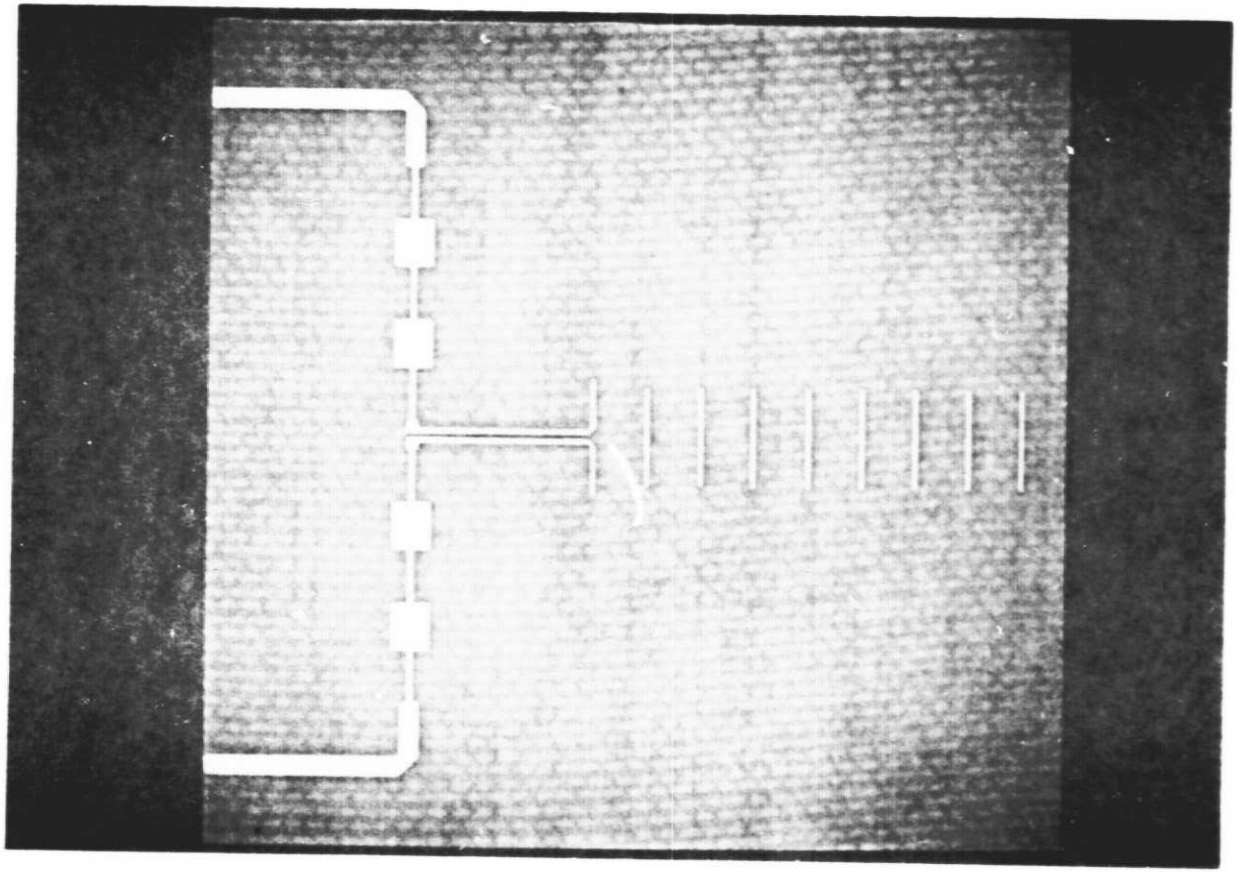

Figure 61. Ten Element Yagi Printed onto a Supporting Substrate

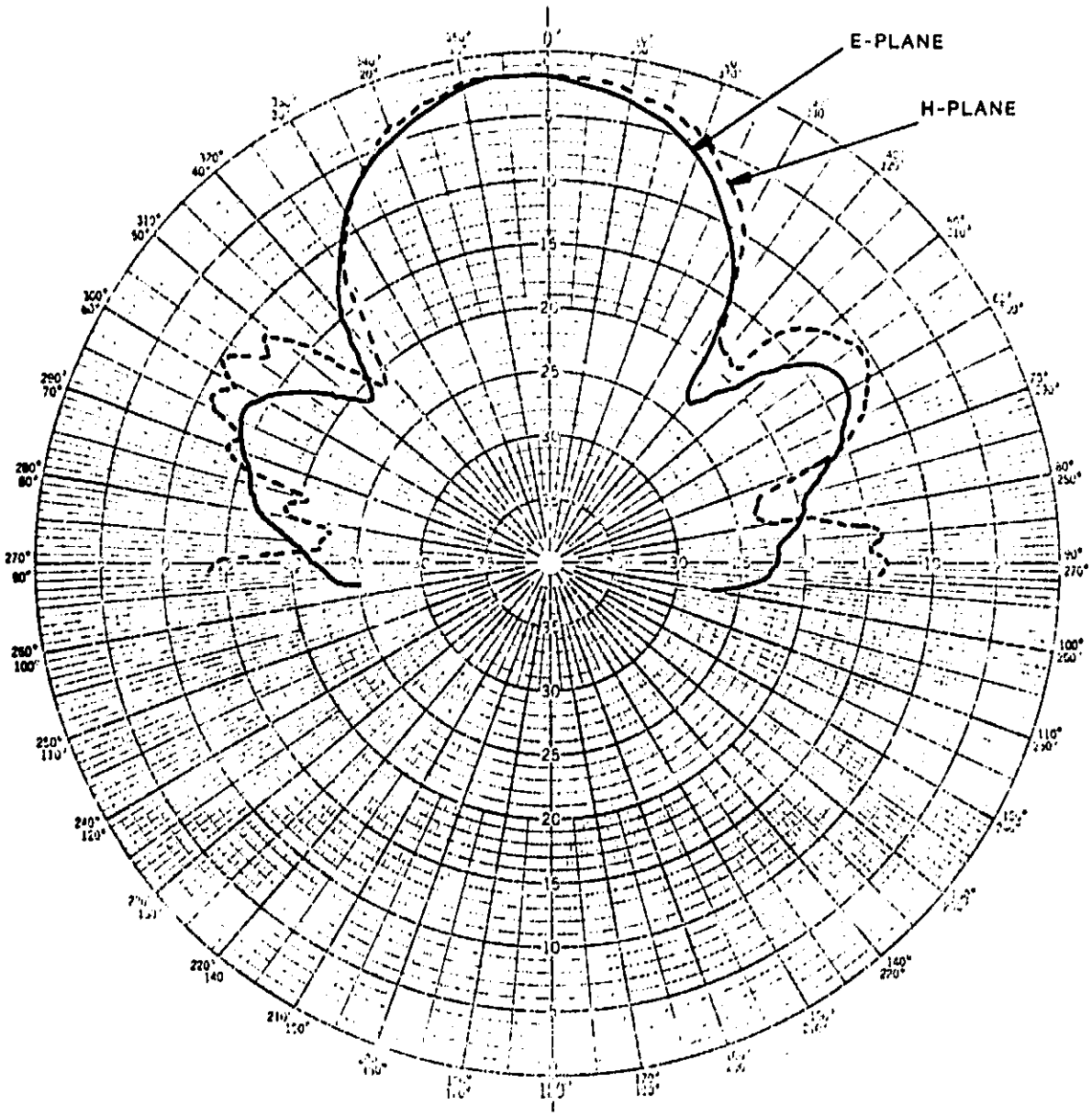

Figure 62. Ten Element 1.8λ Long Dielectric Supported Yagi Measured Principal Plane Patterns

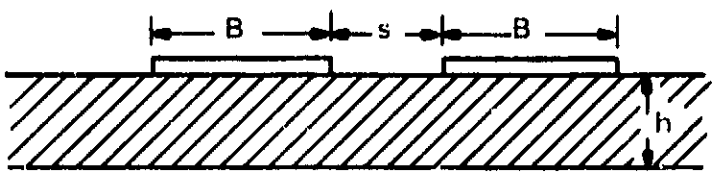

B = CONDUCTOR WIDTHS
s = GAP SIZE
h = SUPPORTING SUBSTRATE THICKNESS

Figure 63. Balanced Yagi Feed Line Configuration

The calculated real and imaginary parts of the driven element feed point impedance for the 15 element, 4.2 λ long yagi design of Figure 58B is shown in Figure 64. As seen in the plot, the resistive portion R has a nominal value of 25 Ω over the band of interest while the reactive part X is centered about zero ohms. To match the 25 Ω feed point impedance to the 100 Ω balanced line, the open dipole driven element of the design of Figure 58B may be replaced by an equal length folded dipole to effect an impedance transformation. The transformation ratio T_z is given by*

$$T_z = \frac{Z_f}{Z_r} = \left[1 + \frac{\cosh^{-1}\left(\frac{a^2 - b^2 + 1}{2a}\right)}{\cosh^{-1}\left(\frac{a^2 + b^2 - 1}{2ab}\right)} \right]^2$$

where

Z_f = folded dipole impedance,
Z_r = unfolded dipole impedance,
$a = d/r_1$
$b = r_2/r_1$

with r_1 and r_2 being the radii of the dipole arms and d being their centerline spacing. For a printed dipole with arm widths w_1 and w_2, the equivalent radii are approximated by

$$r_1 = 0.25\ w_1$$
$$r_2 = 0.25\ w_2 \ .$$

Therefore to match the dipole driven element to the 100 Ω feed line impedance, the transformation ratio T_z must be equal to 4. This corresponds to the special case of parameter values b equal to 1 and a greater than or equal to 2.

The width of the folded dipole arms may be conveniently chosen to be equal to the conductor widths of the balanced feed line. A drawing of the folded dipole yagi driven element is given in Figure 65.

---

* Jasik, Antenna Engineering Handbook, McGraw-Hill, 1961, Section 3.3

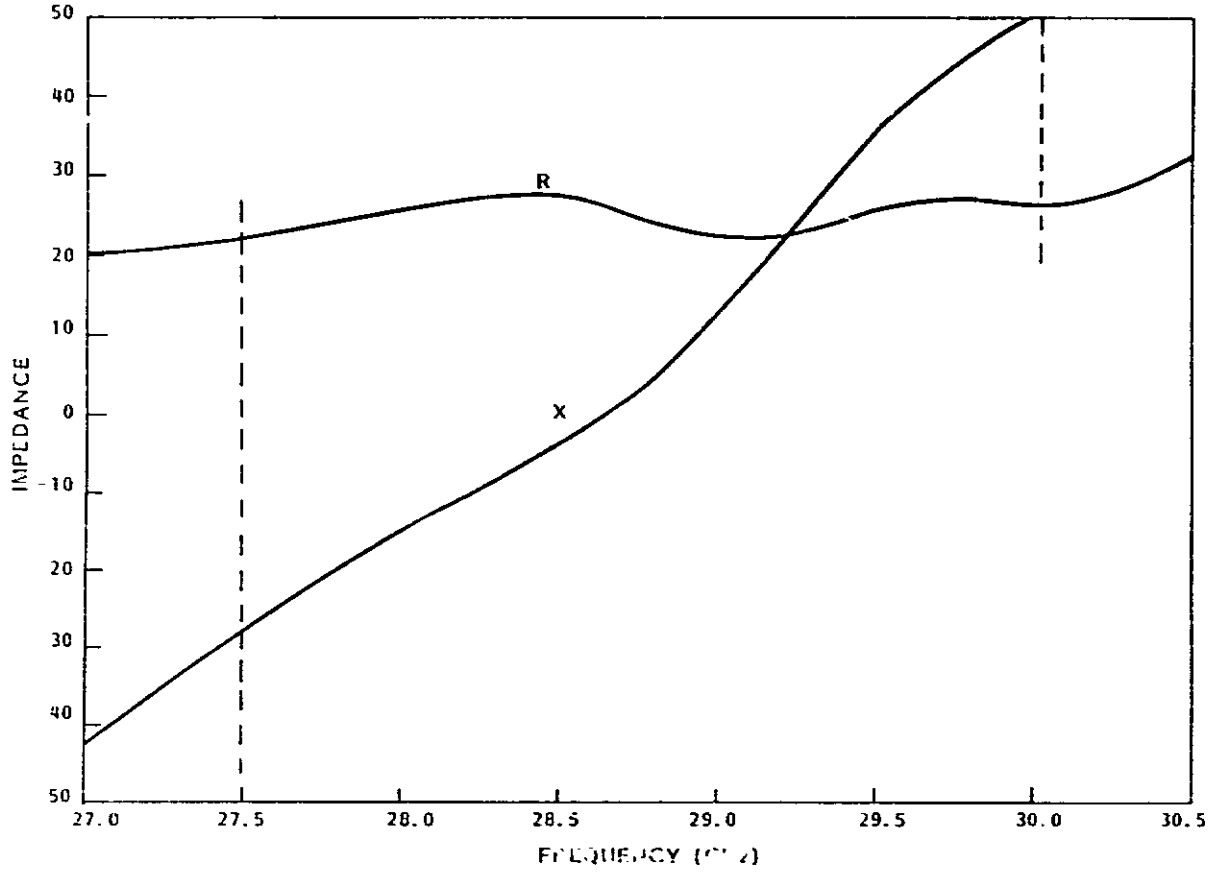

Figure 64. Input Impedance of 15 Element 4.2 λ Long Yagi with 4.57 mm (0.1798") Long Unfolded Dipole Driven Element

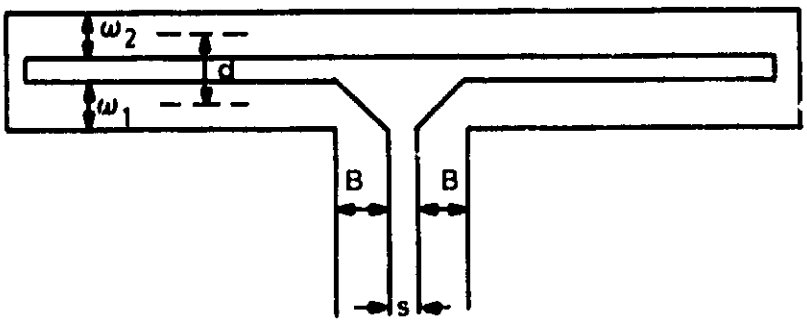

$\omega_1 = \omega_2$ = 0.254 mm (0.010")

d = 0.381 mm (0.015")

B = 0.254 mm (0.010")

s = 0.117 mm (0.0046")

Figure 65. Folded Dipole Driven Element for 15 Element, 4.2λ Long Yagi

The balanced yagi feed is transitioned to the microstrip format of the monolithic circuitry via a printed circuit balun*. A coaxial balun and its printed circuit equivalent are shown in Figure 66. The printed version locates the microstrip line and the balanced line on opposite sides of the supporting substrate with the balanced conductor forming a portion of the microstrip ground planes. Z_a and Z_b are the impedances of the coaxial or microstrip lines while Z_{ab} is the impedance of the balanced section.

From examination of the balun circuit, the impedance Z' may be written as

$$Z' = -j\, Z_b \cot \theta_b + \frac{j R\, Z_{ab} \tan \theta_{ab}}{R + j\, Z_{ab} \tan \theta_{ab}}.$$

If the electrical lengths θ_{ab} and θ_b are made equal

$$\theta_b = \theta_{ab} = \theta$$

then

$$Z' = \frac{R\, Z_{ab}^2 + j \cot \theta \left[R^2 (Z_{ab} - Z_b \cot^2 \theta) - Z_b Z_{ab} \right]^2}{Z_{ab}^2 + R^2 \cot^2 \theta}.$$

Further, if the unbalanced lines have equal impedances and the balanced line impedance is equal to that of the load,

$$Z_a = Z_b$$

and $$Z_{ab} = R,$$

then

$$Z' = R \sin^2 \theta + j (\cot \theta)(R \sin^2 \theta - Z_a).$$

The input impedance is matched,

$$Z' = Z_a = Z_{in}$$

at the two frequencies which yield

$$\theta = \sin^{-1} \sqrt{Z_a/R}.$$

---

* Bower and Wolfe, "A Printed Circuit Balun for Use with Spiral Antennas," IRE Transactions on Microwave Theory and Techniques, Vol. MTT-8, pp. 319-325, May 1960.

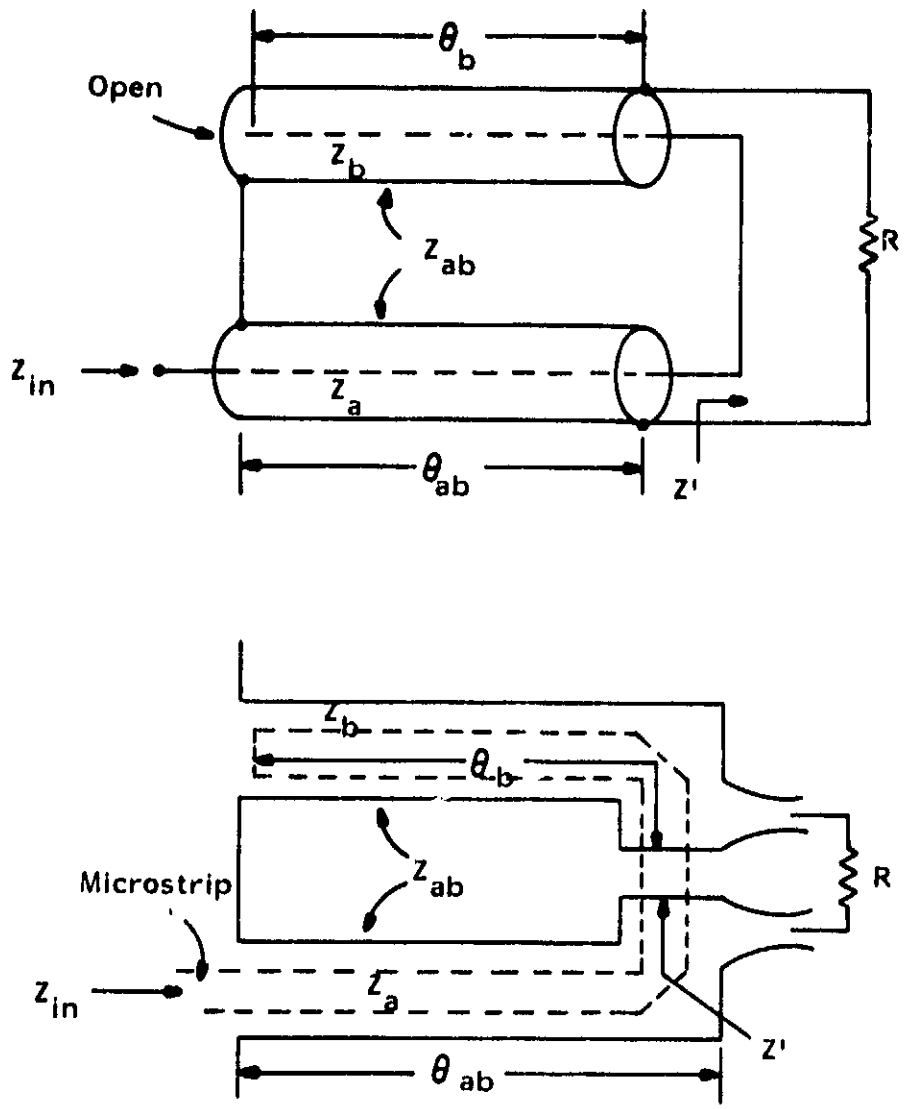

Figure 66. Coaxial Balun Design and Printed Circuit Equivalent

The median of these two frequencies is the frequency at which θ equals 90°. Therefore the balun input match exhibits a double tuned characteristic. For the special case of a 1:1 impedance ratio balun (Z_a = R), the match frequencies degenerate to a single frequency.

The impedance of the monolithic microstrip circuitry is nominally 50 Ω while the yagi balanced feed line impedance is 100 Ω. Therefore, the printed circuit balun must provide an impedance transformation ratio of 2:1. The unbalanced microstrip and balanced line sections which comprise the balun have respective impedances of

$$Z_a = Z_b = 50\,\Omega$$

and $$Z_{ab} = R = 100\,\Omega\ .$$

The electrical line lengths may be selected to be 90° at center band, which yields an input VSWR of 2:1 at this frequency. The input to the balun will be matched to the 50 Ω monolithic circuitry when the electrical lengths of the balun lines are

$$\theta = \theta_b = \theta_{ab} = 45°,\ 135°.$$

A perfect match will not be achieved with this design since due to the slightly different phase velocities of the microstrip and balanced line sections, their electrical lengths are not simultaneously equal to 45° or 135°. Alternatively, the balun may be designed so as to make the lines lengths both equal to 45° or 135° at center band which will then yield a perfect match at this frequency.

For a 0.254 mm (0.010 inch) thick alumina substrate, a 50 Ω microstrip line will have a width of 0.249 mm (0.0098 inch). Since the balanced line conductors comprise the microstrip ground plane within the balun, their line widths are selected to be approximately three times the microstrip width or 0.71 mm (0.028 inch). The spacing between the balanced conductors is set so as to give a line impedance Z_{ab} of 100 Ω. This spacing, determined as for the balanced line feeding the yagi driven element, is 0.279 mm (0.0110 inch). A balun design with the line electrical lengths equal to 90° at center band (28.75 GHz) is shown in Figure 67.

4.2.2 Mutual Coupling with Yagi Radiating Elements

The mutual coupling effects on the yagi radiating element properties were investigated for two radiator configurations;

1) One excited yagi surrounded by six terminated yagis of like polarization,

2) One excited yagi in the presence of two terminated, close neighbor orthogonally polarized yagis.

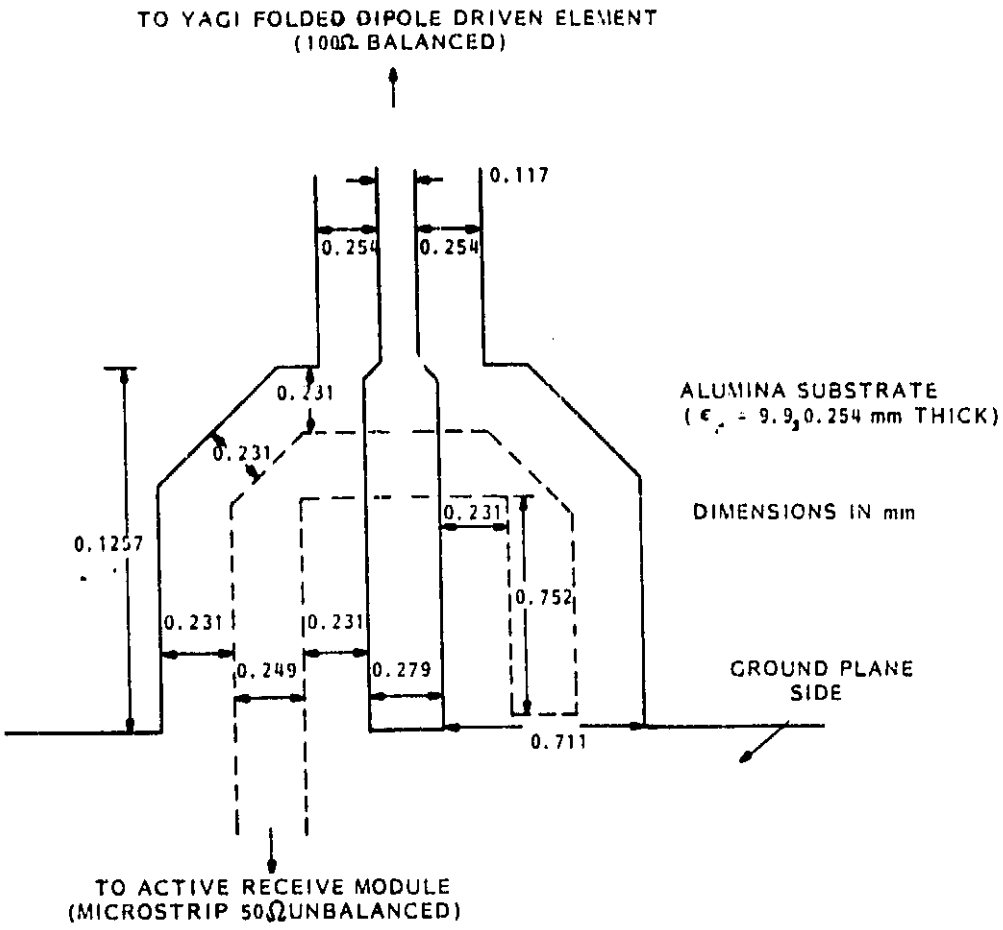

Figure 67. Printed Balun Design with 2:1 Impedance Transformation

The first configuration consists of a total of seven 4.2 λ long yagis arranged on an equilateral triangular grid. This arrangement is shown in Figure 68. The center element is excited while its surrounding neighbors are terminated in their nominal feed point impedance. All yagis are of the same polarization. The sub-array element spacing S is 2.163 λ at center band (1.04 cm).

A method-of-moments computer program was used to model the seven radiator configuration. The in-place element properties (excited element in the subarray environment) are compared with those of an isolated element in Table 19.

TABLE 19. ISOLATED VS IN-PLACE YAGI CHARACTERISTICS

	Isolated Yagi	Yagi in Subarray
Z_{Feed}	29.5-j 1.5 Ω	29.3-j 1.4 Ω
Directivity	14.9 dBi	15.5 dBi
$(\theta_E)_{3\,dB}$	≈ 30°	≈ 24.6°
$(\theta_H)_{3\,dB}$	≈ 31.6°	≈ 25.2°

The feed point impedance is essentially the same for the isolated yagi and the yagi operating in the subarray of like polarized elements. The yagi does exhibit higher directivity and correspondingly narrower E- and H-plane beamwidths when in the subarray environment. This is due to the driven yagi exciting the surrounding subarray elements resulting in an increase of effective aperture.

The second configuration consists of three 4.2 λ long yagis arranged as shown in Figure 69. This configuration was studied to determine the degradation of polarization purity due to the interleaving of orthogonally polarized arrays. The configuration of Figure 70 represents the extremity of assymmetry and is therefore considered a worst case situation. The terminated yagis, shown as vertically polarized, are located at two corners of the equilateral triangular grid. The excited horizontally polarized yagi is located midway between the terminated elements with a spacing S/2 of 1.082 λ.

A method-of-moments computer program was again used for the modeling. The results showing the E- and H-plane principal or horizontally polarized component and the cross- or vertically polarized component are shown in Figure 70. At broadside the cross-polarized component is 26.0 dB down from the principal. This level is marginal for the required system beam isolation. A single isolated yagi, or an array of yagis of a single polarization would theoretically have no cross-polarized far-field components.

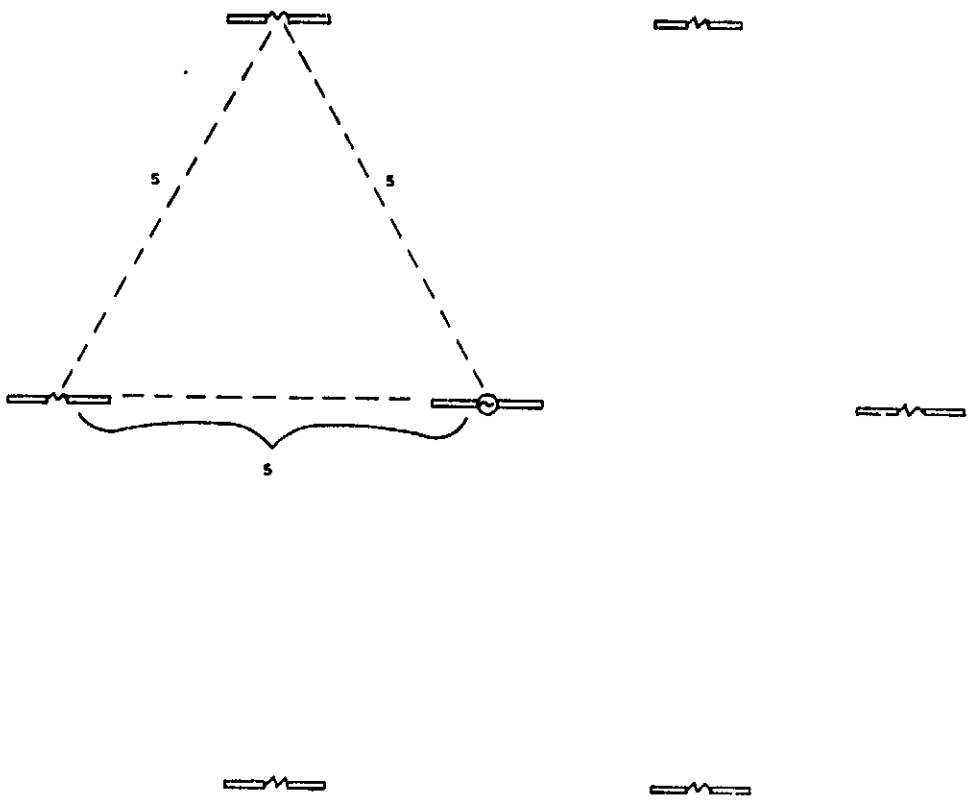

Figure 68. One Excited Yagi Surrounded by Six Terminated Yagis of Like Polarization

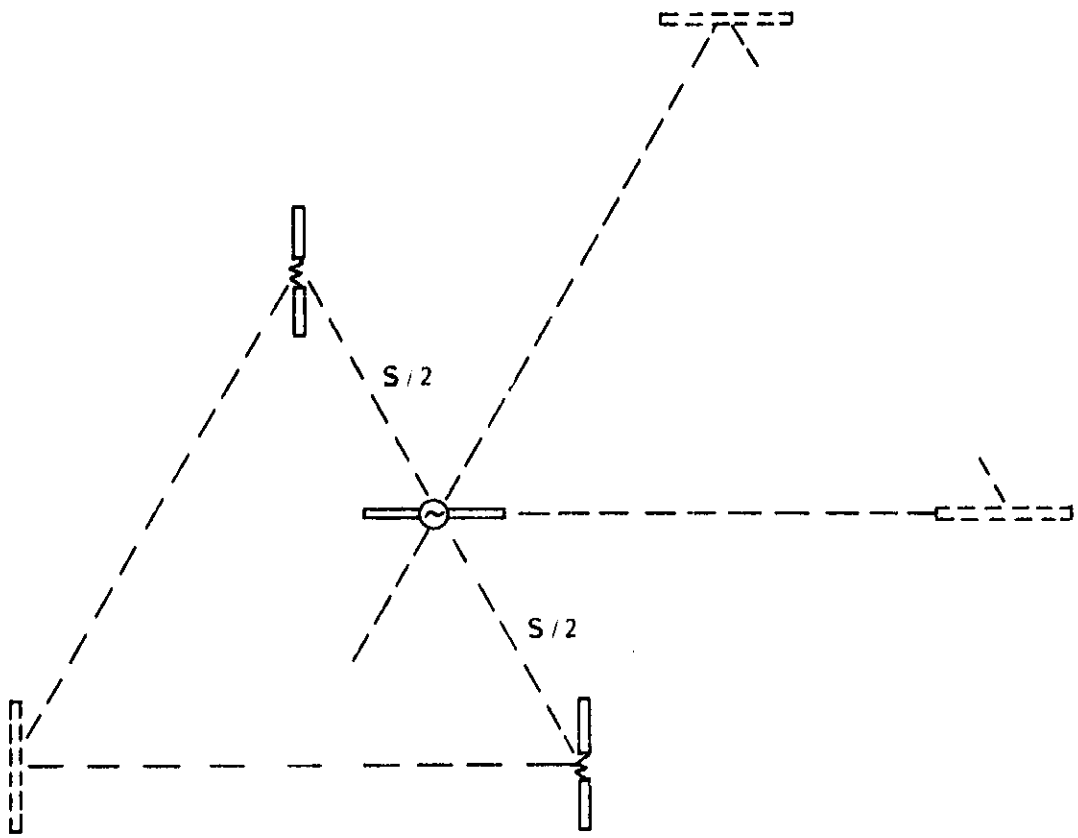

Figure 69. One Excited Yagi with Two Terminated, Close Neighbor Orthongonally Polarized Yagis

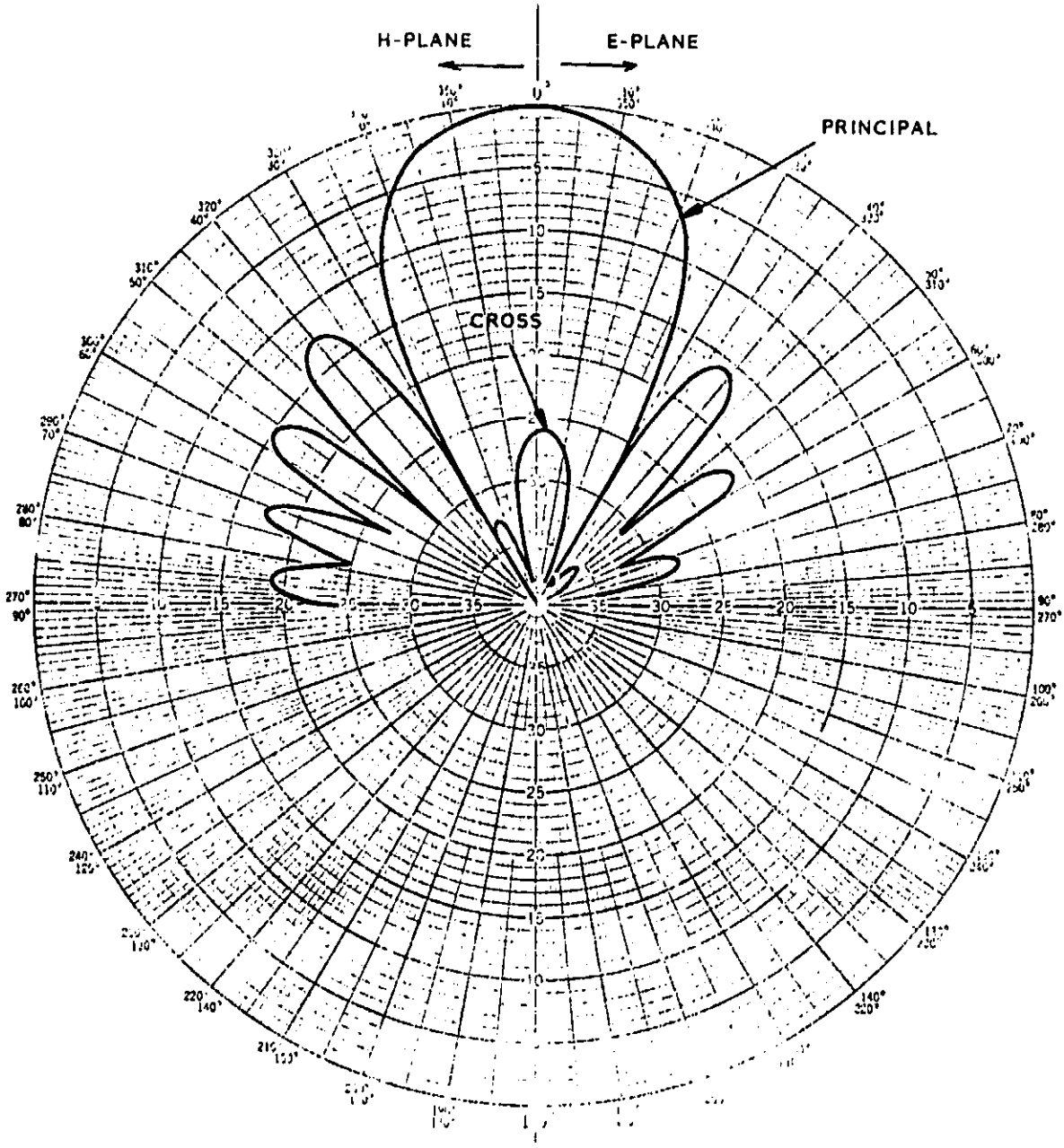

Figure 70. Far-Field Patterns of Three 15 Element Yagis Located at Adjacent Positions in Array Grid (Center Yagi Excited)

5.0 FEED ARRAY DESIGN

5.1 FEED ARRAY ARCHITECTURE COMPARISONS

The active feed arrays for the three primary scanning antenna configurations, Gregorian, Cassegrain, and single reflector, are compared with respect to total number of elements, number of active elements, noise figure, DC power consumption, and relative weight. The noise figure and DC power requirement are also calculated for the dual reflector fixed beam antenna active feed array. The characteristics of the monolithic microwave integrated circuitry and signal combining networks used for the calculation of the feed array electrical performance are outlined in Figures 71 and 72. The values for gain, noise figure, and DC power consumption are based on a study of what monolithic circuit performance can be achieved given presently available devices or on devices that are to become available in the near future. These values are compatible with the submodule requirements specified by NASA/LEWIS for the 30 GHz monolithic receive module.

The MMIC low noise amplifier submodule has a nominal gain of 7 dB per stage. Each stage is impedance matched and biased for low noise operation. The noise figure and DC power consumption is 3.5 dB and 15 mW respectively per stage. Four cascaded low noise amplifier stages are located with each radiating element in all three scanning and the fixed beam antenna configurations. Therefore adequate signal amplification is achieved before combining network losses are encountered thereby minimizing the overall system noise figure.

The MMIC variable gain amplifier submodule is comprised of three stages, each having a gain variable from -10 to +3 dB. The net gain is therefore variable from -30 to +9 dB for a range of 39 dB. This range is compatible with those required by the element amplitude taper schedules. The noise figure for each stage varies from 10 dB (at minimum gain setting) to 4.36 dB (at maximum gain setting). The net noise figure for three stages therefore varies from 30 to 6.06 dB. For calculation purposes, it has been determined that the variable gain amplifier's noise figure may be assumed to be a linear function of gain. The variable gain amplifier has a DC power requirement of 40 mW per stage for a submodule total of 120 mW. A digital controller for each three-stage submodule requires 12.5 mW.

The monolithic phase shifter submodule is comprised of five phase bits. The nominal insertion loss should be independent of the phase state. A value of 8 dB has been estimated. A phase shifter utilizing single gate MESFETs as passive switching elements will have a noise figure numerically equal to its insertion loss. This design also results in an extremely low DC power requirement, estimated to be 10 mW for the entire phase shifter. A digital controller requires an additional 12.5 mW per submodule.

The IF submodule consists of the mixer, I.F. amplifier, and local oscillator. A monolithic active mixer may be employed to achieve frequency translation with minimum conversion loss while requiring low local oscillator power. A design with zero dB conversion loss and a single sideband noise

figure of 6.5 dB has been assumed. The local oscillator drive power requirement would be on the order of -5 dBm. The mixer DC power consumption is 80 mW.

The low frequency I.F. amplifier consists of a single stage and provides approximately 7 dB of gain. Feedback may be used to achieve a flat gain response, and good input and output match over the relatively wide I.F. band. The amplifier has a noise figure on the order of 3 dB and a DC power requirement of 15 mW.

A local oscillator with buffer amplifier is required for each mixer. When multiple local oscillators are employed, each oscillator must be locked to a common reference signal to ensure that they operate at the same frequency and in phase. The oscillator/buffer output power must be adequate to drive the mixer circuitry. The DC power consumption for each oscillator/buffer is approximately 45 mW.

A voltage level set circuit provides the required MMIC voltage levels from the main plus and minus DC bus lines. This circuit has an estimated power dissipation of 50 mW.

The values of insertion loss for the signal combining networks are also given in Figure 72. These estimates are for stripline networks and are a function of the number of divider levels required. The noise figure for these passive circuits is numerically equal to their insertion loss.

The performance of the feed array with respect to noise figure, net gain, and DC power consumption for the dual reflector Gregorian scanning antenna configuration is given in Figure 73. The performance of a system with signal combination at I.F., and a system with signal combination at the R.F. may be compared. Both systems divide each of the 1039 elemental signals of like polarization three ways. An output from each three-way divider is fed to a 1039:1 weighted combiner. The outputs of three of these 1039:1 combiners therefore form the three scanning beams of one polarization. A duplicate system is required to form the three scanning beams of the orthogonal polarization.

The system with signal combination at the I.F. potentially provides the lowest noise figure, 4.40 dB as opposed to 5.18 dB for signal combination at the R.F. The lower noise figure is due to the larger signal gain encountered in the I.F. system prior to dissipative losses in the signal combiner and the assumption that none of the additive noise at the multiple mixers is coherent. If, however, coherent local oscillator noise is added to the I.F. signal at each of the mixer submodules, then the system noise figure will be degraded. In the worst case, if all the mixer additive noise is coherent L.O. noise then the I.F. system's noise figure will become 20.06 dB.

The Gregorian antenna feed array system with I.F. signal combination has a much higher DC power requirement than the R.F. system, 241.6 versus 61.6 watts per scanning beam. In addition the I.F. system is much more complex, requiring an extensive coherent distribution network for the

LOW NOISE AMPLIFIER

Gain = 7 dB/Stage
Noise Figure = 3.5 dB/Stage
DC Power Consumption = 15 mW/Stage

ACTIVE MIXER

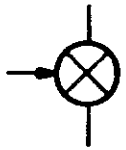

Conversion Loss = 0 dB
Noise Figure = 6.5 dB
DC Power Consumption = 80 mW

VARIABLE GAIN AMPLIFIER

Gain = -10 to +3 dB/Stage
Noise Figure = 10 to 4.36 dB/Stage
DC Power Consumption = 40 mW/Stage

LOCAL OSCILLATOR/BUFFER

DC Power Consumption = 45 mW

5-BIT PHASE SHIFTER

Insertion Loss = 8 dB
Noise Figure = 8 dB
DC Power Consumption = 10 mW

I.F. AMPLIFIER

Gain = 7 dB/Stage
Noise Figure = 3 dB/Stage
DC Power Consumption = 15 mW/Stage

Figure 71. MMIC Performance Used for Noise Figure Calculations

SIGNAL COMBINERS (SCANNING BEAMS)

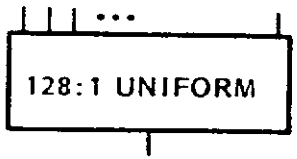

7 Levels
Insertion Loss = 4 dB

SIGNAL COMBINERS (FIXED BEAMS)

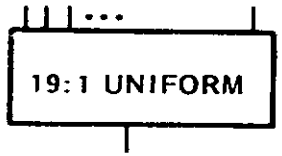

4 Levels
Insertion Loss = 2.6 dB

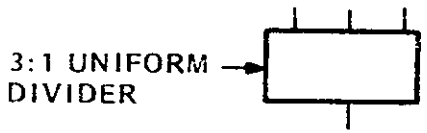

1 Level
Insertion Loss = 0.6 dB

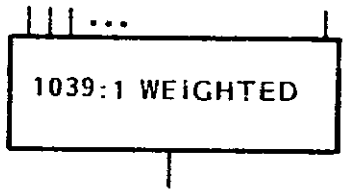

10 Levels
Insertion Loss = 6 dB

DIGITAL CONTROLLER

DC Power Consumption = 125 mW/Variable Gain Stage
12.5 mW/Phase Shifter

VOLTAGE LEVEL SET

DC Power Consumption = 50 mW

Figure 72. MMIC Performance Used for Noise Figure Calculations (Cont)

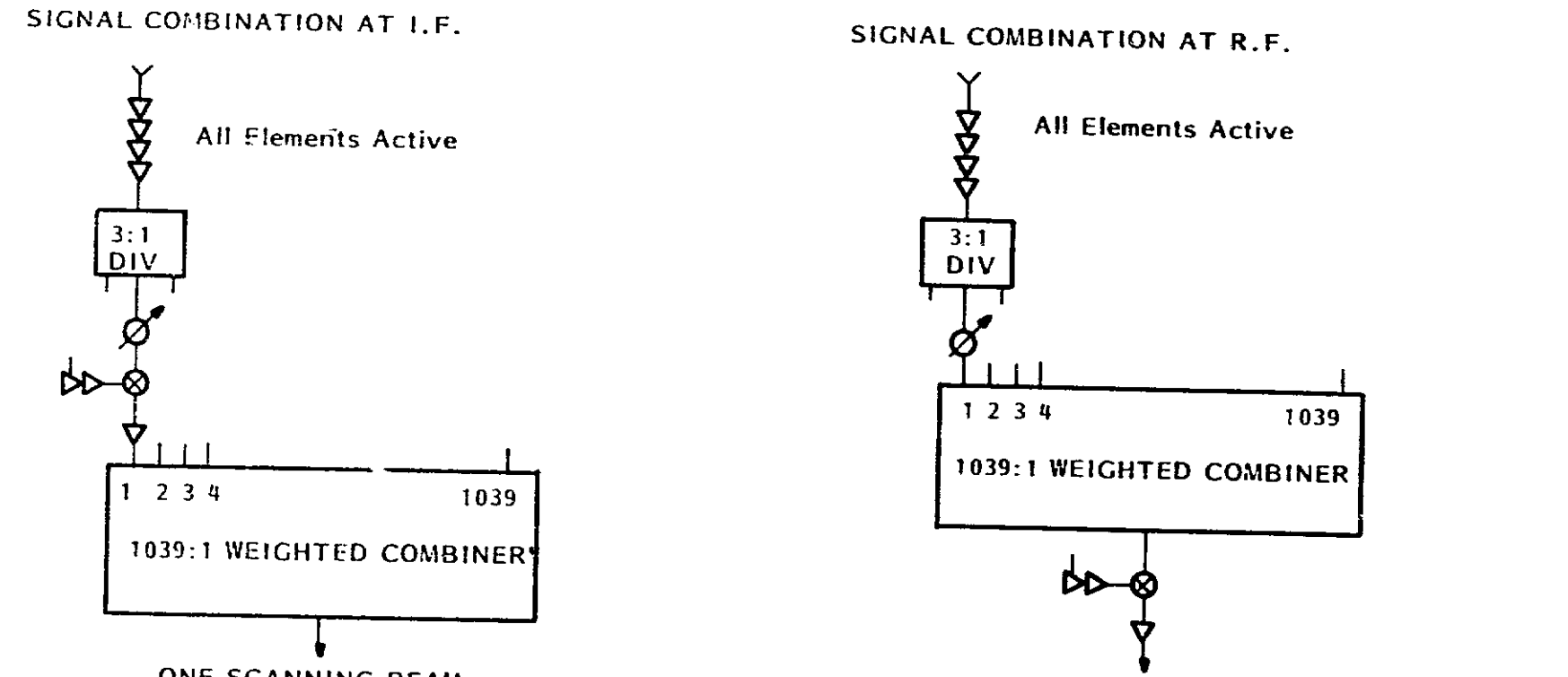

Figure 73. Beam Combining Network Architecture - Performance Comparison for Dual Reflector Gregorian Scanning Configuration

L.O. locking signals. Both the I.F. and R.F. systems have the same net gain of 15.6 dB.

The dual reflector Cassegrain scanning antenna feed array performance with signal combination at the I.F. and R.F. for a sample beam case is given in Figure 74. Both the I.F. and R.F. systems use a total of either 128 or 144 elements for each scanning beam. The total number of elements is dependent on which CONUS section is to be covered. Only 19 of the elements are active (submodules turned "ON") at any one time. The particular 19 elements that are active is a function of the scanning beam position.

The systems' noise figures are a function of the signal level distribution from the active elements as applied to the uniform combiner. These signal levels are set by the variable gain submodules. The ratio of noise applied to the combiner from an "OFF" module to the noise from a radiating element is estimated to be 2. For the case studied, the net noise figure of the I.F. system ranges from 4.20 dB when no coherent local oscillator noise is present to 4.32 dB when all of the mixer additive noise is coherent L.O. noise. This range is much smaller than for the Gregorian antenna I.F. combination feed system since the number of active modules employed in the Cassegrain antenna feed is much less. The net noise figure of the R.F. signal combination system is 5.28 dB. The net gain for both the I.F. and R.F. systems are equal at 15.5 dB. The I.F. signal combination system which requires an I.F. submodule at each input of the uniform combiner requires slightly more DC power than the R.F. system, 10.42 versus 7.90 watts per scanning beam. The I.F. beam system also requires an extensive coherent distribution network for the L.O. locking signals.

The single reflector scanning antenna feed array performance with signal combination at the I.F. and R.F. for a sample beam case is reported in Figure 75. As with the dual reflector Cassegrain configuration, 19 of the total array section elemental receive modules are active at any one time. The 19 elements that are active is dependent upon the scanning beam position. The systems' noise figures are also a function of the signal level distribution of the active elements as applied to the uniform combiner. For the case studied, the net noise figure of the I.F. system ranges from 4.41 dB when no coherent local oscillator noise is present to 4.79 dB when all of the mixer additive noise is coherent L.O. noise. The net noise figure of the R.F. signal combination system is 6.59 dB.

The net gains for the single reflector scanning antenna's I.F. and R.F. signal combining feed array systems are identical at 11.7 dB. The DC power consumption however, is higher for the I.F. system than for the R.F. system, 10.42 versus 7.90 watts per beam. The I.F. system also requires an extensive coherent distribution network for the L.O. locking signals.

The performance of the I.F. and R.F. signal combining feed arrays for the dual reflector fixed beam antenna configuration is given in Figure 76. Up to 19 elements are used to form a spot beam. The signals from these elements are combined in a 19-input port, uniformly weighted combining

SIGNAL COMBINATION AT I.F.

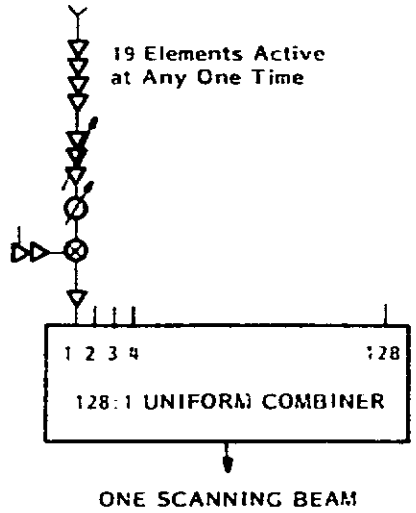

Net Noise Figure 4.20 dB
(No Coherent Noise)

Net Noise Figure = 4.32 dB
(All Mixer Noise Coherent)

Net Gain = 15.53 dB

Total DC Power Consumption = 10.42 Watts (Per Beam)

SIGNAL COMBINATION AT R.F.

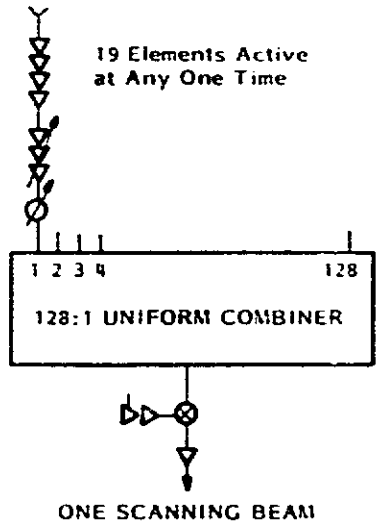

Net Noise Figure = 5.28 dB

Net Gain = 15.53 dB

Total DC Power Consumption 7.90 Watts (Per Beam)

Figure 74. Beam Combing Network Architecture - Performance Comparison for Dual Reflector Cassegrain Scanning Antenna Configuration, Effective F/D = 2.94, Magnification Factor = 2.1

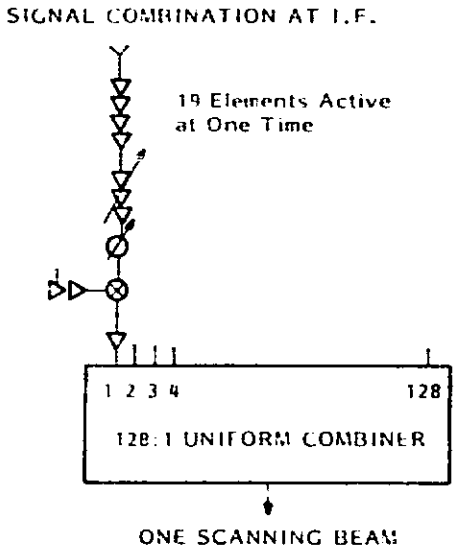

Net Noise Figure = 4.41 dB
(No Coherent Noise)

Net Noise Figure = 4.79 dB
(All Mixer Noise Coherent)

Net Gain = 11.65 dB

Total DC Power Consumption = 10.42 Watts (Per Beam)

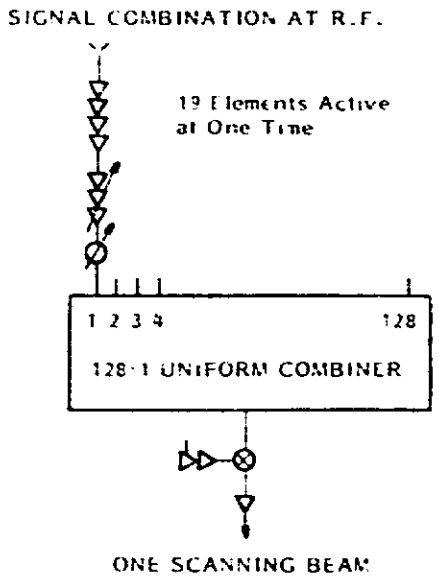

Net Noise Figure = 6.59 dB

Net Gain = 11.65 dB

Total DC Power Consumption = 7.30 Watts (Per Beam)

Figure 75. Beam Combining Network Architecture - Performance Comparison for Single Reflector Scanning Antenna, F/D = 1.2

SIGNAL COMBINATION AT I.F.

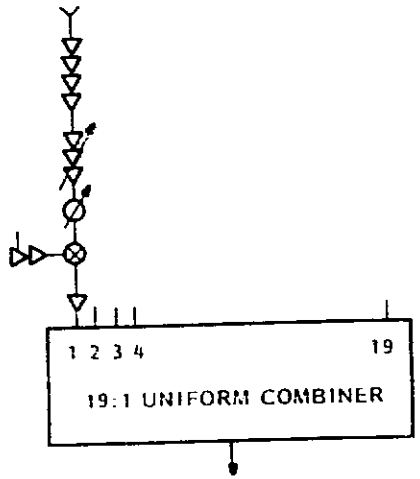

Net Noise Figure = 4.23 dB
(No Coherent Noise)

Net Noise Figure = 4.49 dB
(All Mixer Noise Coherent)

Net Gain = 22.22 dB

Total DC Power Consumption = 7.70 Watts (Per Beam)

SIGNAL COMBINATION AT R.F.

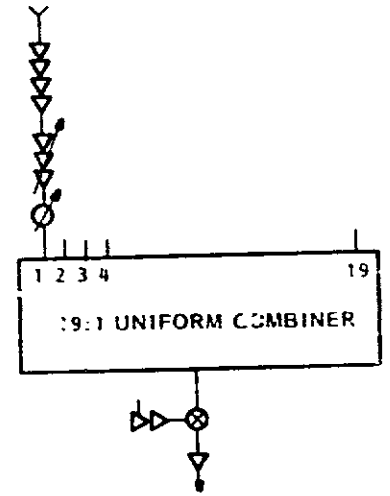

Net Noise Figure = 4.41 dB

Net Gain = 22.22 dB

Total DC Power Consumption 5.18 Watts (Per Beam)

Figure 76. Beam Combining Network Architecture - Performance Comparison for Dual Reflector Fixed Beam Antenna Configuration

network which has an estimated insertion loss of 2.6 dB. For the case studied, the net noise figure of the I.F. system ranges from 4.23 dB when no coherent local oscillator noise is present to 4.49 dB when all of the mixer additive noise is coherent L.O. noise. The net noise figure of the R.F. signal combination system is 4.41 dB.

Both systems have an identical gain of 22.2 dB. The D.C. power requirement for the I.F. system is 7.70 watts per beam while the requirement for the R.F. system is 5.18 watts per beam.

The relative weights of the feed arrays have been estimated for the Cassegrain and the Gregorian scanning antenna designs. Included in the weight estimates are the radiating elements, the MMIC receiver module assemblies, and the beam combining networks (BCN). The BCN was found to contribute the greatest weight by far to the array assembly, with the module weights second in significance, and the radiating element weights the least significant. The Gregorian BCN requires six 1039:1 power combiners plus 2078 3:1 power dividers. The Cassegrain BCN requires six 128:1 or 144:1 signal combiners. The basic weight ratio of the Gregorian to Cassegrain BCN is in the vicinity of 15:1. Taking into account the contribution of the module weights and the radiating element weights moderates this feed array weight ratio to the vicinity of 10:1. The relative feed array weights is reported in Table 20.

TABLE 20. RELATIVE FEED ARRAY WEIGHTS

	Gregorian	Cassegrain
Radiating Elements	0.01	0.04
Receiver Module Assemblies	1.99	0.39
Beam Combining Networks	8.00	0.57
Total	10.00	1

5.2 CORPORATE SIGNAL COMBINING NETWORK DESIGN

Stripline circuitry has been selected for the transmission media of the corporate RF signal combining network. Since a large number of binary level combiners and interconnecting lines must be located within a small area, the self-shielding property of stripline will minimize the detrimental effects of transmission line radiation and coupling. The printed circuit fabrication techniques for stripline result in accurate and reproducible networks which have wide flexibility with respect to combiner design and layout.

A cross-sectional view of stripline transmission media consisting of a flat center conductor located between two parallel plate ground planes is shown in Figure 77. Two types of construction are shown, that of an air fill dielectric between the two ground planes with the center conductor printed on a thin supporting substrate, and a solid dielectric fill with an imbedded center conductor. In practice, mechanical spacers are required to locate the center conductor substrate of the air fill line, and solid fill line is comprised of two bonded together dielectric sheets with the center conductor printed onto the surface of one of the sheets. The advantages and disadvantages of each type of construction, denoted by + and -, are given in the figure. While the air filled stripline has the lowest dissipative losses, it is prone to location errors of its center conductor which may lead to the excitation of undesired (non-TEM) transmission modes. Therefore, the solid dielectric fill construction is preferred. Both the air and solid dielectric construction would have the same approximate weight.

The ground plane spacing of the stripline circuitry must be sufficiently small so as to place the cutoff frequency of circumferential TE modes above the operating band. A graph which shows this cutoff frequency as a function of ground plane spacing, center conductor thickness, dielectric constant, and line impedance is given in Figure 78. For dielectric fill with a relative dielectric constant of 2.2, a ground plane spacing of 1.59 mm (1/16"), and a center conductor thickness of 0.036 mm (1 oz. of copper cladding per square foot), the TE cutoff frequency for a 50 Ω line is approximately 59 GHz. The lowest impedance line that may be used with a TE mode cutoff frequency just above the operating band (31 GHz) is approximately 26Ω.

The calculated line impedances and losses as a function of center conductor width for the 1.59 mm ground plane spacing, 2.2 relative dielectric constant stripline are reported in Table 21. Losses may be reduced by increasing the ground plane spacing, however, this would lower the cutoff frequencies of the undesired TE modes and increase the weight of the signal combining network.

A variety of binary level combiners may be used in the corporate signal combining network. Five types are shown in Figure 79. The combiners featuring load resistors provide isolation between the two input ports (ports 2 and 3) and are therefore preferred for the corporate combiner. The side coupled combiner is limited in coupling by the maximum achievable even-mode impedance of the two parallel line sections. Coupling values greater than -10 dB are not practical for this design and therefore they are not recommended for application in the corporate combiner. The branch-line combiner has its two input ports in phase quadrature. Thus, the use of this combiner design would require the addition of 90° offset lines to achieve an overall corporate signal combiner with in-phase inputs.

---

[1] Packard, "Optimum Impedance and Dimensions for Strip Transmission Line", IRE Transactions on Microwave Theory and Techniques, Vol. 5, pp. 244-247, October 1957.

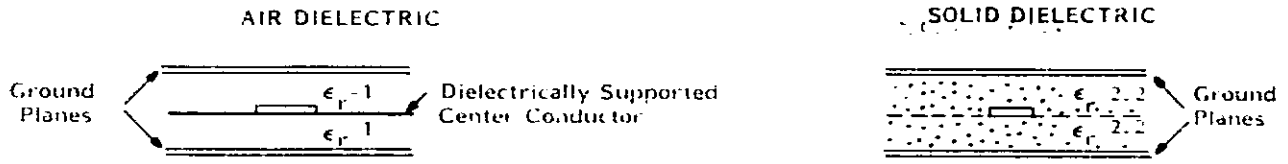

G.P.S. ≈ 1.16" FOR BOTH CONFIGURATIONS

- Lowest Loss
- Uniform Dielectric Constant Throughout

  Requires Special Mechanical Support System for Center Conductor

  Location Errors of Center Conductor May Excite Undesired Modes

- Precise Location of Center Conductor
- Structurally Rugged

Figure 77. Construction of Stripline Signal Combining Network

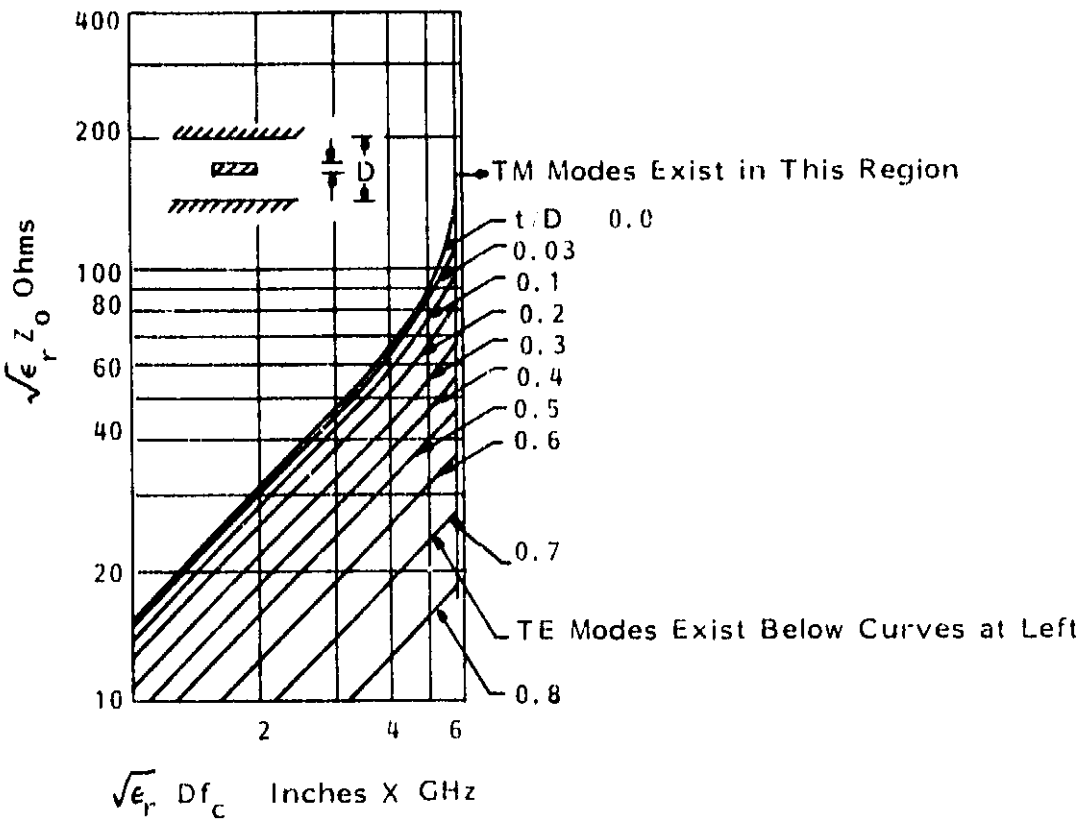

Figure 78. Minimum Characteristic Impedance vs Higher Mode Cutoff Frequency

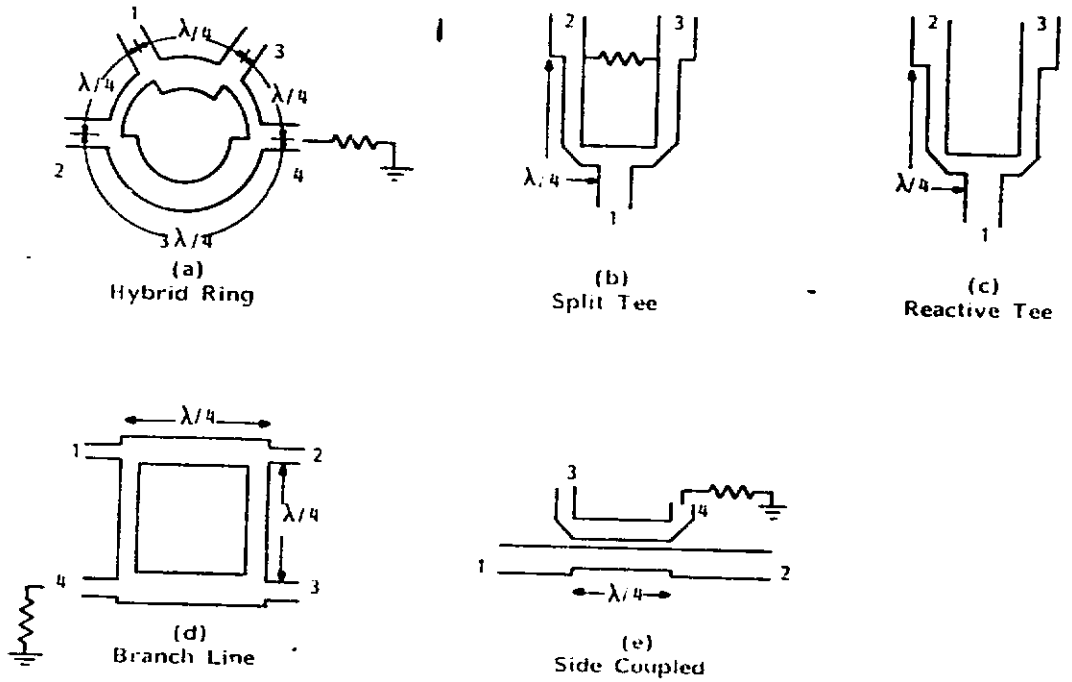

Figure 79. Printed Signal Combiners

TABLE 21. LINE IMPEDANCES AND LOSSES AS A FUNCTION OF CENTER CONDUCTOR

STRIP LINE ANALYSIS

```
                                                    CONDUCTOR RS/RSCU
-------------------------------------------------------  1.050
          A = 0.031300 INCH
  -----   T = 0.001400 INCH                              1.050
          A
-------------------------------------------------------  1.050

          B = 0.064000 INCH
        T/B = 0.021875
```

FREQUENCY-GHZ 28.750

DIEL CONSTANT 2.200
DIEL LOSS TAN 0.001000
LAMBDA-INCHES 0.277

ALF DIEL 0.02729 DB/LAM 0.09859 DB/IN

ZO OHMS	W INCH	W/(B-T)	ALF-COND DB/LAM	ALF-TOT DB/LAM	ALF-TOT DB/INCH
10.0	0.367	5.869	0.01575	0.04304	0.15550
20.0	0.169	2.694	0.01745	0.04474	0.16165
30.0	0.102	1.636	0.01915	0.04644	0.16779
40.0	0.069	1.107	0.02086	0.04814	0.17394
50.0	0.049	0.790	0.02256	0.04984	0.18008
60.0	0.036	0.578	0.02426	0.05154	0.18623
70.0	0.027	0.427	0.02596	0.05325	0.19237
80.0	0.020	0.315	0.02856	0.05585	0.20179
90.0	0.015	0.237	0.03285	0.06014	0.21729
100.0	0.011	0.179	0.03752	0.06481	0.23416
110.0	0.008	0.135	0.04241	0.06970	0.25182
120.0	0.006	0.100	0.04744	0.07473	0.26998
130.0	0.004	0.072	0.05256	0.07985	0.28849

The hybrid-ring combiner (with input ports 2 and 3) and the split-tee combiner feature input port-to-port isolation, in-phase inputs, and a large range of possible coupling values including equal. At the operating band of interest, the physical line length of a quarter wave section in the stripline media approaches the line width. Therefore, due to layout considerations, the hybrid-ring combiner may be preferred over the split-tee. A length of open ended lossy line (stripline center conductor printed with a resistive material) may be substituted at the isolated port in place of the hybrid-ring's grounded load resistor.

The transition between column and row stripline corporate combiners, and between column combiners and elemental microstrip receiver modules are made with minature plunge style coaxial connectors. It is desirable to limit operation of these connectors to the fundamental TEM mode. Therefore, the cutoff frequency of the next higher TE_{11} mode should be placed above the operating band. This higher order cutoff frequency fc_{TE11} is given approximately by

$$fc_{TE11} \approx \frac{c}{\sqrt{\varepsilon_r}\,\pi\,(a+b)} \qquad (1)$$

where c is the free space light velocity, ε_r is the relative dielectric constant of the material filling the coax, and a and b are the radii of the shield and center conductors respectively.

The coaxial connectors should also have a characteristic impedance equal to that of the corporate combiner ports and receiver module output (50 Ω). The impedance Z_o for the coaxial section is given by

$$Z_o = \frac{60}{\sqrt{\varepsilon_r}} \ln\left(\frac{a}{b}\right). \qquad (2)$$

In addition, the connectors must be designed to have minimum or compensated for parasitics (excess shunt capacitance or series inductance) at the points where they transition from the stripline corporate combining networks and the microstrip receiver modules.

A candidate coaxial connector type is the miniature plunge style OSSP series designed by Omni-Spectra. These connectors have a characteristic impedance of 50 Ω and a TE_{11} mode cutoff frequency of approximately 49 GHz.

5.3 CONTROL DATA DISTRIBUTION FOR FEED ARRAY SCAN

Each of the six sections of the scanning antenna feed array consists of approximately 128 receiver modules of a common polarization. Each of the receiver modules include a phase shifter and variable gain amplifier which must be commanded to a certain state to effect array scan in a desired

direction. The control signals for the phase shifters and variable gain amplifiers must be distributed throughout the feed array section from a remote controller to each module. The control signal format and distribution scheme should be the simplest possible while having sufficient flexibility and speed required for scanned beam relocation.

The receiver module phase shifter consists of 5 bits. The variable gain amplifier consists of three stages each with 5 possible levels plus an "OFF" state. Therefore, the variable gain amplifier has 16 unique settings and requires 4 bits of control. Each receiver module, therefore requires a total of 9 bits of control data to be reset for a new scanning beam position.

A control scheme has been studied which sends the command data to each of the modules of an array section in a sequential fashion. The system is diagrammed in Figure 80. Modules are addressed via column and row lines. These address lines form the lattice shown in the upper portion of the figure. Modules are located at alternate lattice points to form the triangular grid as shown. Control data for the modules are sent in a sequential fashion. To address the module of which the control signals on the data line are to be sent, the appropriate row and column address lines are placed high. A data clock signal ensures the beamsteering signals are read into a module only during the appropriate time period. The control signals for a new scanning beam position are read into each module and stored during the dwell period of a beam. With a high signal on the strobe line, all modules change state simultaneously to form the new beam. This control technique requires only two address lines, one data line, a clock line, and a strobe line to be interfaced with each receive module. The later three lines are common for all modules in the array section while the address lines are only unique for different rows or columns. The serial in-parallel out register and latch/drivers shown in the figure are integrated into each module.

To form a scanning beam, only a cluster of 19 modules are active or "ON". Therefore to minimize the time period required to reset the array section for a new scanning beam position, it is possible to set all of the section modules simultaneously to the "OFF" state by placing all row and column address lines high, and then resetting just the 19 active modules sequentially to the required state. If D is the bit rate at which the control signals are sent, then the time period, t, required for array section recommand is

$$t = \frac{(9 \text{ bits})(1 \text{ section "OFF"} + 19 \text{ module resets})}{D} = \frac{180}{D} . \qquad (1)$$

If shorter recommand periods are required and the data rate can not be increased, then the control scheme must be modified so that multiple receive modules are addressed and sent data simultaneously as opposed to a sequential fashion.

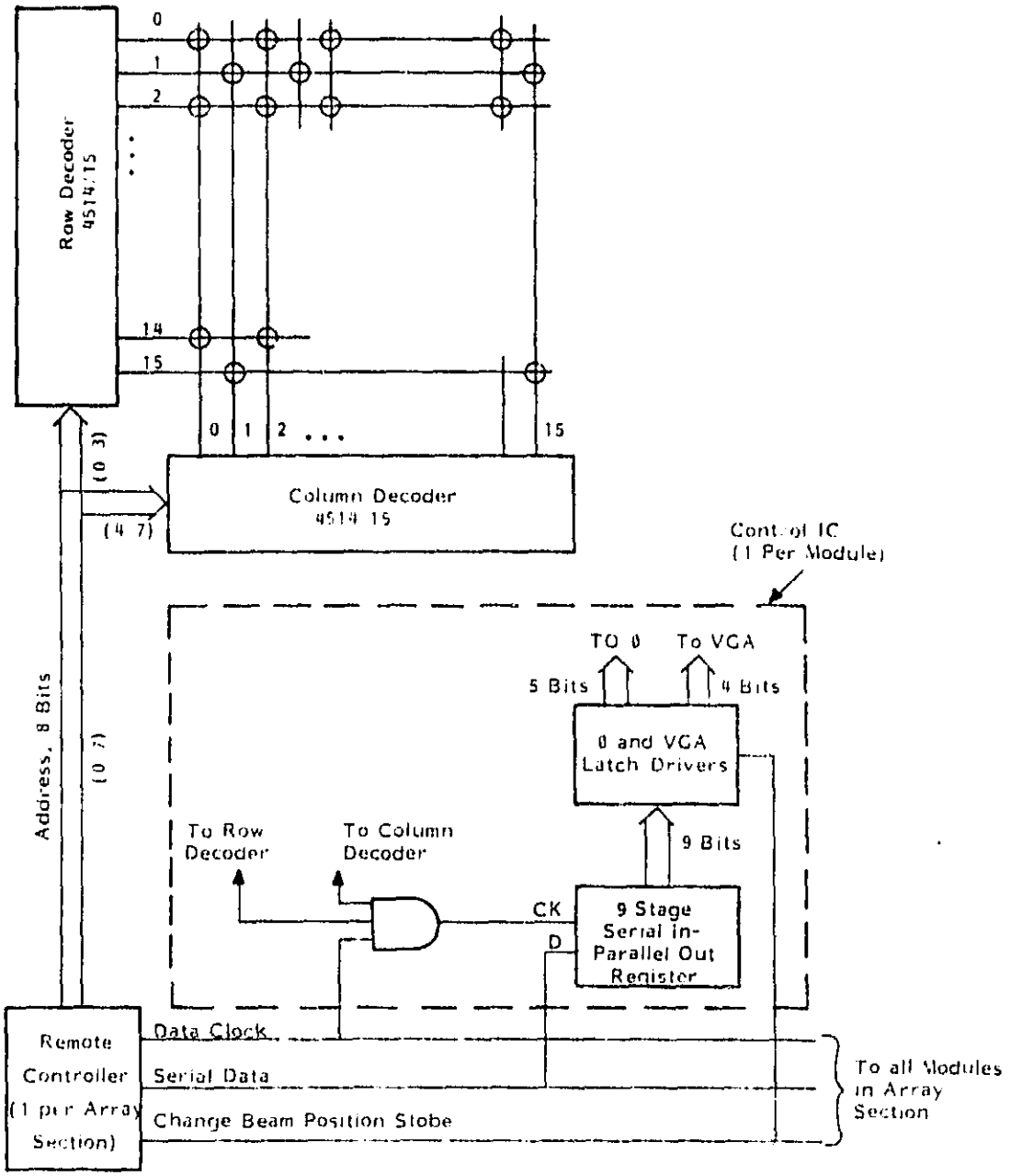

Figure 80. Scanning Array Section Control System

5.4 FEED ARRAY CONSTRUCTION

The active receive feed array of the scanning antenna is subdivided into six electrically independent rectangular sections. As has been described, these sections are located in overlapping portions of the array and are of alternate vertical and horizontal polarization. Each section forms one scanning beam and is comprised of a RF corporate signal combining network, DC power and control signal distribution systems, MMIC elemental receive modules, and conical horn radiating elements.

An isometric view of the scanning antenna feed array is shown in Figure 81. The conical horn radiating elements are arranged on the front face of the array in an equilateral triangular grid. The aperture size of the horns is maximized thereby making adjacent elements tangential. Each horn may be coupled for vertical and/or horizontal polarization. Both polarization couplings are used when the horn is shared between two overlapping array sections. When viewing the array from the front face, the conical horns form a CONUS image.

Located with each of the horn radiating elements are the MMIC active receive modules. The horns and modules are integrated into a single assembly for highest reliability. An elemental receive module is used for each polarization. Therefore, if a feed horn is shared between a vertical and horizontal array section, then it is integrated with two complete modules.

The module/horn assemblies plug into the RF corporate signal combining network via a miniature plunge style coaxial connector and into the DC power and control signal distribution system via a 12-pin miniature connector. The power and control signal distribution system consists of a multilayer printed wiring board oriented parallel to the array face as shown in Figure 81. Prime power of a positive and negative voltage, and address and beamsteering commands are sent from a central location to each of the array modules.

A separate corporate RF signal combining network is employed for each of the six rectangular array sections. Stripline has been selected for the combiner circuit media. As shown in Figure 81, signals from the elemental modules are first combined in a column fashion. The column combiners within an array section are identical, and have either 8 or 9 input ports dependent on the particular array section. Sixteen of these combiners are used for each section giving a possible 128 or 144 element positions. At combiner inputs where no module/horn assembly is used (element locations outside of the CONUS image) the port is loaded in the combiner's characteristic impedance. Column combiners located at overlapping array sections are fabricated as a two-layer structure.

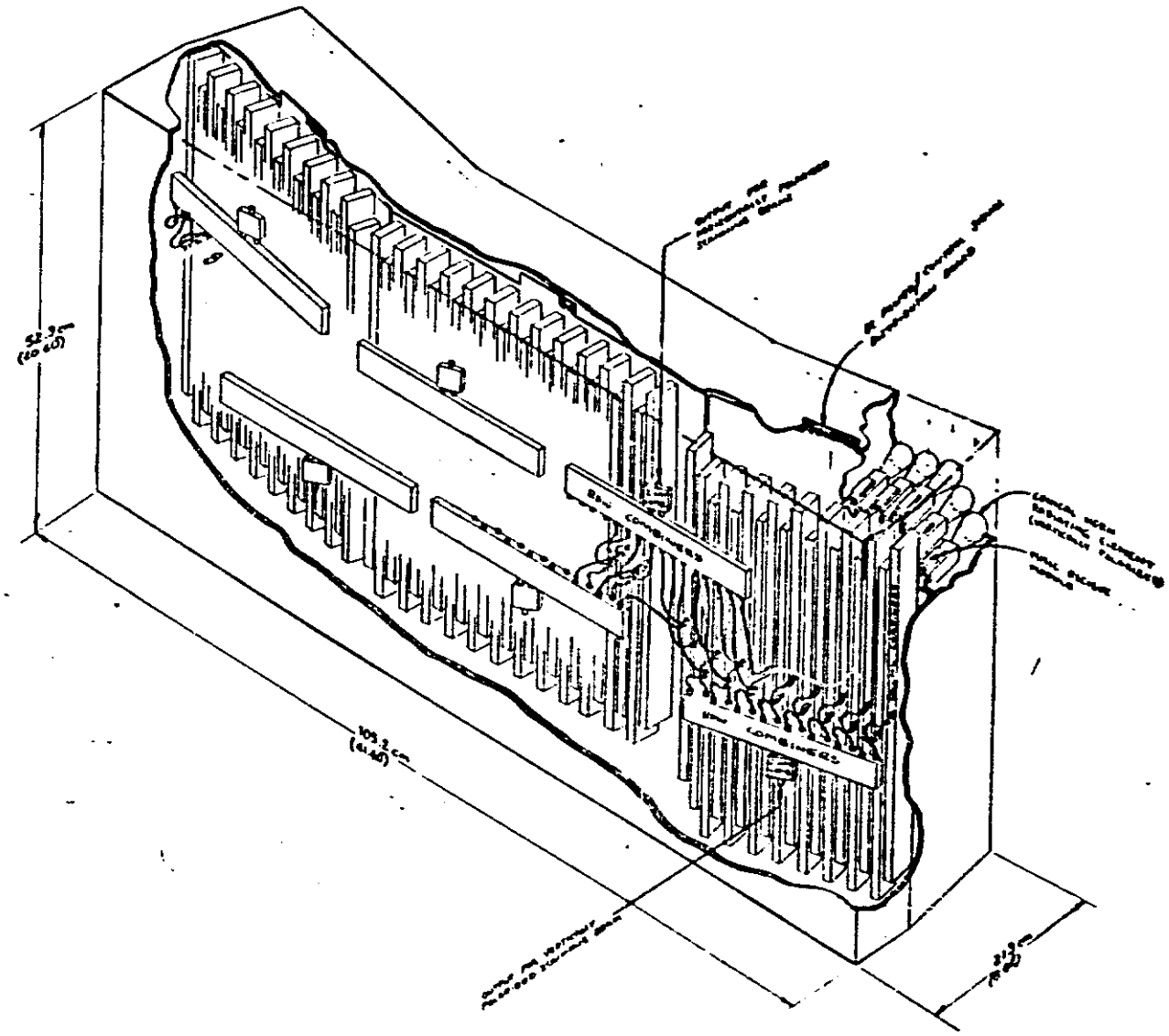

Figure 81. Isometric View of Scanning Antenna Feed Array

The outputs from an array section's sixteen column combiners are brought together with two 8-way row combiner networks. These are also shown in Figure 81. The interconnections are made with equal length coaxial cables to allow for a curvature of the array face. The design of the row combiners are identical to the 8-way column combiners. The output from a section's two row combiners are brought together in a single 2-way combiner whose output is an array section's scanning beam. This scanning beam output will have either vertical or horizontal polarization.

The overall size of the scanning antenna feed array is approximately 52.3 cm high by 105.2 cm wide by 21.3 cm deep. Views of the scanning antenna feed array from the top, side, and back face are shown in Figure 82. The conical horn radiating elements, MMIC receive modules, and stripline corporate combining networks are evident in the top view. The curved array face is shown as being approximated by three flat segments.

The array side view shows the module/radiating element assemblies within the support structure. A cut-away view of the two-layer stripline column combiner is given with the hybrid-ring binary level signal combiners evident.

The multi-layer printed wiring boards which comprise the DC power and control signal distribution system are shown in the back view of the feed array. The outline of the conical horn radiating elements which make up the east coast of the CONUS image may also be seen in this view.

A detailed drawing of the receive module/radiating element assembly is given in Figure 83. A module includes a 4-stage low noise amplifier, a 3-stage variable gain amplifier, and a 5-bit phase shifter MMIC submodules, plus beamsteering control and voltage level set integrated circuits. The control IC converts the serial beamsteering data to a parallel format with latching and provides a driver for the variable gain and phase shifter MMICs. The voltage level set circuit provides the required MMIC voltage levels from the plus and minus DC bus lines. The module/element assembly shown is used in an overlapping section of the array and therefore features two complete receive modules (one for each polarization).

The integrated circuits are mounted directly to a metal base plate to provide grounding and heat sinking. Interconnects between the circuits on the top side are made with bond wires and with printed lines on an alumina substrate frame. The interface between the module/element assembly and the stripline corporate combiners are made with miniature plunge style coaxial connectors. The interconnect to the DC power/control signal distribution system is made with a 12-pin miniature connector. A two-side printed wiring board routes signals from this connector to feed-through pins for connection to the control and voltage level ICs. The receive modules are hermetically sealed with a ceramic cover which is bonded to the top side alumina frame.

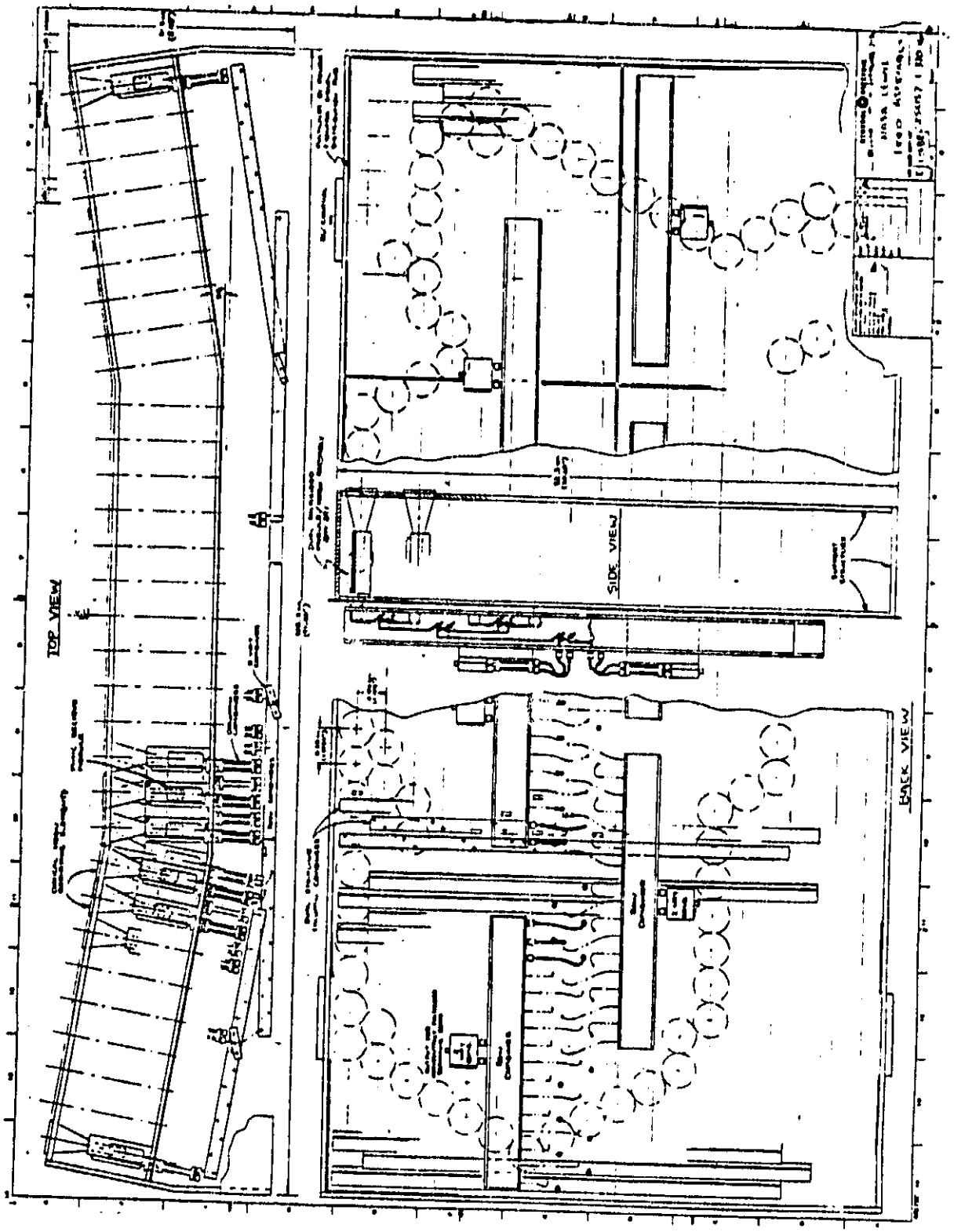

Figure 82. View of Scanning Antenna Feed Array from Top, Side, and Back Faces

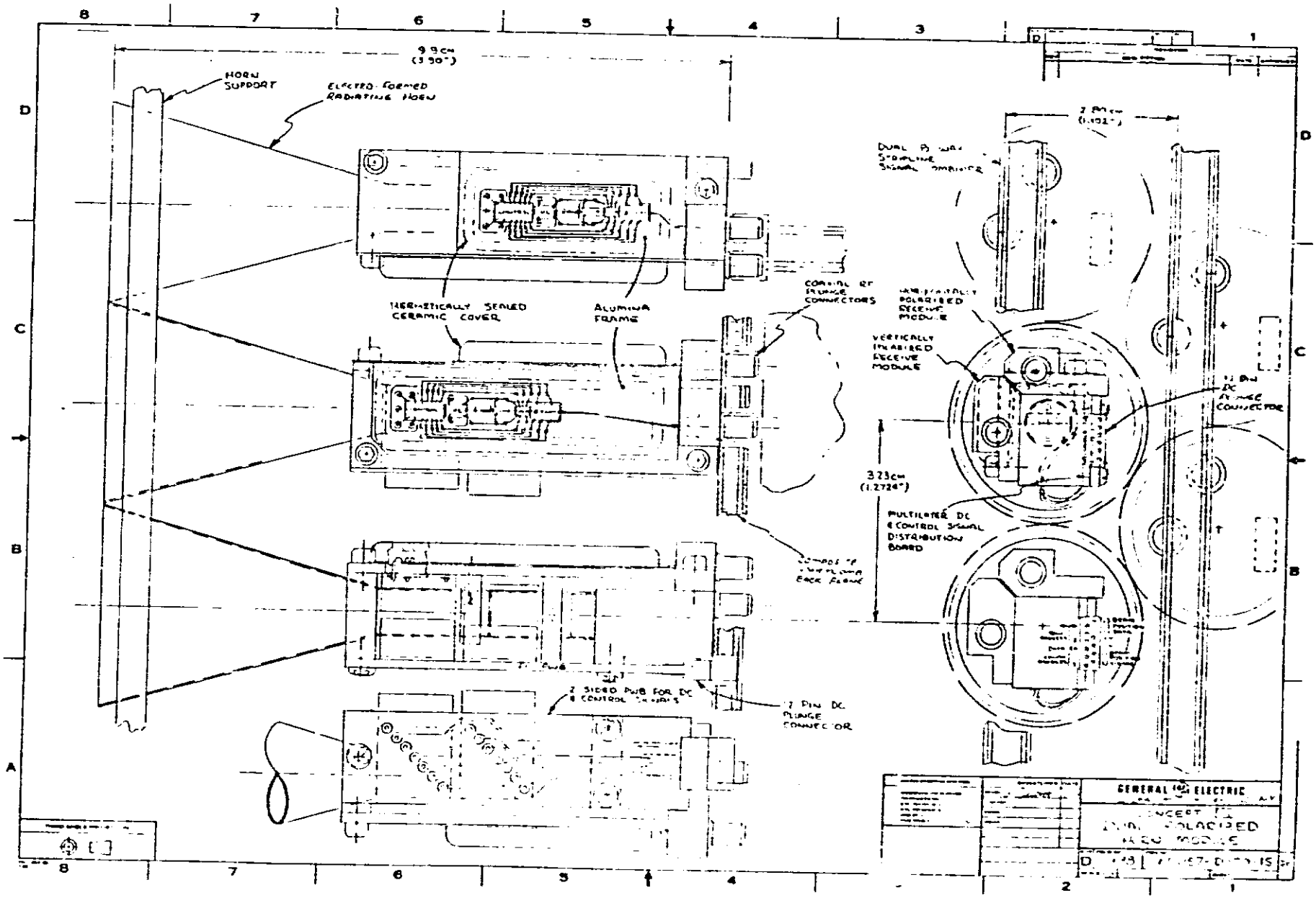

Figure 83. Design of Conical Horn Radiator/MMIC Receive Module Assembly

5.5 THERMAL MANAGEMENT OF FEED ASSEMBLY

The thermal management of the feed assembly is of particular concern for several reasons. FET maximum temperatures are of critical importance to reliability. Even though large amounts of power are not involved, the array is densely packed creating an essentially one-dimensional heat flow situation - front and back. In addition, the ultimate space application precludes any convective cooling; conduction and radiation cooling must be the heat transfer modes.

Some design aspects of the feed assembly have not yet been addressed and many details of the spacecraft are not known. However, based on present knowledge, some basic assumptions have been made to allow the definition of a preliminary thermal management system design and to permit the calculation of a maximum FET temperature. The basic assumptions which have been made are:

1. Heat dissipated is .25 watts per module and .50 watts per horn.

2. The worst case chip has a microstrip FET (with power of 40 mW, width of 125 μm, "gate" spacing of 37.5 μm, "gate" heat source dimensions of 1 μm) on a 100 μm thick GaAs chip.

3. Heat is conducted from the FET chip to the horn and is radiated from its outside surface; this is the only heat path.

4. The horns look primarily at deep space and are subject to solar radiation; no other heat sources are included.

5. The horn's external surfaces are painted white or finished with some other low solar absorptivity, high emissivity surface.

These basic assumptions and other necessary design assumptions have been made as realistically as possible. In cases where data is not availabe, conservative assumptions have been made.

Using these assumptions as needed, a thermal resistance network analysis has been made for the horn module. This analysis indicates that the maximum FET temperature is approximately 124°C. The backside of the GaAs chip is estimated to be 99°C. The temperature of the horn radiating surface is about 80°C.

These results indicate that the design of the feed assembly is adequate with respect to thermal managment for the intended synchronous orbit application. As the design of the feed assembly and spacecraft becomes firmer, the thermal management design can also be further defined and refined.

5.5.1 Thermal Management Analysis

1. Temperature of Horn Surface

$$Q_7 + \alpha_S Q_S A_S = \sigma \varepsilon A T^4 \qquad \text{(Steinberg, p.149)}$$

$$.5 + .15\ (.9)(1.25) = (3.66\ E\text{-}11)(.94)(1.25)\ T^4$$

$$T = 353°K = 80°C$$

Assumes:

- horns look primarily at deep space
- total power horn = .5 watts
- horn surface solar absorptivity = .15 — white paint or similar finish
- horn surface emissivity = .014
- horn radiating area = 1.25 in^2
- incident solar radiation = .9 w/m^2

2. Thermal Resistance of Horn

$$R = \ell / kA$$

$$= 2.5\ in/[5.5\ w/in\text{-}°C][\pi\ (.8\ in)(.010\ in)] = 18.1\ °C/W$$

Assumes:

- average path length = 2.5 inches (horn radiates thermally over entire flared portion)
- horn is .010 thk aluminum
- average conducting area = $\pi dt = \pi(.8)(.010)$

3. Thermal Resistance of Substrate and Bracket

$$R = \ell / kA$$

$$= 2.0\ in/[5.5\ w/in\text{-}°C][(.62\ in)(.06\ in)] = 9.8\ °C$$

Assumes:

- average path length = 2 inches
- substrate and bracket are .06 thk aluminum (conservative: bracket is .12 thk)
- substrate and bracket width are each .62 in.

4. Interface Resistances from GaAs Backside to Horn Radiating Surfaces.

Contact Resistances = .5 °C-in^2 /w

Area (Metal Substrate to Bracket) = [(.12 in)(.62)][2] = .149 in^2

$\Sigma R = .5/.149 + .5/.415 = 3.4 + 1.2 = 4.6$ °C/W

Assumes:

- dry contact interface
- brazed or soldered interfaces (GaAs to metal substrate and bracket to horn) have negligible thermal resistance.

5. Constriction Resistance

Constriction resistance is estimated to be 5° C/W

6. Temperature of Backside of GaAs Chip

Σ R (Horn Surface to GaAs Chip) = $R_{horn} + R_{substrate}$ and bracket + $R_{i/f} + R_{construction} = 18.1 + 9.8 + 4.6 + 5 = 37.5$ °C/W

Assuming total power/horn = .5 watts

Δ T (chip to horn surface) = (.5)(37.5) = 19°C

Temperature at GaAs chip = $T_{horn} + \Delta T = 80 + 19 = 99$°C

7. ΔT From Gate to Chip Nonactive Side

Worst Case Assumed to be on Var Gain Chip

3 Channels; 1.5×5.0 mils; 40 mW each

Assumes:

- width = 5 mils = 125 μm
- "gate" spacing = 1.5 mils = 37.5 μm
- "gate" heat source dimension, d, = 1 μm (worst case)
- reference temperature = 99°C (T_o)
- substrate thk = 4 mils = 100 μm
- GaAs conductivity = .033 W/°C-mm (at T_o = 99°C)

From: GaAs FET Principles and Technology, p. 323, Figure 6, etc.

Thermal Impedance (T_o = 60, k = .038, d = 4) = 58°C-mm/w

Thermal Impedance (T_o = 99, k = .033) = 67°C-mm/w

Thermal Impedance ((+12 for d = 1 "best fit") = 79°C-mm/w

Power = 40 mw = .04 watt = .04 w/125 μm = .04 w/.125 mm = 3.2 w/mm

$\tau - T_o = .32\ (79) = 25$°C

$T - T_O \cong 25°C$

Gate
Temperature = Chip Backside Temperature + $(T - T_O)$

= $99 + 25 \cong 124°C$

6.0 FINAL DESIGN OF REFLECTOR/FEED ARRAY

6.1 DISCUSSION OF FINAL DESIGN SELECTION

The parametric study concluded with a design point consisting of a Cassegrain dual reflector which satisfied both the fixed beam and scanning beam requirements. Due to several factors discussed here, the final design process led to a distinction between the final dimensions of the two designs. These differences include:

- Downward revision of available element gain due to change of element from yagi to horn. Change was made to avoid unacceptable cross-pol coupling.

- This caused upward pressure on the aperture diameter to meet the 56 dB gain requirement.

- To permit one design to use a small (250 λ) aperture, the scanning beam functional requirement of 53 dB gain over CONUS was considered to be met by a continuously steerable beam of at least 54 dB gain. This allows a 1 dB margin for pointing accuracy and beam-steering resolution.

- The element spacing was reduced to the minimum possible value permitted by physical constraints such as sizes of parts and multi-wire connectors.

- With a larger aperture to make up for lost element gain, by reducing spillover, etc., the secondary element pattern becomes narrower. To design for a continuously steerable beam capability, with a fixed minimum element spacing, the focal length had to be increased to reduce the angular separation of the secondary beams to the point of approximately 3 dB crossover levels. Performance capable of continuous steering is required even in the fixed beam case because the elements of adjacent city arrays are packed close together and even overlap in multiple ways. The desired beam angle for a given city will not necessarily correspond to the peak of a single secondary element pattern.

- The wider East-West scan is done in azimuth to minimize deviations of magnification of the subreflector off axis, due to offset. Significant gain variations exist with scan angle in a dual reflector, due to the decreasing magnification of the hyperboloidal subreflector as the scan angle is increased away from the subreflector axis. The effect is to increase the gain of an element, but also to increase the angular separation of the peaks of secondary element patterns, thus degrading sidelobe control. For an offset dual reflector system, the subreflector illumination over the entire range of scan in the offset plane is typically all to one side of the subreflector axis. This

asymmetry aggravates the varying magnification of the subreflector. Attempts to reduce this effect by tilting the subreflector axis or increasing the subreflector focal length both result in an increased main reflector offset. Therefore we have chosen to perform the widest scan in azimuth in order to use the subreflector symmetrically in that plane and reduce the maximum degradation that will occur in any scan direction.

- The minimum element spacing in the feed array was limited to 3.1λ based on packing and assembly considerations, mainly the physical dimensions of connectors, modules, transitions. This fact put upward pressure on the F/D ratio of the initial design point in order to achieve the desired crossover level of the constituent beams in the far field.

- The approach taken was to design for an array/reflector capable of forming a well-formed beam with generally low sidelobes. This is in contrast to identifying the zones in the sidelobe region in which interfering signals are expected, and controlling sidelobes in only those regions. For instance, in a scanning beam case with 6 regions as shown in Figure 4, the sidelobes in the rest of the zone of a given beam may not need to be controlled. Exploiting this fact may permit use of fewer elements in a beam. However, this alternative was not chosen.

6.2 DISCUSSION OF QUANTIZATION ERRORS

The basic array design process was completed assuming continuously variable amplitude and phase weights. Some margin was allowed for quantization errors, primarily in the sidelobe criteria. The results of the quantization study are presented here. Four basic cases from the final design for the 6 scanning beam configuration were used as representative starting points. The four cases used were:

- 0° scan, one principal element
- 0° scan nominal, three principal elements
- 3° scan nominal, one principal element
- 3° scan nominal, three principal elements.

All four cases used 19 elements to form the beam. Cases with one principal element have the composite beam peak near an element beam peak. Cases with three principal elements have the composite beam peak between three individual element beam peaks.

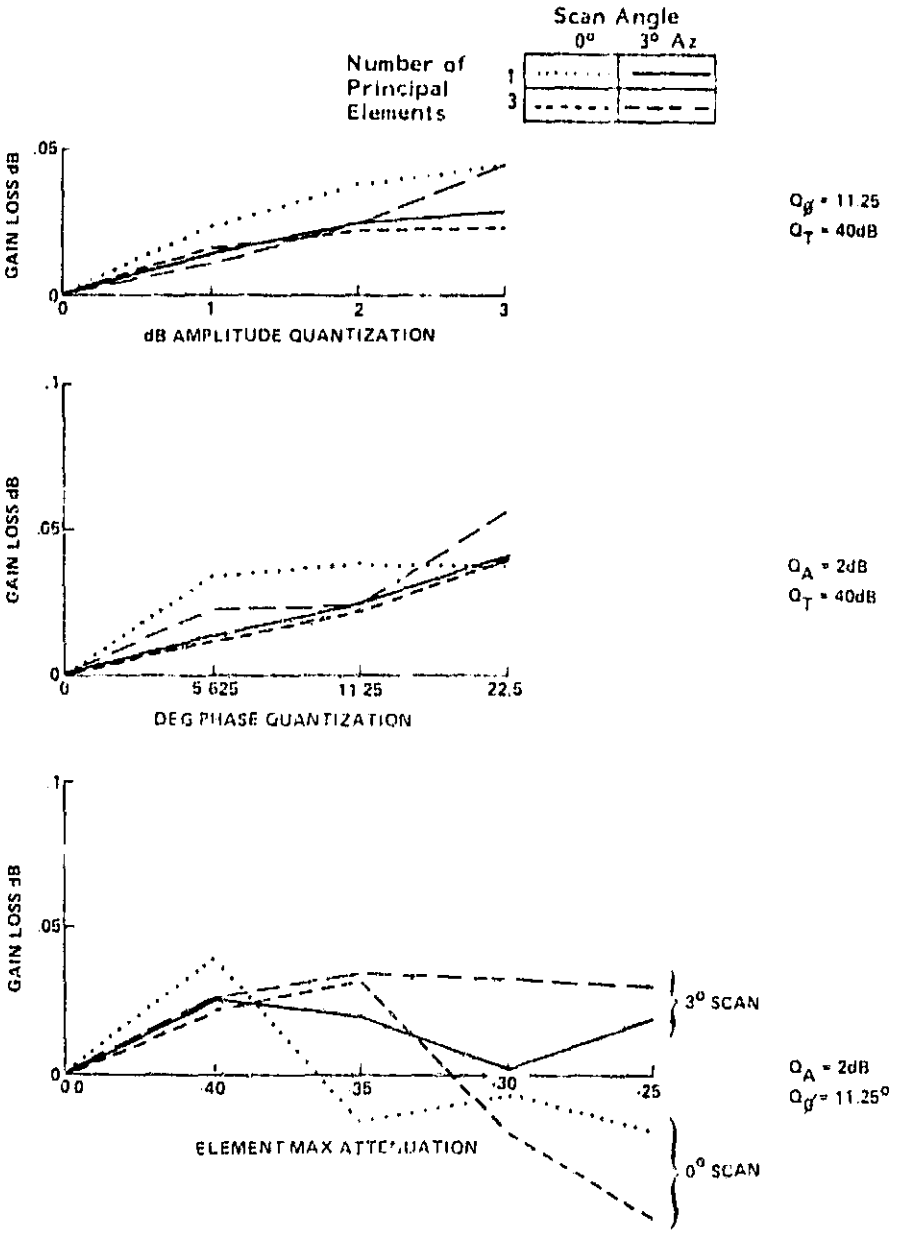

Figure 84. Gain Loss Due to Quantization

An ensemble was obtained by repeatedly applying uniformly distributed errors to the ideal phase and amplitude weight settings for these cases, evaluating the resulting patterns, and comparing to the ideal pattern. This was a much more efficient procedure than to obtain the same number of samples by using a fixed set of quantization levels, ideal element weights from many different scan angles, and fit these ideal weights to the fixed levels. Either way, the error on an individual phase or amplitude weight is approximately uniformly distributed.

The standard value for amplitude quantization levels is compared at 0, 1, 2, and 3 dB. The actual set of levels available is given in Table 22. These are obtained by cascading 3 variable gain amplifiers having individual settings also given in Table 22, with all settings normalized to maximum of 0 dB.

TABLE 22. AVAILABLE AMPLITUDE WEIGHT LEVELS

0	0		0	0	
-3	- 3	3	1.5	1.5	Constant
-6	- 6	3	6	3	1.5 Step
-10	- 9	3	10.5	4.5	
-13	-10	1	12	6	
OFF	-12	2	OFF	7.5	
	-13	1		9	
Individual	-15	2	Individual	10.5	
VGA Settings	-16	1	VGA Settings	12.	
	-18	2		13.5	
	-19	1		15.	
	-20	1		16.5	
	-22	2		18.	
	-23	1		19.5	
	-25	2		21.	
	-26	1		22.5	
	-29	3		24.	
	-30	1		25.5	
	-32	2		27.	
	-33	1		28.5	
	-36	3		30	
	-39	3		31.5	
	OFF			33.	
	LEVEL	STEP		34.5	
				36	
				OFF	

The sparseness of levels available at levels higher than -10 dB means beam pointing errors are best represented by the 3 dB quantization step. The sidelobe errors are best represented by the performance of a level near the 2 dB step, since from -10 to -26 dB the step size averages about 1.5 dB, and from -26 to -39 the step size averages about 2.2 dB. Results of these samples are shown in Figures 84 through 86.

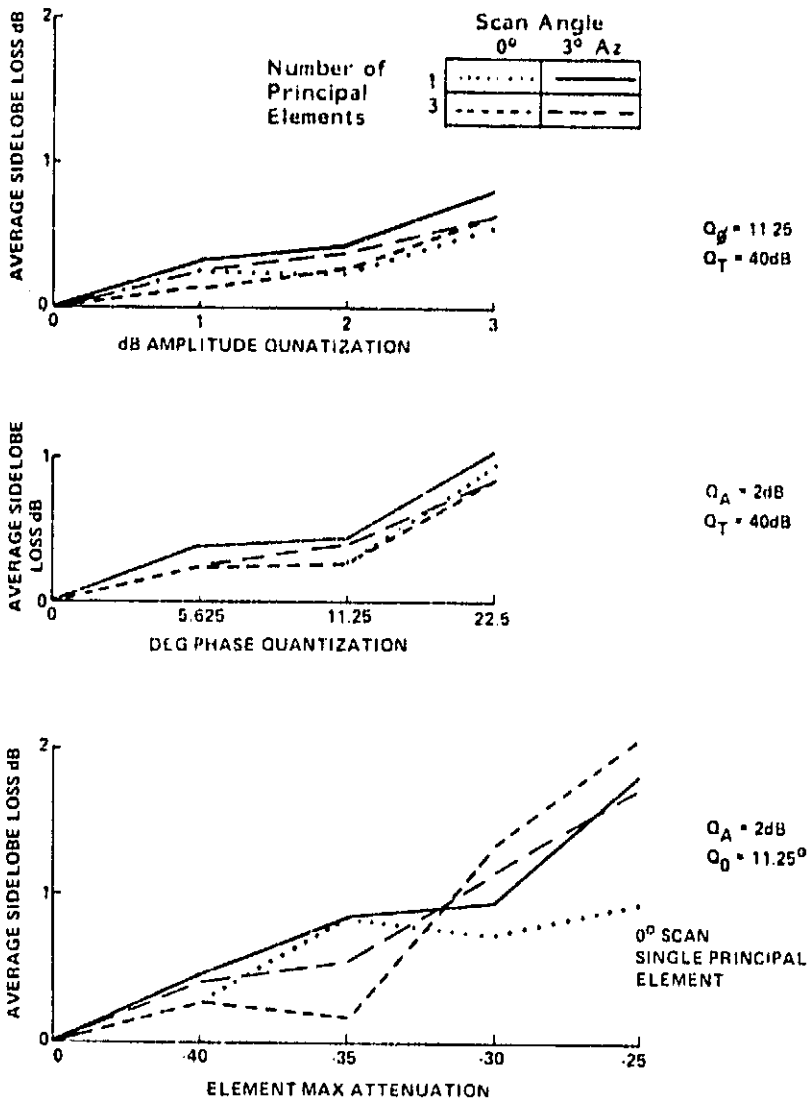

Figure 85. Average Sidelobe Increase Due to Quantization

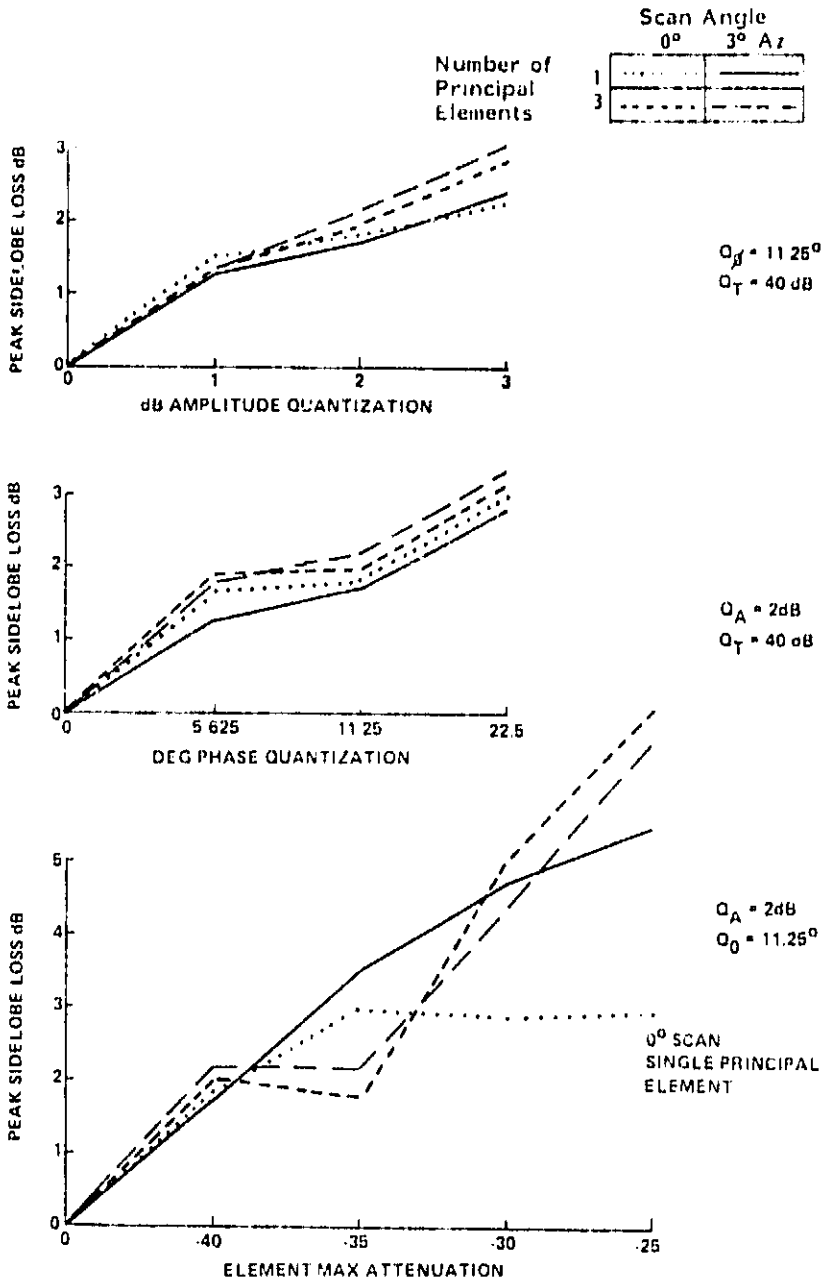

Figure 86. Peak Sidelobe Increase Due to Quantization

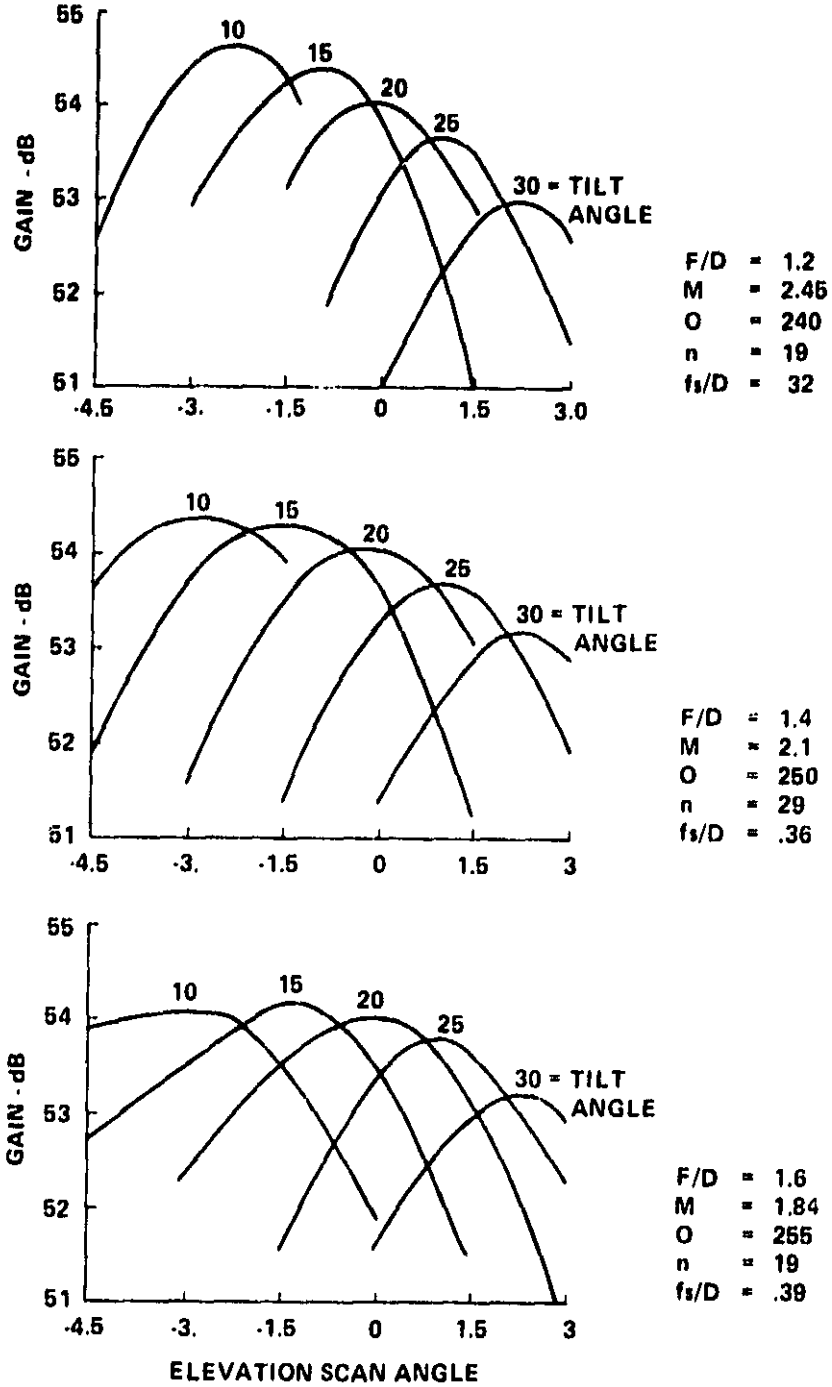

Figure 87. Secondary Pattern Gain vs Scan vs Tilt Angle of a Planar Array Face Constant F/D*M = 2.94

Considering the 5 given levels of the VGA as chosen subject to some other rule, such as only using 1 VGA in an elemental signal path, this application in which 3 VGA's are cascaded could benefit from a more appropriate choice of levels. A possible suggested set is given in Table 22. This provides an even distribution of available levels which is useful, decreases the overall range, which was already more than necessary, and eliminates some redundancy in settings. The levels were chosen in this manner. For a uniform step size of X, number of units to be cascaded N, number of levels per unit M; initial step is X, next step is (N+1)*X; next step $(N+1)^2$*X, etc. This is done symmetrically away from both the 0 dB max level and the yet unknown lowest level. This lowest level is determined by matching the absolute levels at the center point.

Given that a 5 bit phase shifter would be available, the pattern error versus amplitude quantization level samples were run with an 11.25 phase quantization level. To show the significance of this phase accuracy, samples were run with 1 bit more and less phase setting accuracy, as shown in Figures 84 through 86.

To demonstrate the significance of the level of the threshold below which an element is turned off, the pattern error versus three threshold levels is plotted in Figures 84 through 86.

The errors plotted are average errors. In all cases it is possible for the pattern of the quantized elements to have one performance parameter better than it was for the unquantized case. This is true because the optimum point used is a "global" compromise among gain, average sidelobe, and peak sidelobe levels. Also, any particular sample could have a much worse than average performance parameter.

Inspection of Figures 84, 85, and 86 reveals only two types of errors which show correlation with the particular scan condition being considered. Gain loss versus element turnoff threshold becomes negative, a gain increase, for high thresholds near 0° scan. Larger scan angles maintain a gain loss although it appears to reach a limit. The other condition which stands out is the sidelobe level degradation at 0° scan for a single principal element, as a function of element shutoff threshold. The degradation for this case appears to reach a limit, while the other cases continue degrading.

The entire range of quantization errors considered here was found to have only a very small effect on pointing angle. The maximum error for any particular error sample for any case was never greater than .04°. These large errors occurred only for the 3 dB amplitude quantization step, for the case having three principal elements. Errors for all other cases were less than .02°, relative to half-power beamwidths of .28°.

6.3 ARRAY CURVATURE AND TILT REQUIREMENT

It is well known that the focal surface for an offset Cassegrain reflector antenna is a non-symmetrical curved surface. However, there was pressure from the array designers to design if possible an array with a flat face. Thus, an investigation of gain loss was made at the single element level to assess the impact of a flat array face.

This trade was done for 3 250 λ main reflectors, with a constant F/D - magnification factor product of 2.94. As seen in Figure 87, the larger magnification design yields a sharper peak of gain vs scan for a flat array face. The larger magnification also has another disadvantage, in that the envelope of the gain curves has its maxima at a larger scan angle. This increase in gain is due to decrease spillover loss due to a decrease in the actual subreflector magnification realized over the portion of it which is used. This is accompanied by an increase in the apparent element spacing, which is a distinct disadvantage. Since the envelope of these gain curves are a good approximation to the gain vs scan curve for an ideally located and pointed element, clearly the smaller magnification is desirable. Also, the maximum gain is asymmetric with respect to the boresight scan direction. These considerations lead to the choice of a small magnification, and the implementation of the ± 3° scan in azimuth, so that the performance will be symmetrically distributed about the center point. The ± 1.5° scan now done in elevation is not subject to the layer errors encountered by a ± 3° elevation scan.

The aray curvature and tilt was based on an iterative selection of the best pointing angle for the 3° azimuth scan element. Projection of this angle on the offset plane yields the array tilt, and the normal component of the angle yields the curvature requirements. Using a cylindrical surface satisfied the performance criteria in elevation scan for the 6 scanning beam case. For the 18 fixed beam case, some city clusters need to be individually pointed, but the surface of this feed array is not constrained to preserving a continuous sequence of elements.

Use of a cylindrical surface through the optimum location and pointing angle of the wide azimuth scan element leads to some forward defocus of elements near boresight. This defocus condition has been modeled and causes only slight degradation in a region where there is plenty of margin.

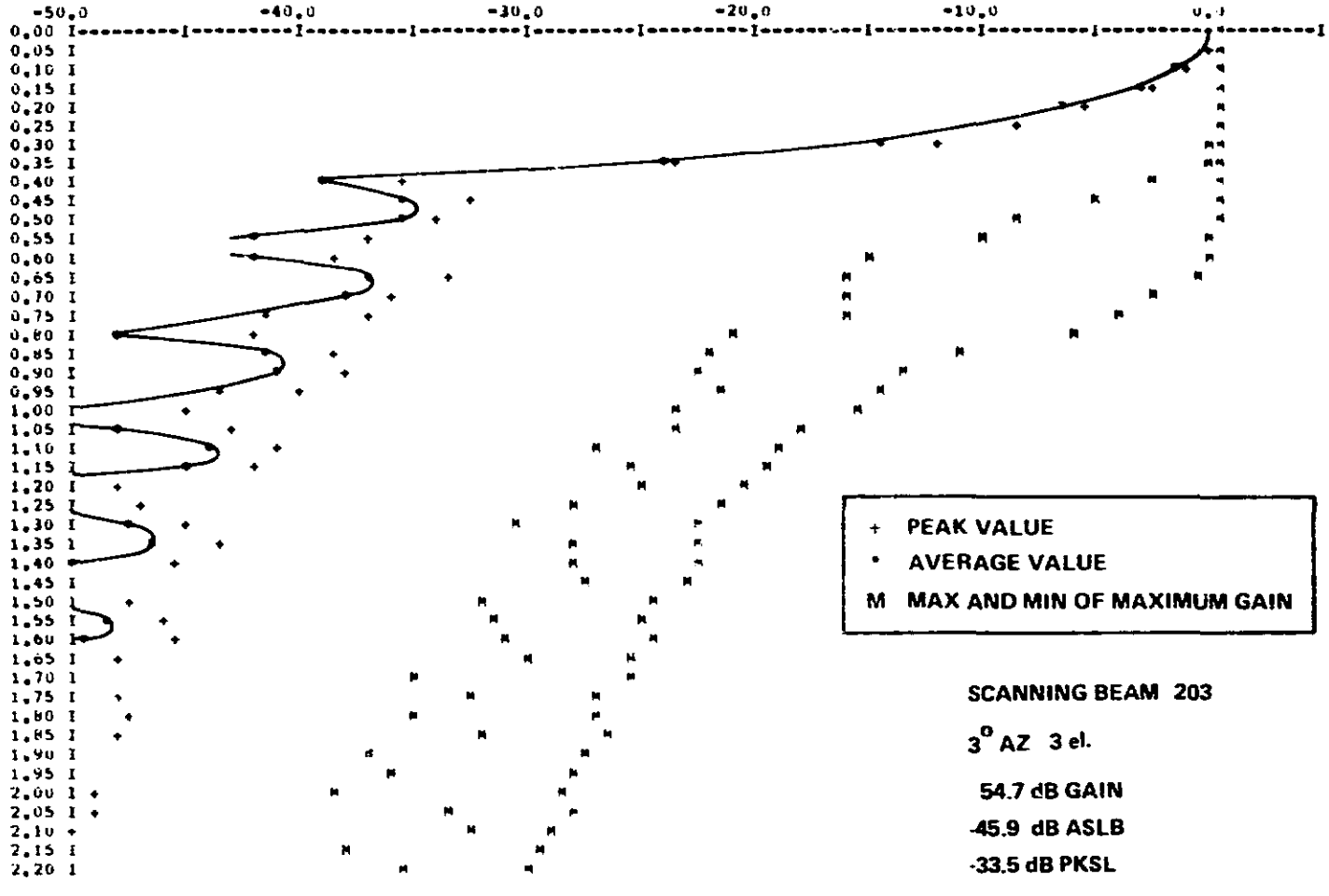

Figure 88 . Plot of Peak and Average Sidelobe Levels in Rings Around Main Beam

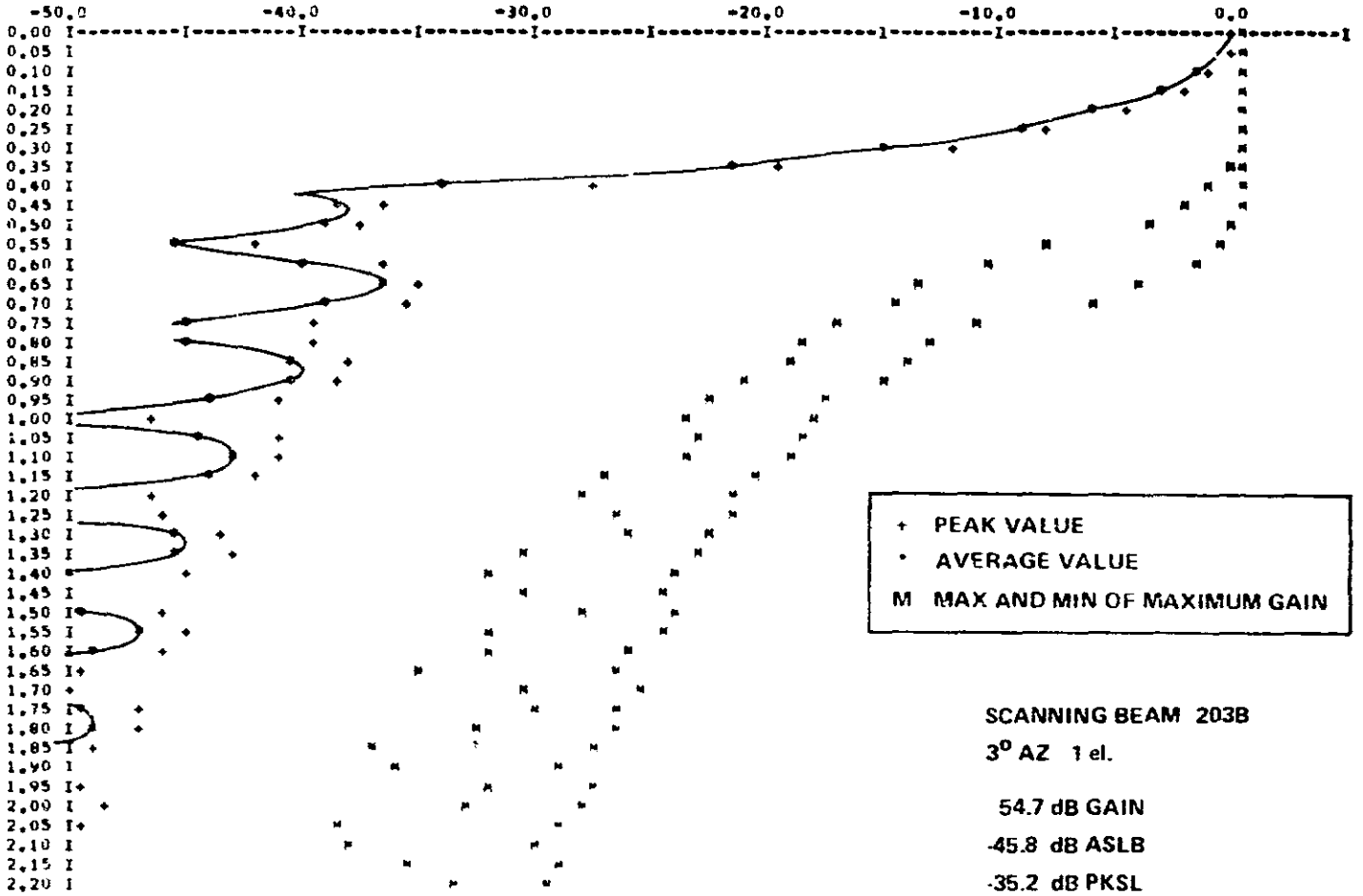

Figure 89 . Plot of Peak and Average Sidelobe Levels in Rings Around Main Beam

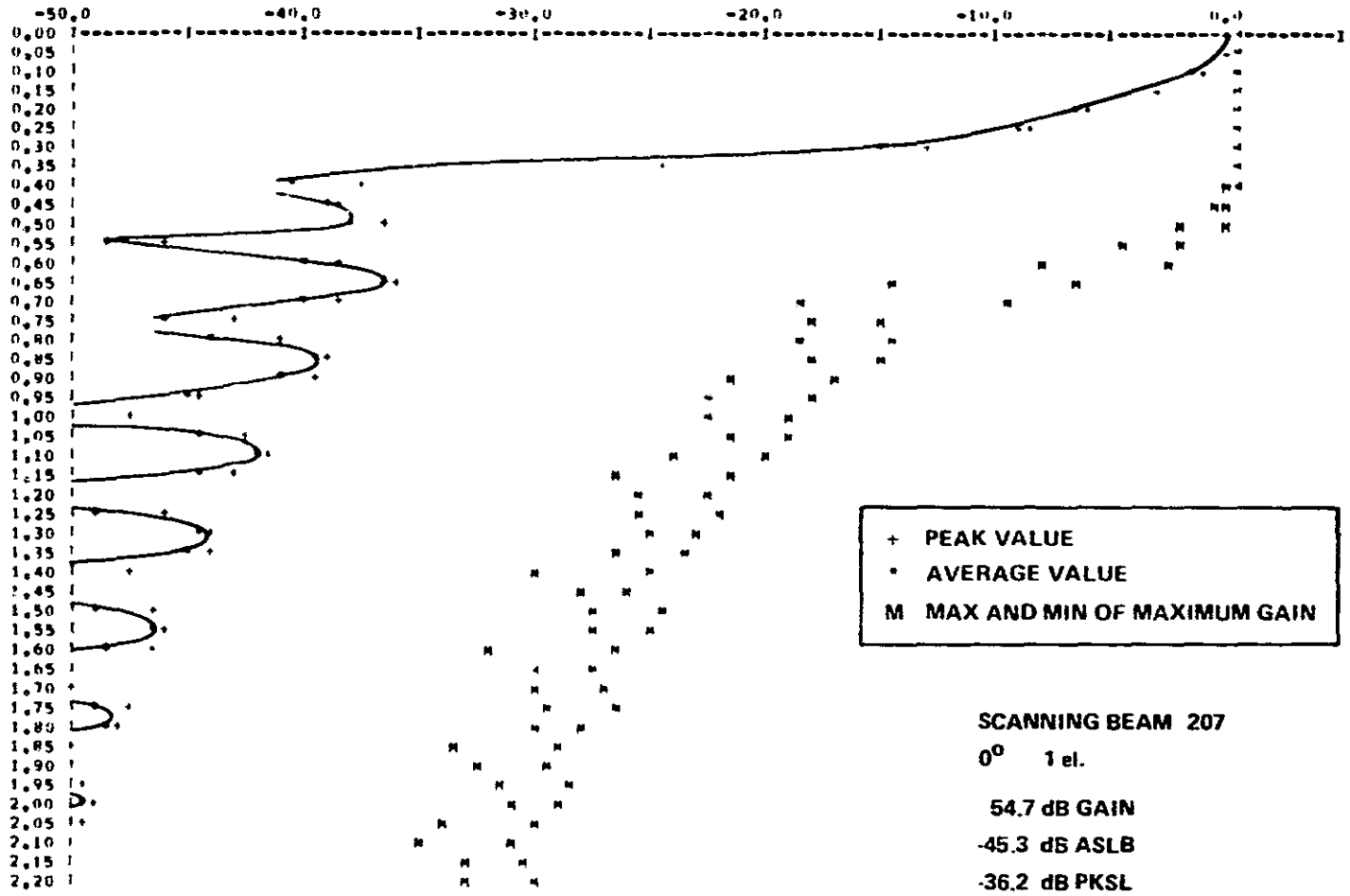

Figure 90. Plot of Peak and Average Sidelobe Levels in Rings Around Main Beam

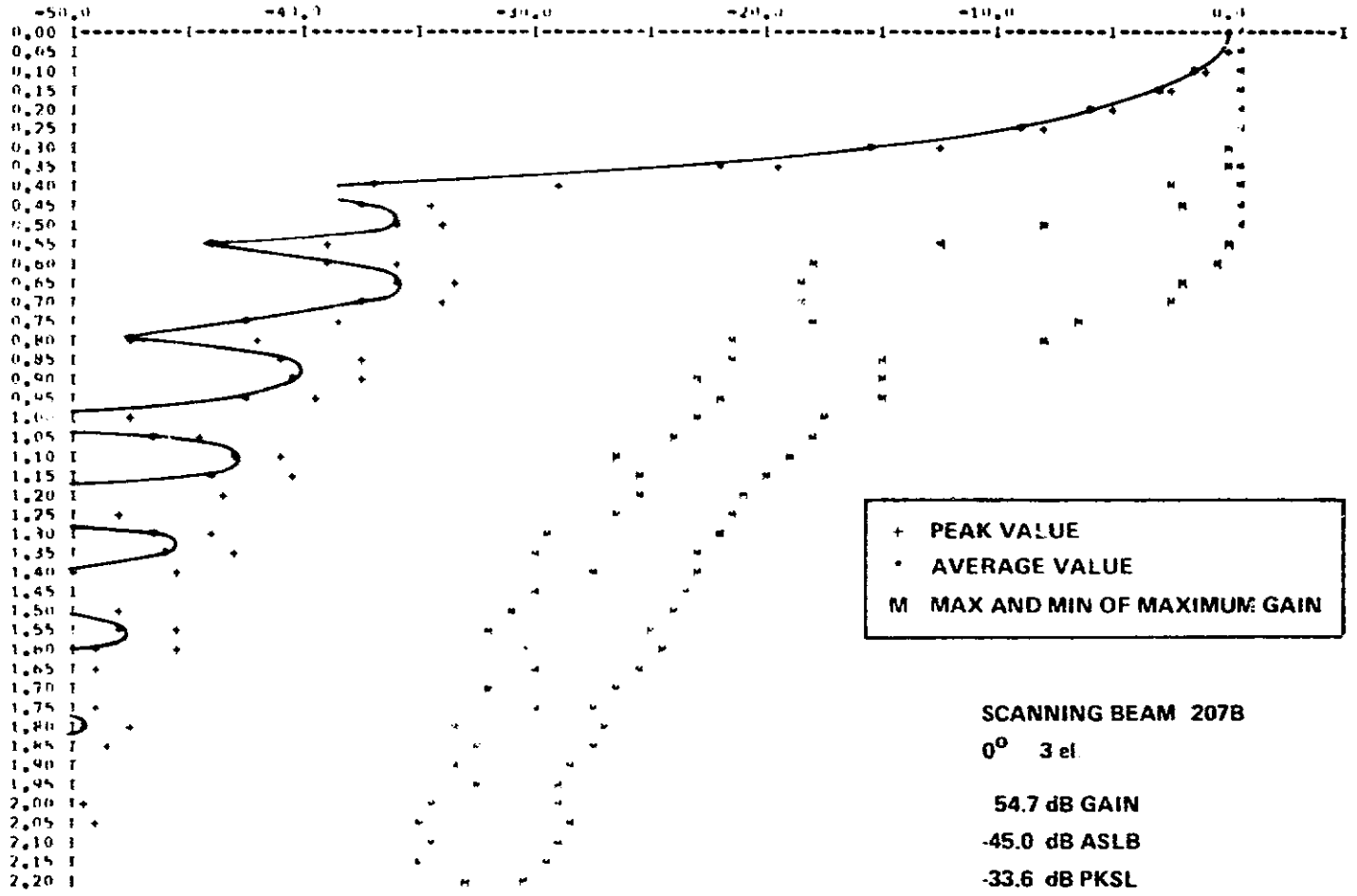

Figure 91. Plot of Peak and Average Sidelobe Levels in Rings Around Main Beam

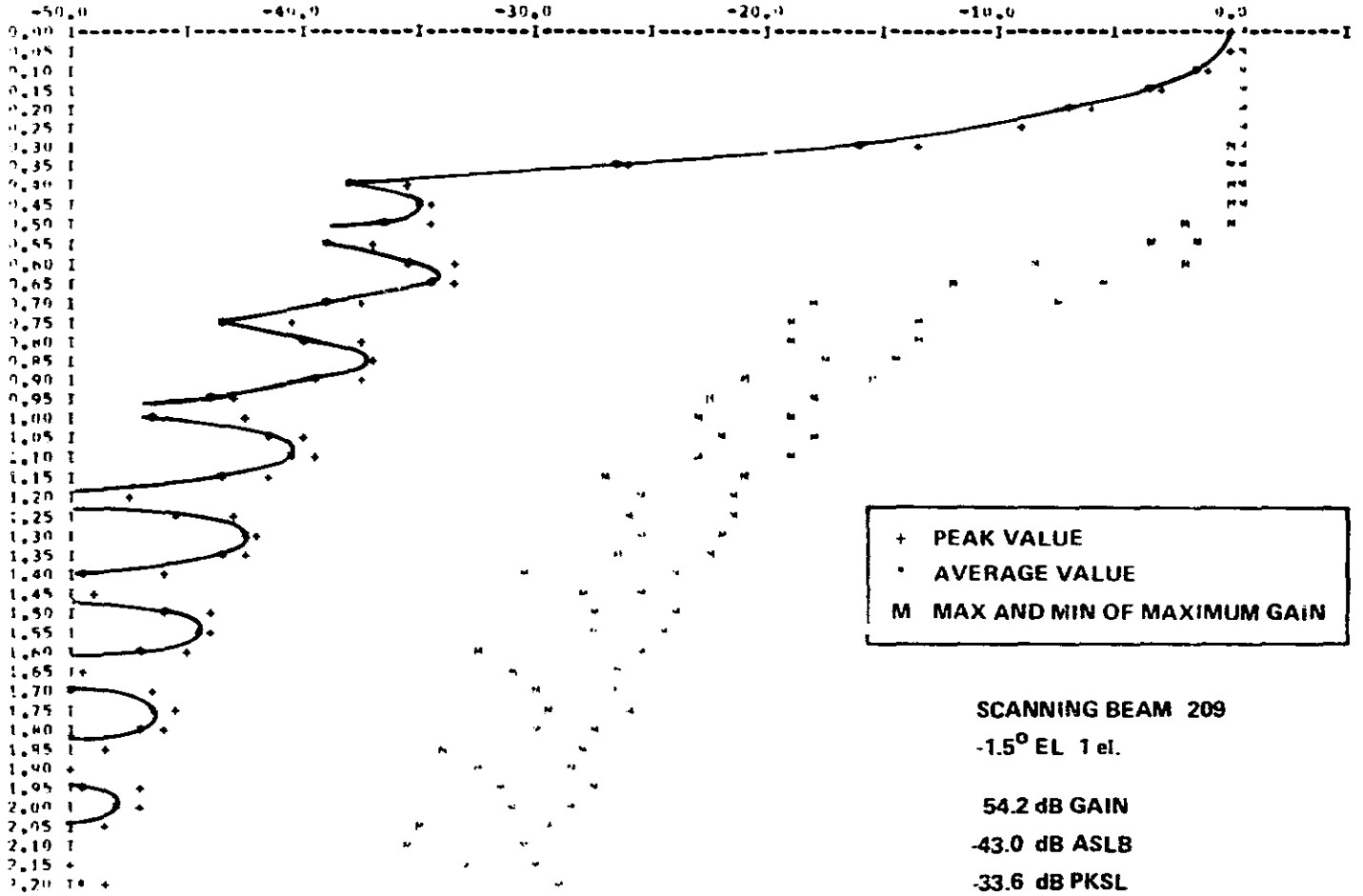

Figure 92. Plot of Peak and Average Sidelobe Levels in Rings Around Main Beam

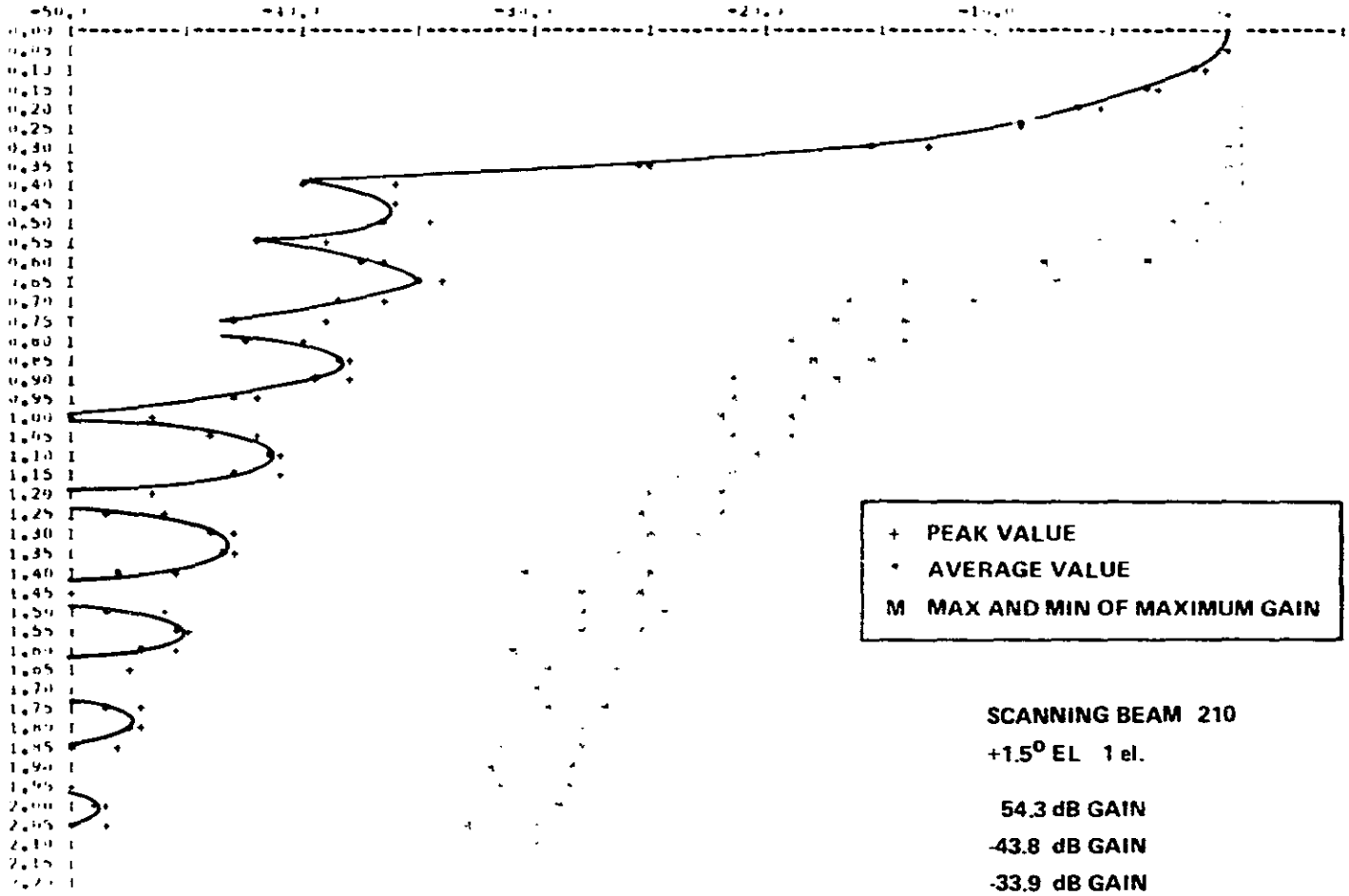

Figure 93. Plot of Peak and Average Sidelobe Levels in Rings Around Main Beam

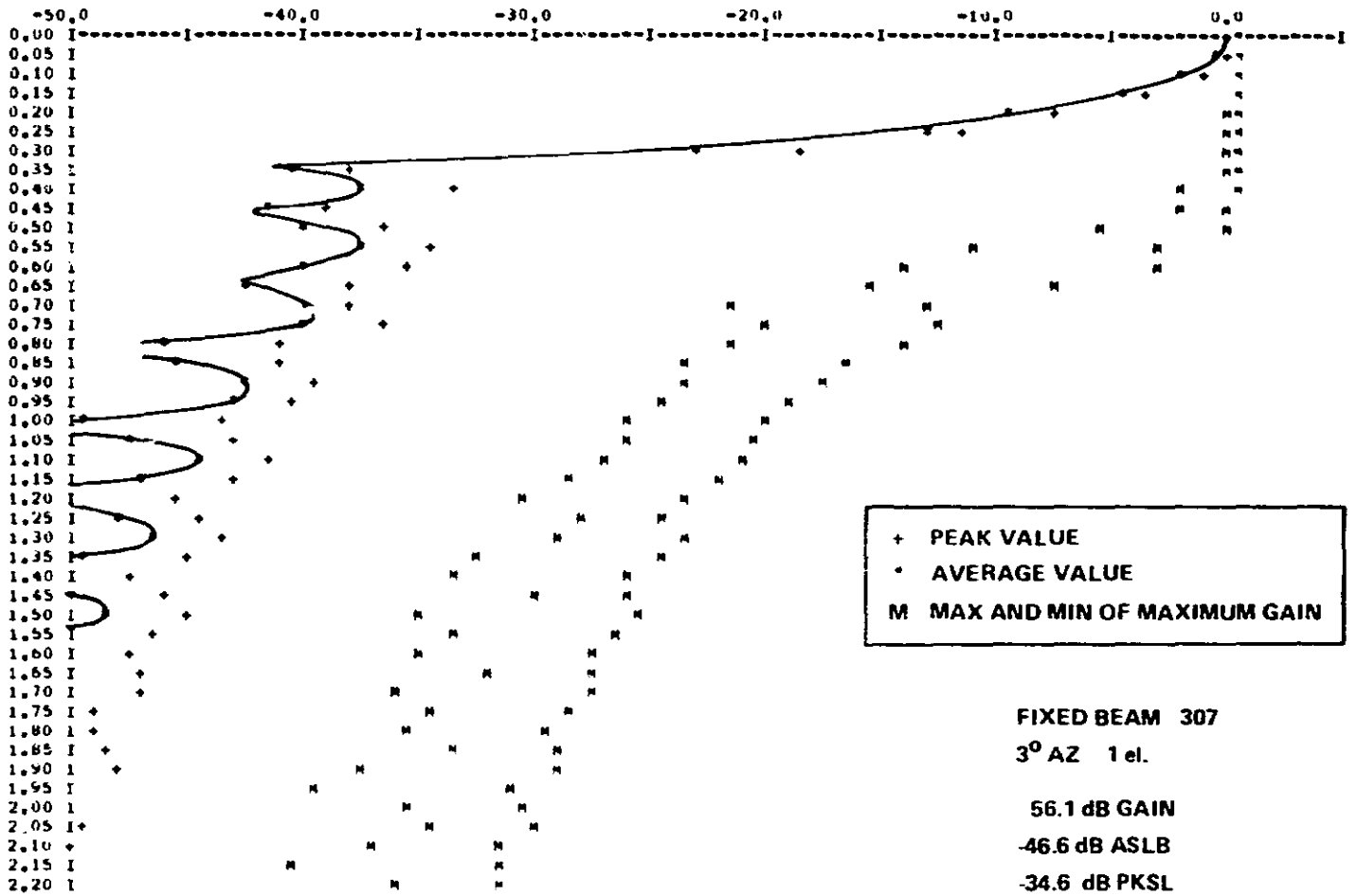

Figure 94. Plot of Peak and Average Sidelobe Levels in Rings Around Main Beam

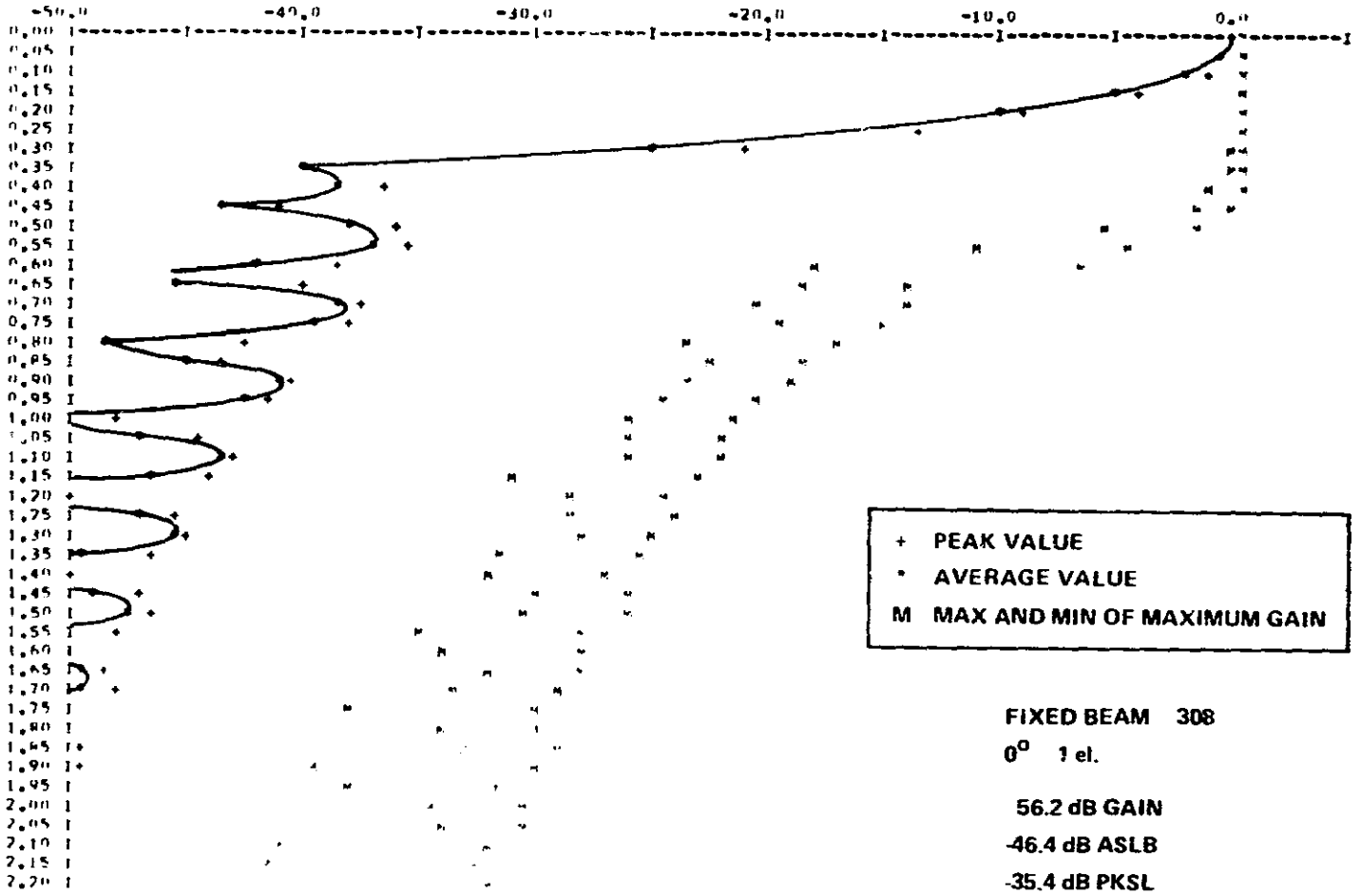

Figure 95. Plot of Peak and Average Sidelobe Levels in Rings Around Main Beam

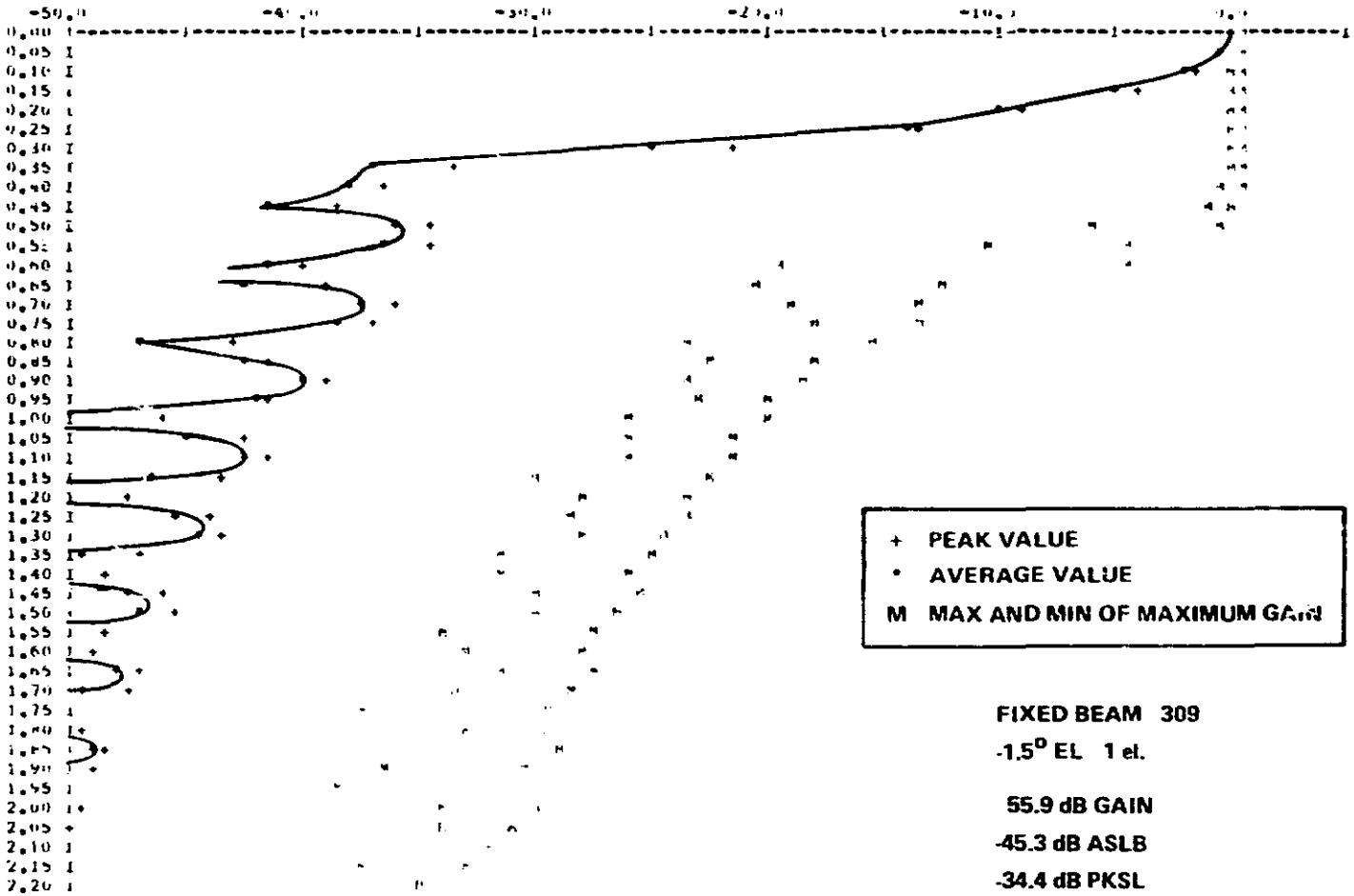

Figure 96. Plot of Peak and Average Sidelobe Levels in Rings Around Main Beam

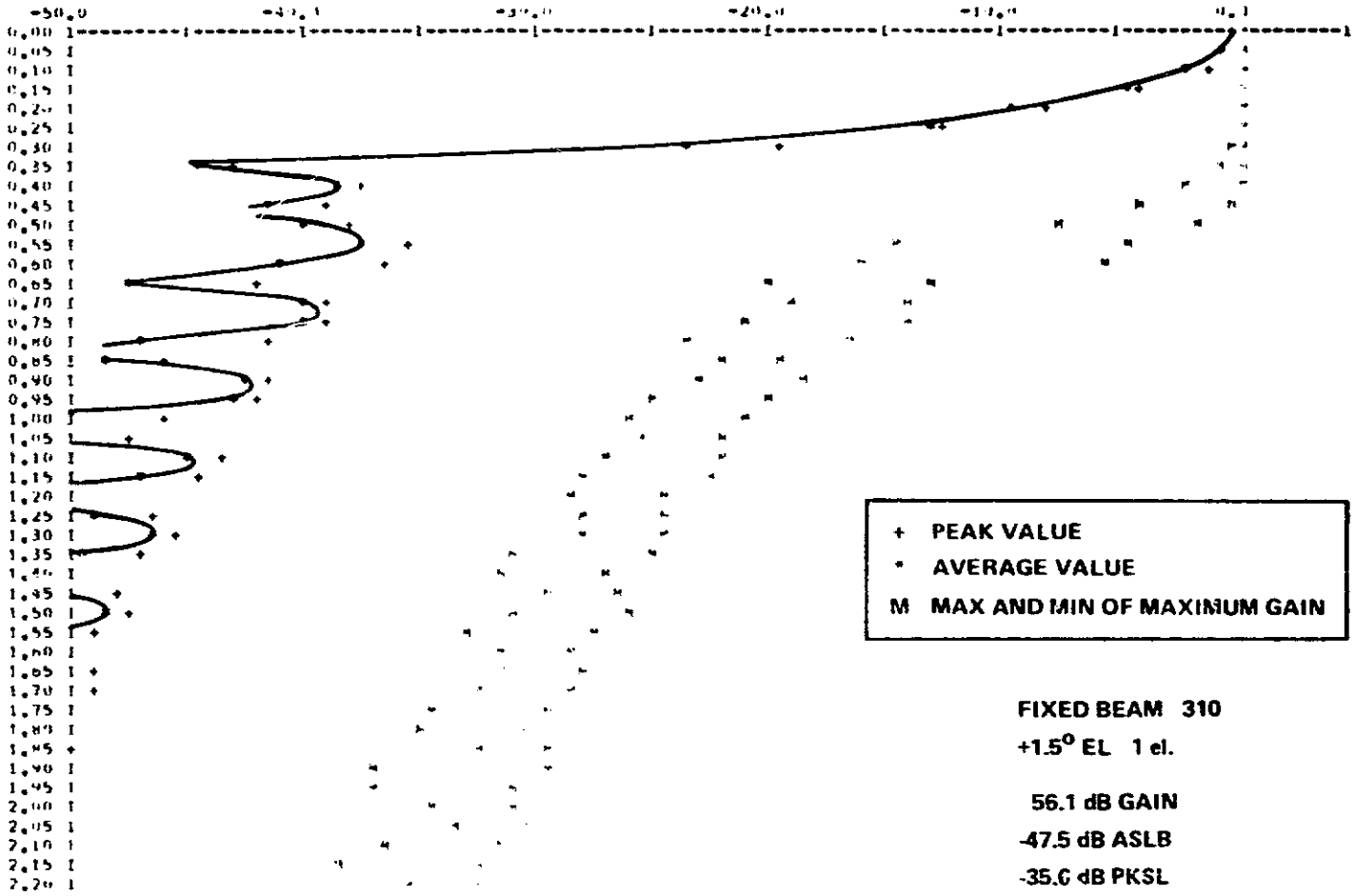

Figure 97. Plot of Peak and Average Sidelobe Levels in Rings Around Main Beam

6.4 ANTENNA PATTERNS

Antenna patterns for the two selected designs are presented in this section. Figures 88 through 93 are for the 6 scanning beam antennae. Figures 94 through 97 are for the 18 fixed beam antennae.

Due to the large amount of pattern data available, a statistical method of presenting the data in a more readily meaningful form was chosen. Since the antennas were designed to have low sidelobes in general, rather than just in zones, it is convenient to present the data as a function of distance from the center of the main beam. Thus a point on the curve presents the statistics of the antenna pattern in an annular ring around the main beam. Three parameters are plotted. First is the average power gain around a ring. Second is the peak power gain of any single point in the ring. Third is the maximum and minimum of the maximum gain envelope. This is not an antenna pattern, but the envelope of the main beam gain under maximum gain conditions as discussed in Section 3.2.7. The maximum and minimum values occurring in each ring around the main beam are plotted. This illustrates that the gain ripple in the region of useful electronic scan is les than .5 dB.

Also indicated on the figures is the number of elements operating at nearly full gain, either 1, 2, or 3. This provides evidence that good beams can be formed whether the power in the focal plane is focused on a single element or focused at a point between two or three adjacent elements.

6.5 COMPOSITE ELEMENT PATTERNS

The composite primary feed patterns for two low sidelobe excitations are shown in Figures 98, 99 and 100, along with a single element pattern in Figure 101. The main reflector subtends an angle of 24° on the primary pattern. Outside of this region, grating lobes do appear in the expected locations based on the element spacing in the array.

The oversized subreflector will intercept some grating lobe energy. Diffraction of this energy by the edge of the subreflector is not accounted for in the computer program. Some grating lobe energy will not be shadowed by the subreflector and may be incident on the earth. The relative level of this energy is computed for a typical case.

Gain of primary element pattern	+18.9 dBi
Array factor of array excitation	+ 6.1 dB
Relative primary grating lobe gain	-10.0 dB
Overall antenna gain	-56.2 dBi
	-41.2 dB

Thus the impact of a feed grating lobe on overall system performance is negligible, being well below the peak sidelobes of any recommended design. However, due to the offset of the feed and subreflector, a feed grating lobe may fall within the coverage area for some beams.

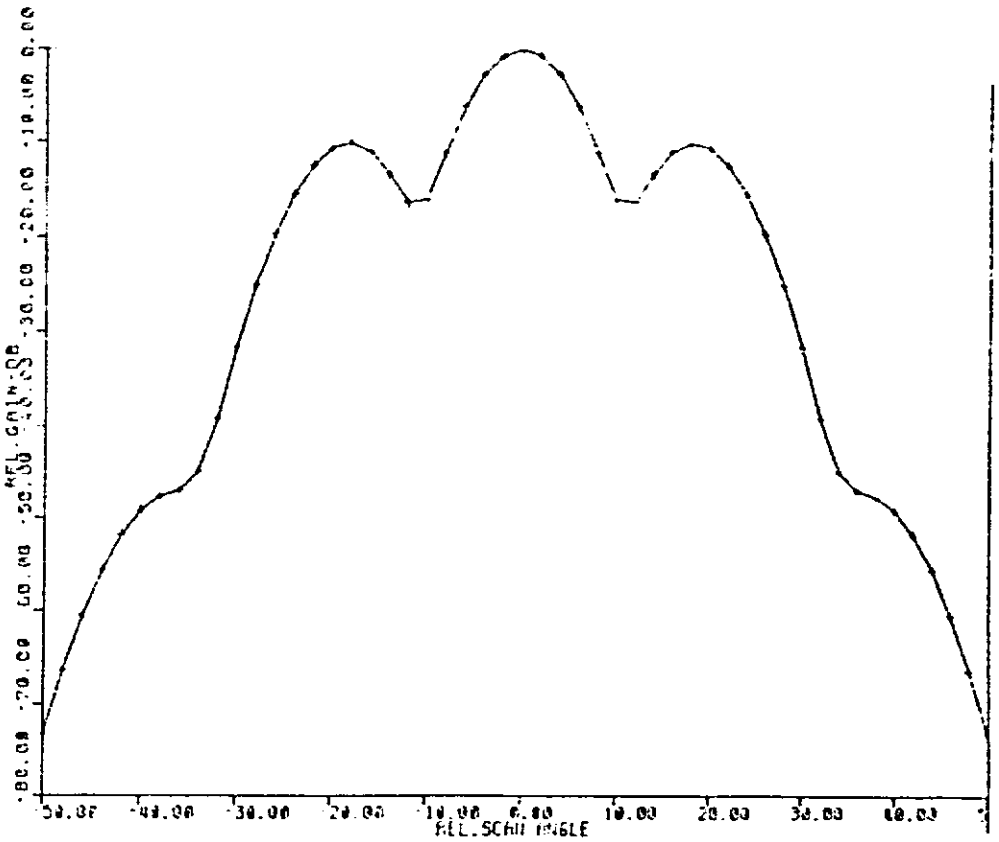

Figure 98. Composite Primary Pattern of 19 Element Cluster
Weighted for 0° Scan
Fixed Beam Case
0° Cut

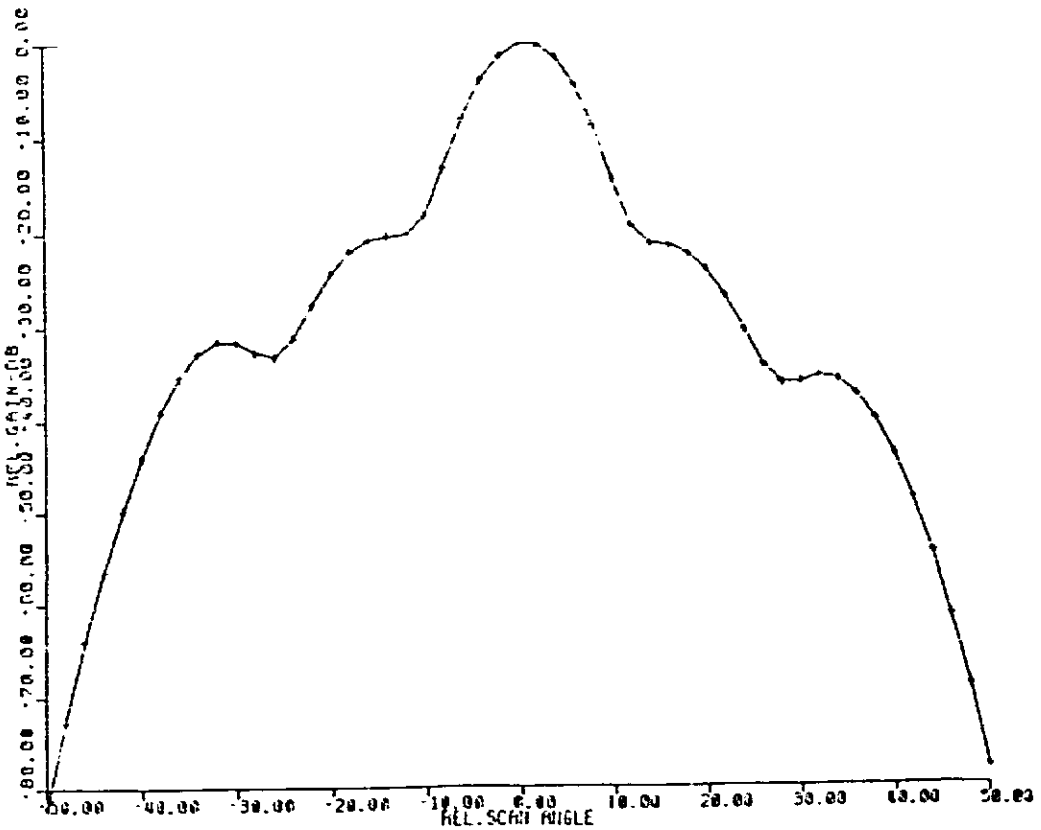

Figure 99. Composite Primary Pattern of 19 Element Cluster
Weighted for 0° Scan
Fixed Beam Case
90° Cut

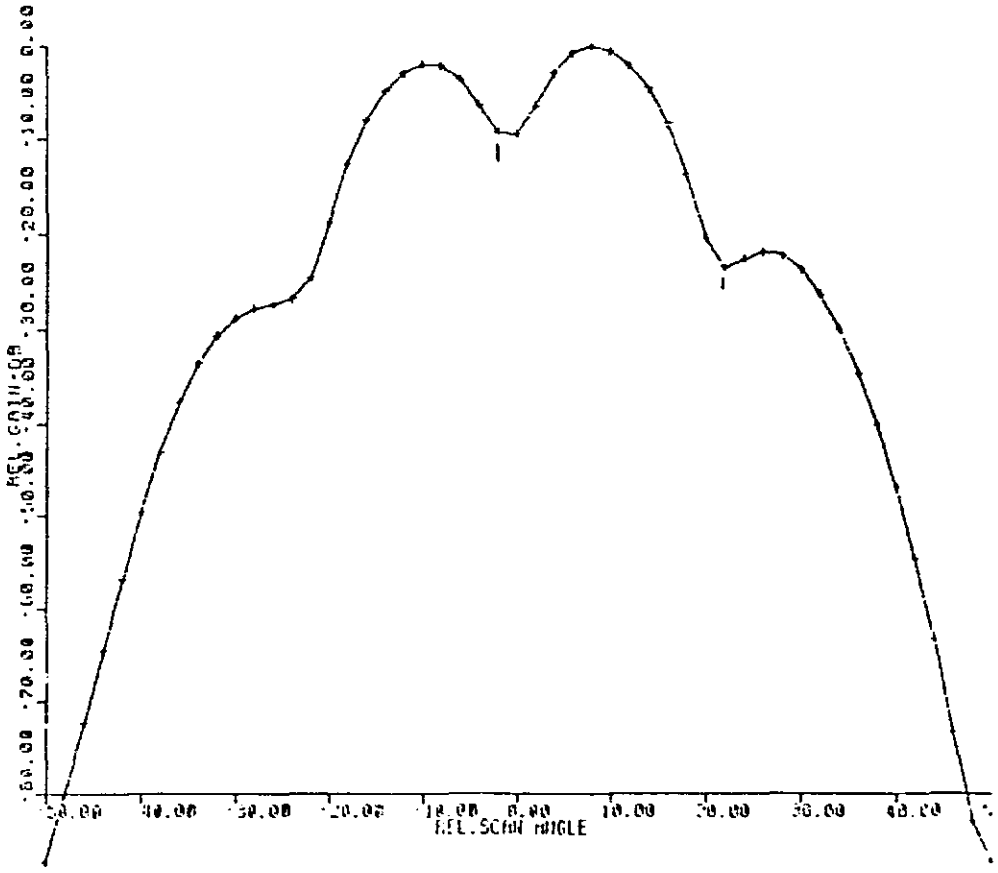

Figure 100. Composite Primary Pattern of 19 Element Cluster Weighted for 3° Azimuth Scan Fixed Beam Case

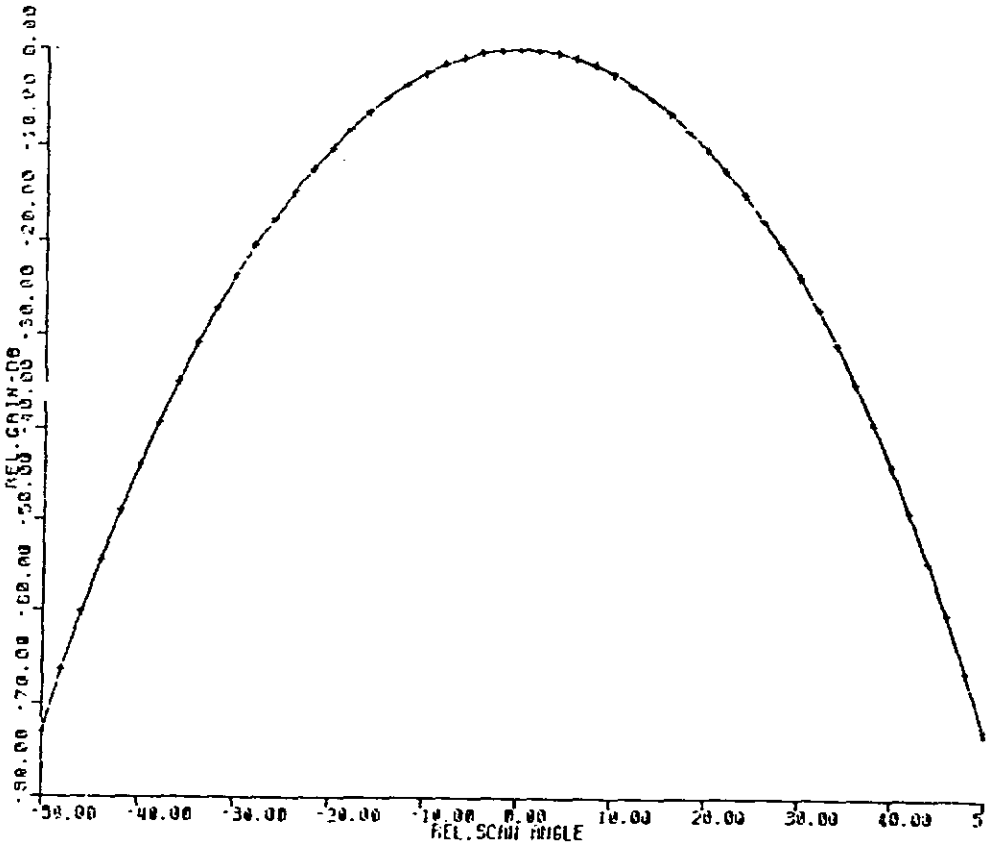

Figure 101. Primary Pattern of Single Element
$\cos^n \theta$ n = 19